Role of fluctuations in finite-dimensional glassy systems

Charlotte Rulquin

Université Pierre et Marie Curie - Paris

École Doctorale Physique en Île de France

T H È S E

pour obtenir le titre de

Docteur en Sciences, spécialité

Physique

Présentée par

Charlotte Rulquin

Rôle des fluctuations dans les systèmes vitreux de dimension finie

---

Thèse dirigée par Gilles Tarjus et co-dirigée par Marco Tarzia

préparée au Laboratoire de Physique Théorique de la Matière Condensée

soutenue le 6 novembre 2017

devant le jury composé de :

Rapporteurs :	Michael A. Moore
	Tommaso Rizzo
Présidente du jury :	Leticia Cugliandolo
Examinateurs :	Ludovic Berthier
	Silvio Franz
Directeur de thèse :	Gilles Tarjus
Invités :	Giulio Biroli
	Marco Tarzia

Remerciements

Trois années et un mois se sont écoulés depuis le début de ma thèse, il va sans dire que de nombreuses personnes en ont été acteurs à mes côtés.

Je pense pour commencer à mes deux rapporteurs, Mickael Moore et Tommaso Rizzo, et je les remercie d'avoir accepté la tâche possiblement ardue de relire en détail ce manuscrit. Leurs commentaires ont permis la construction d'un document plus complet et leurs rapports favorables l'aboutissement de ces années de thèse en une soutenance. Mes pensées se tournent alors vers mes examinateurs, Ludovic Berthier, Leticia Cugliandolo et Silvio Franz, au delà des interactions individuelles que j'ai eues avec chacun d'eux, soit en conférence ou en cours, ils ont montré un intérêt pour mon travail dont je les remercie.

Ce travail n'aurait certainement pas été possible sans l'aide et le soutien inconditionnel des mes responsables : Gilles, Marco et Giulio. Je remercie Giulio d'avoir été de nombreuses fois disponible pour discuter des différents problèmes rencontrés durant ma thèse, qu'ils soient techniques ou conceptuels, et aussi, évidemment, pour la découverte de différentes activités marines ayant pour but de faire filer au gré du vent toute chose flottante munie d'une voile à la très agréable école d'été de Beg Rohu. Je voudrais ensuite remercier Marco pour avoir été présent à chaque fois qu'il fallait comprendre comment résoudre un problème (je pense en particulier aux calculs de diagrammes dans la base LRA !), pour m'avoir prêté main forte de nombreuses fois et bien sûr pour les discussions dans la salle café. Je remercie enfin Gilles pour toutes les discussions physiques pleines de recul dont il m'a fait profiter et suite auxquelles j'ai souvent été remotivée, pour sa capacité à recentrer un problème sur la question d'intérêt à chaque fois que l'esprit s'égarait, pour sa précieuse "manie" à ne jamais laisser tels quels un texte ou une présentation non suffisamment claire à son goût, pour sa participation plus qu'active à la construction d'un manuscrit clair, pour ses calculs de diagrammes (encore eux !) et enfin pour sa sympathie et son humour infaillible.

Entre les deux couloirs qui forment le LPTMC j'ai notamment eu l'occasion d'échanger avec les chercheurs, et pour les différentes discussions je remercie Pascal, Bertrand D. et Bertrand G., Nicolas S., Julien, Annie, Matthieu, Dominique, Ludovic et tout particulièrement Rémy et Olivier qui m'ont beaucoup aidée récemment dans ma recherche de post-doc.

Ensuite, bien évidemment, il y a les thésards et le post-doc du LPTMC. Entre repas, cafés, parties de tarot, bières, ou stops à l'orée des bureaux, il y en a eues des occasions d'échanger sur nos histoires personnelles, nos problèmes de thésards, nos déboires de labo et nos problèmes de physique, de LaTeX ou autre chose du même acabit. Pour tous ces moments partagés je voudrais remercier Chloé, Elsa, Charlie, Can, Pierrilien, Elena, Fred, Andreas, Thibault, Simon, Félix, Jean-Baptiste et Marie. Il y a aussi l'inconditionnel du libanais, le constant visiteur du LPTMC, l'amateur de bière de qualité : le Stanley ! Et il y a des thésards et des post-docs dans une tripotée d'autres laboratoires, que j'ai pu rencontrer en conférence, en école d'été, en bar ou au détour d'un couloir, je ne m'amuserai pas à faire une liste exhaustive de leurs prénoms mais merci à eux.

Viennent alors mes amis qui m'ont soutenue et ont égayé mon quotidien depuis souvent plus longtemps que la thèse, qui parfois ont été un peu négligés lorsque la rédaction battait son plein, mais qui invariablement restait dans mon esprit. Merci à Estelle, Camille, Giulia, Danijela, Mathieu, Eliott, Bassir, Jeferson, et à tous ceux que j'aurais oubliés.

Je remercie cette fois ma famille, qui m'a offert un cadre agréable et ensoleillé à chaque fois que la grisaille parisienne ou les difficultés de la recherche me devenaient trop lourdes à porter. Merci donc à mon père avec qui passer du temps est toujours un plaisir, à ma mère qui a presque invariablement su

être gentille, à ma sœur pour son caractère bien marqué qui peut par moments être agréable, et à ma grand-mère pour le temps passé ensemble à discuter longuement et son infinie gentillesse. Quoi qu'il puisse arriver, je vous porte à tous une immense affection.

Le temps vient enfin de remercier celui qui a progressivement rempli mon cœur, pour en devenir la raison principale de son tic-tac incessant. Tu as été à mes côtés sans défaillir (sauf peut-être depuis ce dernier mois où tu es un peu loin...) pendant ces trois ans, tu as écouté mes doutes, mes envies, mes peines, mes bonheurs, mes colères, tout absolument tout, avec une patience et une attention que jalouseraient beaucoup. Les instants passés à tes côtés me reviennent telle une belle symphonie aux rares fausses notes. Cher Nicolas, j'ose espérer que cette douce mélodie perdurera.

Introduction

The name of "glass" and the appellation "glassy" are used for systems whose dynamics is very slow and with no sign of conventional long-range order. At low temperature, these systems can end up in some arrested out-of-equilibrium state, the so-called glass, corresponding to a dynamics that is too slow to be detectable (the relevant degrees of freedom look frozen on experimental time scales) and then appear as mechanically rigid as a solid can be. A huge variety of materials, called "glass formers", can form a glass: this is for example the case of polymer glasses (plastics), molecular glasses, colloidal gels, foams, spin glasses, vortex glasses, electron glasses. In the above examples, the "glassy" degrees of freedom are associated with molecules, monomers, colloidal particles, bubbles, spin magnetic dipoles, vortices or electrons. [1]

In this thesis we will be concerned by two kinds of glassy systems: the structural glasses [2, 3, 4] and the spin glasses [5, 6]. In the former the degrees of freedom are molecules and the disorder is self-induced when the temperature diminishes; in the latter the degrees of freedom are spins and there is quenched disorder due to the presence of frozen-in magnetic impurities and defects.

The two classes of systems introduced above (and more generally glassy systems) are subject to a phenomenon that is called frustration: it corresponds to the impossibility to minimize the total energy of the system by minimizing sequentially the interactions between degrees of freedom. In structural glasses, the frustration is geometrical and arises when one tries to arrange locally the molecules to optimize the local energetic cost and does not manage to generalize this optimization to the whole space. In spin glasses the mechanism of the frustration which is shown in figure 1 is linked to the presence of quenched disorder which prevents one from satisfying the local spin-spin interactions without arriving at a contradiction. The frustration is accompanied by a large degenerescence of the states of low energy and can therefore be responsible for the existence of complex free-energy landscapes.

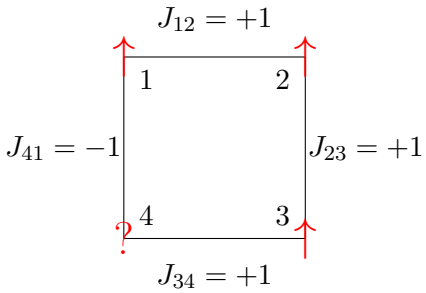

Figure 1: Frustration in an Ising spin-glass model of four spins $(1, 2, 3, 4)$ represented by red arrows, $\uparrow$ or $\downarrow$, whose Hamiltonian is $H = -\sum_{i=1}^{4} J_{i,i+1} S_i S_{i+1}$, with $S_5 = S_1$. The four couplings J_{ij} are distributed between the two values ± 1 with some probability distribution: here, 3 interactions are ferromagnetic $J_{12/23/34} = +1$ and one is anti-ferromagnetic $J_{41} = -1$. Satisfying sequentially the local interactions one arrives at a contradiction and the system is frustrated. There are several states of minimal energy which correspond, *e.g.*, to ? $= \uparrow$ or $\downarrow$ and therefore the ground state is degenerate.

In three-dimensional structural glasses the slowing down of the dynamics has not been given (yet) a widely accepted explanation: there are for instance proposals to associate it to the existence of an underlying thermodynamic phase transition [7, 8, 9], or to to the existence of an underlying dynamical transition [10, 11]. In three-dimensional Ising spin glasses, this slowing down is accepted to be associated

with the existence of a thermodynamic phase transition at finite temperature, from a paramagnetic to a spin-glass phases; however many questions are still open concerning the nature of the spin-glass phase [12, 13, 14]. Structural and (Ising) spin glasses will be presented in more details in the chapter 1.

In general, a good starting point to try to understand a problem in statistical physics is to study its mean-field approximation. On the one hand, since this approximation neglects long-range spatial fluctuations, it is simpler to study than the exact theory in three dimensions. On the other hand, the mean-field approximation often gives interesting qualitative information on the macroscopic physics of the system of interest even in finite dimensions.

The mean-field approximations of structural glasses and spin glasses [15, 16, 17] have been shown to be exact in the limit of infinite dimensions [18, 19, 20, 21, 22]. (We will often contrast infinite dimensions to finite dimensions, which include the three-dimensional case.) Both mean-field theories predict thermodynamic phase transitions at some finite temperature from a paramagnetic phase to an "ideal"-glass phase (for structural glasses) or to a spin-glass phase (for Ising spin glasses). However, they are intricate theories that are, *e.g.*, written in terms of a $n \times n$ overlap matrix order parameter with $n \to 0$ [16] and associated to complex free-energy landscapes with the presence of ubiquitous metastability. The latter appears to be a central ingredient in the mean-field description of the glass transitions and glass phases. For structural glasses, as pictorially represented in figure 2, the mean-field free energy is for low-enough temperatures *above* the thermodynamic transition temperature a rough and hilly landscape with degenerate metastable minima whose number is exponential in the system size. For Ising spin glasses, the mean-field free energy for temperatures lower than the transition one is characterized by an infinite hierarchy of minima [23] (each minimum is divided in several smaller minima, themselves divided in other smaller minima, *etc.*).

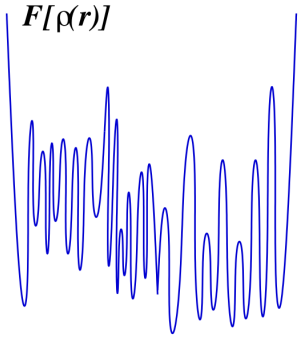

Figure 2: Structural glass: Pictorial mean-field free energy $F[\rho(r)]$ as a function of the density field $\rho(r)$ for lower-enough temperatures larger than the glass-transition temperature with a huge number of metastable minima.

One can wonder which signatures of the mean-field metastability remain in the thermodynamics of finite-dimensional systems. Metastability may indeed be considered as an irrelevant mean-field artifact since fluctuations destroy it in finite dimensions. To answer this, one should include fluctuations to the mean-field descriptions and see their effect on the mean-field scenarios. A method of choice to perform this is the renormalization group [24] which allows one to treat the fluctuations beyond the mean-field description. This method is presented in chapter 2 with an emphasis on nonperturbative approaches [25, 26]. Since studying the role of fluctuations directly on realistic models of structural and spin glasses is a hard task, we try to somehow sidestep the difficulty by investigating fluctuations in simpler related finite-dimensional models.

In chapter 3, we study the return to convexity of the free energy of a simple one-dimensional toy

model as its size increases. The finite size of the system indeed constrains the spatial fluctuations, which for instance allows some form of metastability and a nonconvex shape of the thermodynamic potential. As this is the situation in computer simulations of glassy systems, one may wonder what kind of information on the system in its thermodynamic limit and if the proper effective theory to describe it can be extracted from systems of small to moderate sizes. For the case of the return to convexity in the one-dimensional φ^4 theory, we also investigate possible approximation schemes for the nonperturbative renormalization group [25, 26] that could take into account the strong, nonperturbative, effect of the spatial fluctuations that destroy ordering.

Due to the complex structure of the mean-field theory for structural glasses, it is still unclear what is the nature of the relevant spatial fluctuations that lead to the glassy phenomenology in finite (say, three) dimensions. In chapter 4, by investigating simple glass-forming systems, known as plaquette spin models [27], on Bethe lattices of varying coordination number and comparing with results on Euclidean lattices, we try to disentangle the effect of "short-range" fluctuations, associated with the local environment, and that of "long-range" fluctuations in the glassy properties of these models.

In chapter 5, we analyze spatial correlations in the dynamics, a phenomenon associated with the development of dynamical heterogeneities in glass-forming systems. To shed light on the origin of these correlations and contrast them with the putative correlations responsible for the strong slowing down of the dynamics in glass formers, we study analytically a non-glassy finite-dimensional model with a simple non-glassy yet thermally activated dynamics.

Finally in chapter 6, we study the more standard problem of the role of large-scale fluctuations on the critical behavior of the Ising spin glass (in the absence of an applied-magnetic field). We do so by applying the nonperturbative renormalization group, in an effort to extend this method to glassy systems characterized by a complex order-parameter field.

Chapter 1

Structural and spin glasses: a perspective

Contents

1.1 Structural glasses

1.1.1 Phenomenology

Liquids that have been cooled "fast enough", such that the standard first-order transition leading to the crystalline phase is avoided, reach an equilibrium metastable phase named supercooled liquid phase. The terminology "fast enough", commonly used by the experimentalists, can be clarified: below the melting temperature T_m, if one wants to avoid nucleation of the stable crystalline phase, the cooling rate must be higher than the nucleation rate, so that the system is not given enough time to form a stable nucleus and start crystallization. At the same time, the cooling rate must not be *too* large, or the system would not manage to equilibrate. The supercooled liquid phase is a locally stable state, albeit with a higher free energy than the true stable state which is the crystal phase. In the supercooled liquid phase, the viscosity η of the system begins to grow in a very dramatic way when the temperature decreases (typically, the viscosity grows by 14 orders of magnitude when T is decreased by $30-40\%$). η is linked to the relaxation time τ of the system, *i.e.* the time required to reach equilibrium. By convention, when the relaxation time is of order $\tau \sim 10^2 - 10^3$ sec and larger, corresponding to a viscosity around $\eta \sim 10^{12}\, Pa.s$ and more, the system in practice falls out of equilibrium on the experimental time scale: this corresponds to the experimental glass transition temperature T_g which then represents a dynamical crossover rather than a true phase transition. As a consequence, one is unable to equilibrate the supercooled liquid below T_g, which reaches one of the numerous possible out of equilibrium states

called *glasses*, depending on the initial conditions. See [28, 2, 3, 4] for reviews/book where more on the supercooled liquids phenomenology can be found.

The above phenomenon is schematically represented on figure 1.1, which represents the enthalpies of the crystal and of the liquid/supercooled-liquid/glass phases.

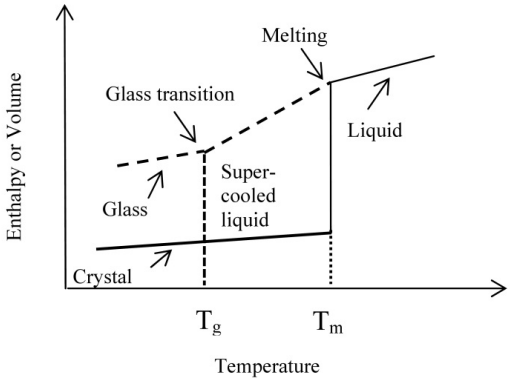

Figure 1.1: Volume or enthalpy of a liquid at constant pressure as a function of temperature. The different phases evoked in the previous paragraph are represented: liquid, crystal, supercooled liquid and glass. T_m is the melting temperature. A "fast enough" cooling yields a glass transition at a temperature T_g which depends on the cooling rate. Reprinted from [29], where it was adapted from [30]

In the following, we will be concerned by the *equilibrium* (metastable) supercooled liquid phase, and not the *out-of-equilibrium* glass.

Growing time scale

From experimental results, supercooled liquids are usually classified according to their "fragility", which characterizes the temperature dependence: see figure 1.2. [31] At one end of the spectrum, "strong" glasses whose relaxation time follows an Arrhenius temperature dependence, $\tau \sim e^{\Delta E/(k_B T)}$, are network glasses where dynamics is dominated by the constant energy barrier ΔE associated with breaking covalent bonds between constituents.

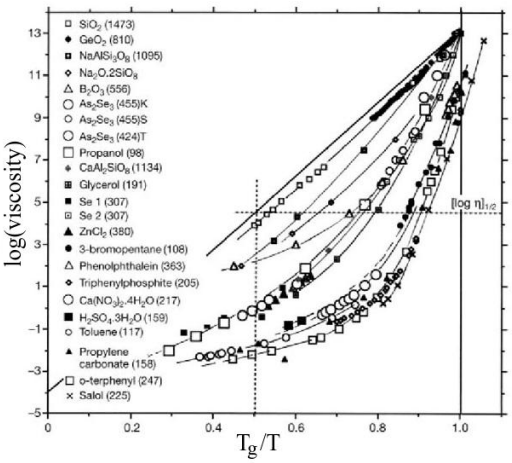

Figure 1.2: The Angell plot from [32], representing the log of the viscosity $\eta \sim \tau$ as a function of the inverse of the temperature rescaled with T_g classifies the liquids according to their fragility, *i.e.*, the deviation from Arrhenius behavior $\tau \sim e^{\Delta E/k_B T}$.

"Fragile" glass formers (the vast majority of polymeric and molecular liquids) are characterized by a faster-than-Arrhenius, a super-Arrhenius, temperature dependence of the relaxation time: $\tau \sim$

$\exp\left[\Delta E(T)/(k_B T)\right]$ with $\Delta E(T)$ increasing as one approaches the glass transition. A popular fitting formula to describe this behavior is the Vogel-Fulcher-Tamman (VFT) expression [33, 34, 35]

$$\tau \sim \exp\left(\frac{A}{T - T_0}\right), \tag{1.1}$$

where A and T_0 are adjustable parameters. This expression suggests a divergence of the relaxation time at an unreachable temperature T_0 below the experimental glass transition T_g. In any case, the growth of the activation barriers as one cools the fragile liquid toward T_g is indicative of a collective phenomenon, necessarily accompanied by the growth of some correlation length. [36]

Growing length scale?

In standard phase transitions, the growth of a time scale is associated to the concomitant growth of a length scale. The most easily accessible length scale is that obtained from the classical two-point density-density correlation function. One can consider the radial correlation function $g(r)$ which gives information about the structural properties of standard liquids: $g(r)$ gives the average probability to find a particle at a distance r from any particle. Its Fourier integral gives the static structure factor $S(q)$, which is directly measured in experiments. These two quantities do not show any marked change as one cools the liquid down to T_g, as one can see on figure 1.3.

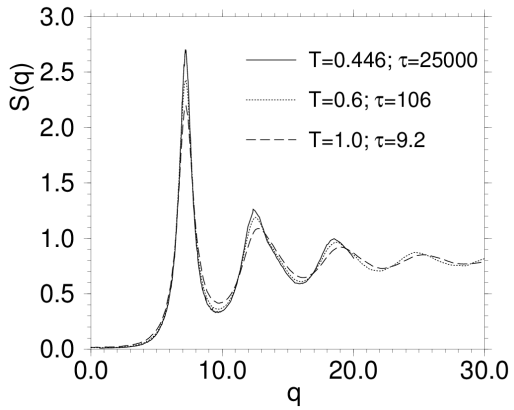

Figure 1.3: Structure factor $S(q)$ as a function of the momentum q for three different temperatures obtained from a computer simulation of a glass-forming liquid model, reprinted from [37].

An understanding and a detailed identification of the collective behavior at the origin of the growing of relaxation times has been a recurring quest in the physics of glasses. [3, 1] We will discuss the subject of growing length scales associated to collective behavior in the glass formation further down in the manuscript.

Entropy

Another quantity which can be experimentally measured is the heat capacity at constant pressure C_P, from which we can determine the total entropy S_{sl} of the supercooled liquid as $C_P = T\, dS_{sl}/dT$. One can plot the entropies of the supercooled liquid S_{sl} and of the crystal S_{cr} as a function of the temperature, see figure 1.4. One observes that the entropy of the liquid decreases much more rapidly than that of the crystal. If the data are extrapolated below T_g, one could reach a temperature T_K at which the two entropies are equal, a rather strange phenomenon. [38] This, together with the empirical observation that $T_K \simeq T_0$ (where T_0 is defined above) within 10% or so, is suggestive of the possible existence of an ideal, and unreachable, glass transition at T_K.

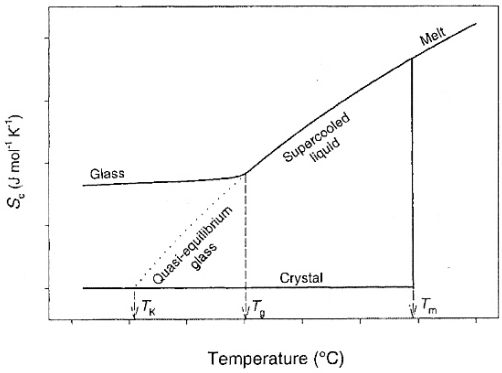

Figure 1.4: Entropies of the supercooled liquid S_{sl} and the crystal S_{cr} as a function of temperature. By extrapolation, one finds the Kauzmann temperature T_K, at which $S_{sl} = S_{cr}$. Reprinted from [38].

Dynamical heterogeneities

The heterogeneous character of the dynamics in glass-forming liquids has been established in the last two decades. When approaching the glass transition at T_g, one observes, *e.g.* by confocal microscopy in colloidal suspensions or by computer simulations of liquid models, the presence of fast and slow moving regions, which stay so over an increasing time scale. [39, 40]

A snapshot from a computer simulation is shown in figure 1.5 (a), where the fastest particles are colored in dark red, whereas the slowest are in blue, and a gradation covers the intermediate regimes. On the second panel, figure 1.5 (b), are represented the vector displacements of the particles, by mean of arrows of different lengths and pointing in different directions, on a time scale comparable to the *structural* relaxation time $\tau = \tau_\alpha$, which is the time needed by the configuration to relax. Both figures show that the mobility varies among the particles, but also that particles with similar mobilities have the tendency to gather spatially.

(a) 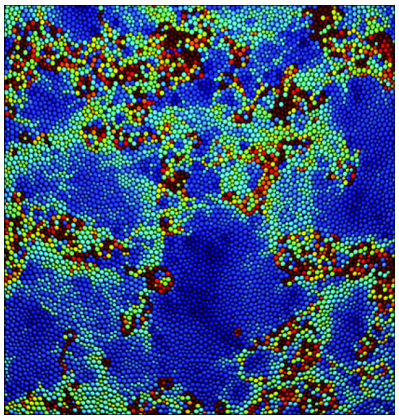 (b) 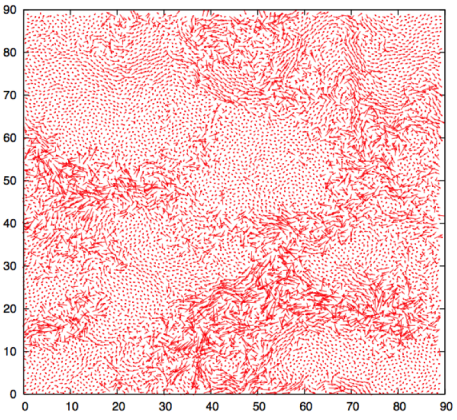

Figure 1.5: (a) Simulation of supercooled liquid showing dynamical heterogeneities: particles change colors depending on their mobility, dark red is for the fastest, dark blue for the slowest, and the gradation stands for the intermediate regimes. Reprinted from [41]. (b) Arrows represent particles displacements on a time scale of the order of the structural relaxation time. Both figures show that mobility varies among particles, and also that particles sharing the same mobility are probable to be side by side. Reprinted from [3].

These dynamical heterogeneities are a form of space-time fluctuations and can be characterized by correlations and an associated length scale. Such correlations in the dynamics cannot be unveiled by conventional pair correlation functions. They require multi-point space-time correlation functions.

Consider for instance a local probe of the motion for atom j between two times 0 and t, *e.g.*, $f_j(q,t) = \Re\left\{e^{iq(r_j(t)-r_j(0))}\right\}$. The average dynamics is characterized by the usual auto-correlation function (self-intermediate scattering function) $F_s(q,t) = N^{-1}\sum_{j=1}^{N}\langle f_j(q,t)\rangle$ represented in figure 1.6 (a). The fluctuations in the dynamics, with $\delta f_j(q,t) = f_j(q,t) - \langle f_j(q,t)\rangle$, can be characterized by higher-order correlation functions such as

$$g_4(r,t) = \frac{1}{N^2}\sum_{i,j=1}^{N}\delta(r_{ij}-r)\,\langle \delta f_i(q_0,t)\delta f_j(q_0,t)\rangle\ , \tag{1.2}$$

with q_0 usually taken as the location of the peak of $S(q)$ represented in figure 1.3. The quantity g_4 is a 4-point space-time correlation function from which one can extract a "dynamical" correlation length $\xi_d(t)$ describing how far the motion of particles is correlated during an elapsed time t. A less detailed description is embodied in the "nonlinear dynamic susceptibility"

$$\chi_4(t) = \frac{N}{V}\int d^3r\, g_4(r,t)\,. \tag{1.3}$$

At fixed temperature, $\chi_4(t)$ has a nonmonotonic behavior (see figure 1.6) and goes through a maximum for a time t of the order of the α-relaxation time. At this time, the correlations in the dynamics are maximum. (Although this nonlinear susceptibility is not directly accessible in experiments on molecular liquids, several proxies have been studied that all display the same behavior.)

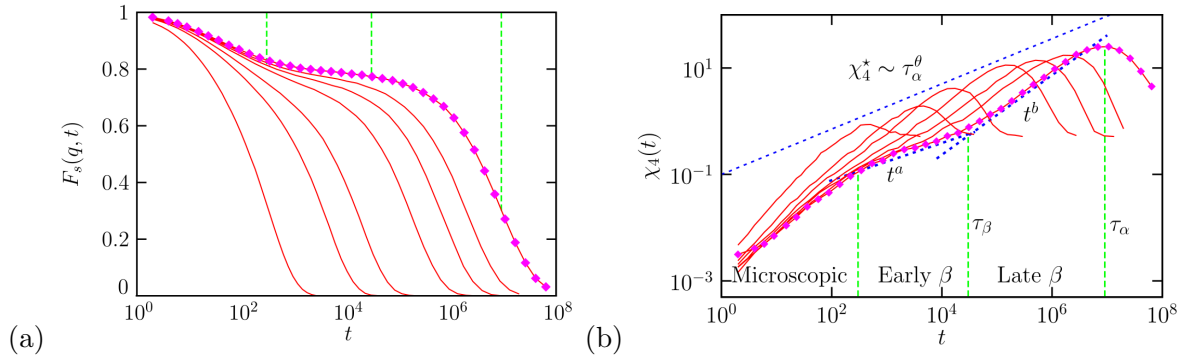

Figure 1.6: Measure of $F_s(q_0,t)$ (here $q \equiv q_0$ of the text) (a) and corresponding regime of $\chi_4(t)$ (b) in Lennard-Jones supercooled liquids simulations. In particular $\chi_4(t)$ has a maximum around $\tau = \tau_\alpha$, time lapse at which the particles dynamics is maximally correlated. Reprinted from [3].

The peak is found to grow when the temperature is decreased. Typically, in simulations, it grows by two orders of magnitude between the highest temperature at which it appears and the lowest temperatures at which the system can be equilibrated. Therefore the dynamical volume over which dynamics is correlated is observed to grow with the inverse temperature, which suggests that the glass transition is a collective phenomenon. For various estimates, the length scale characterizing such correlations in the dynamics appears however to grow not bigger than 5 to 10 molecular diameters at T_g. [39, 40]

1.1.2 Mode-coupling theory

The mode-coupling theory (MCT) predicts a dynamical arrest of the liquid structural relaxation at some temperature T_{MCT} based only on the modest variation of the auto-correlation function. Formally, the MCT derives a set of nonlinear self-consistent equations [10] describing the evolution of the time-dependent auto-correlation function $C(t)$ of the local density field at time t, $\rho(\vec{r};t) = N^{-1}\sum_{i=1}^{N}\delta(\vec{x_i}(t)-$

$\vec{r}$), that characterizes the supercooled liquid composed by N particles evolving in a continuous volume V. In Fourier space, $\rho_{\vec{q}}(t)$ is the density fluctuation of wavelength q and defines

$$C(t) = \left\langle \rho_{\vec{q}_0}(t)\rho_{\vec{q}_0}(0)^* \right\rangle - \left\langle \rho_{\vec{q}_0} \right\rangle^2 , \tag{1.4}$$

which can be measured in supercooled liquids by neutron scattering or computer simulation. At high temperature (yellow curves on figure 1.7 (a)), the dynamical relaxation follows a standard exponential decay $C(t) \sim \exp(-t/\tau)$. When the temperature decreases (red curves), a "plateau" develops and the relaxation now displays two steps: a rapid β and a slow α regimes. The α relaxation step is often described by a stretched exponential, $C(t) \sim e^{-(t/\tau)^\beta}$, with $0 < \beta < 1$.

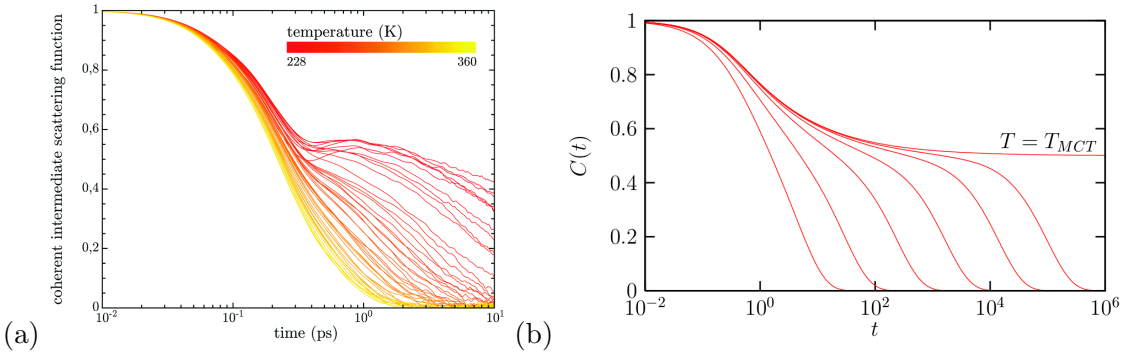

Figure 1.7: Typical shape of the dynamical auto-correlation function $C(t)$ in log-time scale obtained for different temperatures. At high temperature the relaxation is exponential and below some temperature it displays a two-step relaxation characteristic of low-temperature supercooled liquids: the fast β- and slow α-relaxation regimes. (a) $C(t)$ from water supercooled liquids experiments, here $C(t)$ is the coherent intermediate scattering function. Reprinted from [42]. (b) $C(t)$ from the solution of the MCT non-linear self-consistent equations, for different temperatures approaching T_{MCT}. Reprinted from [3].

MCT equations can be derived using the Zwanzig-Mori formalism [43, 44] and have the form of generalized Langevin equations, with a time-dependent memory kernel. The memory kernel is then obtained in a specific, mode-coupling approximation, and is expressed in terms of the static structure factor $S(q)$. The nonlinearity of the equations gives rise to a sharp feedback between static structure and dynamics, and even a small change in the static structure factor leads to a strong slowing down of the relaxation.

The solution of the MCT equations displays a relaxation in two steps, similarly to what is observed in experimental supercooled liquids. These solutions are represented on figure 1.7 (b) for different temperatures.

At some temperature T_{MCT} the system exhibits a dynamical arrest, corresponding to a transition from an ergodic to a nonergodic state. No concomitant singularity in thermodynamic quantities and in the structure of the system are observed. The MCT α-relaxation time is found to diverge as a power law:

$$\tau_\alpha = \frac{1}{(T - T_{MCT})^\gamma} . \tag{1.5}$$

The profound difference with the dynamical arrest predicted by the empirical VFT fit (1.1) when approaching T_g indicates that

$$T_{MCT} > T_g > T_0 . \tag{1.6}$$

The dynamical transition at T_{MCT} is avoided in real supercooled liquids, as shown in figure 1.8, and at best persists as a dynamical crossover.

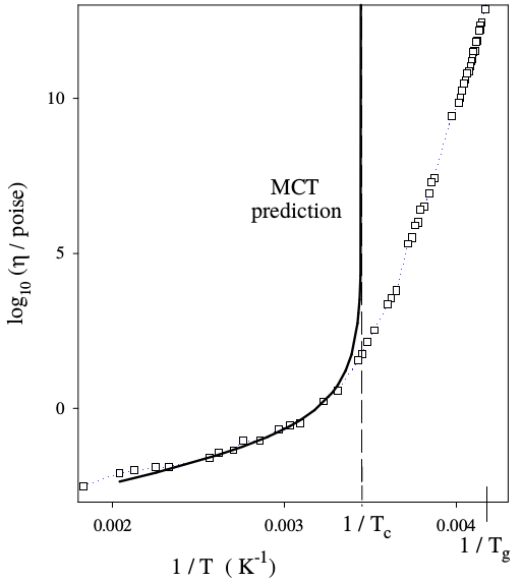

Figure 1.8: $\log_{10}$ of the viscosity $\eta \sim \tau$ as a function of the inverse temperature for liquid ortho-terphenyl from Ref. [45]. The solid line is the mode-coupling prediction of the relaxation time, it fits well the high temperature region, but breaks down at some point and diverges at T_{MCT}, which is interpreted as a crossover temperature.

To conclude, mode-coupling approach can thus describe at best the dynamics of moderately supercooled liquids at temperatures $T > T_{MCT}$. Possibly, it can also apply to the fast β-relaxations even below T_{MCT}. However it misses the deeply-supercooled regime in which the dynamics is better described as thermally activated.

1.1.3 Mean-field theory of glasses

The mean-field theory of glasses originates in the physical picture that the slowing down of relaxation in glass-forming liquids is a consequence of the existence of a complex free-energy landscape with numerous minima that the system has to explore in order to relax. [46, 47, 48]

Kirkpatrick, Thirumalai and Wolynes looked for other simpler mean-field models in which such free-energy landscape could exist, and where a phenomenology similar to the structural glasses occurs. [48, 49] This is the case of the Potts-glass model and of the spherical p-spin model with infinite-range interactions, for example. This analogy was also supplemented by a crude mean-field density functional theory of glass-forming liquids [47, 50] and by a scaling theory that one now refers to as the "random first-order transition" (RFOT) theory [7]; see [51, 9] for reviews.

1.1.3.1 The spherical p-spin model

For illustration we consider below the spherical p-spin model. The behavior of the Potts-glass model is similar. The p-spin model was introduced in [52]. Its Hamiltonian is:

$$\mathcal{H}(\{\sigma_i\}) = - \sum_{i_1,\ldots,i_p=1}^{N} J_{i_1,\ldots,i_p} \sigma_{i_1} \ldots \sigma_{i_p} \,, \tag{1.7}$$

where the sum runs over all possible ensembles of p spins among the N spins of the system, the interactions are therefore fully-connected and there is no lattice structure. The σ_i's are Ising spins

or spherical spins with constraint $\sum_{i=1}^{N}\sigma_i^2 = N$, and the $J_{i_1,...,i_p}$'s are quenched random couplings distributed accorded to a Gaussian probability density with zero mean and variance $p!/(2N^{p-1})$.

The origin of the disorder is different between supercooled liquids and p-spin model, as in the former it is *self induced* while the temperature is lowered whereas in the latter the disorder is *quenched* and put by hand, by the introduction of random coupling constants.

The spherical p-spin model with $p \geq 3$ nevertheless provides a convenient framework to introduce a mean-field theory presenting a complex free-energy landscape and a phenomenology related to that observed in real supercooled liquids, see below.

One first defines the partition function, summing the Boltzmann weights over all N-spin configurations $\{\sigma_i\} = (\sigma_1, ..., \sigma_N)$ and introducing a site-dependent external field h_i that will be used to compute configurations corresponding to free-energy minima,

$$Z\left(\{h_i\}\right) = \sum_{\{\sigma_i\}} \exp\left[-\beta\mathcal{H}(\{\sigma_i\}) + \beta\sum_{i=1}^{N} h_i\sigma_i\right]. \tag{1.8}$$

The Gibbs free energy is the Legendre transform of the Helmholtz free energy obtained from $-\beta^{-1}\log Z\left(\{h_i\}\right)$ with the magnetization per site i: $m_i = -\left[\beta Z\left(\{h_i\}\right)\right]^{-1}\partial Z\left(\{h_i\}\right)/(\partial h_i) = \langle\sigma_i\rangle$. It is given by

$$F\left(\{m_i\}\right) = -\beta\log Z\left(\{h_i^\star\}\right) + \sum_{i=1}^{N} h_i^\star\, m_i, \tag{1.9}$$

where the external field configuration has to be fixed such that the relation

$$-\beta\,\frac{\partial\log Z\left(\{h_i\}\right)}{\partial h_i}\Big|_{\{h_i\}=\{h_i^\star\}} + m_i = 0 \tag{1.10}$$

is verified. F has been named the TAP free-energy from the names of Thouless, Anderson and Palmer who first introduced it. [53]

It appears that F is composed of many minima, which can be found by searching for the configurations $\{m_i^\star\}$ satisfying the equation

$$\frac{\partial F\left(\{m_i\}\right)}{\partial m_i}\Big|_{\{m_i\}=\{m_i^\star\}} = 0. \tag{1.11}$$

The remarkable property of this model when $p \geq 3$ is that the number of solutions of the solutions of the above equation, and more restrictively the number of minima, is exponentially large in the system size N for a whole range of temperature. One is interested in computing the thermodynamic properties of this collection of minima. Since the model is fully connected, the connectivity is equal to the number of degrees of freedom and this precludes the formation of finite clusters where the order parameter takes different values. As a result, barriers between locally stable states are extensive, infinite in the thermodynamic limit; thus, when the system enters a locally stable state it cannot escape from it to reach the global minimum, and stays for an infinite time in a metastable state. The sharp separation between configurations within one free-energy minimum and different minima allows one to perform a well-defined coarse graining. One computes first the free-energy density of one minimum (state) μ by summing over configurations $\{\sigma_i\}$ belonging to this minimum μ

$$f_\mu = -\frac{1}{\beta N}\log\sum_{\{\sigma_i\}\in\mu} e^{-\beta H(\{\sigma_i\})}. \tag{1.12}$$

Introducing the f-dependent configurational entropy (density) $s_c(f) = N^{-1} \log \sum_{\mu=1}^{N} \delta(f - f_\mu)$ counting the logarithm of the number of minima with fixed free-energy density f, one can write the partition function of the system summing on the different states. This is the second step:

$$Z = \sum_{\mu=1}^{N} e^{-\beta N f_\mu} = \int df \, \exp^{-\beta N [f - T s_c(f)]} . \tag{1.13}$$

The free-energy density of the system in the thermodynamic limit can be evaluated by a saddle-point calculation:

$$F = -\frac{1}{N\beta} \log Z = \min_f \left[f - T s_c(f) \right] . \tag{1.14}$$

The metastable states dominating the partition function have a free-energy density $f^\star(T)$ which is solution of equation (1.14). This defines rigorously the configurational entropy, or complexity (in the spin-glass community), which counts the number of statistically available states, as

$$s_c(T) = s_c(f^\star(T)) . \tag{1.15}$$

By analyzing the behavior of $s_c(T)$ when the temperature is varied, one identifies two characteristic temperatures, T_d and T_K: at T_d, the equilibrium configuration entropy first emerges as a nonzero quantity (the number of relevant states is then exponentially large in N) and at $T_K < T_d$, this configurational vanishes.

For $T > T_d$, the configurational entropy drops to zero *discontinuously*. Above T_d only one global free-energy minimum exists, corresponding to the the high-temperature paramagnetic phase. Mean field free-energy barriers separating metastable states being of infinite height, the system remains stuck in one metastable state below T_d and the relaxation time τ diverges at T_d; consequently, the dynamics is out of equilibrium below T_d. This breaking of ergodicity corresponds to a transition which is purely dynamical, and no singularity in the free energy is found. Actually this singularity is a mean-field artifact, as the fully-connected nature of the description prevents the existence of thermal fluctuations allowing the system to relax between minima. The temperature T_d is the equivalent of T_{MCT} of section 1.1.2 at which a similar dynamical transition occur.

At T_K, the configurational entropy linearly vanishes giving back an entropy crisis *á la* Kauzmann (see figure 1.4). A thermodynamic phase transition occurs toward a new amorphous state corresponding to the minimum in which the system is stuck, which is now an equilibrium ideal glass state. This RFOT (which also goes under the name of "one-step replica symmetry breaking", see below) is second order in the usual thermodynamic sense (with no latent heat) but accompanied by a discontinuous jump of the order parameter as in first-order transitions.

The spherical p-spin model also displays a MCT-like two-step relaxation (as plotted in figure 1.7 (a)) and aging properties akin to what is observed in real structural glasses. [52, 54, 17]

1.1.3.2 Order parameter: overlap matrix

As for the Sherrington-Kirkpatrick Ising spin glass [16, 12, 55, 56, 57, 58], the order parameter $\mathbb{Q}$ of this mean-field glass transition is a complicated object, a $(n \times n)$ matrix of overlaps with $n \to 0$, which measures the average structural similarity between configurations in different minima.

Replica trick

Historically this order parameter comes from the fact that a convenient way to compute the free energy in models with quenched disorder is to use the replica trick. It allows one to compute the free energy averaged over disorder, namely $\overline{F} = -\beta^{-1} \overline{\log Z}$, by using the exact equality $\overline{\log Z} =$

$\lim_{n\to 0}\left[(\overline{Z^n}-1)/n\right]$. Hence, by letting n be an *integer*, the partition function has to be *copied* n times before the product of exponential is averaged

$$\overline{Z^n} = \sum_{\{\sigma^{a_1}\},\ldots,\{\sigma^{a_n}\}} \overline{e^{-\beta\sum_{i=1}^{n}\mathcal{H}[\{\sigma^{a_i}\}]}}\,. \tag{1.16}$$

Then n *replicas* of the system formally identified by indexes $(a_1,...,a_n)$ appear. Each one is in a configuration $\{\sigma^{a_i}\}$, and all of them are submitted to the *same* quenched disorder, leading to the possibility to integrate Z^n over an unique disorder distribution. This leads to an effective coupling between replicas and one finally has to perform the usually uncontrolled procedure of letting n go to zero after a continuation to noninteger values of n in order to obtain the correct averaged free energy $\overline{F}$.

The *overlap* between two replicas, or configurations, $\{\sigma^a\}$ and $\{\sigma^b\}$, shows up naturally in the calculation of $\overline{F}$ and provides an order parameter. One can define

$$Q_{ab} = \frac{1}{N}\sum_{i=1}^{N}\sigma_i^a\sigma_i^b\,, \tag{1.17}$$

with $Q_{ab}=1$ if the two configurations a and b are identical, $Q_{ab}=-1$ if they are anti-correlated, and $Q_{ab}=0$ if they are uncorrelated. The self-overlap is $Q_{aa}=1$ due to the Ising or spherical constraint.

Overlap matrix

Then, one can construct the $(n\times n)$ matrix of overlaps Q_{ab} and $\langle Q_{ab}\rangle$ which is the order parameter [16] Physically, the continuous version of the matrix of average overlaps is linked to the probability distribution of having some overlap q between configurations of the system averaged over the disorder $\overline{P(q)}$. Mathematically, $\overline{P(q)}$ is equal to the fraction of elements $\langle Q_{ab}\rangle$ of the overlap matrix equal to q:

$$\overline{P(q)} = \lim_{n\to 0}\frac{1}{n(n-1)}\sum_{a\neq b}\delta\left(q-\langle Q_{ab}\rangle\right)\,. \tag{1.18}$$

If the replicas are all symmetric and $\langle Q_{ab}\rangle = q_0$ for all a and b different, the probability distribution is just one Dirac-δ centered in q_0: $\overline{P(q)}=\delta(q-q_0)$. The overlap matrix is then "replica symmetric".

Having just one possible value of overlap precludes the existence of more than one state. (A spin reversed state must also of course exist and the overlap between the two states in then $-q_0$. We consider here only positive values of the overlap.) If α and β are two states, then two configurations $\{\sigma^{a_1}\}$ and $\{\sigma^{a_2}\}$ belonging to α are more similar than two configurations $\{\sigma^a\}$ and $\{\sigma^b\}$ respectively from α and β. The thermally averaged overlap must therefore take two values: $\langle Q_{a_1a_2}\rangle = q_1$ and $\langle Q_{ab}\rangle = q_0$, with $q_1 > q_0$. The probability distribution has two δ-peaks, $\overline{P(q)} = m_1\delta(q-q_1) + (1-m_1)\,\delta(q-q_0)$ (with m_1 the probability of being in the same state), and characterizes a "first step of replica symmetry breaking" (1-RSB) of the overlap matrix. As $n\to 0$ is necessary to recover the correct physics, one also takes the limit $m_1\to 0$.

The overlap matrix for r steps of replica symmetry breaking can be constructed following the scheme represented on figure 1.9. For the p-spin model described above, only one step of replica-symmetry breaking is needed (when $p\geq 3$). We will see that for the mean-field Ising spin-glass case (see section 1.2.3) the phase transition is described in terms of a matrix where the symmetry between replicas has been fully broken (full-RSB), meaning that the number of steps goes to infinity $r\to\infty$. [16]

The order parameter, which is zero in the disordered (paramagnetic) phase and nonzero in the ordered (spin-glass) phase, is a single parameter, say q_0, akin to the Edwards-Anderson [59] parameter $q^{EA} = N^{-1}\sum_{i=1}^{N}\overline{\langle\sigma_i\rangle}^2$, when the system remains replica symmetric but becomes a full function in the full-RSB case [12].

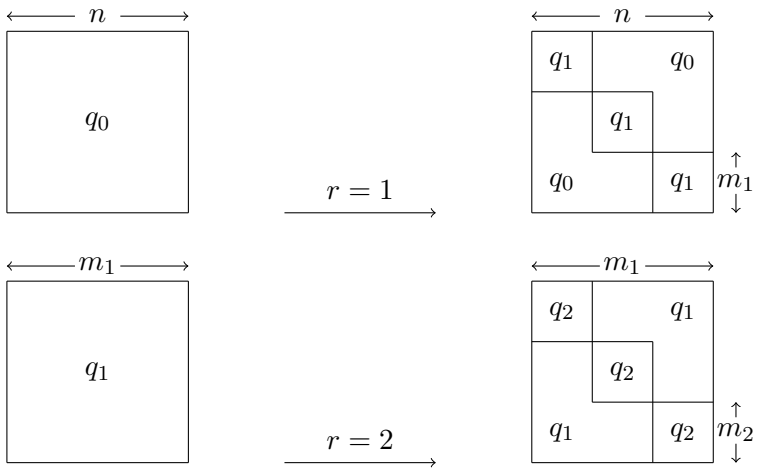

Figure 1.9: Construction of the overlap matrix for $r = 1$ and $r = 2$ steps of replica symmetry breaking, with $n > m_1 > m_2 > ... > m_\infty \geq 0$. One can iterate it r times to reach any step r of replica symmetry breaking. When $r = \infty$, the full Parisi replica symmetry breaking overlap matrix, order parameter of the Ising spin glass transition in the mean-field theory, is obtained. On the diagonal, the elements are $Q_{aa} = 1$.

1.1.3.3 Glass-forming liquids in infinite spatial dimension

The RFOT scenario occurring in mean-field p-spin and Potts-glass models has also been found in several liquid models when treated within mean-field-like approximations. [47, 60, 61, 62] More importantly, the RFOT scenario has recently been shown to occur exactly for the glass formation and the glass phase of liquids in infinite spatial dimensions [21, 22, 63, 64]: this definitely confirms the RFOT 2-temperature scenario as the mean-field theory of glass-forming liquids.

Some tools from spin-glass theory [6], such as the replica method and generating functional approaches, have been developed to study the mean-field version of supercooled liquids models. [65, 66, 17] This requires to work with the density functional $F[\{\rho(r)\}]$ which is written as an integral over the volume of the system of functions of the whole density field $\rho(r)$. It contains all information on the positions of the particles in the system, but is potentially highly complex. The configurational space has $3N$ dimensions, with N the number of particles (atoms), which makes any free-energy landscape hard to visualize. On figure 2 we pictured an overly schematic view of $F[\{\rho(r)\}]$ as a function of $\rho(r)$.

1.1.3.4 Franz-Parisi potential

However, instead of working with the free-energy functional, one can construct a reduced free energy which already contains interesting information. In the context of the mean-field theory of glasses, the order parameter of the glass transition is the overlap of a configuration a with a reference configuration r. [1] The probability distribution function of the overlap between a and r is naturally associated to a large deviation function, the Franz-Parisi potential $V(q)$ [67]. It measures the free-energy cost to maintain a configuration with a fixed average overlap q with a reference one r and is illustrated in figure 1.10. (Note that figure 1.10 corresponds to a mean-field description in which the potential is nonconvex.)

The knowledge of which minima are likely to be visited by the system among the exponentially large number of potential ones (below some temperature) is reduced to the knowledge of the minima

[1] This description has transformed the self-induced disorder of supercooled liquids into a quenched one, represented by the fixed reference configuration.

of $V(q)$.

When $T > T_d$, $V(q)$ has a unique minimum and the corresponding phase is symmetric, with an order parameter $q^{EA} = 0$. At $T = T_d$, $V(q)$ develops a spinodal at some positive value of q. When $T < T_d$, $V(q)$ has a secondary minimum. The equilibrium order parameter is always $q^{EA} = 0$ as all the available configurations are statistically equally accessible. At $T = T_K$ the secondary local minimum of $V(q)$ becomes stable and the order parameter jumps discontinuously to $q^{EA} \neq 0$.

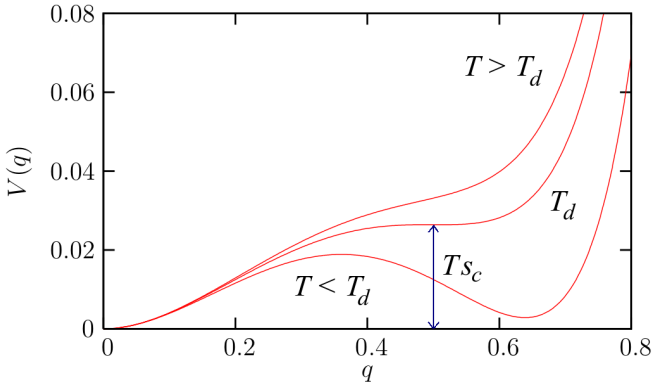

Figure 1.10: Franz-Parisi potential $V(q)$ as a function of the average overlap q between a system configuration and an equilibrium reference one for different temperatures. Reprinted and adapted from [3].

The height difference between the global minimum and the metastable minimum gives access to the configurational entropy (density) $s_c(T)$. Indeed maintaining the system in the metastable minimum between T_d and T_K yields an entropic cost of $T\, s_c(T)$ coming from the non-exploration of the other metastable states. The shape of $V(q)$ also illustrates the first-order character of the glass transition, as the order parameter appears discontinuously at T_K.

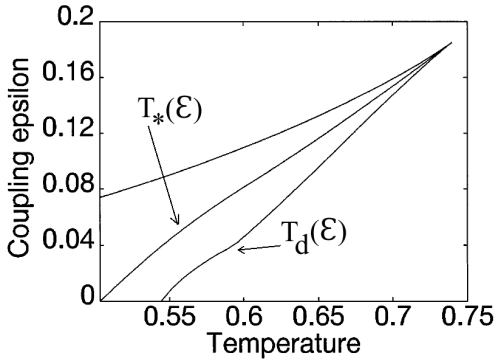

Figure 1.11: Phase diagram in temperature-coupling phase space, separating a high-temperature low-overlap phase from a low-temperature high-overlap phase for the mean-field p-spin model with $p = 4$. There are three curves, the rightmost is the spinodal of the metastable state which touches $\varepsilon = 0$ at T_d; the middle one is the first-order transition line reaching $\varepsilon = 0$ at $T_K > 0$; the leftmost is the spinodal of the $q \simeq 0$ minimum. The three curves match at a terminal critical point. Reprinted from [68].

From the shape of $V(q)$, one also concludes that a first-order transition from low- to high-overlap phases must exist when an external field ε linearly coupled to the overlap is turned on between T_d and T_K. [68, 69] Such a line of transitions is potentially interesting because they occur at higher temperatures than that at T_K in $\varepsilon = 0$ and could therefore be easier to detect. The free energy $F(\varepsilon)$ of the system

is obtained *via* a Legendre transform

$$V(q) = F(\varepsilon) + q\,\varepsilon \quad \text{with} \quad q = -\frac{\partial F(\varepsilon)}{\partial \varepsilon}\,, \tag{1.19}$$

and corresponds to a tilted $V(q)$. If $\varepsilon > 0$, the high-q minimum of $V(q)$ is favored and will appear upon lowering the temperature at $T_d(\varepsilon) > T_d(0) = T_d$. The first-order transition will occur at $T_\star(\varepsilon) > T_K$, hence creating a line between low- and high-q phases in the T-ε plane. The line of first-order transition ends in a critical point at some value ε_c and $T_c = T_\star(\varepsilon_c)$ (see figure 1.11).

1.1.4 Beyond the mean-field theory

The question is to know whether the mean-field theory of glasses presented above is the correct effective theory to describe supercooled liquids in finite dimensions or not, *i.e.*, remains robust to the introduction of fluctuations. Either the thermodynamic glass transition at $T_K > 0$ persists or disappears, one has to find the fluctuation mechanisms responsible for the relaxation of finite-dimensional systems below T_d and above T_K.

1.1.4.1 Phenomenological arguments

Assuming that the mean-field theory of glasses is qualitatively correct in finite-dimensional systems, the fluctuations can be tentatively accounted for through phenomenological arguments of nucleation and the "mosaic scenario". [7]

Nucleation destroys metastable states in finite dimensions

In the above mean-field description the properties of the system were computed as if it was characterized by a collection of metastable states with infinite lifetime.

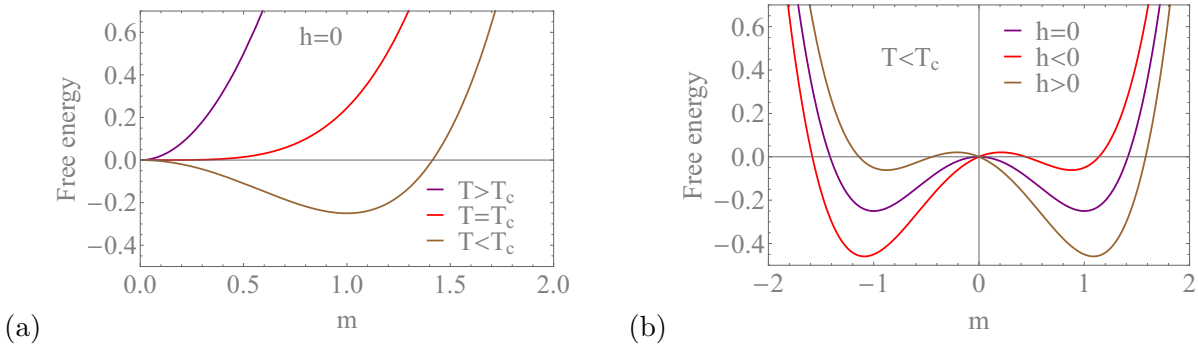

Figure 1.12: Free-energy of the Curie-Weiss model as a function of the magnetization m. (a) For three values of the temperature, $T > T_c$, $T = T_c$ and $T < T_c$. (b) $T < T_c$, for three values of the external field $h > 0$, $h = 0$ and $h < 0$. For $h \neq 0$, a metastable state appear in the free-energy.

Metastable states are present within the Ginzburg-Landau description of the fully connected Ising model (Curie-Weiss model) in an external field, when looking at the free energy as a function of the magnetization m, near the phase transition, see figure 1.12. Below a certain temperature it presents two minima with different extensive free energies. The free energy is therefore *nonconvex*. The barrier between minima is extensive and the system in the thermodynamic limit will remain an infinite time in the metastable minimum even if it is not the one of lowest free energy.

In a finite-dimensional system, nonuniform configurations are relevant and the free energy does not retain the nonconvex shape. A fluctuation of the order parameter when the system is in a metastable

state takes the form of a nucleation bubble. [70, 28] Consider for instance the d-dimensional Ising model below T_c in the presence of an external positive magnetic field h. In this case the stable state has a positive magnetization and the metastable state of the mean-field description has a negative magnetization (see figure 1.12 (b)).

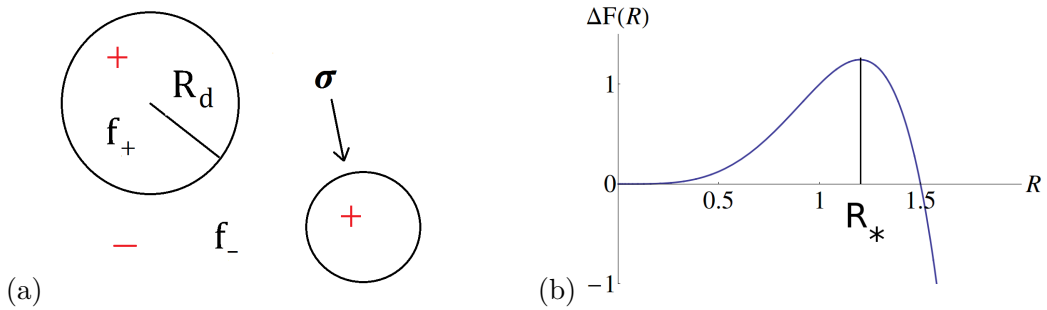

Figure 1.13: (a) Nucleation region for the Ising model for $h > 0$ in 2 dimensions. The two phases of different magnetization + (stable) and − (metastable) coexist and have respective energy f_+ and f_-; σ is the surface tension. (b) The nucleation bubble of radius R_d relaxes in the outer phase if it is larger than a critical value $R_\star$ depending on the different energies, found as the radius where ΔF is maximal.

Imagine we insert a bubble of radius R of the stable phase within the metastable phase, as represented in figure 1.13 (a). It exists a typical radius $R_\star$ below which the free-energy cost to maintain the bubble within the metastable phase is positive and the bubble therefore shrinks and disappears. Above this radius, the nucleation bubble is free-energetically favorable and grows without bound such that the metastable state disappears. The free-energy cost of the bubble is $\Delta F(R) = \sigma R^{d-1} - \Delta f R^d$, whose typical shape is plotted in figure 1.13 (b). The first term is the free-energy cost associated with the creation of an interface, with σ the surface tension between the metastable and the stable phases. The second term is the difference of the bulk free-energy density between the metastable and stable phases, $\Delta f > 0$. $R_\star$ is defined as the location of the maximum of $\Delta F(R)$.

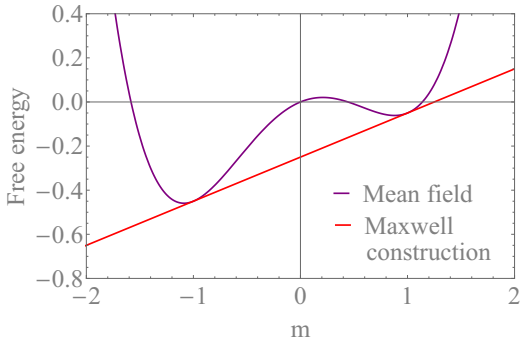

Figure 1.14: Free-energy of the Curie-Weiss model as a function of the magnetization m for $T < T_c$ and $h < 0$. The free energy is nonconvex in mean field (purple line), and performing a Maxwell construction (red line) allows one to recover the needed convexity property of the free energy for finite-dimensional systems.

The above phenomenological approach justifies that the escape of the system from a metastable state to reach the stable state is described by the nucleation (and further growth) of a droplet: this leads to activated dynamics. As a result, finite-dimensional systems always present a convex free energy, which one can approximate from the mean-field result by the Maxwell construction (see figure 1.14).

This convexity implies that metastability disappears. The system in the thermodynamic limit is either in the global minimum of the free energy when the latter is unique or in one of the two pure states if there is a phase transition and a coexistence curve. However, systems smaller than the typical length scale of the relevant fluctuations will essentially behave as systems "without" fluctuations for which the mean-field approximation is well suited.

"Mosaic" scenario for glass-forming liquids in finite dimensions

Schematically, the mosaic picture states that a finite-dimensional supercooled liquid in the regime $T_K < T < T_d$ is composed of finite domains of linear size ξ in different states corresponding to minima of the complex free-energy landscape, with equal free-energy densities. This requires the existence of interfaces, whose energetic cost is proportional to a surface tension Y. In supercooled liquids the interface between different states can be very rough with effective dimension $\theta \leq d-1$. Thus, a nucleus of linear size R has an interface free-energy cost of $\Delta F_{int} = Y R^{\theta}$.

For the Curie-Weiss model the balancing term was the free-energy density difference $\Delta f > 0$. Here free-energy densities of all states are the same. However, localizing the system in one state among the exponentially large number has an entropic cost, the competing term is thus $\Delta F_{ent} = T\, s_c(T)\, R^d$. The free energy of a droplet of size R is then

$$\Delta F(R) = Y R^{\theta} - T s_c(T) R^d \,. \tag{1.20}$$

This can be associated to a length scale, the mosaic length, found by setting equation (1.20) to zero:

$$\xi \propto \left(\frac{Y(T)}{T s_c(T)} \right)^{\frac{1}{d-\theta}} . \tag{1.21}$$

The mosaic length captures the emergence of a cooperative behavior. Indeed, it is inversely proportional to the configurational entropy (density) $s_c(T)$. As the latter decreases with T below T_d, it leads to an increase of ξ that finally diverges at T_K as $s_c(T_K) = 0$. (The critical nucleus obtained as the maximum of $\Delta F(R)$ scales in the same manner.)

It has been argued that the mosaic length scale is directly connected to a "point-to-set" correlation length ξ_{PTS}. [71] This has given support to the mosaic scenario, as the point-to-set length can be computed in long-range-interaction models (Kac models, see below) [72] and in computer simulations [73, 74, 75]: it gives the spatial extent over which the effect of equilibrium amorphous boundary condition propagates, see figure 1.15.

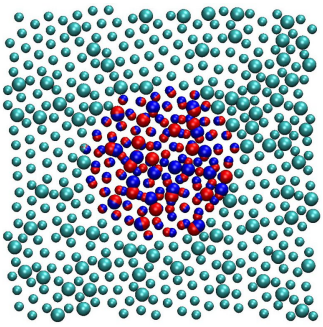

Figure 1.15: Point-to-set length scale from [76].

Starting with an equilibrium configuration of the system, a cavity of radius R is created outside which the particles are frozen. The particles inside the cavity can rearrange, and the system evolves with this constraint, the outer particles acting as a pinning field. The point-to-set length scale is defined

as the minimal cavity radius such that the similarity between the new and the initial configurations goes to zero at the center. Metastability and a mean-field like description then have some physical meaning on linear scales smaller than ξ_{PTS} *only*.

The point-to-set length also yields an upper bound for the relaxation time $\tau < e^{c\,\xi^d_{PTS}/T}$ (c a constant) [36, 77] which predicts that a diverging relaxation time implies a diverging length scale. The relaxation time is expected to be given by an Arrhenius-like law, $\tau = \tau_0 \exp\left[\Delta E(T)/(k_B T)\right]$, with the barrier $\Delta E(T)$ growing with ξ with another critical exponent ψ,

$$\Delta E(T) \sim \Delta_0\, \xi^{\psi}\,. \tag{1.22}$$

Replacing the T-dependent barrier $\Delta E(T)$ by its expression in equation (1.22) and the configurational entropy (density) by $s_c \underset{T\to T_K}{\sim} (T - T_K)$, one obtains a relaxation time τ which would diverge at T_K as

$$\tau \sim \exp\left[\left(\frac{Y(T)}{T - T_K}\right)^{\frac{\psi}{d-\theta}}\right]. \tag{1.23}$$

The above expression of τ is similar to the phenomenological VFT law given in equation (1.1) when $T_0 \simeq T_k$ and is equal to it when $\theta = d/2$ and $\psi = \theta$ as argued in [7].

1.1.4.2 Fluctuations beyond mean field: a review of past and ongoing work

One would like to study through first-principle methods the influence of spatial fluctuations in finite dimensions on the mean-field description of the glass transition. For instance, one knows that by definition (a Legendre transform) the equilibrium free energy of the finite-dimensional system has to be convex. One would thus like to find statistically relevant fluctuation mechanisms by which metastability and nonconvexity of the free energy that are central in the mean-field treatment disappear in finite dimensions.

Yet, at the mean-field level, the nature of metastability and of the metastable states of the density functional $F[\{\rho(x)\}]$ is quite elusive [71, 78, 79] and the effective or coarse-grained landscape of minima and saddle-points is expected to be very complex, with a number of minima that is exponentially large in the system size. Finding the mechanism by which fluctuations alter this mean-field free-energy landscape, *e.g.*, via some form of nucleation events, is therefore a very challenging task.

Several steps have been recently achieved in investigating the role of fluctuations beyond the mean-field theory of glasses:

- "Instanton" calculations have been performed on the effective Franz-Parisi potential of the replicated theory and give an estimation of the surface tension of some droplet. [80, 78, 79]

- Kac models have been studied: these models have long-range interactions and, depending on the order in which one takes the thermodynamic limit and the limit where the range of interactions goes to infinity, they are exactly described either by the conventional mean-field results (where the free energy can be nonconvex) or by an improved version in which nonuniform configurations are allowed and convexity of the free energy is recovered. Kac models have been used to provide an analytic determination of the mosaic length scale [72]. Instanton calculations also allowed the determination of a "glassy coherent length" [78], argued to lead to a relaxation time [81] that would be in agreement with the phenomenological mosaic scenario.

- Real-space Migdal-Kadanoff renormalization group methods applied on spin-glass models supposed to be in the same universality class as finite-dimensional structural glasses (which is exact in $d = \infty$) have found that in large but finite dimensions the glass transition could be controlled by a nontrivial zero-temperature fixed point. [82, 83]

- The dynamics of the finite-dimensional glass-formers near T_d, known to be a dynamical crossover (from experiments), has been thoroughly investigated. Using MCT equations that can be written to study the dynamics of glass-forming models near T_d [84, 85], analytical computations of the effect of long-range fluctuations (added perturbatively) on this dynamical transition have been performed. [86, 87, 88, 89] This yields an avoided dynamical transition in finite-dimensional systems. Dynamical heterogeneities and activated dynamics then also naturally emerge.

- A mapping of supercooled liquids in finite dimensions onto Ising-like systems with disorder is also suggested.

It has been shown that the critical fluctuations of the overlap close to the dynamical transition are in the same universality class as the spinodal point of the random-field Ising model (RFIM) [2]. [95] If one thinks of the liquid below T_d as formed of finite-size domains in which a local Franz-Parisi potential can be defined, the local (domain) configurational entropy would play the role of an applied random field and the local (domain) overlap that of the local magnetization. [95, 96]

Then, when an external field ε is applied, glassy systems presenting a RFOT in mean-field develop a first-order transition line in the $T - \varepsilon$ plane (see section 1.1.3.4). Such line has been detected in computer simulation of finite-dimensional systems. [97, 98, 99, 100] Studies have predicted that its terminal critical point (in T_c, $\varepsilon_c > 0$) is in the universality class of the RFIM. [101, 102] A glass transition line can also be obtained in the $T - c$ plane when "pinning" a certain fraction c of particles in the system. It is predicted on the basis of mean-field glassy models [103] and claimed to be observed in simulations of finite-dimensional liquid models [104]. It was established [105] that fluctuations close to the critical endpoint can also be mapped onto the RFIM, in agreement with other results. [103, 106]

Additional suggestions of mapping of supercooled liquids in finite dimensions onto Ising-like systems with disorder has also appeared in various numerical computer simulations [107, 98, 99, 100]. The same conclusion has been obtained in computer simulations of finite-dimensional glassy plaquette models in an external field [108, 109].

- Another mapping has been proposed in [110] where it is argued that the effective theory for the glass transition is in the universality class of an Ising spin glass in a field. This would invalidate the possibility of a nonzero temperature glass transition in finite-dimensional systems, similarly to the absence of a de Almeida-Thouless line for Ising spin glasses in finite dimensions argued by the authors (see also section 1.2.3). A real-space RG treatment has been performed in support of this idea. [111]

1.1.5 A diversity of theoretical approaches

Explaining the glass transition and the slowing down of relaxation that leads to it remain an open and controversial issue. The established existence of a mean-field theory does not preclude alternative theories focusing directly on 3-dimensional glass-forming systems with no reference to this mean-field scenario. As stressed above, spatial fluctuations can be for glass formation in $d = 3$ and one may as well try to postulate the nature and the effect of these fluctuations based on physical intuition. Among the many attempts, one could notice those based on the existence of some locally-preferred order and its

[2] The RFIM is a paradigmatic model showing a competition between ferromagnetic interactions and quenched disorder. [90, 91, 92, 93, 94]. Its Hamiltonian (in its simplest form) is like the simple Ising one, but with random fields h_i (following some probability distribution that can be Gaussian) applied on each sites i of the lattice: $H[\{\sigma_i\}] = -J\sum_{\langle i,j\rangle}\sigma_i\sigma_j - \sum_{i=1}^{N} h_i\sigma_i$, where $\sigma_i = \pm 1$ are Ising spins, and $\sum_{\langle i,j\rangle}$ is over nearest neighbors. From the mean-field infinite-range treatment, if disorder strength $\overline{h_i^2}$ is too strong compared to the ferromagnetic coupling, the system is paramagnetic at all temperatures. If it is smaller than some critical value, the system can present a phase transition at some temperature between a high-temperature paramagnetic phase and a low-temperature ferromagnetic one. This mean-field description is qualitatively correct above the upper critical dimension which is $d_u = 6$ [90].

possible frustration at large distance [8, 112] or, in a quite well different vein, those relying on a purely dynamical description in terms of mobility defects and dynamical facilitation [113]. In the following, we will only discuss the latter because we will come back to it again in chapter 4.

1.1.5.1 Dynamic facilitation

In the Dynamical Facilitation Theory (DFT) [11], it is postulated that the physics of glass-forming liquids can be understood purely at the dynamical level, with no need for any thermodynamic or landscape description.

Dynamic facilitation is the fact that a mobile region, called mobility defect, prompts the mobility of others nearby regions, generating highly rearranging domains and dynamical heterogeneities. [113] The rest of the system is essentially frozen. Hence relaxation comes with cooperative moves in real space, which become harder and harder the more the temperature decreases. Therefore glassiness is the consequence of effective dynamical constraints in the motion of particles when the temperature is lowered, irrespective of the thermodynamics of the system. [114]

Kinetically constrained models

DFT is realized in simple models with trivial thermodynamics but with dynamical rules enforcing kinetic constraints. Examples are the Fredrickson-Andersen model [115] and the East model [116].

The Fredrickson-Andersen model is a lattice-gas model of particles that can be either mobile $n_i = 1$ or immobile $n_i = 0$. Its Hamiltonian is given by:

$$H(\{n_i\}) = J \sum_{i=1}^{N} n_i. \tag{1.24}$$

The constant J is the energy scale arising from the production of a mobility defect $n_i = 1$ on site i. The thermodynamics of the model is therefore trivial and has no singularity at nonzero temperature. The dynamics however is nontrivial due to the introduction of a kinetic constraint: a variable is allowed to change state at a given site if and only if a minimum number of its nearest neighbors are empty. On can also define models with some asymmetry in the dynamical constraint, as the East model [11]. The relaxation time is generally found to diverge at zero temperature only, either in an Arrhenius-type of behavior for "noncooperative" models or in a super-Arrhenius way for "cooperative" models [11]. Dynamical facilitation and properly chosen KCM's are able to reproduce the salient features of the dynamics of supercooled liquids [117]. However, there remains some arbitrariness in the choice of the proper KCM and an instability to describe thermodynamical features of real glass-formers such as the rapid decrease of the entropy.

Plaquette spin models

In these lattice spin models the local interactions involve spins belonging to plaquettes. Different plaquette models have been studied in the literature, which are characterized by the number p of spins around an elementary plaquette, the number c of plaquettes attached to a given site, and more generally by the lattice type. When $p = c$, their dynamics on Euclidean lattices can be fully described by localized defects and the dynamic-facilitation theory. [118, 119, 114, 27]

For example the Hamiltonian of the square-plaquette model on a square lattice ($c = p = 4$) is given by

$$H[\{\sigma_i\}] = -J \sum_{\mu} \sigma_{\mu 1}\sigma_{\mu 2}\sigma_{\mu 3}\sigma_{\mu 4}, \tag{1.25}$$

where μ labels the square plaquettes, $\sigma_{\mu i} = \pm 1$ the four Ising spins composing μ, and $J > 0$ is the energy coupling strength. If the spin variables are changed into plaquettes variables $\sigma_{\mu 1}\sigma_{\mu 2}\sigma_{\mu 3}\sigma_{\mu 4} \rightarrow$

S_μ, the above Hamiltonian becomes that of a noninteracting model of variables $S_\mu = \pm 1$ and its thermodynamics is therefore trivial. Its dynamics however is not simple, as a simple spin flip changes the state of all the plaquettes to which it belongs to. It has been shown that the dynamics of this model can be studied by looking at the -1 plaquettes only, which play the role of mobility defects as they favor the -1 transformation of the surrounding plaquettes variables, and can be described as resulting from effective kinetic constraints. These models are thus akin to KCM's. [114].

When the number of spins per plaquette is even, such as the square-plaquette model or the cubic plaquette model on a cubic lattice ($c = p = 8$), the model is characterized by a relaxation time that follows an Arrhenius law, like strong glass formers. [120, 121, 27, 122, 123]

Models with an odd number of spins per plaquette have also been studied on 2-dimensional and 3-dimensional Euclidean lattices. In the triangular-plaquette model, the ferromagnetic interactions involve the 3 spins of each upward-pointing triangle in a triangular lattice ($c = p = 3$) and in the square-pyramid model they involve the 5 spins of each upward-pointing square-based pyramid on a body-centered cubic lattice ($c = p = 5$). They represent "fragile" glass-formers, for which the relaxation time τ grows with decreasing temperature T in a super-Arrhenius manner with $\log \tau \propto 1/T^2$. [119, 114, 27] These models have been extensively investigated in relation to the theory of glass formation, more specifically for their connection to simple glass-forming models with kinetic constraints, see [27] for a review.

The main advantage of these models is their dual nature: they appear as KCM's and good models for the DFT at the defect (plaquette) level (when $c = p$), yet represent *bona fide* models with nontrivial thermodynamics and local, unconstrained, dynamics at the spin level. In consequence they provide a framework to understand the possible connection between theories of the glass transition, based whether on a nontrivial dynamics (DFT) or on a nontrivial thermodynamics (mean-field theory of glasses). We will consider them in chapter 4.

1.2 Spin glasses

1.2.1 Phenomenology

The magnetic moments that compose spin glass materials are submitted to random ferromagnetic and antiferromagnetic interactions due to frozen-in structural disorder in the system. Indeed, the scattering of the conduction electrons leads to indirect interactions between spins that oscillate strongly with the distance. Therefore, as distance between spins is random, some interactions will be positive, favoring ferromagnetic alignment, others will be negative, favoring anti-ferromagnetic alignment. The spins are in the impossibility to find an alignment that satisfies all the interactions: this phenomenon is called frustration [124] (see figure 1 were it is sketched for four Ising spins). As a consequence and as represented on figure 1.16, no conventional long range order can be established, with all spins pointing in the same direction (ferromagnetic order), or in alternate directions (antiferromagnetic order).

Nevertheless, at some critical temperature T_c, the system presents a second-order phase transition [126] toward a phase with a new kind of order: with spins $\vec{\sigma}_i$ pointing in random but well defined directions, such that the magnetization is zero $N^{-1}\sum_{i=1}^{N}\langle\vec{\sigma}_i\rangle = 0$ but $N^{-1}\sum_{i=1}^{N}\langle\vec{\sigma}_i\rangle^2$ is different from zero, where the brackets denote a thermal average. This phase has been called the spin-glass phase, and its nature is still not understood (see below). Experimentally and from computer simulations one can approach the critical point from the high temperature side only, as the relaxation time is infinite in the spin-glass phase. The system then falls out of equilibrium and displays aging behavior. [127] It seems that the combination of randomness and frustration is the source of this new kind of phase transition.

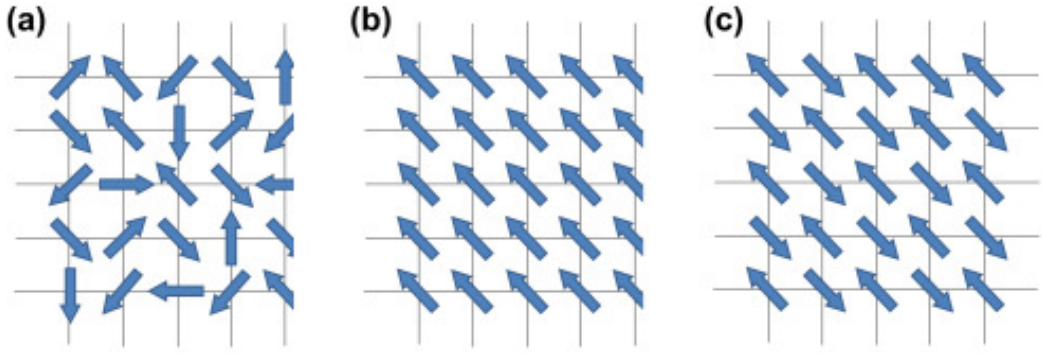

Figure 1.16: Pictorial comparison between different orders on a two-dimensional discrete lattice: (a) spin glass, (b) ferromagnetic and (c) antiferromagnetic. Reprinted from [125].

1.2.2 Edwards-Anderson model

The first effective model of spin glasses was introduced by Edwards and Anderson (EA) in [59]. They proposed the following effective spin-glass Hamiltonian, in the case of Ising spins $\sigma_i = \pm 1$,

$$H = -\sum_{\langle i,j \rangle} J_{ij}\sigma_i\sigma_j - h\sum_i \sigma_i \,, \tag{1.26}$$

where the sum $\langle i,j \rangle$ runs over all distinct nearest neighbors sites of a lattice of N sites, and h is an external magnetic field that will often be set to zero in the following. The J_{ij} are finite-range random interactions that can be ferromagnetic or antiferromagnetic and mimic the oscillating interactions of experimental spin glasses. They follow some probability distribution $P(J_{ij})$, that can be chosen as Gaussian with zero mean, $\overline{J} = 0$, where the overline denotes an average over the quenched disorder. The different observables are computed for fixed configurations of the quenched disorder, over which an average is finally performed.

Edwards and Anderson argued that this model should present a spin-glass phase transition at a critical temperature T_c, with a paramagnetic high-temperature phase and a spin-glass low-temperature phase. The order parameter of this transition, since called Edwards-Anderson parameter (see also section 1.1.3.1), is the "overlap" between spin configurations averaged over disorder,

$$q^{EA} = \frac{1}{N}\sum_{i=1}^{N} \overline{\langle \sigma_i \rangle^2} \,, \tag{1.27}$$

where $\langle \, . \, \rangle$ is a thermal average for a fixed configuration of the disorder. q^{EA} is zero above T_c and grows continuously for $T \leq T_c$, showing that the transition is second order.

The phase transition in the EA Ising spin glass was put in evidence in computer simulations in dimension $d = 3$ in [128, 129] and with renormalization calculations in [130]. It is also now confirmed by large scale computer simulations. [131, 132] Several studies [133, 134, 135, 136, 137] have been devoted to the determination of the lower critical dimension d_l, defined as the dimension at which the transition disappears. They agree on a value of the lower critical dimension between 2 and 3 (possibly $d_l \simeq 2.5$).

1.2.3 Mean-field theory

Sherrington and Kirkpatrick (SK) studied the Hamiltonian (1.26) in the fully-connected version where the J_{ij} are of infinite range, [15] showing the existence of a mean-field spin-glass transition at a tem-

perature T_c from a paramagnetic phase to a mean-field spin-glass phase. See [5, 138] for reviews where the mean-field theory of spin glasses is developed.

The free energy (averaged over the quenched disorder) of the system, $F = -\beta^{-1}\overline{\log Z}$, can be formally computed by use of the replica trick (see section 1.1.3.2). This generates n replicas of the system with a $n \to 0$ limit to evaluate in order to recover the initial physical situation. One can rewrite the partition function in terms of an overlap between replicas a and b, $Q_{ab} \equiv N^{-1}\sum_{i=1}^{N}\sigma_i^a\sigma_i^b$ (i is the lattice position). The Edwards-Anderson parameter is directly linked to this quantity as

$$q^{EA} = \lim_{n\to 0}\frac{1}{n(n-1)}\sum_{a\neq b}\langle Q_{ab}\rangle \ . \tag{1.28}$$

The high-T and low-T phases are studied by finding the singularities of the free energy in the framework of the replica method. Sherrington and Kirkpatrick considered a replica symmetric (RS) solution with $Q_{ab} = Q$ when $a \neq b$. The EA parameter in this case is just $q^{EA} = \langle Q\rangle$. Under this hypothesis, they found two solutions: $q^{EA} = 0$, supposed to correspond to the high-temperature phase, and $q^{EA} \neq 0$, supposed to describe the low-temperature (spin-glass) phase. They also computed the critical exponents of this second-order transition. This yielded the upper critical dimension as the dimension for which the scaling relation $2\beta + \gamma = d_u\nu$ is verified for the mean-field critical exponents, hence $d_u = 6$ for the spin-glass universality class. [3]

The stability of a phase is determined by computing the curvature(s) (called "masses" in field theory) at the corresponding extremum of free energy. If there are many directions, as in the case of a replicated theory, the curvatures in all directions are obtained from a $\frac{n(n-1)}{2}\times\frac{n(n-1)}{2}$ matrix of second derivatives of the free energy (called Hessian matrix) with respect to the fields $\delta Q_{ab}\delta Q_{cd}$ (with $a < b$, $c < d$). Its eigenvalues give access to the stability of the solution along the corresponding eigendirection. A positive eigenvalue corresponds to a stable eigendirection, along which if the system is perturbed it will end in the same state; the contrary happens for a negative eigenvalue, and any fluctuation occurring in the corresponding eigendirection will make the system escape from its state. A zero eigenvalue is related to a eigendirection said "marginal", and generically one has to compute the third order derivative of the free energy evaluated at the extremum to determine the stability.

The first solution, $q^{EA} = 0$, yields a diagonal Hessian matrix. Its eigenvalues λ_1 are all degenerate and are given by, when $n = 0$,

$$\lambda_1 = 2\,\frac{T - T_c}{T_c}\,. \tag{1.29}$$

The paramagnetic state, $q^{EA} = 0$, is stable for temperatures $T > T_c$ as $\lambda_1 > 0$. The properties of the high-temperature phase are therefore well described by a replica symmetric order parameter. As expected in phase transitions, this phase becomes marginally stable at $T = T_c$ ($\lambda_1 = 0$) and is completely unstable for $T < T_c$ ($\lambda_1 < 0$). To correct this the system usually has to break a symmetry, acquiring a nonzero order parameter so that the eigenvalues become non-negative.

Such a symmetry breaking corresponds to the other, nontrivial, solution with $q^{EA} \neq 0$. It should describe the low-temperature phase. It is usually expected to be stable for $T < T_c$. This yields a symmetric stability matrix that can be diagonalized [140]: it has three distinct n-dependent eigenvalues, two of them being degenerate when $n = 0$. The related three eigendirections and their respective n-dimensions are the replicon "R" ($\frac{n(n-3)}{2}$), the anomalous "A" ($n-1$) and longitudinal "L" (1) ones.

[3] For the mean-field spin-glass transition they are given by $\beta = 1$, $\gamma = 1$ and $\nu = 1/2$ hence $d_u = 6$. [139]

When $n = 0$, the eigenvalues are given by (A and L are degenerate)

$$\begin{aligned} \lambda_{A,L} &= 2\,\frac{T_c - T}{T_c}, \\ \lambda_R &= -\frac{4}{3}\left(\frac{T_c - T}{T_c}\right)^2. \end{aligned} \tag{1.30}$$

One immediately sees for $T < T_c$ that this solution, $q^{EA} \neq 0$, is stable along the anomalous and longitudinal eigendirections ($\lambda_{A,L} > 0$), but unstable along the replicon one ($\lambda_R < 0$). The replica-symmetric solution cannot therefore be the right description of the low-temperature phase for $T < T_c$.

The correct description of the mean-field Sherrington-Kirkpatrick model for the low-temperature phase was obtained by Parisi [16, 12, 55, 56, 57, 58]. It involves an additional symmetry breaking, namely the breaking of the replica symmetry when computing the relevant saddle-point in the mean-field treatment. The replica symmetry is continuously broken and involves an infinite number of stages ($r \to \infty$ in section 1.1.3.2) that leads to an overlap order parameter which is now a whole function. The physical interpretation of this solution is that the low-temperature phase is characterized by an infinite number of pure states (which generalizes the two pure states found in a simple ferromagnetic model) with an ultrametric organization [23]. By studying the stability of this solution, it has been shown that it is stable, albeit marginally stable, in all directions. [141]

1.2.4 Beyond the mean-field theory

For spin glasses, it has been shown that the mean-field approximation is quantitatively correct in infinite-dimensions. [18, 19, 20] Fluctuations of field, that are by definition absent in mean field, are present in finite dimensions and may modify the scenario for finite-dimensional systems. In the case of spin glasses, is the nature of the low-temperature phase the same as predicted in the mean field, as it occurs in the Ising model, for example? The situation is not clear and is still today not settled. One should however distinguish what happens for the (critical) transition itself and for the low-temperature spin-glass phase.

For the former, the conventional scenario appears to apply: the spatial fluctuations present in finite-dimensional systems modify the mean-field critical exponents only below an upper-critical dimension $d_u = 6$ and do not change the qualitative features of the critical point and of the associated scaling behavior above a lower critical dimension d_l between 2 and 3. The critical exponents have been computed in a perturbative renormalization group treatment in $d = 6 - \varepsilon$, $\varepsilon > 0$. [139]

Quite different is the issue of the nature of the low-temperature phase. As it has been briefly discussed above, the mean-field theory predicts an intricate spin-glass ordered phase characterized by an infinite number of pure states and obtained through a spontaneous breaking of the replica symmetry when $n \to 0$. How fluctuations alter this phase is still contentious as no successful renormalization group treatment has been developed, at least below the putative upper critical dimension $d_u = 6$ [141].

An alternative theoretical framework formulated directly in low dimensions focuses on fluctuations associated with low-energy "droplet" excitations and predicts a low-temperature phase with only a finite number of pure states (see below).

1.2.5 Droplet theory

A quite different theoretical approach is the droplet theory, independently developed by Bray and Moore [13, 142, 143] and Fisher and Huse [14, 144, 145]. This approach directly focuses on the spin-glass phase in finite dimensions and on the role of spatial fluctuations. The number of pure states is

assumed to be finite, essentially two as in ferromagnets, and the criticality of the low-temperature phase is explained by the presence of large-scale excitations described as droplets. This approach is motivated by real-space renormalization studies on "domain walls" [146, 134, 130]. These studies predict that the lower-critical dimension for the existence of the spin-glass phase is between 2 and 3: $2 < d_l < 3$.

A key difference in the predictions of the mean-field and droplet theories is that in the presence of a uniform (or random) applied field, there is no transition in the droplet theory whereas there is still a finite-temperature transition with replica-symmetry breaking in the mean-field description.

Chapter 2

Theoretical tools

Contents

2.1 Method of instantons

In classical statistical mechanics, the partition function is the quantity one needs to compute in order to extract the thermodynamic characteristics of a system at equilibrium. It is given by the expression

$$Z(\beta) = \sum_{\{\sigma\}} e^{-\beta H(\{\sigma\})}\,, \tag{2.1}$$

where $\beta = 1/(k_B T)$, $\{\sigma\}$ represents all the possible configurations of the system and $H(\{\sigma\})$ is the Hamiltonian. Using Feynman path integral formalism and taking the continuum limit, one can go from classical statistical mechanics to statistical field theory. The field $\varphi(x)$ is a function of space. The partition function is rewritten under the form of an integral over all the paths $\varphi(x)$,

$$Z(\beta) = \int \mathcal{D}\varphi\, e^{-\beta H[\varphi]}\,. \tag{2.2}$$

There are situations, *e.g.* when $\beta \to \infty$ (or $T \to 0$) or in the mean-field limit, where one is interested in the configurations or paths that minimize the energy,

$$\frac{\delta H[\varphi]}{\delta \varphi(x)}\Big|_{\varphi(x)=\varphi_\star(x)} = 0\,. \tag{2.3}$$

These minimum energy configurations, also called classical solutions in a more general setting, can be uniform (this is what gives the conventional mean-field description) or not. An instanton is a localized solution whose energy or action $H[\varphi_\star]$ is finite (and nonzero). [147, 148, 149] In the above, we have considered the partition function appropriate for an equilibrium state in classical physics but the whole formalism can be generalized to describe space-time behavior either in quantum-field theory or for the dynamics of classical systems. In chapter 5 of this manuscript, we will consider the dynamics of a system of particles in the low temperature limit $T \to 0$, and make use of the instanton formalism: having a finite action, instantons indeed provide the dominant contribution to describe the dynamics in this limit.

Let us illustrate here the instanton method for the simple case of the equilibrium behavior of a one-dimensional scalar-field theory, with potential $V(\varphi(x))$ and the lowest order gradient term. [148] The Hamiltonian (or action in field theory) in this case reads:

$$H[\varphi] = \int_x \left\{ \frac{c}{2} \left(\partial_x \varphi(x)\right)^2 + V(\varphi(x)) \right\} , \tag{2.4}$$

where $c > 0$ is a parameter. We are looking for solutions of equation (2.3), which here becomes:

$$c \frac{\partial^2 \varphi_\star(x)}{\partial x^2} - \left. \frac{\partial V(\varphi(x))}{\partial \varphi(x)} \right|_{\varphi_\star} = 0 . \tag{2.5}$$

By making the formal replacements ($x \to t\,;\ \varphi_\star(x) \to X(t)$) this equation corresponds to Newton's equation for a particle at position in time $X(t)$ with kinetic energy $\frac{c}{2}\left(\dot{X}(t)\right)^2$ into the reversed potential $-V(X(t))$, see figure 2.1 (a). For example, for a double-well potential $V(\varphi(x)) = \frac{r}{4}\left(\varphi(x)^2 - \varphi_0^2\right)^2$ (then it corresponds to the φ^4 theory), with $r > 0$ and $\varphi_0 > 0$, a uniform solution of (2.5) is given by $\varphi_\star = \pm\varphi_0$ and a localized solution of (2.5) is simply:

$$\varphi_\star(x) = \pm\varphi_0 \, \tanh(x/\sigma) , \tag{2.6}$$

where $\sigma = \sqrt{2c/r}$ is the width of the instanton (not to be confused with σ of equation (2.1)). The boundary conditions of the solution also minimize the energy: $\varphi_\star(x \to -\infty) = \mp\varphi_0$ and $\varphi_\star(x \to +\infty) = \pm\varphi_0$. The resulting "instanton" $\varphi_\star(x) = \varphi_0 \tanh(x/\sigma)$ (the "kink") is represented on figure 2.1 (b) for $\varphi_0 = 1$ and $\sigma = 0.3$; its $x \to -x$ reverse, $\varphi_\star(x) = -\varphi_0 \tanh(x/\sigma)$, is the "anti-kink".

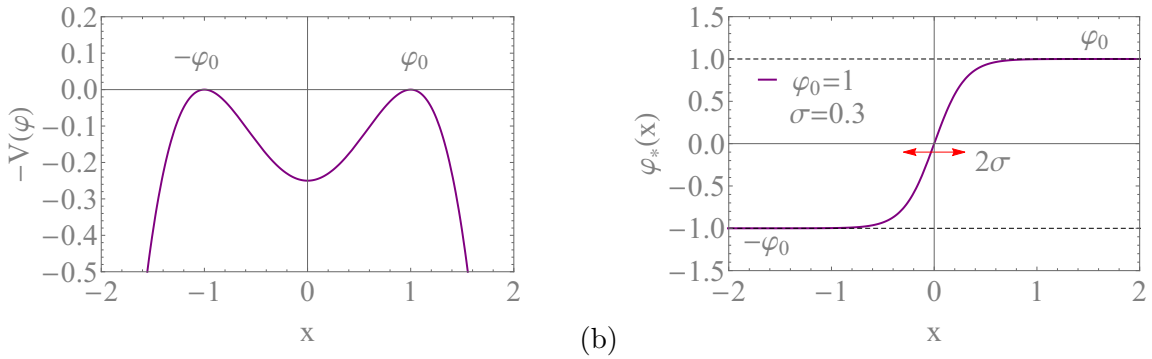

Figure 2.1: One-dimensional φ^4 theory. (a) Reversed potential $-V(\varphi)$ for the $1d$ φ^4 theory. The instantonic trajectory (b) corresponds with formal replacements ($x \to t\,;\ \varphi_\star(x) \to X(t)$) to a particle $X(t)$ living in $-V(X(t))$ and going from position $-\varphi_0$ at $t \to -\infty$ to $+\varphi_0$ at $t \to +\infty$. (b) Instanton: $\varphi_\star(x) = \varphi_0 \tanh(x/\sigma)$ for $\varphi_0 = 1$ and $\sigma = 0.3$.

Originally, the method of instantons was developed in order to compute passage probabilities of tunneling in quantum mechanics, see [148]. Indeed, $\exp(-\beta S_\star)$, with $S_\star$ the "action" of an instanton, is the probability of tunneling from $-\varphi_0$ to φ_0 in the potential $+V[\varphi]$. In the classical mechanics case, this corresponds to a particle climbing an energy barrier $S_\star$. The action corresponding to the instantonic solution can be rewritten as

$$S_\star = \int_{-\varphi_0}^{\varphi_0} dx \, \left[2\, V(\varphi_\star(x))\right]^{1/2} , \tag{2.7}$$

and is a finite quantity (even in the thermodynamic limit).

One can easily prove that instantons are very localized and rare objects [148]. Therefore on an interval on length L, or of duration τ, a typical configuration of the system at low temperature will be

composed by a succession of $2n$ kink and anti-kink instantonic events (like the kink shown in figure 2.1 (b)) centered on positions $x_1, x_2, \cdots, x_{2n}$, as shown schematically for $n = 2$ on figure 2.2. Here we consider periodic boundary conditions hence the number of instantons must be even.

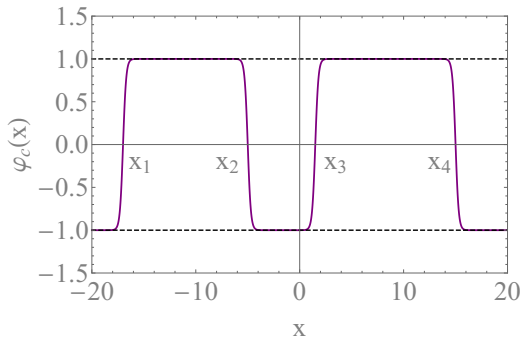

Figure 2.2: One-dimensional φ^4 theory. A possible configuration $\varphi_c(x)$ for a linear system of size $L = 40$ with periodic boundary conditions composed by 2 instantons/anti-instantons (like the one of figure 2.1 (b)) centered in positions x_1, x_2, x_3, x_4.

The partition function of the system can then be obtained by adding to the contribution of the uniform solutions $\varphi = \pm\varphi_0$ all the possible configurations of $2n$ instantons that can occur on a segment of size L, as the one represented in figure 2.2 for $n = 2$. One has to take into account that the positions x_i can be wherever on the interval $[-L/2; +L/2]$, which gives an entropic factor. In addition, as each instanton costs an energy $S_\star$, and that uniform profiles φ_0 do not cost energy, the total energetic cost of a configuration with $2n$ instantons is simply given by $2nS_\star$. One then has to sum over all possible positions x_i's to obtain $Z(\beta)$. In particular, when $\sigma = 0$, the instantonic trajectories becomes sharp jumps of zero width. In this case the entropic factor is simplified, and is given by:

$$\int_{-L/2}^{L/2} dx_1 \int_{x_1}^{L/2} dx_2 \cdots \int_{x_{n-1}}^{L/2} dx_{2n} = \frac{L^{2n}}{(2n)!} \,. \tag{2.8}$$

One obtains $Z(\beta)$ by summing over all possible configurations going from $+\varphi_0$ (or $-\varphi_0$) in $-L/2$ to $+\varphi_0$ (or $-\varphi_0$) in $+L/2$, which corresponds to summing over all integers n:

$$Z(\beta) = \sum_{n=0}^{\infty} e^{-\beta 2n\, S_\star} \frac{L^{2n}}{(2n)!} \,. \tag{2.9}$$

The case of nonzero width σ is done in chapter 3. In addition, one can also include the fact that the real trajectories occurring in a system at low temperature can be slightly modified with respect to the instantonic trajectories which are exactly valid at $T = 0$. This results in the introduction in the expression of $Z(\beta)$ of a term accounting for the fluctuations of shape, determined by evaluating a Gaussian integral over the second order field derivative $\delta H[\varphi(x)]/(\delta\varphi(x')\delta\varphi(y'))\Big|_{\varphi_\star(x)}$. This involves the computation of the determinant of the operator $-\partial_x^2 + V''[\varphi]$. [148, 149]

2.2 Renormalization group

Phase transitions are ubiquitous in physics. This generic term encodes the fact that a system drastically changes its properties under the variation of some external parameter, for example the temperature T. When it crosses a critical value T_c, particular of the system, the phase transition occurs. This is generally captured by an adequate order parameter, which passes from zero to a nonzero value at the transition.

The most common phases transitions are separated in two classes.

On the one hand, first-order phase transitions, which are characterized by a *discontinuous* emergence of a nonzero order parameter, resulting in the existence of a latent heat (related to the height of the "jump"). The correlation length ξ remains finite in the whole temperature range.

On the other hand, second-order phase transitions, for which the emergence of a nonzero order parameter is *continuous*, which results in the absence of latent heat. The correlation length diverges at the transition, basically meaning that all the degrees of freedom are correlated. The system then shows scale invariance. The key consequence of this scale invariance is that the thermodynamic parameters can be expressed as scaling laws of the distance to the critical external parameter, involving critical exponents. For example, for a temperature T larger than but close to the critical one, the correlation length behaves like

$$\xi \sim (T - T_c)^{-\nu} \tag{2.10}$$

and diverges when $T \to T_c$ with a critical exponent ν. These exponents are part of the more general category of "universal quantities", which are independent on the microscopic details of the systems. They are identical for systems belonging to the same universality class which is characterized for instance by the type of symmetry that is broken at the transition. On the contrary, non-universal quantities depend on the particular system under study: it is the case for the value of the critical temperature, for example.

In this thesis we will be concerned by different universality classes: The chapter 3 deals with the Ising model universality class in which the low temperature phase breaks the two-state $\mathbb{Z}_2$ symmetry. The chapter 4 is concerned by both the pure and the random-field Ising model universality classes. The chapter 6 treats of the Ising spin-glass universality class.

A key theoretical framework to compute universal and non-universal quantities characterizing phase transitions, and more specifically critical points at which scale invariance arises, is the renormalization group (RG) [24]. Although a large body of RG studies have used perturbation expansions (ε expansion with ε the distance to the upper critical dimension, expansion in the coupling constants, etc.) we will be concerned by nonperturbative implementations of the RG.

2.2.1 Real-space renormalization group

The simplest (and usually crudest) way of implementing a nonperturbative renormalization group is the Migdal-Kadanoff procedure [150, 151, 152, 153] that relies on a renormalization of the partition function in real space.

As mentioned above, in the vicinity of second-order phase transitions, it is expected that for the long-distance physics and for universal quantities, the details of what happens at short-length scales do not matter. Therefore, one is aiming at a coarse-graining process that averages the fluctuations which are irrelevant for the physics at large scales and gives access to the long-distance physics.

Consider for instance the Ising model on a triangular lattice in dimension two. To obtain information on thermodynamic quantities, on has to sum over the spin degrees of freedom to obtain the partition function

$$Z = \sum_{\{S_i\}} e^{\beta J^{(0)} \sum_{\langle i,j \rangle}^{N} S_i S_j} \tag{2.11}$$

with $\langle i, j \rangle$ the sum over nearest neighbors sites, the lattice containing N sites. Instead of doing the sum in one breath, the idea behind the RG procedure is to sum recursively on degrees of freedom contained in some groups, or blocks, of spins whose shape depends on the geometry of the initial system. Here, these blocks can be chosen to triangular plaquettes, see figure 2.3. On one block A is defined a new

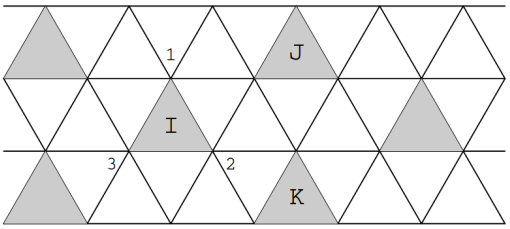

Figure 2.3: Triangular lattice with Ising spins S_i on the vertices, $i = 1, ..., N$. Block-spins $\hat{S}^A$ $(A = I, J, K)$ are defined following (2.12) on triangular plaquettes A, where S_j^A are the three spins of A, $j = 1, 2, 3$. Reprinted from [26].

spin, called block-spin $\hat{S}^A$, which is defined according to some rule: for example, one can choose a "majority rule",

$$\hat{S}^A = \text{sign}(S_1^A + S_2^A + S_3^A)\,. \tag{2.12}$$

One then sums over all the initial degrees of freedom S_i^A yielding this block-spin, making some coarse graining that brings a new effective interaction between the $\hat{S}^A$'s. In the thermodynamic limit the number of sites $N \to \infty$, hence the number of degrees of freedom is let unchanged by the above coarse graining. A difference exists, however, in the effective lattice spacing between block-spins, which is now $> a$. This introduces the last RG operation, a reduction of the scale of the lattice to recover the initial lattice spacing. Doing so, the partition function finally obtained is left invariant.

In general, the process generates new interactions between spins that no longer have the same form as in equation (2.11). To make progress and do actual computations, one must proceed to approximations. A bold one is to neglect all multi-spin interactions except the pair ones, so that the new Hamiltonian for block spins has the same form as the original one. Let's denote by $J^{(1)}$ the effective pair interaction existing between block-spins, where the 1 stands for "one" step. The partition function can therefore be rewritten with $\hat{S}^A$ transformed in S_i (i and A both take values between 1 and ∞) as it is always an Ising spin,

$$Z = \sum_{\{S_i\}} e^{\beta J^{(1)} \sum_{\langle i,j \rangle} S_i S_j}\,. \tag{2.13}$$

The procedure can be repeated with the RG transformations for the couplings, $J^{(n+1)} = \mathcal{R}(J^{(n)})$. At this stage we remember that at the critical point the system is scale invariant. This implies that the above decimation at criticality yields invariant coupling constants, $J^\star = \mathcal{R}(J^\star)$,which correspond to fixed points of the RG transformation. One can then search for the critical fixed point $J^\star$ of this real-space RG procedure and get the critical physics by evaluating Z for this coupling. If one considers a system close to (but not at) criticality, the RG flow of the coupling will spend a long time in the close vicinity of the critical fixed point, before finally flowing away from it to reach one of the two trivial fixed points describing the paramagnetic and ferromagnetic phases.

This real-space RG method is nonperturbative but the approximations that are made are in general uncontrolled and not easy to improve in a systematic way. In one dimension, one can devise real-space RG schemes that are exact. This is what we have done in our study detailed in chapter 3.

2.2.2 Nonperturbative RG in momentum space

An alternative implementation of the nonperturbative RG is to work in momentum space instead of real space. This was originally developed by Wilson [24] and later by others [154, 155, 156]. We will

present here the nonperturbative RG (NPRG) formalism as formulated by C. Wetterich in terms of the effective average action [157, 158, 159, 160, 161]; for reviews see [25, 26].

The NPRG is based on the original idea of Wilson which aims to determine effective actions giving the correct long-distance physics by progressively integrating short-wavelength/high-momentum fluctuations. However, instead of working with the abstract action S_k of the modes which have not been yet integrated out, one computes the effective action Γ_k (or Gibbs free-energy functional) of the modes $(k')^2 > k^2$ that have *already* been integrated out, with $|k| < |k'| < \Lambda$, and Λ the ultraviolet cutoff that is of order of the inverse lattice spacing (or microscopic length scale). This quantity possesses a quite simple physical interpretation, as will be seen.

The effective average action Γ_k verifies the following properties: When $|k| = \Lambda$, no fluctuations have been integrated out and Γ_k is the initial (bare) action of the system

$$\Gamma_\Lambda = S\,, \tag{2.14}$$

and when $k = 0$, all fluctuations are integrated out and Γ_k is the Gibbs free energy of the model

$$\Gamma_0 = \Gamma\,. \tag{2.15}$$

The introduction of the scale k permits to interpolate between the microscopic action and the macroscopic free energy by introducing a family of effective average actions in between. Γ_k is a coarse grained free energy with coarse-graining domains of linear size $|k|^{-1}$, such that all the fluctuations details within the domains have been averaged out.

2.2.2.1 Definition of the effective average action

The partition function can be supplemented by a source term, linear in the field,

$$Z[h] = \int \mathcal{D}\varphi\, e^{-S[\varphi]+\int d^dx\,\varphi(x)h(x)}\,. \tag{2.16}$$

A thermodynamic potential can be defined as

$$W[h] = \log Z[h], \tag{2.17}$$

and it is equal to the Helmholtz free energy F up to some $-\beta^{-1}$ factor. The functional derivative of $W[h]$ with respect to the source gives the connected correlation functions, in particular the thermal average of the field density, the magnetization, is

$$\frac{\delta W[h]}{\delta h(x)} = \langle\varphi(x)\rangle = \phi(x)\,, \tag{2.18}$$

which is used in a Legendre transform to give another thermodynamic potential, the effective action

$$\Gamma[\phi] = -W[h] + \int d^dx\,\phi(x)h(x), \tag{2.19}$$

where $h(x)$ is obtained by inverting the relation (2.18). In statistical physics, this effective action is the Gibbs free energy, and

$$\frac{\delta\Gamma[\phi]}{\delta\phi(x)} = h(x), \tag{2.20}$$

which in absence of external field corresponds to extrema of Γ.

The effective average action Γ_k is a generalization of the above effective action at the scale k. Technically, Γ_k is built by adding a term to the action S which limits the domain of momenta over which the integration is performed, such that the modes $q^2 > k^2$ are averaged and those with $q^2 < k^2$ are not (or weakly) affected. This is the regularization or cutoff term,

$$\Delta S_k[\varphi] = \frac{1}{2}\int d^d q\, R_k(q^2)\, \varphi_q \varphi_{-q}\,, \tag{2.21}$$

where $R_k(q^2)$ plays the role of a mass term, freezing "low-momenta" modes. Actually, the latter enter into the definition of the propagators $P_k(q^2) \propto \left(q^2 + R_k(q^2)\right)^{-1}$, which are integrated in d dimensions on the range $[0;\Lambda]$; $R_k(q^2)$ plays the role of an infrared (IR) cutoff as it suppresses the contributions of the low momenta modes with $q^2 \lesssim k^2$. The regulator term satisfies two properties:

- It is of order k^2 for $q^2 \lesssim k^2$, such that it freezes the contribution of momenta $q^2 \lesssim k^2$,
- It vanishes for $q^2 \gtrsim k^2$, such that the highest momenta are not affected by the presence of the regulator.

A commonly used regulator function is the exponential one, $R_k(q^2) = q^2 \left(e^{q^2/k^2} - 1\right)^{-1}$, which verifies the above conditions. A sharper one called the Litim regulator [162] is also often used, it is given by the expression [1]

$$R_k(q^2) = (k^2 - q^2)\Theta(k^2 - q^2)\,, \tag{2.22}$$

and allows for analytic computations of integrals over the propagators.

The action S thus modified gives rise to a Helmholtz free energy with cutoff k

$$W_k[h] = \log \int \mathcal{D}\varphi\, e^{-S[\varphi]-\Delta S_k[\varphi]+\int d^d x\, \varphi(x)h(x)}\,, \tag{2.23}$$

and the effective average action Γ_k is obtained through the Legendre transform of $W_k[h]$, but modified by the subtraction of the cutoff term, *i.e.*,

$$\Gamma_k[\phi] = -W_k[h] + \int d^d x\, \phi(x)h_k(x) - \Delta S_k[\phi]\,, \tag{2.24}$$

with $\phi(x) = \frac{\delta W_k[h]}{\delta h(x)}$, and $h_k(x)$ obtained by inverting it. Because of the subtraction of $\Delta S_k[\phi]$ the effective average action does not need to be convex, whereas the associated Legendre transform $\Gamma_k + \Delta S_k$ does by definition.

The limit $\Gamma_0 = \Gamma$ can be recovered from the above equation easily as the cutoff ΔS_k vanishes when $k \to 0$. The subtraction of ΔS_k ensures that $\Gamma_\Lambda = S$ is also recovered, without modifying the other limit. [25]

2.2.2.2 Exact flow equation

An exact equation giving the evolution of the effective average action with the change of the fluctuation cutoff k can be derived [163, 160, 161]:

$$\frac{\partial}{\partial k}\Gamma_k[\phi] = \frac{1}{2}\mathrm{Tr}\left\{\left[\Gamma_k^{(2)} + R_k(q^2)\,\mathbb{1}\right]^{-1}\frac{\partial R_k}{\partial k}\right\}\,, \tag{2.25}$$

where $\left[\Gamma_k^{(2)} + R_k(q^2)\,\mathbb{1}\right]^{-1}$ has to be understood as an inverse in the operator sense. The second order functional derivative and the trace term contain absolutely everything on which the theory depends,

[1] In the case where the field is also renormalized, a factor Z_k appears in the expressions of $R_k(q^2)$.

momenta or coordinates and internal indices if they are present:

$$\Gamma^{(2)}_{k;a,b}(q,q') = \frac{\delta^2\Gamma_k[\phi]}{\delta\phi_a(q)\delta\phi_b(q')}\,, \tag{2.26}$$

and

$$\mathrm{Tr} = \sum_a \int d^dx = V^2 \sum_a \int \frac{d^dq}{(2\pi)^d} = V^2 \sum_a \int_q . \tag{2.27}$$

The integral appearing in this flow equation is over *one* loop, or one momentum vector, which simplifies crucially the problem in comparison to the perturbative case in which a term of order n in perturbation implies to compute an n-loop integral. The presence of $R_k(q^2)$ in the integrand regularizes the expression in the ultraviolet (UV) and the IR. For $q^2 \gtrsim k^2$, $\partial_k R_k(q^2) = 0$ and the upper bound in effectively replaced by k; on the other side, all the modes with $q^2 \lesssim k^2$ are given a mass of order k^2 which freezes them, and k acts as an IR cutoff that provides from any $q \to 0$ divergence.

In practice, it is convenient to take the regulator derivative at the end, and the flow equation (2.25) is often expressed as

$$\frac{\partial}{\partial k}\Gamma_k[\phi] = \frac{1}{2}\widetilde{\partial}_k \mathrm{Tr}\left\{\log\left[\Gamma^{(2)}_k + R_k(q^2)\,\mathbb{1}\right]\right\}\,, \tag{2.28}$$

with the introduction of the operator $\widetilde{\partial}_k = \frac{\partial R_k}{\partial k}\frac{\partial}{\partial R_k}$ which acts only on the R_k dependence of the right hand side.

The flow equation (2.25) is an exact equation and its solution contains all the properties of the system. However, despite its apparent simple character, it is in general impossible to solve without introducing some approximations. Indeed, the functionals $\Gamma_k[\phi]$ and $\Gamma^{(2)}_{k;a,b}(q,q')$ depend on the complete profile(s) $\phi_a(q)$, and are extremely complicated mathematical objects.

2.2.2.3 Diagrammatic representation

In the case of a theory without internal indices, the equation (2.25) is more explicitly written in reciprocal space under the form of an integral over q

$$\frac{\partial}{\partial k}\Gamma_k[\phi] = \frac{1}{2}\int \frac{d^dq}{(2\pi)^d}\frac{\partial R_k(q^2)}{\partial k} P_{k;q,-q}[\phi]\,, \tag{2.29}$$

where $P_{k;q,-q}[\phi]$ is the propagator, which depends on the field configuration, defined as

$$P_{k;q,-q}[\phi] = \left[\left(\Gamma^{(2)}_k + R_k(q^2)\,\mathbb{1}\right)^{-1}\right]_{q,-q}\,. \tag{2.30}$$

This equation, and its higher fields derivatives, can be rewritten under the form of Feynman diagram(s) The graphical representation of the above equation (2.29) is [2]

$$\frac{\partial}{\partial k}\Gamma_k[\phi] = \frac{1}{2}$$

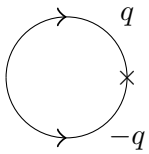

where the cross corresponds to the derivative $\frac{\partial R_k(q^2)}{\partial k}$ and the simple line is the propagator $P_{q,-q}$. If we consider a theory with internal indices, again, these indices have to appear on the diagram.

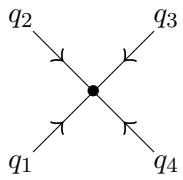

Figure 2.4: Diagrammatic representation of $\Gamma^{(4)}_{k;q_1,q_2,q_3,q_4} = \frac{\delta\Gamma_k}{\delta\phi(q_1)\ldots\delta\phi(q_4)}$.

The evolution equation of any vertex $\Gamma^{(n)}_k$ has also a simple diagrammatic representation. The vertex $\Gamma^{(n)}_k = \frac{\delta\Gamma_k}{\delta\phi(q_1)\ldots\delta\phi(q_n)}$ $(n \geq 3)$ can be represented diagrammatically, for example it is done in figure 2.4 for $n = 4$.

The flow equation for $\Gamma^{(1)}_k[\phi]$ is obtained taking one field derivative of equation (2.29):

$$\frac{\partial}{\partial k}\frac{\delta\Gamma_k[\phi]}{\delta\phi(q_1)} = \frac{1}{2}\widetilde{\partial}_k \int_{q_2,q_3} \Gamma^{(3)}_{k;q_1,q_2,q_3} P_{k;q_3,-q_2}\,. \tag{2.31}$$

Taking the derivative of the diagram representing $\frac{\partial}{\partial k}\Gamma_k[\phi]$ with respect to $\phi(q_1)$ is equivalent to create a leg to this diagram, carrying a momentum q_1, as shown in figure 2.5. At this stage, one has understood

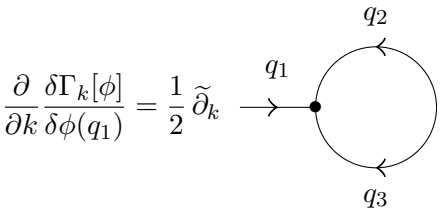

Figure 2.5: Diagrammatic representation of $\frac{\partial}{\partial k}\frac{\delta\Gamma_k[\phi]}{\delta\phi(q_1)}$.

that propagators (and indices) appearing inside a loop are integrated (summed), and the ones present on the external leg(s) are fixed by the field derivative(s).

Similarly, we can take another field derivative of diagram of figure 2.5 to obtain the higher-order flow equation

$$\frac{\partial}{\partial k}\frac{\delta^2\Gamma_k[\phi]}{\delta\phi(q_1)\delta\phi(q_2)} = \frac{1}{2}\widetilde{\partial}_k\left\{\int_{q_3,q_4} \Gamma^{(4)}_{k;q_1,q_2,q_3,q_4} P_{k;-q_4,q_3} - \int_{q_3,q_4,q_5,q_6} \Gamma^{(3)}_{k;q_1,q_3,q_4} P_{k;-q_4,q_5} \Gamma^{(3)}_{k;q_2,q_5,q_6} P_{k;-q_6,q_3}\right\} \tag{2.32}$$

represented on figure 2.6.

[2] In the diagrams the vectors have been omitted to simplify the notation.

$$\frac{\partial}{\partial k}\frac{\delta^2\Gamma_k[\phi]}{\delta\phi(q_1)\delta\phi(q_2)} = \frac{1}{2}\widetilde{\partial}_k\Big\{$$

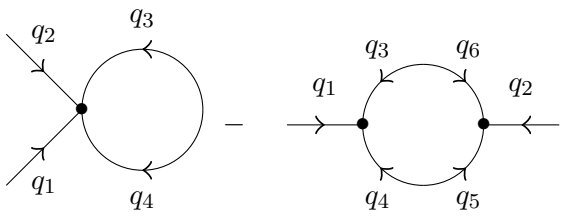

$$\Big\}$$

Figure 2.6: Diagrammatic representation of $\frac{\partial}{\partial k}\frac{\delta^2\Gamma_k[\phi]}{\delta\phi(q_1)\delta\phi(q_2)}$.

Etc.

2.2.2.4 Approximations and truncations

The main difficulty is to find an approximation scheme for the problem at hand. Different general schemes have been proposed and we summarize some of them below.

Derivative expansion

In the study of critical phenomena, we are concerned by the long-distance physics. It is therefore possible to expand the effective average action in gradients of the field (around a uniform field configuration). For illustration, the two lowest truncations of the derivative expansion are:

-*$O(\partial^0)$ Local potential approximation (LPA)*: At the lowest order, the only term kept is the usual gradient squared

$$\Gamma_k[\phi] = \int d^dx \left[U_k(\phi(x)) + \frac{1}{2}\left(\partial_x\phi(x)\right)^2\right], \tag{2.33}$$

where $U_k(\phi)$ is the effective potential, which is equal to the effective average action evaluated for a uniform field (times the volume of the system). The kinetic term is not renormalized during the process.

-*$O(\partial^2)$:*At second order, one has (for a 1-component scalar theory)

$$\Gamma_k[\phi] = \int d^dx \left[U_k(\phi(x)) + \frac{Z_k(\phi(x))}{2}\left(\partial_x\phi(x)\right)^2\right] \tag{2.34}$$

where one now has a new function $Z_k(\phi)$ characterizing the renormalization of the field.

- The derivative expansion approximation can be truncated still at higher orders of derivatives, involving more functions.

Expansion in powers of the field around a nontrivial configuration

If we want to describe the properties of the system near a certain constant profile $\phi_{0,k}$, it may be useful to write Γ_k as an expansion in powers of $\phi(x) - \phi_{0,k}$. Truncated at some order N, this gives

$$\Gamma_k[\phi] = \sum_{n=0}^{N}\frac{1}{n!}\int\left(\prod_{j=1}^{n}d^dx_j\ [\phi(x_j) - \phi_{0,k}]\right)\Gamma_k^{(n)}(x_1,...,x_n;\phi_{0,k}) + O(\phi^{N+1}), \tag{2.35}$$

and if $\phi_{0,k}$ corresponds to a minimum of Γ_k, the first field derivative vanishes, $\Gamma_k^{(1)}(x_1;\phi_{0,k}) = 0$. In the above expression the notation

$$\Gamma_k^{(n)}(x_1,...,x_n;\phi_{0,k}) = \frac{\delta^n\Gamma_k}{\delta\phi(x_1)...\delta\phi(x_n)}\Big|_{\phi=\phi_{0,k}} \tag{2.36}$$

has been used and will reappear in the following.

Mixing the approximations

One can combine the derivative expansion and the expansion in powers of the field (around a nontrivial configuration), *e.g.*,

$$U_k(\phi) = \sum_{n=0}^{N} \frac{1}{n!} U_k^{(n)}(\phi_{0,k}) \, (\phi - \phi_{0,k})^n \, , \tag{2.37}$$

$$Z_k(\phi) = \sum_{n=0}^{M} \frac{1}{n!} Z_k^{(n)}(\phi_{0,k}) \, (\phi - \phi_{0,k})^n \, . \tag{2.38}$$

The so-called LPA' approximation amounts to keeping the full potential $U_k(\phi)$ and truncating $Z_k(\phi)$ at the zeroth order, *i.e.*, $Z_k(\phi) = Z_k(\phi_{0,k})$.

Expansion in invariants

An alternative expansion to that in the field difference from a nontrivial configuration consists in using invariants. This guaranties that the symmetries of the theory are preserved by the truncation. This can be illustrated for the simple case of the φ^4 theory. There is an unique invariant $\rho = \frac{1}{2}\phi^2$, and Γ_k can be expanded as

$$\Gamma_k[\phi] = \int d^d x \, \left[U_k(\rho) + \frac{1}{2} Z_k(\rho) \, (\partial_x \phi(x))^2 + O(\partial^4) \right] . \tag{2.39}$$

The above expression is manifestly invariant by the $\mathbb{Z}_2$ (or $O(N)$) symmetry as is the bare action.

This is relatively easy to perform for a theory with an unique invariant, however this can be more involved for more complex theories with internal indices, for which the symmetry can be described by many index-dependent invariants. In chapter 6, we construct the effective potential U_k for such a theory in the case of the Ising spin-glass model.

2.2.2.5 φ^4 theory within the LPA

As an illustration, we first consider the LPA for the φ^4 theory. As already discussed, this theory has a unique invariant $\rho = \frac{1}{2}\phi^2$, hence its potential U_k can be defined as a function of ρ. With this approximation $\Gamma_k^{(2)}(q, q')$ in a uniform profile ρ is given by

$$\Gamma_k^{(2)}(q, q')\Big|_\rho = \left(q^2 + U_k'(\rho) + 2\rho \, U_k''(\rho) \right) \delta(q + q') \, , \tag{2.40}$$

where the primes on $U(\rho)$ denote derivatives with respect to ρ. In this case the propagator (2.30) is easy to compute. Inserting the LPA ansatz, (2.33), in the exact RG equation, (2.25), leads to

$$\frac{\partial}{\partial k} U_k(\rho) = \frac{1}{2} \int \frac{d^d q}{(2\pi)^d} \frac{\partial_k R_k(q^2)}{q^2 + U_k'(\rho) + 2\rho \, U_k''(\rho) + R_k(q^2)} \, , \tag{2.41}$$

This equation can be solved numerically once a regulator function $R_k(q^2)$ has been chosen.

The physical quantity that will give us the macroscopic properties of the system is $\lim_{k\to 0} U_k(\phi) = U_0(\phi)$. If $\phi_{0,k}$ is the minimum of $U_k(\phi)$, it will be equal to the average order parameter $\phi_{0,k\to 0}$ in the limit $k \to 0$. In the high temperature phase, the average order parameter is zero, hence the potential $U_0(\phi)$ has a unique minimum centered on $\phi_{0,k\to 0} = 0$. In the phase where the symmetry is spontaneously broken, the average order parameter is nonzero, the potential therefore has two minima located in $\pm\phi_{0,k\to 0} \neq 0$. However, $\Gamma_0 = \Gamma$, the Gibbs free energy which is given by a Legendre transform and must be convex at all temperatures by definition. The exact shape of the potential in the low temperature phase is therefore *flat* between the two values $\pm\phi_{0,k\to 0} \neq 0$.

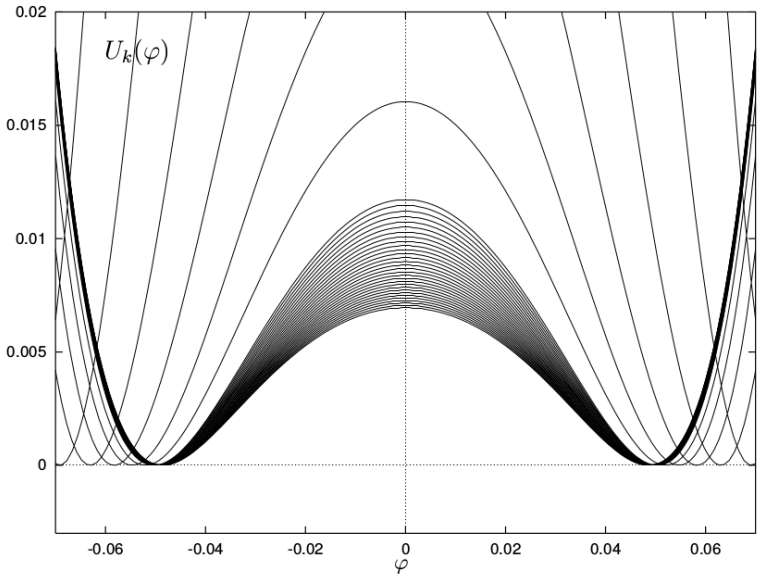

Figure 2.7: Evolution of the average potential $U_k(\phi)$ (here ϕ is noted φ) when the scale k of the included fluctuations is varied. Here is plotted the particular case where the initial condition $U_\Lambda(\phi)$ is a double-well potential which minimum is in position $> \phi_{0,k\to 0}$, hence $U_k(\phi)$ converges toward the broken symmetry phase potential with lowering k. The inner part progressively flattens to recover the convexity property of the Gibbs free energy (times V^{-1}) when $k = 0$. Reprinted form [25].

These behaviors are recovered if one solves the flow equation (2.41) for an initial condition of the average potential at scale Λ which has the shape of a potential in the broken symmetry phase. For a coarse grained Ising model, one can choose an initial condition corresponding to a φ^4 potential, with two symmetric minima located at some finite symmetric values, which can be fine tuned. [3] The initial position of one minimum (the minima are symmetric) is a marker of how much the system is in the low temperature phase: the more it is initially set to be far from the origin, the more the system is in a broken symmetry phase. More explicitly, if the initial minimum is larger than $\phi_{0,k\to 0}$, $U_{k\to 0}(\phi)$ will converge toward the potential of the broken symmetry phase, see figure 2.7, and inversely.

At the critical point, which localizes the limit between the two phases, the average order parameter $\phi_{0,k\to 0}$ is zero. In particular, one observes in the case of the LPA that the minimum at criticality goes to zero when $k \to 0$ with some power of k

$$\phi_{0,k}^2 \propto \rho_{0,k} \underset{k\to 0}{\sim} k^{2-d}, \tag{2.42}$$

corresponding to the dimension of the minimum in reciprocal space (in this case the anomalous dimension $\eta = 0$).

So far we have considered an operation which is the analog of coarse-graining in the real space RG of section 2.2.1. The second step of the RG transformation, *i.e.*, a rescaling of the system under study, is necessary to find the fixed points of the RG transformation. For this we will use scaling dimensions like the one of $\rho_{0,k}$ in equation (2.42) near $k = 0$. One then obtains a *dimensionless* flow equation, and the critical point of the physical system is determined by finding the associated fixed point solution. It contains information about universal quantity.

[3] One has to note that from a polynomial initial condition of the potential, truncated at $O(\varphi^4)$ for example, the inner part of the potential will never be flat. This feature requires to consider the exact, complete expansion, of the potential.

2.2.2.6 Dimensionless flow equation for the LPA

In order to find the critical fixed point associated with scale free behavior, we have to write equation (2.41) in a dimensionless form. If γ_k, u_k and $\tilde{\varrho}$ are the dimensionless equivalent of Γ_k, U_k and ρ, one has:

$$\begin{aligned} \Gamma_k &= k^0\,\gamma_k\,, \\ U_k &= k^d\,u_k\,, \\ \rho &= k^{d-2}\,\tilde{\varrho}\,, \end{aligned} \tag{2.43}$$

where we have used that dimensionally $[x] = k^{-1}$. With the above set of relations, we can compute the dimension of any field derivative of $U_k(\rho)$.

To find a fixed point of the renormalization group procedure, we have to determine the flow equation of the dimensionless potential $u_k(\tilde{\varrho})$. The total derivative $k\frac{d}{dk}u_k(\tilde{\varrho})$ reads

$$k\frac{d}{dk}u_k(\tilde{\varrho}) = k\frac{d}{dk}\left[k^{-d}U_k\left(k^{d-2}\tilde{\varrho}\right)\right] = -d\,u_k(\tilde{\varrho}) + k\partial_k u_k(\tilde{\varrho}) + u_k'(\tilde{\varrho})\,(d-2)\,\tilde{\varrho}\,. \tag{2.44}$$

At this point, we can introduce the dimensionless RG "time" t and the dimensionless derivative $\frac{d}{dt}$ (and ∂_t)

$$t = \log\frac{k}{\Lambda}\,, \quad \frac{d}{dt} = k\frac{d}{dk}\,. \tag{2.45}$$

When a total derivative $\frac{d}{dt}x$ appears, it can be replaced by $\dot{x}$, in analogy with real time derivatives.

The fixed point solution $u_\star(\tilde{\varrho})$ is found by solving $\frac{d}{dt}u_k(\tilde{\varrho}) = 0$, which is given by

$$0 = -d\,u_\star(\tilde{\varrho}) + u_\star'(\tilde{\varrho})\,(d-2)\,\tilde{\varrho} + v_d\,l_0^d\left[u_\star'(\tilde{\varrho}) + 2\tilde{\varrho}\,u_\star''(\tilde{\varrho})\right]\,, \tag{2.46}$$

where the rightmost term is the dimensionless equivalent of the integral in equation (2.41), which is written with help of the "threshold function" l_0^d defined, after using the dimensionless variables $y = q^2/k^2$ and $r_k(y) = R_k(q^2)/k^2$, as

$$l_0^d(w) = \frac{1}{2}\int_0^\infty dy\,y^{d/2-1}\frac{\partial_t r_k(y)}{y + r_k(y) + w}\,, \tag{2.47}$$

where v_d is a factor coming from the integration over angular variables, with Ω_d the solid angle in dimension d,

$$v_d = \frac{\Omega_d}{2(2\pi)^d}\,, \quad \Omega_d = \frac{2\pi^{d/2}}{\Gamma(\frac{d}{2})}\,. \tag{2.48}$$

The values of the above threshold function l_0^d for the Litim regulator (2.22) can be found in [26].

Fixing a regulator function $r_k(y)$, equation (2.46) can be numerically solved. Although it seems to admit an infinity of solutions, it has been shown that the physical solution corresponds to a particular $u_\star(\tilde{\varrho})$ which is regular in $\tilde{\varrho}$ [156, 164].

The average potential can also be studied for more complex $O(N)$ theories, the φ^4 theory corresponding to $N = 1$. They are all described in terms of an unique invariant, implying that the average potential is a function of one variable which can be found by solving one differential equation. However, for theories involving more than one invariant we are faced with functions of several variables and a system of differential equations has to be solved. In practice, this is doable is the number of invariants is not too large.

2.2.3 Fixed points and stability

The system of dimensionless flow equations (for the LPA and more involved truncations) can admit several fixed points, one of them corresponds to the critical point in the dimension d at which the problem is studied. The latter is unstable, with only one relevant direction [4].

The stability of the fixed point is studied by linearizing the dimensionless flow equations around the fixed point. In the case where the functions are expanded around some field configuration and one has flow equations for couplings constants, this gives rise to a matrix, whose eigenvalues encode the stability of the fixed point. More generally, one may have to solve a system of partial differential equations. With our choice of RG time $t = \log \frac{k}{\Lambda}$, an unstable direction corresponds to a negative eigenvalue.

The eigenvalues of a critical fixed point are all positive (the stable eigendirections) excepted one: the eigendirection associated to the temperature, which is unstable as it automatically drags the system out of criticality if different from T_c. In the case where an external field h is applied, a second eigenvalue is negative in the eigendirection associated to the external field.

The unstable directions correspond to *relevant* coupling constants, when the stable ones are linked to *irrelevant* couplings. One can also find a zero eigenvalue, which corresponds to a *marginal* direction: one therefore needs to go beyond the linear perturbation to know if it is relevant or irrelevant.

In field theory, the Gaussian theory contains a simple-well potential term, centered on 0:

$$H_G = \int d^d x \left[\frac{1}{2} (\partial_{\vec{x}} \phi(x))^2 + \frac{1}{2} \phi(x)^2 \right] . \tag{2.49}$$

The RG procedure can be exactly performed, as only simple Gaussian integrals appear, and the dimensionless flow equations admit one fixed point, called the Gaussian fixed point. Actually, this fixed point is stable for systems in dimension d above the upper critical dimension d_u and the critical exponents are the classical ones predicted by the mean-field theory.

Generally, one is more interested in the critical properties of systems below the upper critical dimension, real systems being generally contained in the dimension interval $d \in [1; d_u[$. In this case, fluctuations become important, and they are not described by the above Gaussian theory. The trivial Gaussian fixed point hence becomes unstable (repulsive), meaning that the universal physics is described by an other, nontrivial fixed point.

2.2.4 Critical exponents

The anomalous dimension accounts for the effect of field renormalization and describes the critical behavior of the pair correlation function:

$$G^{(2)}(r) \underset{T=T_c}{\propto} \frac{1}{r^{d-2+\eta}} . \tag{2.50}$$

When approaching the critical point, the behavior of the correlation length is governed by a power law with critical exponent ν:

$$\xi \sim (T - T_c)^{-\nu} . \tag{2.51}$$

The critical exponent ν can be obtained from the knowledge of the eigenvalues of the stability matrix around the critical fixed point. Generically, ν is given by the inverse of the relevant eigenvalue λ_1 (in the case where the is no external field):

$$\nu = \frac{1}{|\lambda_1|} . \tag{2.52}$$

[4] In the presence of an external field, there is an additional relevant direction.

Other critical exponents can be determined from the scaling relations that are verified in the framework of the nonperturbative RG:

$$\begin{aligned} \alpha &= 2 - \nu\, d\,, \\ \gamma &= \nu(2-\eta)\,, \\ \delta &= \frac{d+2-\eta}{d-2+\eta}\,, \\ \beta &= \frac{\nu}{2}(d-2+\eta)\,. \end{aligned} \tag{2.53}$$

Therefore, only ν and η are independent critical exponents (at least when there is no additional dangerously irrelevant operator as it is the case, for instance, for the critical point of the random-field Ising model [165]).

Chapter 3

Non-perturbative fluctuations in a simple model with metastability

Contents

The results of this chapter have been published in [166].

The activated dynamics that is expected to play a fundamental role in supercooled liquids below the dynamical transition T_d is intimately related to the presence of metastability in the systems. This metastability takes place in the complex mean-field free-energy landscape in the form of an exponential number (in the system size) of metastable minima.

No one knows what is left from the mean-field theory in finite dimensions. Studying directly the effect of fluctuations starting from the mean-field theory is an extremely hard task. This is partly due to the very intricate nature of the associated replica-field theory which involves a $n \times n$ overlap matrix order parameter, with n that must be analytically continued to zero, and also to the necessity to introduce nonperturbative events. Some of the different attempts that have been done in this direction are reported in section 1.1.4.2.

One can then prefer to work with effective theories, which basically encode the main physical mechanisms while leaving out the inessential ones and are usually easier to study. These theories then contain the long-distance properties of the system under study all in having washed out the irrelevant small-length-scale details of the original system. Their effective Hamiltonian, that can be strikingly different (and, as one hopes, simpler) from the microscopic theory, are expressed in terms of effective parameters which are not known *a priori*, and the fundamental step for a correct description of the macroscopic physics in terms of an effective theory is then to find these parameters.

A possible effective theory for supercooled liquids is a RFIM-like theory, and the interested reader is redirected to section 1.1.4.2 where several references where it is argued for that are given. One possibility to proceed would then be to consider the finite-dimensional results of simulations, that take into account, virtually exactly, of all the spatial fluctuations of the system including highly nonperturbative ones, in order to determine the effective parameters of the effective theory describing the system in the thermodynamic limit. One finds that supercooled liquids in finite (small-enough) sizes eventually behave in a mean-field manner, if the relevant fluctuations responsible for the disappearance of the metastability occur on a length scale larger than the system size, and one can measure a nonconvex

Franz-Parisi potential $V(q)$. [167] This potential was introduced in section 1.1.3.4. Studying for an ensemble of reference liquid configurations the average value of $V(q)$ and its fluctuations in such-finite-size systems should provide a way to access these parameters. [102] Once they are known, predictions of the effective theory on long length scales could be further checked against other numerical or experimental observations.

One however has to design a method to extract the effective parameters from the nonconvex shape of $V(q)$ measured in finite-size computer simulations. This requires a better understanding of the role played by nonperturbative fluctuations and the development of a theoretical approach able to capture them at all scales.

The aim of this chapter is to study this problem on a toy model that is simple enough to be thoroughly investigated. We propose the study of a simple model presenting metastability when studied on small-enough-finite sizes. Its mean-field like double-well structure gradually evolves when finite-size (and finite-dimensional) fluctuations are progressively introduced, in practice by increasing the size over which the model is defined. The model can be fully investigated from analytic and numerical computations. We will then characterize completely the fluctuations present in the system. We will understand how they affect the potential, from its mean-field like shape in small sizes to the the expected convex shape in the thermodynamic limit, and will determine from this evolution the parameters of the effective theory. In order to mimic the situation in structural glasses, in parallel to exact computations valid when the temperature goes to zero, $T \to 0$, we perform numerical simulations and numerical calculations on finite-size systems at low but finite T. Once analyzed by scaling arguments, these results allow to characterize fully the relevant fluctuations that bridge the gap from small-sizes results to the thermodynamic limit and to determine the effective parameters of the effective theory.

3.1 One-dimensional model

The model that we focus on is the one-dimensional φ^4 scalar field theory defined by the Hamiltonian

$$H_L[\varphi] = \int_0^L \mathrm{d}x \left[\frac{c}{2}(\partial_x\varphi)^2 + V(\varphi(x))\right] , \tag{3.1}$$

where L is the system size, $c > 0$, and the local potential $V(\varphi)$ has a double-well form

$$V(\varphi) = \frac{r}{4}(\varphi^2 - 1)^2 , \tag{3.2}$$

with $r > 0$. We are interested in the low-temperature regime. There, the physics of the model is governed by strong nonperturbative fluctuations: these are kinks or domain walls of small width between the positively magnetized and negatively magnetized phases (to use the language of magnetic systems), and the order parameter varies from ∓ 1 to ± 1 on a very small distance. These spatially localized defects are *a priori* energetically unfavorable: they have a finite energetic cost. Hence, their density is always finite, albeit very small at low temperature (it follows a Boltzmann distribution). However, by redistributing the positions of these kinks the system can gain entropy. The standard balance between energy and entropy gives the kinks/anti-kinks redistribution winner: it is therefore their presence that destroys the phase transition which is predicted at the mean-field level and remains in a perturbative treatment.

Mirroring the current situation in glasses, the problem we consider is one in which we want to infer the parameters of a theory that we conjecture to be of the Ising/φ^4 type from the results of simulations and to further check that the effective microscopic theory we have in mind is the correct one. The input from simulations and other essentially exact computations that we consider as available knowledge is

the probability of observing a given average value ϕ of the field in a system of finite size L, or, more precisely, its logarithm,

$$U_L(\phi) = -\frac{1}{\beta L} \ln P_L(\phi) \tag{3.3}$$

where $P_L(\phi)$ is the probability density to observe $\frac{1}{L}\int dx\varphi(x)$ equal to ϕ in a system of size L with periodic boundary conditions and $\beta = 1/(k_B T)$. We will call $U_L(\phi)$ *the finite-size effective potential* since it takes into account all fluctuations exactly, up to the length-scale L. In the $L \to 0$ limit it coincides with the bare potential $V(\phi)$, whereas in the thermodynamic limit it is equal to the exact effective potential (Gibbs free energy) as a function of ϕ.

Of course, in the case of the one-dimensional φ^4 field theory we know from the start that the proper effective theory is just that given in equation (3.1). Nevertheless, the problem of inferring the bare parameters of the theory, c, r, and the energy of a kink from the behavior of finite-size systems is not straightforward. Moreover, understanding in detail the evolution of $U_L(\phi)$, *i.e.*, how the change in shape of the finite-size effective potential is related to the progressive integration of nonperturbative fluctuations is also very instructive. The knowledge gained in the case of this simple problem will likely be useful for tackling more difficult and still unsolved ones.

We also tried to develop an approach that progressively takes into account fluctuations, including the nonperturbative ones, and allows one to eventually describe the macroscopic behavior. The theoretical method of choice for progressively bridging the gap from microscopic to macroscopic physics is the renormalization group (RG) (see section 2.2). In particular the nonperturbative renormalization group (NPRG) could be able to catch the effect of all kinds of fluctuations, from perturbative to nonperturbative ones. The NPRG starts from an exact flow equation for the running effective action $\Gamma_k[\phi]$, which can be solved successfully if one manages to find a simple yet rich enough truncation for it.

In both of the above situations, *i.e.*, either in a system of finite size L or within the NPRG in a system in the thermodynamic limit but in the presence of an infrared cutoff on fluctuations of wavelength larger than $1/k$, fluctuations are limited. As a result, the relevant potential, be it the finite-size one $U_L(\phi)$ or the running effective one $U_k(\phi) = \Gamma_k[\phi]/(\beta L)$, need not be convex. Just like in the mean-field limit where no fluctuations are taken into account, which in the present case leads to a Landau potential equal to the bare $V(\phi)$, metastability can thus be present. As the length scale over which fluctuations are allowed increases, *i.e.*, with increasing L or decreasing k, metastability should become less pronounced and in the macroscopic limit, $L \to \infty$ or $k \to 0$, both $U_L(\phi)$ and $U_k(\phi)$ should converge to the convex exact effective potential.

The typical evolution with L of $U_L(\phi)$ is shown in figure 3.1 (a) and that of the running effective potential $U_k(\phi)$ is plotted in figure 3.1 (b). (In the latter case, we have obtained the result by using the so-called Local Potential Approximation (LPA) of the exact NPRG equation.) The progressive disappearance of metastability is clearly observed in the two cases. The question we want to address in the former case is as follows: Say we are given some numerical data in the form of figure 3.1 (a); how can one extract information about the corresponding effective theory and its parameters? On the other hand, in the latter case, it is possible to develop a suitable approximation scheme of the effective action such that the NPRG is able to reproduce the main features associated with the nonperturbative fluctuations in the present model?

3.2 The finite-size effective potential

In this section we study the behavior of the finite-size effective potential $U_L(\phi)$ and its evolution with the system size L. We first describe intuitively the shape of $U_L(\phi)$ and explain the ideas on how to extract the relevant quantities such as the correlation length ξ and the surface tension γ from the evolution of

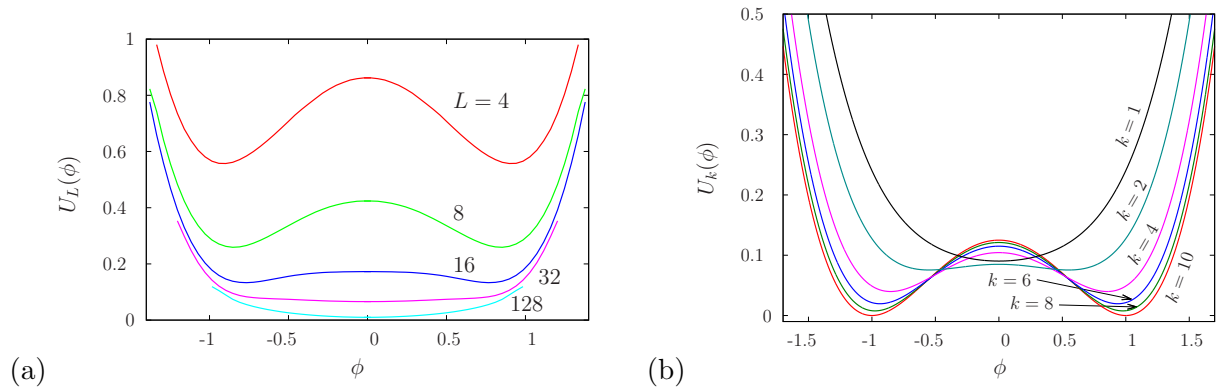

Figure 3.1: 1-dimensional φ^4 scalar field theory. (a) Plot of the finite-size effective potential $U_L(\phi)$ as a function of ϕ for different values of L, as obtained by MonteCarlo simulation: $L = 4, 8, 16, 32, 128$ for model parameters $r = 2$, $c = 4$, $\beta = 1$. (b) Plot of the running effective potential $U_k(\phi) = \Gamma_k(\phi)/(\beta L)$ as a function of ϕ for different values of k obtained by using the Local Potential Approximation (LPA). The model parameters are $c = 1$, $\beta = 1$, $r = 1/2$, and $\Lambda = 1$. The flow equation is obtained with a regulator of the form[162] $R_k(p) = (k^2 - p^2)\Theta(k^2 - p^2)$: $\partial_k U_k(\phi) = -\pi^{-1} U_k''(\phi)[U_k''(\phi) + k^2]^{-1}$. Note that there is a k-dependent but ϕ-independent contribution that is not included (hence the apparent difference of behavior with that in (a).

$U_L(\phi)$, by focusing in particular on the behavior of two quantities: the curvature of $U_L(\phi)$ in $\phi = 0$, $\kappa_L = U_L''(0)$, and the height of the barrier of $U_L(\phi)$ between the maximum in $\phi = 0$ and the minima in $\phi_{min} \simeq \pm 1$ (when present), $\Delta_L = U_L(0) - U_L(\phi_{min})$. We then present detailed analytic results for $U_L(\phi)$ in the limit of zero temperature, which are obtained through the instanton technique, and use them as a benchmark to check the validity of our recipes for extracting the correlation length and the surface tension. Finally, we numerically determine the behavior of $U_L(\phi)$ at finite temperature, *i.e.* at finite (but large) ξ. To this aim, we have combined Monte-Carlo (MC) simulations and perturbation expansions based on a real-space RG and transfer matrix treatments. We then apply again the recipes for extracting the temperature dependence of ξ and γ and compare the output with the direct numerical computation of these quantities.

3.2.1 The shape of $U_L(\phi)$ and its evolution with L

At any given finite temperature, *i.e.*, at any given finite correlation length ξ, if the system size goes to infinity, then the magnetization distribution goes to a Gaussian centered at $\phi = 0$, due to the central limit theorem, and eventually converges to a Dirac-delta function. (We use in this section the language of magnetic systems and call ϕ the magnetization, or, more properly, the magnetization density.) Thus, in the thermodynamic limit, the finite-size effective potential displays an unique (parabolic) minimum in $\phi = 0$. On the other hand, at any given finite system size, as the temperature goes to zero and the correlation length goes to infinity, the magnetization goes to either plus or minus one with probability one. For $\xi \gg L$ the finite-size effective potential is given by two symmetric minima centered in ± 1. As a result, a nontrivial distribution of $P_L(\phi)$ and a nontrivial shape of $U_L(\phi)$ arise between the two opposite limits considered above.

In order to figure out intuitively the evolution of $P_L(\phi)$ and $U_L(\phi)$ with the system size, let us first focus on the typical configurations of the field $\varphi(x)$ which, at least at low enough temperature, dominate the Gibbs measure. These are the configurations associated with the ground states of the system, corresponding to constant positive or negative magnetization profiles $\varphi(x) = \pm 1$, and the

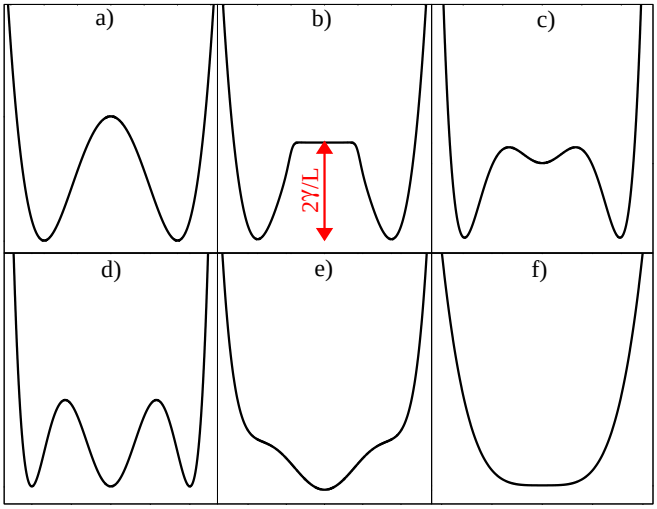

Figure 3.2: Sketch of the evolution of the shape of the finite-size effective potential $U_L(\phi)$ for different system sizes L: a) $L < 2\sigma$; b) $2\sigma \ll L \ll \xi$; c) $L \lesssim \xi$; d) $L \simeq \xi$; e) $L \gtrsim \xi$; f) $L \gg \xi$.

lowest excitations above them, involving domain walls (*i.e.*, kinks and anti-kinks), which correspond to instantons that minimize the hamiltonian and connect positively and negatively magnetized regions (see chapter 2). At low enough temperature (large enough correlation length), the typical configurations of the field are thus well described by regions with almost constant ± 1 magnetization separated by narrow domain walls. The width σ of a domain wall is the typical size of an interface. The energy of a domain wall, $S^\star$, is, by definition, proportional to the microscopic surface tension γ of the model, which is defined as the energy cost associated with the creation of an interface between two regions with opposite magnetization. It is easy to show (see below for more details) that the typical distance between domain walls is of the order of the correlation length ξ, which is proportional to $e^{\beta S^\star}$.

If L is smaller than 2σ, no domain walls can be present in the system. (We consider periodic boundary conditions, so that the number of domain walls must be even.) Thus, $P_L(\phi) \simeq e^{-\beta L V(\phi)}$ and $U_L(\phi) \simeq V(\phi)$ (see figure 3.2 (a)). Therefore, from equation (3.2), $\Delta \simeq r/4$ and $\kappa \simeq -r$.

For $L > 2\sigma$ but still much smaller than the correlation length ξ, the probability of finding a domain wall is very small. The typical field configurations are then approximately constant ± 1 magnetization profiles plus some small thermal fluctuations, whose amplitude depends on $V''(\phi = \pm 1) = 2r$. On the other hand, configurations with zero magnetization correspond to field profiles with $2n$ domains walls, with $n \in \mathbb{N}^*$, that are suitably placed between 0 and L (obviously, $2n\sigma \leq L$). The thermodynamic weight of such configurations is proportional to $e^{-2n\beta S^\star}$ and the probability of having $\phi = 0$ is obtained as

$$P_L(\phi = 0) \propto \frac{L}{2}\left[e^{-2\beta S^\star} + \frac{(L-4\sigma)^2}{8}\, e^{-4\beta S^\star} + \frac{(L-6\sigma)^4}{192}\, e^{-6\beta S^\star} + \dots\right], \tag{3.4}$$

where the terms $(L-4\sigma)^2/8$, $(L-6\sigma)^4/192$, etc., correspond to the combinatorial factors accounting for the number of field configurations with 4, 6, etc., domain walls between 0 and L that have zero magnetization (see the next section for more details). As long as $2\sigma \ll L \ll \xi$, all configurations with more than a single kink/anti-kink pair are highly suppressed and their contribution can be neglected. Therefore, $P_L(\phi = 0)$ is dominated by field profiles with only two domains walls. Since all such profiles have the same combinatorial factor (and thus the same probability), independently of the distance between the kink and the anti-kink, all intermediate magnetization values, sufficiently away from ± 1, occur with approximately the same probability. As a result, for $2\sigma \ll L \ll \xi$ the finite-size effective

potential $U_L(\phi)$ is given by two deep narrow symmetric minima around $\phi_{min} \simeq \pm 1$ (whose curvature is simply given by $2r/L$) that are separated by a central region where $U_L(\phi)$ is approximatively constant. This is sketched in figure 3.2 (b). The barrier height $\Delta_L = U_L(0) - U_L(\phi_{min})$ is then given by $2S^\star/L$, and the curvature in $\phi = 0$ is $\kappa_L = U_L''(0) \simeq 0$.

The qualitative shape of $U_L(\phi)$ does not show any significant change until $L \lesssim \xi$. At this point, the terms of equation (3.4) corresponding to field configurations with more than two domain walls start to give a significant contribution to $P_L(\phi)$. Since there are exponentially many more configurations of the domain walls corresponding to zero magnetization with respect to configurations yielding positive or negative magnetization, $P_L(\phi)$ starts to develop a secondary maximum around $\phi = 0$ as a result of this entropic effect. Correspondingly, $U_L(\phi)$ develops a secondary minimum in zero, as sketched in figure 3.2 (c). In this regime the behavior of the barrier height Δ_L and of the curvature κ_L are model-dependent and cannot be determined by simple intuitive argument: they must be computed in some explicit way, as we do in the following subsections.

For $L \simeq \xi$ the barrier Δ_L is expected to disappear as the value of the potential in $\phi = 0$ crosses that in $\phi \simeq \pm 1$ (see figure 3.2 (d)). As L further increases the minima in ± 1 become higher and eventually disappear. However, the potential may still remain nonconvex, as illustrated in figure 3.2 (e). Full convexity is recovered only for $L \to \infty$. It is then easy to show that the finite-size effective potential coincides with the Gibbs free-energy density (or exact effective potential) $U(\phi)$ of the system:

$$U_L(\phi) = U(\phi) + o\left(\frac{1}{L}\right), \tag{3.5}$$

where $U(\phi)$ is defined as the Legendre transform of the Helhmoltz free energy,

$$U(\phi) = \beta^{-1} f(\beta, h) + h\phi\,, \tag{3.6}$$

where h is the external magnetic field and $\langle\varphi\rangle = -\partial f(\beta,h)/\partial(\beta h) = \phi$ (we have again used the magnetic language). As a consequence, for $L \gg \xi$ the finite-size effective potential is a convex function of ϕ and presents a unique minimum in $\phi = 0$: see figure 3.2 (f). In the thermodynamic limit the curvature κ_L approaches $\kappa_\infty = U''(0) = \chi^{-1}$, where χ is the magnetic susceptibility defined as $\chi = \partial\langle\varphi\rangle/\partial h|_{h=0} = (\langle\varphi^2\rangle - \langle\varphi\rangle^2)|_{h=0}$.

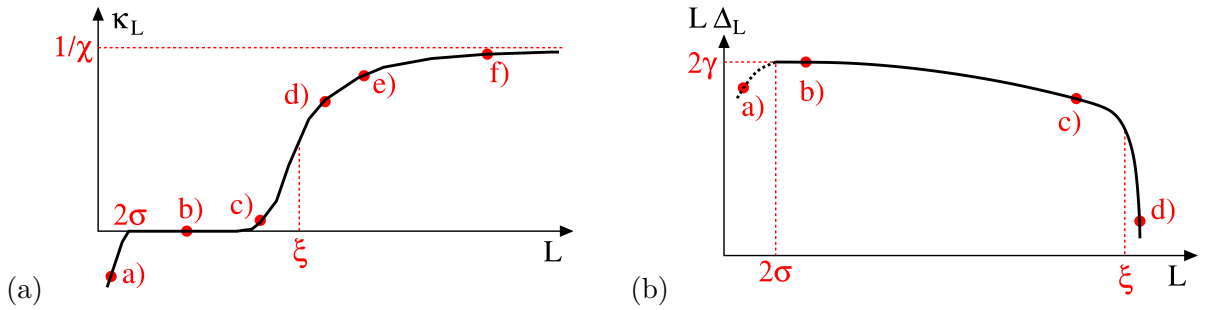

Figure 3.3: Schematic plot of the curvature $\kappa_L = U_L''(0)$ (a) and of the barrier height $\Delta_L = U_L(0) - U_L(\phi_{min})$ times the system size L (b) as a function of L. The barrier height is shown on a log-log plot. The labels a)-f) correspond to the shapes of $U_L(\phi)$ of figure 3.2. Note that the behavior of $L\Delta_L$ at small $L \lesssim 2\sigma$ is not universal and depends on the bare parameters.

Based on the intuitive arguments discussed above, we can qualitatively determine the behavior of the quantities of interest for us, κ_L and Δ_L, as a function of L. They are schematically represented in figure 3.3. On very short length scales, $L < 2\sigma$, the curvature is negative, $\kappa_L \simeq -r$. Then, for

$2\sigma \ll L \ll \xi$, κ_L is approximately zero. For $L \lesssim \xi$, κ_L starts to grow and for $L \to \infty$ it approaches $1/\chi$ as $1/L$. In turn, the barrier height Δ_L behaves roughly as $2\gamma/L$ for $2\sigma \ll L \ll \xi$ and rapidly vanishes for $L \gtrsim \xi$.

We can therefore extract the important physical quantities by focusing on the behavior of κ_L and Δ_L. For instance, one possible recipe is to try to collapse the curves of κ_L versus L obtained at different temperatures onto a master curve by rescaling the axes by adjustable parameters. The parameters that provide the best collapse should then be $\chi(T)^{-1}$ for κ_L (vertical axis) and $\xi(T)$ for L (horizontal axis). Another possibility would be to plot $L\Delta_L$ as a function of L and, knowing the correlation length $\xi(T)$ from the previous operation, to look for a plateau or a region of weak dependence on L for $L < \xi$: at low enough temperature, the height of the plateau should then be twice the surface tension $\gamma(T)$. (Alternatively, one could do a log-log plot as in figure 3.3 (b).) In the next subsections we will implement and check these ideas in a quantitative way.

3.2.2 $U_L(\phi)$ in the $T \to 0$ ($\xi \to \infty$) limit

As explained above, at very small temperature the Gibbs measure is dominated by the ground state of the system and the lowest excitations above it. The ground states of equation (3.1) correspond to constant field configurations $\varphi(x) = \pm 1$. The lowest excitations above the ground states correspond to nonuniform kink and anti-kink instantonic profiles that are obtained by minimizing the Hamiltonian:

$$\left.\frac{\delta H_L[\varphi(x)]}{\delta\varphi(x)}\right|_{\varphi^\star} = 0 \quad \Rightarrow \quad c\,\frac{\partial^2\varphi^\star(x)}{\partial x^2} = \left.\frac{\partial V(\varphi(x))}{\partial\varphi(x)}\right|_{\varphi^\star}, \tag{3.7}$$

with the boundary conditions $\varphi^\star(x \to -\infty) = \mp 1$ and $\varphi^\star(x \to +\infty) = \pm 1$. This differential equation can be solved exactly for the φ^4 theory in $d = 1$, yielding

$$\varphi^\star(x) = \pm \tanh(x/\sigma)\,, \tag{3.8}$$

with $\sigma = \sqrt{2c/r}$. The energy cost associated to such domain walls can be obtained by plugging equation (3.8) into equation (3.1) (momentarily, we have redefined the system from $-L/2$ to $L/2$ and taken the instanton center far away from the edges); this gives $S^\star = \int H_L[\varphi^\star(x)]\,\mathrm{d}x \approx \sqrt{8rc/9}$. Note that we can make more precise now the notion of "low-temperature regime": It is obtained by letting either β or r be large, such that the Boltzmann factor associated with the presence of a domain wall, $\exp(-\beta\sqrt{8rc/9})$, is much smaller than 1.

Small fluctuations of the field around the instantonic profile can be easily taken into account at a Gaussian level. After expanding the Hamiltonian around the instantonic solution up to second order in $\delta\varphi(x) = \varphi(x) - \varphi^\star(x)$, the thermodynamic weight of a single instanton is expressed as

$$Z_1 \simeq e^{-\beta S^\star} \int \mathcal{D}\varphi\, e^{-\frac{\beta}{2}\int \mathrm{d}x\,\mathrm{d}y\, \left.\frac{\delta^2 H_L}{\delta\varphi(x)\delta\varphi(y)}\right|_{\varphi^\star} \delta\varphi(x)\,\delta\varphi(y)}. \tag{3.9}$$

In order to compute the functional integral above one thus need to diagonalize the operator corresponding to the kernel

$$M(x,y) = \beta\left[-c\frac{\partial^2}{\partial x^2} + V''(\varphi^\star(x))\right]\delta(x-y)\,, \tag{3.10}$$

which yields

$$Z_1 \simeq e^{-\beta\tilde{S}^\star} = e^{-\beta S^\star + \frac{1}{2}\ln(2\pi/\det M)}\,. \tag{3.11}$$

In the present low-temperature limit, it can be shown, following the arguments of *e.g.* [149], that $\det M \sim \beta r$ and, thus, $\tilde{S}^\star \simeq S^\star - (1/2)\beta^{-1}\ln(\beta r) + \mathrm{O}(\beta^{-1})$.

At very low temperature the typical configurations of the field are therefore described by a dilute gas of domain walls separated by regions with constant $\varphi = \pm 1$. The partition function of the system can thus be written as a sum over the number n of kink/anti-kink pairs (as discussed above, the number of domain walls must be even to be compatible with the periodic boundary conditions) weighted by the energy cost $e^{-2n\beta\tilde{S}^\star}$ times an appropriate combinatorial coefficient I_{2n} accounting for all the possible configurations of the positions of $2n$ domain walls between 0 and L:

$$Z_L = \sum_{n=0}^{[L/2\sigma]} I_{2n}(L)\, e^{-2n\beta\tilde{S}^\star}\,, \tag{3.12}$$

where $[x]$ denotes the integer part of x. Note that, since the instantons have a finite width σ, we cannot place more than $(L/2\sigma)$ kink/anti-kink pairs between 0 and L. The problem of determining the combinatorial coefficients I_{2n} is equivalent to computing the entropy of a gas of $2n$ hard spheres of size σ on a ring of length L (see appendix A.1). The resulting expression is

$$I_{2n}(L) = \frac{1}{n}\,\frac{L}{(2n-1)!}(L-2n\sigma)^{2n-1}\,. \tag{3.13}$$

Two length scales thus naturally emerge from the calculation: σ, the typical size of an interface, and $e^{\beta\tilde{S}^\star}$ (here and in the following we have set the microscopic length scale $1/\Lambda$ to unity), which corresponds to the typical distance between two consecutive instantons. Following arguments similar to those in [168] the latter can easily be shown to be (up to a trivial proportionality constant) the correlation length ξ of the system as obtained from the exponential decay of the two-point connected correlation function.

After introducing the rescaled variables $\zeta = L/e^{\beta\tilde{S}^\star}$ and $\alpha = \sigma/L$, the partition function finally reads

$$Z_L(\zeta,\alpha) = 2\sum_{n=0}^{[1/(2\alpha)]} \frac{\zeta^{2n}}{(2n)!}(1-2n\alpha)^{2n-1}\,. \tag{3.14}$$

The computation of the magnetization probability distribution $P_L(\phi)$ in the $T \to 0$ limit can be carried out in a similar way. Note that an analogous computation has already been done for the Ising model in $d = 1$ [168] (see also below).

For each given instantonic configuration with $2n$ alternate kinks and anti-kinks we define x_i, $i = 1,\ldots,2n$, as the lengths of the regions with constant $\varphi = \pm 1$. In terms of these variables, the extensive magnetization M reads

$$M = \int_0^L \varphi(x)\,\mathrm{d}x = \pm\sum_{i=1}^{n}(x_{2i-1} - x_{2i})\,. \tag{3.15}$$

Note that thanks to the translational invariance, one can choose without loss of generality to place the first domain wall at $x = 0$. The sign of M in front of the sum thus depends on whether the first instanton is from $\varphi = -1$ to $\varphi = +1$ or *vice versa*. Since each domain wall has a width σ, we also have that

$$\sum_{i=1}^{2n} x_i = L - 2n\sigma\,. \tag{3.16}$$

In consequence, the extensive magnetization is bounded as $|M| \leq L - 2n\sigma$. When enforcing the constraints given by equations (3.15) and (3.16) one obtains

$$P_L(M) = \frac{1}{Z_L}\Big[\delta(M-L) + \delta(M+L) + 2\sum_{n=1}^{[(L-|M|)/2\sigma]} J_{2n}(M,L)\, e^{-2n\beta\tilde{S}^\star}\Big]\,, \tag{3.17}$$

where Z_L is defined in equation (3.12). Again, the combinatorial factors $J_{2n}(M, L)$ can be computed exactly (see appendix A.1). After introducing the rescaled variables ζ, α defined above and the magnetization density $\phi = M/L$ and using the fact that $\delta(L\phi) = (1/L)\delta(\phi)$ and $P_L(L\phi) = (1/L)P_L(\phi)$, we finally obtain:

$$P_L(\phi) = \frac{1}{Z_L(\zeta,\alpha)}\left[\delta(\phi-1)+\delta(\phi+1)+2\sum_{n=1}^{[(1-|\phi|)/2\alpha]}(\zeta/2)^{2n}\,\frac{\left[(1-2n\alpha)^2-\phi^2\right]^{n-1}}{n!(n-1)!}\right], \tag{3.18}$$

where $Z_L(\zeta,\alpha)$ is given in equation (3.14). It is easily checked that $P_L(\phi)$ is properly normalized, $\int_{-1}^{1} P_L(\phi)\,\mathrm{d}\phi = 1$. One also finds that in the limit $\sigma \to 0$, *i.e.*, when the domain walls become infinitely sharp, and for $\tilde{S}^\star = 2J$, equations (3.14) and (3.18) give back the exact results derived for the one-dimensional Ising model.[168]. These calculations are explicitly done in appendix A.1.

The finite-size effective potential and its evolution with the system size can be now explicitly determined in the $T \to 0$ limit from the relation in equation (3.3). $U_L(\phi)$ behaves as anticipated in the previous section: It presents two narrow minima in $\phi = \pm 1$, corresponding to the δ-functions, [1] and a secondary minimum in $\phi = 0$ due to the entropic term in equation (3.18). As L increases (*i.e.*, α decreases) the minimum in $\phi = 0$ becomes deeper and deeper, as the sum over n in equation (3.18) grows exponentially fast with ζ/α. For $L \simeq \xi$ the value of the minimum in $\phi = 0$ crosses that of the two symmetric minima in $\phi = \pm 1$ (strictly speaking the value of the minima in $\phi = \pm 1$ is defined only for a nonzero temperature; otherwise, one has to consider the weight of the delta peaks). Nevertheless, at any finite L the potential remains nonconvex due to the vestiges of the two minima in ± 1. It is only in the thermodynamic limit that $U_{L\to\infty}(\phi) = U(\phi)$ recovers full convexity.

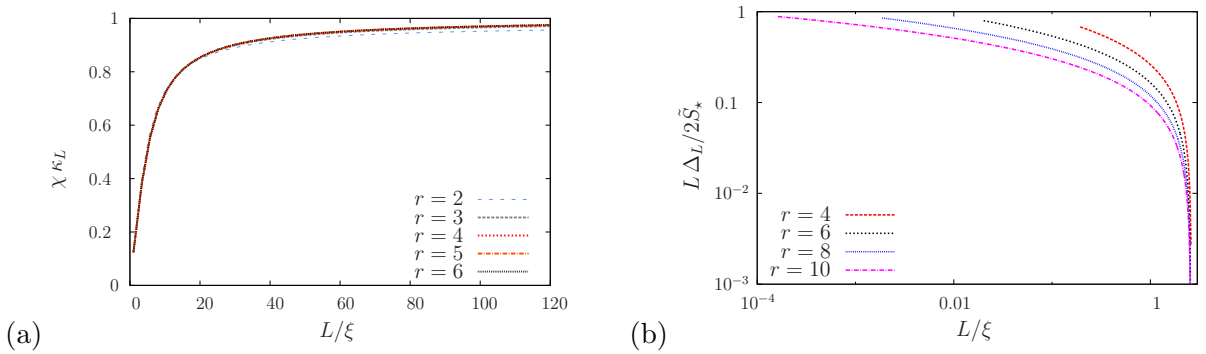

Figure 3.4: (a) Rescaled curvature $\chi\kappa_L$ as a function of L/ξ for the φ^4 field theory in $d = 1$ in the low-temperature regime for $\beta = 1$, r varying from 2 to 6, and for $c = 2r$. (b) Log-log plot of the rescaled barrier, $L\Delta_L/(2\tilde{S}^\star)$, as a function of L/ξ for the φ^4 field theory in $d = 1$ for $\beta = 1$, r varying from 4 to 10, and $c = 2r$. The curves stop on the low side for $L = 2\sigma + a$ and the barrier is not defined within the instanton treatment for $L < 2\sigma$.

From equations (3.3), (3.14), and (3.18), one can compute all the desired characteristics of $U_L(\phi)$, such as the curvature in $\phi = 0$, κ_L, and the barrier height (when present), Δ_L. Following the ideas presented in the previous section, we plot in figure 3.4 (a) the curvature κ_L multiplied by the magnetic susceptibility χ as a function of the system size L divided by the correlation length ξ, for different

[1] Note that at small but finite temperature, the two δ-functions in $\phi = \pm 1$ acquire a finite width due to the small gaussian thermal fluctuations of the fields around $\phi(x) = \pm 1$. Locally, the amplitude of such thermal fluctuations is simply related to $V''(\phi = \pm 1) = 2r$. Therefore the curvature of the two minima of $U_L(\phi)$ in $\phi = \pm 1$ is $2\beta r/L$.

temperatures. [2] We have set $\beta = 1$, $c = 2r$ and a range of r from 2 to 6 (as discussed above, the low-temperature limit here means that $\exp(-\beta\sqrt{8rc/9}) = \exp(-4r/3) \ll 1$). The curves show a perfect collapse, as expected. Via the instanton calculation we indeed have access to all physical quantities of the present simple model. This is a consistency check of the recipe discussed above and an illustration of the range of temperatures where the asymptotic results apply. We show in figure 3.4 (b) the evolution of the barrier height Δ_L multiplied by the system size L and divided by twice the domain-wall (free) energy $\tilde{S}^\star$ as a function of L/ξ for $\beta = 1$, $c = 2r$, and for r varying from 4 to 10. This log-log plot is very similar to the sketch in figure 3.3 (b). The value $L\Delta_L/(2\tilde{S}^\star) \approx 1$ (implying $\gamma \simeq \tilde{S}^\star$ as expected) is observed for $L \sim 2\sigma$, which corresponds to very small values of L/ξ, especially at low temperature. There is then a broad regime, up to $L/\xi \lesssim 1$, where one observes a small decay, by less than a factor of 10. Finally, for $L \gtrsim \xi$ there is a fast (exponential) decay.

These plots validate at a quantitative level the proposed ways of extracting the parameters of the theory from the behavior of the finite-size effective potential. We now turn to the same exercise but in the finite temperature regime where the analytical solution via the instantons is no longer a sufficient description.

3.2.3 $U_L(\phi)/L$ for finite but large ξ

In this section we apply and test the empirical recipes to extract ξ, χ and γ proposed above on a system at large but finite correlation length (corresponding to small but finite temperature). We obtain a numerical estimate of the finite-size effective potential $U_L(\phi)$ for a range of values of L through several methods.

First, we have performed MC simulations. To this aim, we first discretize the continuum field theory of equation (3.1) by replacing the gradient by its discrete lattice version. The Hamiltonian thus becomes

$$H_L(\{\varphi_i\}) = a \sum_{i=1}^{L} \left[\frac{c}{2a^2} (\varphi_i - \varphi_{i+1})^2 + V(\varphi_i) \right] . \tag{3.19}$$

We set the lattice spacing a to 1 (note that for $c = 2r$ the width of a domain wall is then $\sigma = 2 > a$) and we consider periodic boundary conditions: $\varphi_{L+1} = \varphi_1$.

The numerical simulations are performed with a Metropolis algorithm: At each time step we pick a site i at random, and attempt to change the value of φ_i by a random quantity, $\delta\varphi_i$, extracted from a gaussian distribution with zero mean and variance σ_φ. We then compute the energy difference $\Delta H_L = c\,\delta\varphi_i(\delta\varphi_i + 2\varphi_i - 2\varphi_{i+1}) + V(\varphi_i + \delta\varphi_i) - V(\varphi_i)$ and accept the move with the Metropolis probability $p = \min\{1, e^{-\beta\Delta H_L}\}$. Time is advanced by $1/L$. The typical width of the field shifts σ_φ is optimized recursively during the dynamics by enforcing that the acceptance rate of the moves (averaged over the last 100 MC steps) is approximately equal to 0.3.

We start from a given initial condition (for instance $\varphi_i = +1\ \forall i$) and let the system evolve and equilibrate. The equilibration time τ, which of course depends on β, r, and L, can be extracted from the exponential decay of dynamical correlation functions such as $(1/L)\sum_i \langle \varphi_i(t+t')\varphi_i(t')\rangle \simeq \langle \varphi^2 \rangle\, e^{-t/\tau}$. In order to compute the magnetization probability distribution, $P_L(\phi)$, we measure the instantaneous magnetization $\varphi(t) = (1/L)\sum_i \varphi_i(t)$ at regular time intervals corresponding to several times the equilibration time, say 10τ. This allows us to make sure that the values of $\varphi(t)$ measured during the dynamics are statistically independent. In this way we construct a histogram of the magnetizations which gives

[2] Note that in the $T \to 0$ limit, the correlation function has a simple exponential form, $G_c^{(2)}(r) \simeq e^{-r/\xi}$. As a consequence, the magnetic susceptibility becomes $\chi = 2\int G_c^{(2)}(r) \propto 2\xi$ and $\kappa_\infty = 1/(2\xi)$. This result can be obtained analytically, as shown in appendix A.2.

an estimate of $P_L(\phi)$ and, from equation (3.3), we obtain $U_L(\phi)$. Results for $\beta = 1$, $r = 2$, $c = 2r$, and L varying from 4 to 128 are shown in figure 3.1 (a).

Note that in order to obtain an accurate enough estimate of $P_L(\phi)$ and of $U_L(\phi)$, we need to sample rare events, which take place with an exponentially small probability in the system size. As a consequence, the number of measurements of the instantaneous magnetization must scale exponentially with L. Since the computational time of a single MC step scales linearly with the system size, this implies that the total computational time of our MC simulations scales as $\tau L e^L$. Therefore, MC results are limited to not too large values of L, typically $L \lesssim 10^2$.

In order to overcome this limitation and study larger system sizes, we have used a $1/L$ perturbation expansion combined with an exact computation of the (Helmholtz) free energy of the model through both a real-space RG approach and a transfer-matrix technique.

Let us start with the definition of the magnetization probability distribution,

$$P_L(\phi) = \frac{\mathrm{Tr}_{\{\varphi_i\}} \delta(L\phi - \sum_i \varphi_i) e^{-\beta H_L}}{\mathrm{Tr}_{\{\varphi_i\}} e^{-\beta H_L}} , \tag{3.20}$$

where $\mathrm{Tr}_{\{\varphi_i\}} \equiv \int \prod_i \mathrm{d}\varphi_i$. By using the integral representation of the δ-function, one easily obtains

$$P_L(\phi) = e^{L\beta f_L(\beta,0)} \int_{-i\infty}^{i\infty} \mathrm{d}\mu \, e^{-L[\beta f_L(\beta,\mu) + \mu\phi]} , \tag{3.21}$$

and

$$U_L(\phi) = -\frac{1}{\beta L} \ln \int_{-i\infty}^{i\infty} \mathrm{d}\mu \, e^{-L[\beta f_L(\beta,\mu) + \mu\phi]} - f_L(\beta, 0) , \tag{3.22}$$

where $f_L(\beta, \mu)$ is the Helmholtz free-energy density of a system of size L in the presence of an external uniform magnetic field μ/β:

$$f_L(\beta, \mu) = -\frac{1}{\beta L} \ln \mathrm{Tr}_{\{\varphi_i\}} e^{-\beta H_L + \mu \sum_i \varphi_i} . \tag{3.23}$$

For large enough L the integral in equations (3.21) and (3.22) is dominated by the maximum in $\mu = \mu^\star$, which is given by [3]

$$\left. \frac{\partial \beta f_L(\beta, \mu)}{\partial \mu} \right|_{\mu^\star} + \phi = 0 . \tag{3.24}$$

Expanding the argument of the exponential around $\mu^\star$ leads to

$$\beta f_L(\beta, \mu) + \mu\phi = \beta f_L(\beta, \mu^\star) + \mu^\star \phi + \frac{\beta}{2} f_\star^{(2)} (\delta\mu)^2 + \frac{\beta}{3!} f_\star^{(3)} (\delta\mu)^3 + \frac{\beta}{4!} f_\star^{(4)} (\delta\mu)^4 + \dots ,$$

where $f_\star^{(n)} = \partial^n f_L(\beta, \mu)/\partial\mu^n|_{\mu^\star}$ and $\delta\mu = \mu - \mu^\star$. One can thus treat all terms beyond the gaussian level in a perturbative way and obtain a systematic expansion of $P_L(\phi)$ and $U_L(\phi)$ in powers of $1/L$. From a straightforward calculation, one finds up to the order $1/L^2$:

$$U_L(\phi) \simeq f_L(\beta, \mu^\star) + \frac{\mu^\star}{\beta}\phi - f_L(\beta, 0) - \frac{1}{\beta L} \ln \sqrt{\frac{2\pi}{\beta L |f_\star^{(2)}|}} + \frac{1}{\beta L^2} \left[\frac{f_\star^{(4)}}{8\beta |f_\star^{(2)}|^2} + \frac{5[f_\star^{(3)}]^2}{24\beta |f_\star^{(2)}|^3} \right] . \tag{3.25}$$

The above equation deserves some comments:

[3] Since the integrand in equations (3.21) and (3.22) is an analytic function, we can modify the contour in the complex plane.

(1) As already mentioned, in the thermodynamic limit, $U_{L\to\infty}(\phi)$ converges to the Gibbs free-energy density $U(\phi)$, which is defined as the Legendre transform of the Helmholtz free-energy density $f_{L\to\infty}(\beta,h)$ (see equation (3.6)) and is therefore a convex function of the magnetization ϕ.

(2) equation (3.25) is actually an expansion in powers of ξ/L. The successive derivatives of the Helmholtz free energy with respect to the external field μ yield the n-points connected correlation functions, $\beta f_\star^{(n)} = (1/L)\sum_{i_1,\ldots,i_n}\langle\varphi_{i_1}\cdots\varphi_{i_n}\rangle_{con}$, which thus behave as ξ^{n-1}/L. As a result, the expansion of equation (3.25) does not converge for $L/\xi < 1$ (even if L is large) and is expected to poorly behave compared to the numerical simulations in this regime. On the other hand, it should provide a good description of the finite-size effective potential for $L/\xi > 1$.

(3) In order to make some use of equation (3.25) we need to know the expression of the Helmholtz free energy of the model on a ring of L sites, at temperature β, and in the presence of an external uniform magnetic field μ/β.

The calculation of $f_L(\beta,\mu)$ can be done exactly by using a real-space RG approach (see chapter 2), called the Migdal-Kadanoff (MK) scheme. It consists in integrating out iteratively half of the sites of the systems (say the odd sites) at each decimation step, and computing recursively the effective pair interaction potential, $W_n(\varphi,\varphi')$, among the remaining sites. Consider for instance three consecutive sites, i, $i+1$, and $i+2$, at the p-th step of the renormalization procedure. After integrating out the field on the site $i+1$, one finds the following exact recursive equation:

$$W_{p+1}(\varphi_i,\varphi_{i+2}) = -\frac{1}{\beta}\ln\int_{-\infty}^{+\infty} \mathrm{d}\varphi_{i+1}\, e^{-\beta[W_p(\varphi_i,\varphi_{i+1})+W_p(\varphi_{i+1},\varphi_{i+2})]}\,, \tag{3.26}$$

with the initial condition:

$$W_0(\varphi,\varphi') = \frac{c}{2a^2}\left(\varphi-\varphi'\right)^2 + \frac{1}{2}\left[V(\varphi)+V(\varphi') - \frac{\mu}{\beta}\left(\varphi+\varphi'\right)\right]. \tag{3.27}$$

For a system of size $L=2^p$, after $p-1$ decimation steps, there are only two sites left and the Helmholtz free-energy density can be obtained as a simple integration:

$$f_L(\beta,\mu) = -\frac{1}{2^p\beta}\ln\int_{-\infty}^{+\infty}\mathrm{d}\varphi\,\mathrm{d}\varphi'\, e^{-2\beta W_{p-1}(\varphi,\varphi')}\,. \tag{3.28}$$

This procedure allows one to obtain very accurate numerical values of $f_L(\beta,\mu)$ and of its derivatives, provided that the size of the system is an integer power of 2. In order to access other values of the system size L, we have complemented the RG calculation by a transfer-matrix (TM) approach.

Indeed, the partition function of the system can be written as, with $\lambda_1 > \lambda_2 > \cdots > \lambda_L$:

$$Z_L(\beta,\mu) = \mathrm{Tr}_{\{\varphi_i\}} T_{\varphi_1,\varphi_2}T_{\varphi_2,\varphi_3}\cdots T_{\varphi_L,\varphi_1} = \mathrm{Tr}\mathbf{T}^L = \lambda_1^L + \lambda_2^L + \ldots\,,$$

where the transfer-matrix operator is such that $T_{\varphi,\varphi'} = \exp(-\beta W_0(\varphi,\varphi'))$ with W_0 given by equation (3.27). One can then numerically diagonalize the operator by discretizing the values of the fields φ and φ' and compute its eigenvalues, $\lambda_1,\lambda_2,\ldots$, which leads to an approximate expression for the Helmholtz free-energy density,

$$f_L(\beta,\mu) \simeq -\frac{1}{\beta}\ln\lambda_1 - \frac{1}{\beta L}\, e^{L\ln(\lambda_2/\lambda_1)} + o\left[(\lambda_3/\lambda_1)^L\right].$$

Since the correlation length of the system is given by

$$\xi^{-1} = -\ln\left(\lambda_2/\lambda_1\right)\,, \tag{3.29}$$

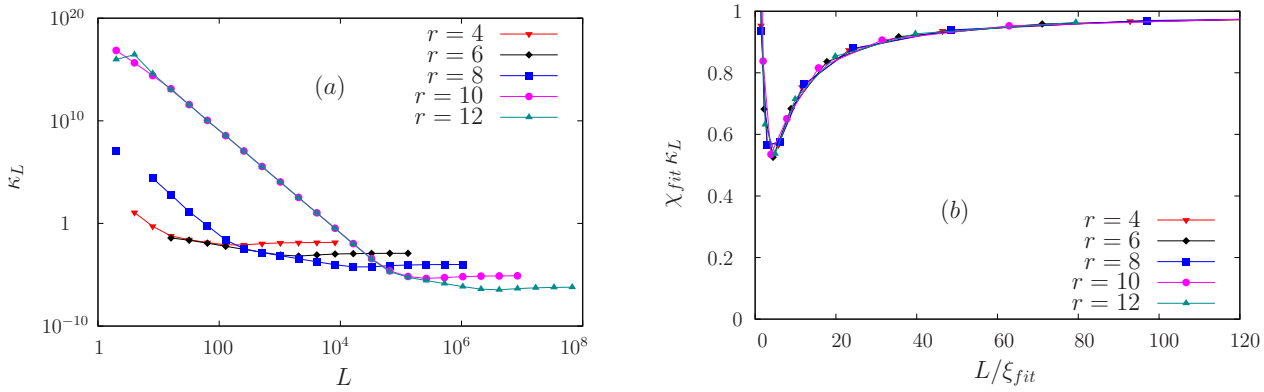

Figure 3.5: (a) Log-log plot of the curvature $\kappa_L = U_L''(0)$ as a function of L for $\beta = 1$, $r = 4$, 6, 8, 10, 12, and $c = 2r$. (b) Same data with a rescaling of the horizontal and vertical axes, as L/ξ_{fit} and $\chi_{fit}\kappa_L$ respectively, to provide the best collapse to a mastercurve.

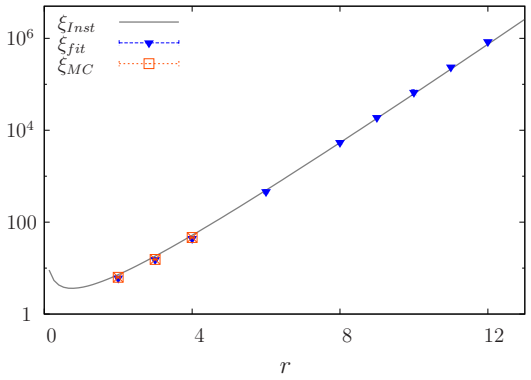

Figure 3.6: Plot of the scaling parameter ξ_{fit} versus r and comparison with the direct computation of the correlation length through MC and instanton techniques. Recall that have set $\beta = 1$, so that the temperature dependence is controlled by r. (Recall that since $c = 2r$, the instanton width $\sigma = \sqrt{2c/r} = 2$.) The error bars associated with the fitting procedure are very small in this case and of the order of the symbol size.

equation (3.29) provides a good approximation for $f_L(\beta, \mu)$ only for $L \gtrsim \xi$.

The finite-size effective potential $U_L(\phi)$ is then obtained from equation (3.25). The numerical results for the curvature κ_L in $\phi = 0$ and for the barrier height Δ_L at small but finite temperature (or rather, correlation length) are displayed in figures 3.5 and 3.7. In figure 3.5 (a), we plot κ_L versus L for several temperatures (actually, values of r as we fix $\beta = 1$) and in figure 3.5 (b) we show the best data collapse on a mastercurve after rescaling both the curvature and the system size by temperature-dependent adjustable parameters. (Note that the curvature κ_L is obtained from the $1/L$ expansion only as the numerical accuracy of our MC data is not high enough to allow a good determination of the curvature.) In figure 3.6 we plot the best-fit parameter ξ_{fit} versus r and compare it to a direct determination of the correlation length through MC simulations and the instanton technique: we find a very good agreement between the two sets of data. The same agreement is obtained for χ_{fit} which is found proportional to the correlation length, ξ_{fit} or ξ, as expected in one dimension.

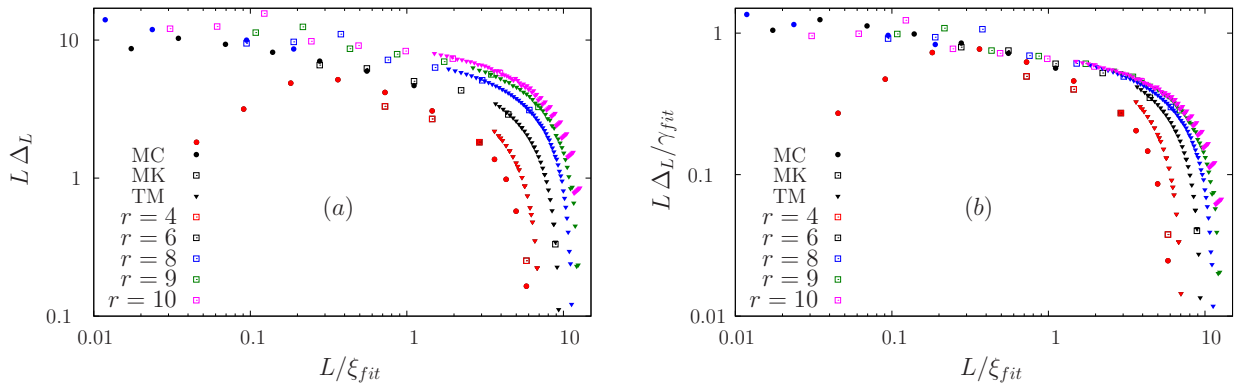

Figure 3.7: (a) Log-log plot of the barrier height times the system size, $L\Delta_L$, versus L/ξ_{fit} for $\beta = 1$, $c = 2r$, $r = 4$, 6, 8, 9, 10. Filled circles correspond to MC data. Empty squares are obtained using the $1/L$ expansion with the real-space RG approach and filled triangles correspond to the $1/L$ expansion with the transfer-matrix approach. (b) Same data with an adjustment of the vertical axis, $L\Delta_L/\gamma_{fit}$, to provide the best collapse for $L/\xi_{fit} < 1$.

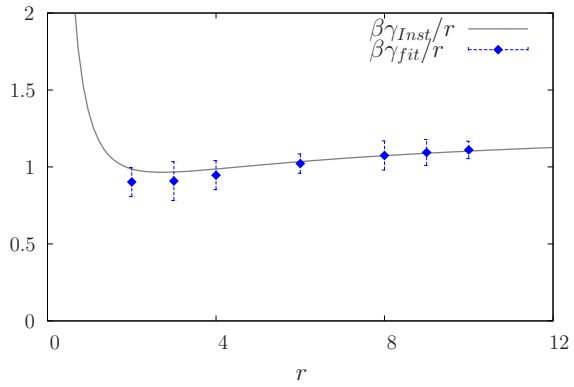

Figure 3.8: Plot of the scaling parameter γ_{fit}, multiplied by β/r, versus r and comparison with the direct instanton computation of the surface tension. The error bars are associated to the uncertainty of the collapse procedure. Recall that we have set $\beta = 1$ and $c = 2r$, so that the temperature dependence is controlled by r, with $\gamma \propto r$. Note also that the instanton calculation breaks down at small r.

In figure 3.7 (a), we display a log-log plot of $L\Delta_L$ versus L/ξ_{fit} where ξ_{fit} is obtained from the previous data collapse in figure 3.5. (As could be anticipated, the $1/L$ expansion fails completely for $L/\xi \lesssim 1$ and is not shown here.) figure 3.7 (b) then shows the same data with $L\Delta_L$ divided by a temperature-dependent adjustable parameter γ_{fit} that ensures the best collapse of all curves for $L/\xi < 1$ (this parameter is determined up to a multiplicative constant). When plotted as a function of r, we find that this best-fit parameter γ_{fit} matches very well the r dependence of the direct estimate of the surface tension of the model through the instanton technique: see figure 3.8. Here, $\beta = 1$ and $c = 2r$, so that $\beta\tilde{S}^\star = 4r/3 - (1/2)\ln r$ for large enough r. We have arbitrarily adjusted the unknown constant in γ_{fit} so that the latter is roughly equal to $2\beta\tilde{S}^\star$: the plot in figure 3.7 (b) is shown with this choice of constant (which merely shifts all curves by a constant amount on the log scale).

These plots therefore confirm that the ideas and recipes we have proposed to extract the correlation length ξ, the susceptibility χ and the surface tension γ (or alternatively the amplitude of the gradient

term c) from finite-size numerical data for the effective potential work nicely. Without *a priori* knowledge one can empirically determine the relevant parameters of the underlying (effective) theory from observations on finite-size systems.

3.3 Nonperturbative renormalization group

We also attacked the same problem by using a specular and complementary approach: starting from a known microscopic (or to the least effective) theory and trying to include the fluctuations, in particular possibly strongly nonperturbative ones, to describe the observed macroscopic behavior. The method of choice that could possibly achieve this is the RG, more precisely the nonperturbative RG (NPRG), see section 2.2. Being able to capture the effect of nonperturbative fluctuations via a NPRG approach (supposed capable to taken then into account efficiently) on the model under study could open the way to new ideas for treating the effect of activated phenomena in supercooled liquids, where they are ubiquitous. All details of this section are relegated to appendix A.3, as it does not enter directly in the topic of this thesis.

Applications of the NPRG formalism to the one-dimensional φ^4 theory have been previously considered. [169, 170, 171, 172] In these studies it was found that simple approximation schemes fail to recover the low-temperature physics of the model, in particular the activated scaling form of the correlation length ($\xi \propto e^{\beta S^\star}$). To understand the underlying reason for this failure, an exact asymptotic low-temperature form of the running effective action $\Gamma_k[\phi]$ has to be derived by using the instanton approach and a mapping to the one-dimensional Ising model.

We tested different approximation schemes for the expression of the effective action. The first one is the so-called derivative expansion, where the running effective action at scale k is expanded in gradients of the field. Unfortunately finite truncations of the derivative expansion are unable to reproduce the exact features of the low-temperature physics. The lowest order in the derivative expansion is given by the LPA. In this case the return to convexity of the potential $U_k(\phi)$ when k is lowered is observed, as it can be seen on figure 3.1 (b), determined using the Litim regulator given in equation (2.22). The LPA provides a good description for values of T higher than the energy barrier of the double well, or more precisely than the instanton energy cost $S^\star$. Nevertheless, it fails to reproduce the low-temperature results with a thermally activated dependence of the correlation length, $\propto \exp(\beta S^\star)$. For instance, the curvature of the effective potential in zero, $\kappa_{k=0} = U''_{k=0}(0)$, which should vanish exponentially when $T \to 0$ as $\exp(-\beta S^\star)$ (see also section 3.2) is generically found to vanish as a power law of T instead. The nonperturbative regime associated with the rare localized events, which is captured by the instanton calculation, is therefore completely missed.

Actually, going to any finite order of the truncation of the derivative expansion, one always finds an inconsistency in the higher order flow equation. The right-hand side is of higher order in $\exp(\beta S_k^\star)$ than the left-hand side and precludes from the extraction of an asymptotic behavior when $\beta S_k^\star \to \infty$. This is however corrected by cancellation of terms in the non-truncated approximation, effect that cannot take place at all orders when the truncation is finite. The appropriate ansatz of $\Gamma_k[\phi]$ would therefore contain an infinite sum of derivative terms of the form $(\partial\phi(x))^{2l}$. This however leads to an infinite set of differential equations that cannot be treated with standard methods. Another routes have been tried, they are briefly explained in appendix 2.2. All of them have failed to properly describe the nonperturbative physics of the one-dimensional φ^4 at low temperature. More work is needed to possibly find a solution to this unsatisfactory theoretical situation.

3.4 Conclusion

We have studied the φ^4 theory at low temperature in the regime where the behavior of the system is completely dominated by nonperturbative instantonic fluctuations. The variation of the "maximal" spatial extent of these fluctuations, possibly controlled by the size of the system, gives rise to nontrivial shape of the effective potential. It has a double-well shape when fluctuations are "absent" (small sizes), suffers nontrivial changes when they are progressively included (size increases), and converges toward a convex shape when fluctuations occur at all scales (thermodynamic limit).

This shape variation is intimately related to the parameters of the underlying microscopic or effective theory. For the φ^4 theory studied here, surface tension and correlation length can be extracted from empirical analysis of the curvature in zero and of the barrier height of the effective potential obtained from the numerical study of finite-size systems. This strategy could be very useful in the analysis of finite-size numerical simulation of glassy systems where a Franz-Parisi potential can be defined. Such analysis of this potential and its fluctuations could allow to extract the parameters of the effective theory of supercooled liquids in the thermodynamic limit, which would supposedly map on a RFIM-like theory.

We also illustrate the difficulty to describe the low-temperature nonperturbative physics of the one-dimensional φ^4 theory through truncations of the NPRG.

Chapter 4

Short- and long-range fluctuations in glassy plaquette spin models

Contents

The results of this chapter have been published in [173].

When coupling different copies of glassy systems, and when considering the similarity or averaged overlap between configurations as an order parameter, the mean-field theory of glasses predict a first-order transition line in the temperature (T)−coupling (ε) plane separating a low-overlap from a high-overlap phase and terminating in a critical point (see also section 1.1.3.4). In particular, this line terminates at $\varepsilon = 0$ (which then corresponds to the usual physical situation for glass formation) at a temperature $T_K > 0$, corresponding to a realization of the entropy crisis of the RFOT scenario.

Such field-induced transitions were also recently found in several computer simulations for 3-dimensional Lennard-Jones or hard-spheres glass-forming liquids, albeit for small systems. [97, 98, 99, 100] The presence of this first-order transition for some positive value of ε was sometimes viewed as an indirect evidence of the existence of a RFOT scenario (at $\varepsilon = 0$) in finite-dimensional glass-formers. However, since as soon as ε is too small the system equilibrates on out-of-experimental time scales and no transition line can be found, this assumes that a smooth extrapolation of the $\varepsilon > 0$ transition line can be done down to $\varepsilon = 0$, which is not evident since, *e.g.*, some singularity could be present around $\varepsilon \simeq 0$.

Recently, the thermodynamic behavior of coupled plaquette spin models models (see also section 1.1.5.1) with $p = c$ was studied in dimensions $d = 2$ and $d = 3$, [174, 108, 109] which correspond respectively to the triangular-plaquette model (TPM) with $p = c = 3$ and the square-pyramid model (SPyM) with $p = c = 5$. These works presented strong numerical evidence for the existence of a transition line in the $T - \varepsilon$ plane. What appears specific, though, about the thermodynamic transition line

in these plaquette spin models is that it exactly goes to zero temperature at $\varepsilon = 0$, $T_K = 0$, and does so in a singular manner.

This raises an interesting possibility, namely, that fluctuations present in finite-dimensional systems could generically depress the thermodynamic glass transition temperature T_K predicted by the mean-field theory to zero temperature. In particular, this would prevent the appealing extrapolation of the computer-simulation results of a $T - \varepsilon$ transition line for $\varepsilon > 0$ down to $\varepsilon = 0$.

To address the issue of the effect of fluctuations on the first-order transition line, a possibility is to study the thermodynamic behavior of plaquette spin models of glasses in the presence of a coupling between replicas of the system, on a lattice where spatial fluctuations of the order-parameter field are not present, or nearly. In order to do this we can distinguish between long-range and short-range fluctuations. The distinction appears somehow arbitrary because fluctuations may of course appear on a continuum of scales. What is meant by "long-range fluctuations" are long wave-length fluctuations whose correlations in space may become scale-free, *e.g.*, near critical points. They are responsible for the difference between mean-field and finite-dimensional results at criticality or for the disappearance of metastability in finite dimensions; they can be present in (infinite) Euclidean lattices, but not in Bethe lattices and other tree-like or fully-connected structures in which the spatial correlations are intrinsically limited. "Short-range fluctuations" instead denote here fluctuations that are associated with the local environment, as, *e.g.*, the connectivity of the lattice, and that never become scale-free: such fluctuations are present in Bethe lattices (and Euclidean lattices as well of course) but are absent in the fully connected lattice which is typically a fluctuation-less system.

This study will give us more insight on the proper effect of long-range and short-range fluctuations in specific glassy systems that are plaquette (spin) models.

4.1 The plaquette spin models

The Hamiltonian of the plaquette spins models reads

$$H[\mathcal{C}] = -\frac{J}{2} \sum_{\mu} \sigma_{\mu 1} \cdots \sigma_{\mu p} \tag{4.1}$$

where $\mathcal{C} \equiv \{\sigma_i\}$ denotes the spins configuration on a lattice of N sites, J is a positive coupling, $\sigma_{\mu\alpha} = \pm 1$, μ is the index characterizing the elementary plaquettes of the lattice, and α spans the p sites around the plaquette. This Hamiltonian is the same as the p-spin model one given in equation (1.7) where the random coupling between spins J_{ij} has been replaced by the constant J, and the interactions do not occur between p randomly chosen spins but on one plaquette containing p spins.

We will study two cases with $c = p$, either the TPM where $c = p = 3$ and the SPyM where $c = p = 5$. Both plaquette models Euclidean lattice structure are represented on figure 4.1: the TPM is designed for a triangular lattice, where the plaquettes are the upward-pointing triangles; the SPyM is constructed on a body-centered cubic lattice, where each square-based upward pyramid is a plaquette.

We recall (see also section 1.1.3.2) that the overlap at site i between two configurations $\mathcal{C} \equiv \{\sigma_i\}$ and $\mathcal{C}' \equiv \{\sigma'_i\}$ (measuring the similarity between them) is defined as

$$q_i = \sigma_i \, \sigma'_i \, . \tag{4.2}$$

As $\sigma_i = \pm 1$, it is clear from its definition that it is also an Ising variable, with $q_i = \pm 1$.

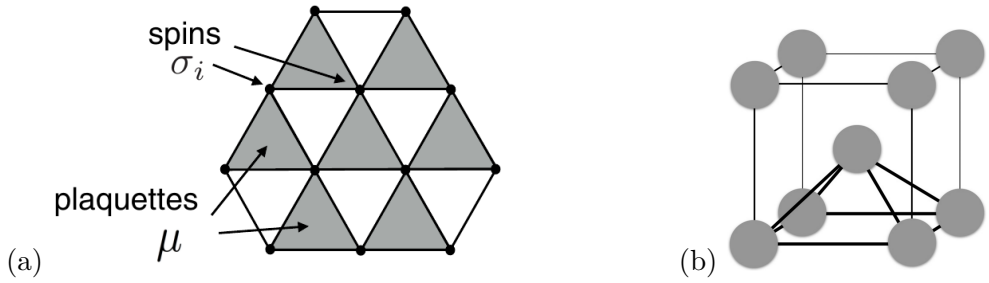

Figure 4.1: TPM and SPyM on Euclidean lattices. (a) Triangular plaquettes ($c = p = 3$) enlightened in gray, the ferromagnetic interactions involve the 3 spins of each upward-pointing triangle in a triangular lattice. (b) Square-pyramid plaquette ($c = p = 5$), interactions involve the 5 spins (gray balls) of each upward-pointing square-based pyramid on a body-centered cubic lattice. Both reprinted from [108].

4.1.1 Different couplings between configurations

Garrahan, Turner and Jack studied coupled systems in two different settings: an "annealed" one, where two coupled replicas of the system evolve together, for the 2-d (TPM) and 3-d (SPyM) systems [174, 108] and a "quenched" one, where the configurations of the system are biased to be similar to a fixed reference configuration, for the 3-d (SPyM) case [109].

In all cases one has to study the thermodynamics in the presence of an attractive coupling between configurations. The two settings are presented in detail below.

Quenched coupling

In this case one is interested in the distribution of the overlap between the system's configurations and a fixed reference equilibrium configuration $\mathcal{C}_0$ [67, 68]. The probability of a configuration $\mathcal{C}$ in the presence of an attractive coupling ε with $\mathcal{C}_0$ is then given by

$$p_\varepsilon[\mathcal{C}|\mathcal{C}_0] = \frac{1}{Z_\varepsilon[\mathcal{C}_0]} e^{\frac{\beta J}{2}\sum_\mu \sigma_{\mu 1}\cdots\sigma_{\mu p} + \beta\varepsilon \sum_i \sigma_i \sigma_i^0}\,, \tag{4.3}$$

where i and μ respectively denote the sites and the elementary plaquettes of the lattice, and ε is the strength of the attractive coupling.

From the normalization factor $Z_\varepsilon[\mathcal{C}_0]$ one defines $(-\beta)$ times the free energy of the system as a function of ε: $W_\varepsilon[\mathcal{C}_0] = \ln Z_\varepsilon[\mathcal{C}_0]$.

Due to the dependence on $\mathcal{C}_0$ this is a random function and it can be characterized by its cumulants, $W_1(\varepsilon) = \overline{W_\varepsilon[\mathcal{C}_0]}$, $W_2(\varepsilon,\varepsilon') = \overline{W_\varepsilon[\mathcal{C}_0] W_{\varepsilon'}[\mathcal{C}_0]} - \overline{W_\varepsilon[\mathcal{C}_0]}\;\overline{W_{\varepsilon'}[\mathcal{C}_0]}$, etc., where the overline denotes an average over the reference configuration. Although one could investigate the influence of a reference configuration equilibrated at a different temperature than the physical one $T = 1/\beta$ ($k_B = 1$), we focus here on the most relevant case where the reference configuration is drawn from the equilibrium Boltzmann distribution at temperature T:

$$p[\mathcal{C}_0] = \frac{1}{Z} e^{\frac{\beta J}{2}\sum_\mu \sigma^0_{\mu 1}\cdots\sigma^0_{\mu p}}\,. \tag{4.4}$$

The so-called Franz-Parisi potential $V(q)$ (more precisely $\beta\, V(q)$) corresponds to the Legendre transform of $(-W_1(\varepsilon))$ [1],

$$\beta V(q) = -W_1(\varepsilon) + \beta\varepsilon\, q\,, \qquad \text{with} \qquad q = \partial W_1(\varepsilon)/\partial\varepsilon\,, \tag{4.5}$$

where q is the average overlap $q = N^{-1}\sum_{i=1}^N \sigma_i\,\sigma_i^0$. More details on the Franz-Parisi potential $V(q)$ can be found in the section 1.1.3.4, together with references.

[1] $W_1(\varepsilon)$ will be abusively called free energy in the following.

Annealed coupling

In this case one focuses on two coupled replicas $\mathcal{C} \equiv \{\sigma_i\}$ and $\mathcal{C}' \equiv \{\sigma'_i\}$, both equilibrated at the same temperature $T = 1/\beta$ with the Hamiltonian

$$H_\varepsilon[\mathcal{C}, \mathcal{C}'] = H[\mathcal{C}] + H[\mathcal{C}'] + \beta\varepsilon \sum_i \sigma_i \sigma'_i \,, \tag{4.6}$$

where $H[\mathcal{C}]$ is given by equation (4.1). The free energy [2] for the coupled replicas is defined as

$$W^{an}(\varepsilon) = \ln \mathrm{Tr} \exp(-\beta H_\varepsilon[\mathcal{C}, \mathcal{C}']) \,, \tag{4.7}$$

where the trace is over the spin variables $\sigma_i, \sigma'_i = \pm 1$.

4.1.2 From coupled replicas to plaquette models in a field

When $c = p$ the plaquette spin models have a dual representation in which one switches from the Ising spins, σ_i, defined on the sites of the original lattice with connectivity c to the Ising plaquette variables, $S_\mu = \prod_\alpha \sigma_{\mu\alpha}$, placed on the dual lattice with the same connectivity c. As shown for instance in [118, 119, 27, 174], the mapping from one representation to the other is one-to-one with appropriate boundary conditions (at least for the TPM and SPyM studied here).

In terms of the plaquette variables, one can reexpress the Hamiltonian in equation (4.1) as

$$H[\mathcal{C}] = -\frac{J}{2} \sum_\mu S_\mu \,, \tag{4.8}$$

which corresponds to a noninteracting Ising model in an external field $J/2$. This representation in terms of plaquette variables is particularly useful to study the quenched and annealed Franz-Parisi potential.

We first rewrite the Hamiltonian of a interacting spins system in a configuration $\mathcal{C}$ and coupled to a configuration $\mathcal{C}_0$ in terms of the overlap variables $q_i = \sigma_i \sigma_i^0$, introducing the constraint $\sum_{\{\sigma_i = \pm 1\}} \prod_i \delta(q_i - \sigma_i \sigma_i^0) = 1$:

$$e^{-\beta \mathcal{H}_\varepsilon[\{q_i\}|\mathcal{C}_0]} = \sum_{\{\sigma_i = \pm 1\}} e^{\frac{\beta J}{2} \sum_\mu \sigma_{\mu 1} \cdots \sigma_{\mu p} + \beta\varepsilon \sum_i \sigma_i \sigma_i^0} \prod_i \delta(q_i - \sigma_i \sigma_i^0) \,. \tag{4.9}$$

Due to the properties of Ising variables, $(\sigma_i^0)^2 = 1$, one has $\sigma_i = q_i \sigma_i^0$, and $\mathcal{H}_\varepsilon[\{q_i\}|\mathcal{C}_0]$ can be expressed as

$$\mathcal{H}_\varepsilon[\{q_i\}|\mathcal{C}_0] = -\frac{J}{2} \sum_\mu \sigma^0_{\mu 1} \cdots \sigma^0_{\mu p} \, q_{\mu 1} \cdots q_{\mu p} - \varepsilon \sum_i q_i \,. \tag{4.10}$$

By using the dual representation $\sigma^0_{\mu 1} \cdots \sigma^0_{\mu p} = S^0_\mu$ for the configuration $\mathcal{C}_0$, we finally find

$$\mathcal{H}_\varepsilon[\{q_i\}|\mathcal{C}_0] = -\frac{J}{2} \sum_\mu S^0_\mu \, q_{\mu 1} \cdots q_{\mu p} - \varepsilon \sum_i q_i \,. \tag{4.11}$$

In summary, we started with a Hamiltonian with spins variables interacting *via* constant pair interactions, and coupled to random applied fields determined by the reference equilibrium configuration $\mathcal{C}_0$, and eventually found a Hamiltonian with overlap variables (that also are Ising spins) whose pair interactions are now random and coupled to a constant external field ε.

We now consider separately the annealed and the quenched settings.

[2] The same shortcut will be done for $W^{an}(\varepsilon)$.

4.1.2.1 Mapping in the annealed case and self-dual line

We start with the simpler annealed case. The Franz-Parisi potential is obtained from the annealed free energy, which from equations (4.6), (4.7), and (4.11) is given by

$$W^{an}(\varepsilon) = \ln \sum_{\{q_i=\pm 1\}} \left(\sum_{\{S'_\mu=\pm 1\}} e^{\frac{\beta J}{2} \sum_\mu S'_\mu (1+\prod_{\alpha=1}^p q_{\mu\alpha})} e^{\beta\varepsilon \sum_i q_i} \right) , \tag{4.12}$$

where the configuration $\mathcal{C}_0 \equiv \mathcal{C}'$ in equation (4.11) is now considered as annealed and we have therefore replaced the subscript 0 by a prime on S_μ. By performing the sum over the plaquette variables explicitly, one ends up with

$$W^{an}(\varepsilon) = \ln \sum_{\{q_i=\pm 1\}} e^{-\beta \mathcal{H}^{an}_\varepsilon[\{q_i\}]}$$

where the Hamiltonian $\mathcal{H}^{an}_\varepsilon[\{q_i\}]$ reads

$$\mathcal{H}^{an}_\varepsilon[\{q_i\}] = -\frac{1}{\beta} \sum_\mu \ln \left[2\cosh \left(\frac{\beta J}{2} \left(1 + \prod_{\alpha=1}^p q_{\mu\alpha} \right) \right) \right] - \varepsilon \sum_i q_i \, . \tag{4.13}$$

The above expression $\ln \left[2\cosh \left(\frac{\beta J}{2} \left(1 + \prod_{\alpha=1}^p q_{\mu\alpha} \right) \right) \right]$ assumes two values depending on $\prod_{\alpha=1}^p q_{\mu\alpha}$,

$$\mathcal{H}^{an}_\varepsilon[\{q_i\}] = \begin{cases} \ln\left[2\cosh\left(\beta J\right)\right] & \text{if} \quad \displaystyle\prod_{\alpha=1}^p q_{\mu\alpha} = 1 \\ \ln 2 & \text{if} \quad \displaystyle\prod_{\alpha=1}^p q_{\mu\alpha} = -1 \, , \end{cases} \tag{4.14}$$

which gives the effective Hamiltonian:

$$\begin{aligned} \mathcal{H}^{an}_\varepsilon[\{q_i\}] &= -\frac{1}{\beta} \sum_\mu \left\{ \frac{\ln\left[2\cosh\left(\beta J\right)\right]}{2} \left(1 + \prod_{\alpha=1}^p q_{\mu\alpha} \right) + \frac{\ln 2}{2} \left(1 - \prod_{\alpha=1}^p q_{\mu\alpha} \right) \right\} - \varepsilon \sum_i q_i \\ &= -\frac{1}{2\beta} \ln[\cosh(\beta J)] \sum_\mu \prod_{\alpha=1}^p q_{\mu\alpha} - \varepsilon \sum_i q_i + \text{cst} \, , \end{aligned} \tag{4.15}$$

where cst denotes an irrelevant constant.

As first shown by Garrahan [174], the annealed computation therefore amounts to studying a plaquette spin model with a coupling $\tilde{J} = (1/\beta)\ln[\cosh(\beta J)]$ in a uniform external field $\tilde{H} = \varepsilon$. This model is known to have an exact duality property [175, 176, 177], which implies that the partition function $Z(\tilde{J}, \tilde{H})$ associated with the Hamiltonian in equation (4.15) satisfies $Z(\tilde{J}, \tilde{H}) = [\sinh(\beta\tilde{J})\sinh(2\beta\tilde{H})]^{N/2} Z(\tilde{J}', \tilde{H}')$ with $\tanh(\beta\tilde{J}'/2) = e^{-2\beta\tilde{H}}$ and $\tanh(\beta\tilde{H}') = e^{-\beta\tilde{J}}$.

As a result [174, 108], the annealed free energy $W^{an}(J, \varepsilon)$, where we have made the dependence on the coupling J explicit, satisfies

$$W^{an}(J, \varepsilon) - \frac{N}{2} \ln[\sinh(2\beta\varepsilon)] = W^{an}(J', \varepsilon') - \frac{N}{2} \ln[\sinh(2\beta\varepsilon')] \, , \tag{4.16}$$

where $\tanh(\beta J/2) = e^{-\beta\varepsilon'}$ and $\tanh(\beta\varepsilon/2) = e^{-\beta J'}$. There is therefore a self-dual line which is characterized by $\sinh(\beta J)\sinh(\beta\varepsilon) = 1$. If the free energy has a singularity in a point $(\beta J, \beta\varepsilon)$, by equation (4.16) it is also singular in the point obtained by the above transformation. As a result, if the model has a single phase transition, it must take place along the self-dual line which emanates from the point at zero temperature and zero coupling, $T = \varepsilon = 0$. Note that the result is valid for the Euclidean lattices as well as for the Husimi trees, provided $c = p$.

4.1.2.2 Mapping in the quenched case

We now consider the quenched case. The reference configuration $\mathcal{C}_0$ in equation (4.10) represents some quenched disorder. More precisely, from the form of the Hamiltonian in equation (4.10) the disorder appears as random couplings, JS^0_μ. Computing the quenched Franz-Parisi potential is then tantamount to obtaining the partition function of a model with random p-spin interactions in a uniform external field. Therefore it corresponds to ($-1/\beta$ times) the quenched average free energy, which using equations (4.3), (4.11) is given by

$$W_1(\varepsilon) = \overline{\log Z_\varepsilon[\mathcal{C}_0]} \propto \sum_{\{S^0_\mu=\pm 1\}} p(\{S^0_\mu\}) \ln \sum_{\{q_i=\pm 1\}} e^{\beta \frac{J}{2} \sum_\mu S^0_\mu q_{\mu 1}\cdots q_{\mu p} + \beta\varepsilon \sum_i q_i} . \tag{4.17}$$

The distribution of the random interactions (4.4) are given by that of the variable S^0_μ, which for an equilibrium distribution at temperature $T = 1/\beta$ is simply

$$p(\{S^0_\mu\}) \propto \prod_\mu \exp\left[\left(\frac{\beta J}{2}\right) S^0_\mu\right] . \tag{4.18}$$

The average of $\overline{S^0_\mu}$ is $\tanh(\beta J/2)$, whereas the variance is given by $\overline{S^0_\mu S^0_\nu} = \tanh^2(\beta J/2) + \delta_{\mu\nu}[1 - \tanh^2(\beta J/2)]$. Thus, the disorder is such that the average interaction is ferromagnetic and the fluctuations are smaller than the mean value, in particular at low temperature.

The computation of the free energy $W_\varepsilon[\mathcal{C}_0]$ does not lead to further simplifications, such as the self-dual line found in the annealed case.

4.2 Euclidean-lattice triangular and square-pyramid plaquette models

In the annealed case, the two models, TPM (2d) and SPyM (3d), both display a first-order transition line in the $T - \varepsilon$ plane between a phase with a low overlap between the two replicas and one with a high overlap [174, 108]. Thanks to the duality relation (4.16), one knows that the transition line must be along the self-dual line, which is defined by the relation $\sinh(\beta J)\sinh(\beta\varepsilon) = 1$. This line terminates in a critical point that was found to be in the universality class of the Ising model [108], as originally predicted in the work [101]. The results are reprinted on figure 4.2 (a).

In the quenched case, for the 3-d SPyM, numerical simulations by Jack and Garrahan[109] gave evidence for the existence of a first-order critical line terminating in a critical point in the universality class of the random-field Ising model (RFIM), as theoretically predicted [101, 102], see figure 4.2 (b).

The represented transition line (on figure 4.2 (b)) is an estimation, based on a scaling near $\varepsilon \simeq 0$, $T \simeq 0$, which is obtained in two steps. First evaluating the configurational entropy on the transition line $\varepsilon^\star(T)$, given by the height difference of the two minima of $V(q)$ given in (4.5):

$$T\, S_c(T) = V(q \simeq 1) - V(q \simeq 0) \simeq \Delta q\, \varepsilon_\star(T) , \tag{4.19}$$

where $\Delta q \simeq O(1)$ is the overlap difference between minima. One has then to estimate the configurational entropy $S_c(T)$. In plaquette models it is expected to behave as the total Shannon entropy $S = -\sum_i p_i \log p_i$, where p_i is the probability of the state i. [109] (Indeed there is no intra-state entropy since $T \simeq 0$.) At very low temperature, one defect plaquette $S_\mu = -1$ has a probability weight $e^{-J/T}$ and the relevant configurations are only composed by *one* defect, more defects yielding an infinitely less

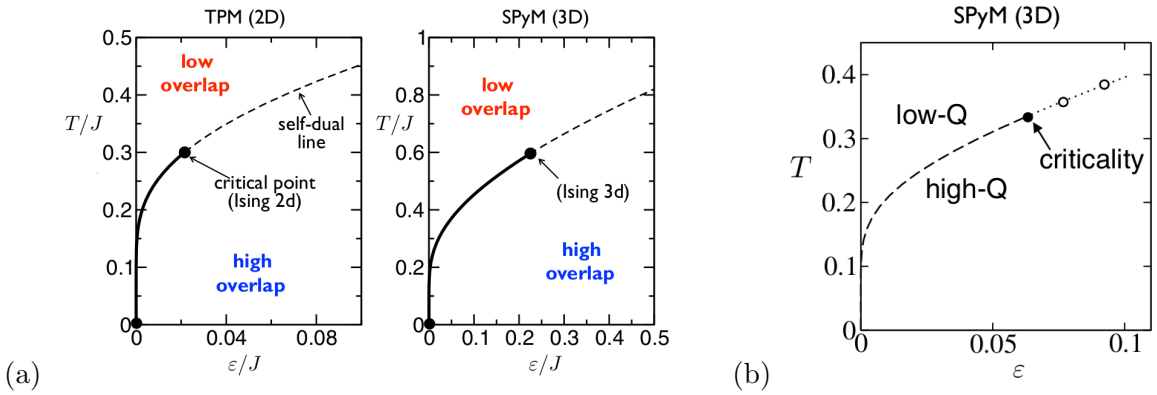

Figure 4.2: Temperature T versus coupling $\beta\varepsilon$ phases diagrams for the plaquette spin models. (a) TPM (2d) and SPyM (3d) in the annealed case. The dashed line is the continuation of the self-dual line, and the terminal critical point are in the Ising universality class. Reprinted from [108]. (b) SPyM (3d) in the quenched case. The large-dashed line is an estimation based on of the scaling $\varepsilon \simeq Ae^{-1/T}$ for $\varepsilon \simeq 0$, $T \simeq 0$ ($A = 1.25$) and passing by the points at which the transition has effectively been detected. Unfilled circles localize a second order transition line. The TPM presents no transition line in the quenched case, as the disorder kills it in 2d (see main text). The terminal critical point is in the random-field Ising model universality class.

favorable configuration when $T \to 0$. Hence the total entropy writes $S \underset{T\to 0}{\sim} J/T\, e^{-J/T}$, which allows to localize the first-order transition line:

$$\varepsilon_\star(T) \underset{T\to 0}{\sim} J\, e^{-J/T}\,. \tag{4.20}$$

This relation is actually valid for the quenched case and the annealed case TPM and SPyM on both Euclidean and Bethe lattice, the above arguments being applicable in all the cases. It is moreover visible on the figures 4.2 for the Euclidean case, and as we shall show, is the same in the Bethe case.

Note that in the quenched case there should be no finite-temperature phase transition for the TPM. Due to the presence of quenched disorder, the existence of the first-order transition line and of a terminal critical point in the universality class of the RFIM is excluded in $d = 2$. The presence of quenched disorder kills the transition in dimensions $d \leq 2$, as it was explained with the Imry-Ma argument [90, 94] and its rigorous formalization by Aizenman and Wehr [178].

In appendix B.1 we give heuristic arguments for why, as expected on general grounds [101, 102], the terminal critical point of the coupled plaquette spin models in the annealed setting is in the Ising universality class of the simple Ising model and that in the quenched setting in the universality class of the RFIM.

4.3 Bethe-lattices triangular and square-pyramid plaquette models

In order to discuss a mean-field version of the TPM and the SPyM that correctly takes into account "short-range fluctuations" we consider plaquette models on Bethe hyper-lattices (or Husimi trees, the analog of a Bethe lattice for systems with plaquette interactions [179]).

In the present case, the lattice is formed of elementary plaquettes of p sites that are connected through a tree-like structure with a fixed connectivity c. Each spin is involved in exactly c plaquettes, hence in c distinct p-spin interactions. Due to the tree structure, spatial fluctuations are restricted and the models have a mean-field character.

We are primarily interested in the Bethe (hyper) lattice versions of the 2-dimensional TPM, which corresponds to $c = p = 3$, and of the 3-dimensional SPyM, which corresponds to $c = p = 5$. In these cases, the lattice is a Husimi tree in which each site is connected to exactly $c = p$ elementary plaquettes, themselves comprising exactly p sites forming a triangle for the TPM and a pyramid for the SPyM: see figure 4.3 for the case $c = p = 3$.

As already mentioned, the mapping between site and plaquette variables, the mapping between coupled replicas and plaquette spin models in a field, and the duality relations hold also for Bethe hyper-lattices. They will be used in the following to simplify the analysis. Although we focus on models with $c = p$, it is also interesting to study cases in which c is different from p in order to discuss the results from a more general perspective. Along the way, we will therefore consider the treatment for generic values of c and p.

4.3.1 Quenched case

When $c = p$, one expects that, if present, the phase transitions consist in a single first-order line terminating in a critical point. On general grounds one expects the mean-field, *i.e.*, Bethe-lattice, critical temperature to be higher than its Euclidean counterpart.

Furthermore, due to the tree structure of the Bethe hyper-lattice, one can derive self-consistent equations that allow one to obtain the phase diagram in the $T - \varepsilon$ plane. This imply to use the so-called cavity method [179, 180, 181, 182], allowing to derive self-consistent recurrence equations on the "cavity field". The cavity field $h_\mu^{(i)}$ represents the effect on site i of plaquette μ of all the spins except those involved in the plaquettes other than μ containing the site i (see figure 4.3). To do so, the primary assumption is that the different cavity fields of a Husimi tree are uncorrelated in the large-size limit. Typical loops are indeed of order log(size) and have a vanishing contribution when the system size goes to infinity.

One sub-tree of connectivity c can be constructed from a plaquette of p sites by adding $(p-1)(c-1)$ branches emanating from $p-1$ sites and by leaving unconnected one "cavity" site. In turn, $(p-1)(c-1)$ such sub-trees, whose cavity fields are known, can be attached to a new plaquette μ to form a new, larger, sub-tree (figure 4.3).

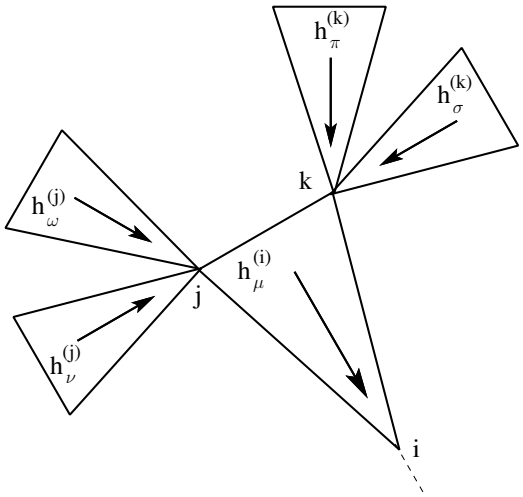

Figure 4.3: Local structure of the Bethe hyper-lattice for $p = c = 3$. The cavity fields that satisfy the recursive cavity equation in equation (4.23) are also shown.

For one configuration $\{q_\mu^{(1)},...,q_\mu^{(p)}\}$ of the plaquette μ, the energy $E_\mu(\{q_\mu^{(1)},...,q_\mu^{(p)}\})$ of the new sub-tree can be written as the sum of the contributions due to the individual effective cavity fields acting on sites $\{1,...,i-1,i+1,...,p\}$ of plaquette μ plus the energy of the plaquette in the presence of a constant external field ε (not counted on site i):

$$E_\mu(\{q_\mu^{(1)},...,q_\mu^{(p)}\}) = -\frac{J}{2}S_\mu \prod_{j\in\mu} q_\mu^{(j)} - \sum_{j\in\mu\backslash i}(\varepsilon + H_\mu^{(j)})q_\mu^{(j)} \tag{4.21}$$

where $H_\mu^{(j)} = \sum_{\nu\ni j\backslash\mu} h_\nu^{(j)}$ is the total cavity field acting on site j. The notations $\backslash i$ and $\backslash\mu$ mean that we exclude the spin i or the plaquette μ from the sum, and Greek letters refer to plaquettes and Latin letters to sites. The mapping from section 4.1.2.2 has been used to write (4.21).

Then, $S_\mu = \pm 1$ (we have dropped the superscript 0 from the notations of the previous section) is a binary random variable taken from the distribution $p[S_\mu = \pm 1] = e^{\pm\beta J/2}/[2\cosh(\beta J/2)]$. Tracing out over the configurations $\{q_\mu^{(1)},...,q_\mu^{(i-1)},q_\mu^{(i+1)},...,q_\mu^{(p)}\}$ gives the effective cavity field $h_\mu^{(i)}$ acting on site i of the plaquette μ via

$$Ce^{\beta h_\mu^{(i)} q_\mu^{(i)}} = \sum_{\{q_\mu^{(1)},...q_\mu^{(p)}\backslash q_\mu^{(i)}\}=\{\pm 1\}} e^{-\beta E_\mu(\{q_\mu^{(1)},...,q_\mu^{(p)}\})} \tag{4.22}$$

with C a normalization constant. Equation (4.22) can be further rewritten as [179]

$$\tanh(\beta h_\mu^{(i)}) = \tanh\left(\frac{\beta J S_\mu}{2}\right) \prod_{j\in\mu\backslash i} \tanh\left[\beta \sum_{\nu\ni j\backslash\mu} h_\nu^{(j)} + \beta\varepsilon\right] . \tag{4.23}$$

Figure 4.3 provides a visual representation of the cavity fields.

The $h_\mu^{(j)}$'s are random variables that depend on the disorder realization. Therefore, we have to follow their whole probability distribution $P(h)$. In the thermodynamic limit, equation (4.23) becomes a self-consistent equation for $P(h)$:

$$P(h) = \sum_{S_\mu=\pm 1} p[S_\mu] \int \prod_{j=1}^{c-1}\prod_{\nu=1}^{p-1} \left[dh_\nu^{(j)} P(h_\nu^{(j)})\right] \delta\left(h - h_\mu^{(i)}\right) \tag{4.24}$$

with $h_\mu^{(i)}$ given by equation(4.23). Note that these cavity equations are valid for all values of c and p.

This equation can be solved numerically by using population dynamics [179, 181, 182], with a population of 10 millions fields.

4.3.2 Annealed case

Thanks to the duality relation, one knows that the transition line on the Bethe lattice must be along the *same* self-dual line as for the Euclidean case, which is defined by the relation $\sinh(\beta J)\sinh(\beta\varepsilon) = 1$. Therefore, only the location of the terminal critical point is different.

The cavity method explained in the previous section can be applied to the simpler annealed case. In the case of annealed setting, the quenched disorder is absent and the plaquette interaction coupling is fixed to $\widetilde{J} = (1/\beta)\ln[\cosh(\beta J)]$. Therefore $P(h)$ (4.24) converges to a Dirac delta function and we have to solve a simple self-consistent recurrence equation on the cavity field h:

$$\tanh(\beta h) = \tanh\left(\frac{\beta\tilde{J}}{2}\right) \tanh\left[\beta(c-1)h + \beta\varepsilon\right]^{p-1} . \tag{4.25}$$

Note that these cavity equations are valid for all values of c and p.

After solving this equation and plugging the solution into the expression of the free energy of the plaquette model model in a field one can reconstruct the phase diagrams. The details of the computation of the intensive annealed free energy from the cavity solution are given in appendix B.2.

4.3.3 Phase diagrams

In both quenched and annealed settings, after solving the equation for the cavity field and plugging the solution into the expression of the free energy of the plaquette model in a field one can reconstruct the phase diagrams. The details of the computation of the intensive quenched and annealed free energies are given in appendix B.2. The first order transition line from a high-overlap to a low-overlap phases is determined by finding, for fixed values of the temperature T, the field $\varepsilon_\star(T)$ for which the intensive free-energy values of the two phases are equal. For each setting, this is done by injecting the two solutions (one for the low-overlap phase and the other for the high-overlap phase) of the above cavity equations into the corresponding free-energy expression. This gives two functions of ε (at fixed T) that has to be varied until they are equal, then $\varepsilon = \varepsilon_\star(T)$.

The phase diagram that we obtain for the SPyM is shown in the upper left panel of figure 4.4 (a) while that for the TPM is shown in the left panel of figure 4.4 (b). In both cases, the transition line emerges from the singular point at $T = 0$ and $\varepsilon = 0$. As anticipated, the transition line in the annealed case is on the self-dual line. It is always above the quenched transition line, as could have also been expected since disorder suppresses the transition.

Both the annealed and the quenched transition lines $T_\star(\varepsilon)$ (or equivalently, $\varepsilon_\star(T)$), display a singular behavior, $\varepsilon_\star(T) \sim J\, e^{-J/T}$ given in equation (4.20), when $T \to 0$.

Finally, the results obtained here for the SPyM and the TPM on Bethe hyper-lattices can be compared with those on Euclidean lattices. For the SPyM they are plotted together with the numerical results and estimates of [109] in figure 4.5. The agreement is quite remarkable in this case. As expected for any mean-field treatment, the critical temperatures are overestimated compared to the $d = 3$ case, but the overall features of the phase diagram, including the singular behavior when T and ε go to zero are similar in both descriptions. For the TPM, the annealed results are in good agreement between the Bethe hyper-lattice and the 2-dimensional (triangular) lattice. As already mentioned, this however can no longer be true for the quenched case: a transition is found on the Bethe lattice whereas it should be absent in $d = 2$.

The main lesson brought by these results is that the singular behavior of the transition line in the TPM and SPyM, with a transition temperature that goes to zero when the coupling goes to zero, is *not* the consequence of the long-range fluctuations, hence not an intrinsic property of finite dimensions. The very same behavior is found in the Bethe-lattice versions of the TPM and SPyM.

4.4 Role of fluctuations in glassy plaquette spin models

4.4.1 Short-range fluctuations

One can probe the role of short-range fluctuations by changing the connectivity c at fixed p for the Bethe hyper-lattice. In the absence of coupling ε, it is known that the plaquette spin models on Bethe lattices can display, as temperature is lowered, a sequence of two transitions [179, 183, 184, 185, 186]: a dynamical one T_d and a static one at T_K, yielding an exact realization of the mean-field RFOT scenario (see section 1.1.3.1). Adding a bias in the form of an attractive coupling ε with other configurations

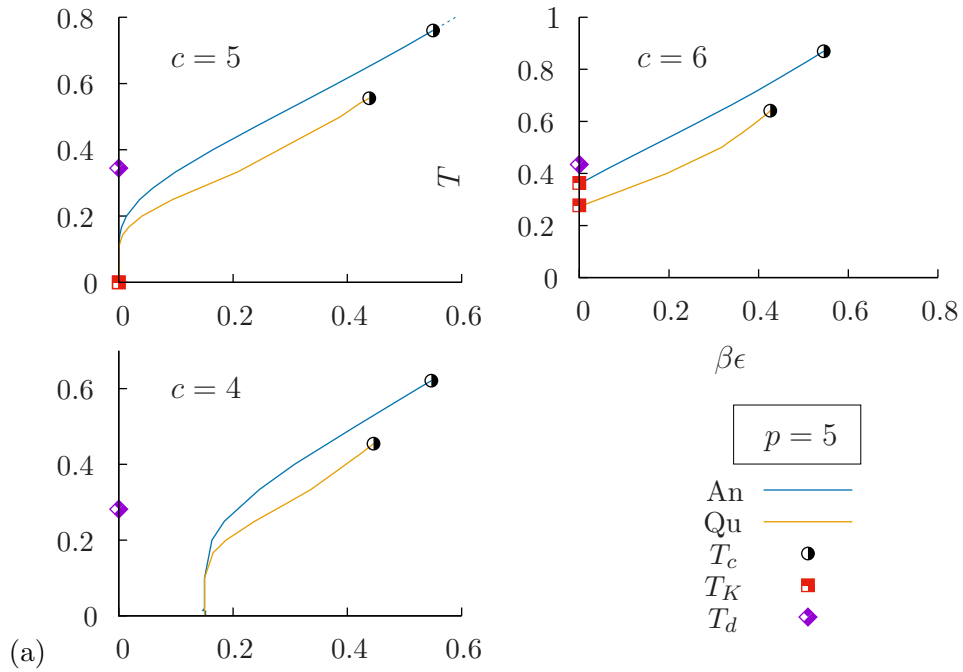

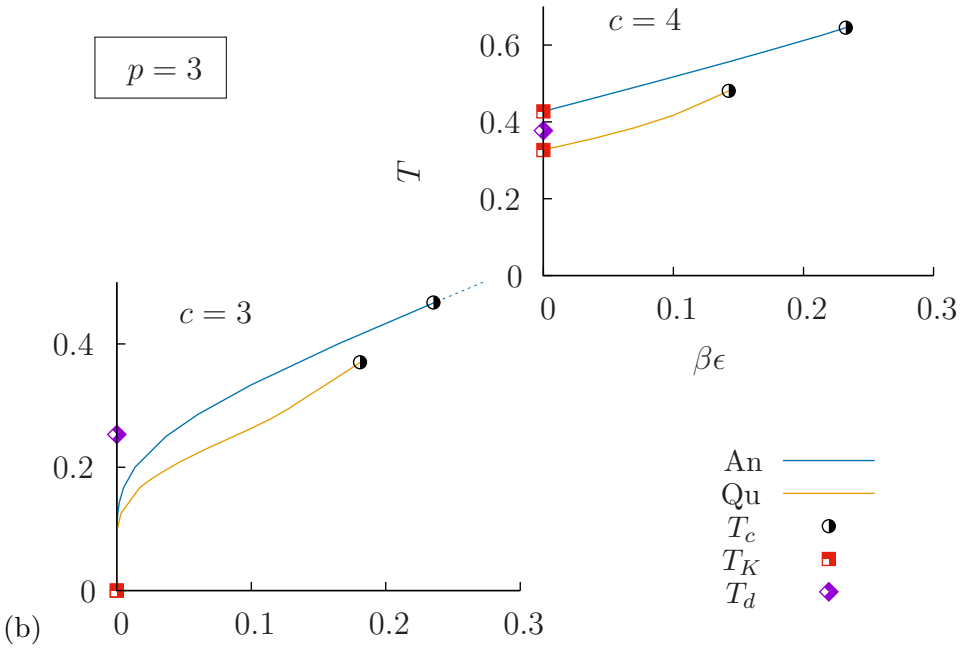

Figure 4.4: Temperature T versus coupling $\beta\varepsilon$ phases diagrams for the plaquette spin models in both the annealed and the quenched descriptions on Bethe hyper-lattices with (a) $p = 5$ and $c = 4, 5, 6$, and (b) $p = 3$ and $c = 3$ and $c = 4$ ($c = 2$ corresponds to the 1-dimensional chain and is of no interest here). The interaction strength J is set equal to 1. The dashed line is the continuation of the self-dual line (see text). We consider $\beta\varepsilon$ instead of ε for the horizontal axis to better compare all cases; otherwise the transition line for $c = 4$ terminates in $\varepsilon_\star = 0$ at $T = 0$, although the situation is quite different from the case $c = 5$ because there is a nonzero configurational entropy at $T = 0$ and $\varepsilon_\star$ actually scales as T and not $J \exp(-J/T)$.

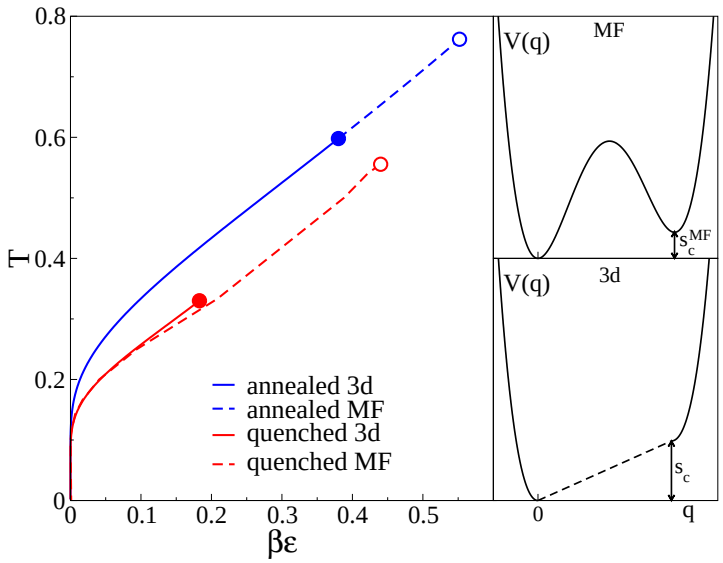

Figure 4.5: Temperature T versus coupling $\beta\varepsilon$ phase diagram of the square-pyramid model (SPyM) in both the annealed and the quenched descriptions for the Bethe hyper-lattice with $c = 5$ (dashed lines) and for $d = 3$ (full lines [109, 108]). The transition lines are between a high-T phase with low overlap and a low-T phase with high overlap. The interaction strength J is set equal to 1. Inset: Sketch of the Franz-Parisi potential $V(q)$ as a function of the overlap in the mean-field description (left) and for $d = 3$ (right).

then produces a line of first-order transitions between a low- and a high-overlap phase that emanates from T_K and terminates at higher T and ε in a critical point.

For $c > p$ one finds that $T_K > 0$. The phase diagram in the T-$\beta\varepsilon$ plane obtained from the cavity equations, is illustrated in the right panels of figures 4.4 (a) and (b). The annealed transition line (in blue) reaches the vertical axis at a temperature larger than the quenched T_K but that may be either smaller ($c = 6, p = 5$) or larger ($c = 4, p = 3$) than T_d. This is the conventional mean-field RFOT scenario with $T_K > 0$, as it also appears in a fully connected lattice ($c \to \infty$) or in infinite dimensions.

On the contrary, when $c < p$ the configurational entropy $S_c(T) \simeq \beta\varepsilon_\star(T)$ from equation (4.19) remains nonzero in $T = 0$ at $\varepsilon = 0$ and there is therefore no Kauzmann transition in the absence of coupling. The transition line persists down to a threshold value c_d of the connectivity but it reaches the zero-temperature line at a nonzero value of the rescaled coupling $\beta\varepsilon_\star$ (see figure 4.4 (a)) [3].

The case $c = p$, which can also be realized in Euclidean space, appears somehow marginal: there is an entropy catastrophe but exactly at zero temperature, *i.e.*, $T_K = 0$.

Short-range fluctuations therefore appear very influent on the thermodynamic behavior of plaquette spin models in zero field. They are responsible of the location of the transition line in $\varepsilon = 0$ and of the existence of a RFOT (either in $T_K = 0$ or > 0) or not. This is in agreement with a previous work where short-range fluctuations were argued to be important for the RFOT scenario. [187]

[3] Both lines terminate at the same value of ε. This is due to the fact that in the zero-temperature limit the couplings do not fluctuate any longer in the quenched case: they all become equal to J. In consequence, quenched and annealed settings coincide.

4.4.2 Long-range fluctuations

The role of long-range fluctuations can be assessed by comparing Bethe and Euclidean lattices with the same $c = p$. As seen from figure 4.5, long-range fluctuations do not change the topology of the phase diagram for the SPyM model, neither in the annealed setting nor, if one compares with the numerical results of [109], in the quenched one. They do of course modify the location of the transitions and change the behavior near the critical terminal points: the values of the critical exponent are the classical (mean-field) ones on the Bethe lattice but are those of the $d = 3$ pure or random-field Ising model in Euclidean space (see also appendix B.1).

Long-range fluctuations also enforce convexity of the potential $V(q)$ (see the sketch in figure 4.5) and prevent true metastability. As a result, the dynamical transition found at T_d in $\varepsilon = 0$, which can be associated to a spinodal point (where a secondary minimum first appears in the potential $V(q)$), is avoided and can at best remain in the form of a crossover. However, all this is akin to what is obtained in a conventional 3-dimensional ferromagnet at a first-order phase transition and does not call into question the qualitative or even semi-quantitative relevance of the mean-field description.

For the 2-dimensional case in the quenched setting long-range fluctuations have a more severe influence. The TPM with $c = p = 3$ displays a transition line in the quenched calculation on the Bethe hyper-lattice but the transition should be absent on the triangular lattice. In Euclidean space, $d = 2$ is indeed the lower critical dimension of the RFIM (see section 4.2), which means that the fluctuations depress the transition to zero temperature and zero random-field strength: no finite-temperature transition therefore exists in the $T - \varepsilon$ plane.

4.5 Remarks

As sketched in figure 4.5, if a transition is present in the presence of a biasing field ε in $d = 3$, $V(q)$ remains singular when $\varepsilon = 0$ (with a linear segment) and a configurational entropy S_c (more precisely T times S_c) can then be unequivocally defined at low enough T as the difference between the two ends of the singular segment of $V(q)$, even in the thermodynamic limit and in finite d. This will be in agreement with the mean-field based assumptions underlying the RFOT theory.

Implications for the dynamics can also be done. It has been recently shown that the dynamics of a plaquette spin model on a random-regular graph/Bethe lattice with $c = p$ (the authors focused on $c = p = 3$ but the conclusion is more general)[188] is equivalent to that of a kinetically constrained model of noninteracting spins. So, plaquette spin models with $c = p$ appear to share similar glassy features on Bethe and Euclidean lattices, even at the dynamical level. The dynamics is therefore ruled by the kinetically constrained motion of localized defects. The latter have a relaxation time diverging at zero temperature exactly, as the thermodynamics is totally trivial for the KCM. In particular τ has been computed for the plaquette models with $c = p$, and it appears to have two distinct behaviors depending on if the parameters $c = p$ are even or odd (see section 1.1.5.1). In particular they present either an Arrhenius like or super-Arrhenius like behavior:

$$\begin{aligned} \ln \tau &\propto 1/T \quad \text{if} \quad c = p \quad \text{even}\,, \\ \ln \tau &\propto 1/T^2 \quad \text{if} \quad c = p \quad \text{odd}\,. \end{aligned} \tag{4.26}$$

However, it is clear that the usual RFOT explanation of glassy dynamics in terms of mosaics and entropic droplets does not apply for these models. It stipulates that the relaxation time behaves following $\tau \propto e^{\Delta E(T)/T}$, where the energy barrier $\Delta E(T)$ is given by equations (1.21), (1.22). Replacing the configurational entropy (density) by its value here $S_c(T) \sim J/T\, e^{-1/T}$, the relaxation time would

be given by:

$$\ln \tau \propto \frac{Y(T)^{\psi/(d-\theta)}}{T} \exp\left[\frac{\psi}{(d-\theta)T}\right], \tag{4.27}$$

with $Y(T)$ the surface tension of the droplets of the mosaic scenario and ψ and θ critical exponents. All these quantities are defined in section 1.1.4.1.

This would be in disagreement with the expressions of equation (4.26) be $c = p$ odd or even. One therefore faces different possibilities: The first one is that the RFOT theory gives a good description of the thermodynamics in three dimensions but that it fails for the dynamics. Another is that the RFOT arguments for the slow relaxation hold but that the proposed scalings for ξ and τ (in equations (1.21), (1.23)) designed for a divergence at some $T_K \neq 0$ do not apply since the point-to-set length diverges at zero temperature only. The approach to a zero-temperature glass transition, which is not the usual situation envisaged by the RFOT theory, might lead to important changes. For example metastable states seem to have zero surface tension in plaquette spin models [123], whereas it was some nonzero function $Y(T)$ in the mosaic theory.

4.6 Conclusion

This chapter is an assessment of the role of the fluctuations on overlap-based phase transitions in plaquette spin models of glasses in the presence of a biasing field. Motivated by the computer simulation results of [174, 108, 109] who found a transition line, in the temperature-coupling plane between a low-overlap and a high-overlap phases, that predicts the realization of a RFOT scenario when the coupling is zero at zero temperature exactly with a singular behavior of the transition line, and argued that $T_K = 0$ could eventually be a more generic effect of fluctuations on the RFOT scenario in glass-formers, we addressed the issue of the fluctuations on these plaquette spin models.

We have distinguished the effect of what we called "long-range fluctuations" and "short-range fluctuations" on the RFOT scenario by comparing the thermodynamics of plaquette spin models on Bethe and Euclidean lattices (which is given by the results evoked in the above paragraph). The latter contains all ranges of fluctuations, by definition, whereas the former presents short-range ones only. The description on Bethe lattices is then an improved mean-field approximation.

At least for the 3-dimensional square pyramid model (SPyM), we have seen that the main properties of the transition line, namely the singular behavior when $\varepsilon \simeq 0$ and $T \simeq 0$, the fact that $T_K = 0$ and the overall shape of the line, are qualitatively the same on Bethe and Euclidean lattices and are therefore quite robust to the introduction of long-range fluctuations. Therefore, it appears that the long-range fluctuations are not responsible for the fact that $T_K = 0$ in the SPyM. However, it also appears that the short-range fluctuations, which are tuned by varying the inter-plaquette connectivity on the Bethe lattice, are responsible for the position of the terminal point of the transition line at $\varepsilon = 0$, the situation where $T_K = 0$ being peculiar to the SPyM-like cases where the connectivity is equal to the number of spins per plaquette, as changing this one can also find $T_K > 0$ or no T_K at all.

The mean-field description for the SPyM in $d = 3$, provided that it correctly encompasses the description of the local environment, appears surprisingly robust to the introduction of the long-range fluctuations. In $d = 2$ however, the mean-field description completely fails to describe the thermodynamic properties of the triangular-plaquette model on Euclidean lattice. Indeed, in two dimensions the disorder kills the line of transition whereas the plaquette model with $c = p = 3$ on the Bethe lattice predicts an in-field line of transition. This scenario is also what occurs for the classical Ising model in one dimension, in which there is no transition whereas the mean-field description predicts it; this nevertheless does not modify the validity of the qualitative information (existence of a transition,

nature of the low temperature phase and of the order parameter, *etc*) given by the mean-field approximation is dimensions higher than one. One can then expect that here, where the effective theory is presumably an Ising-like theory with disorder, the failing of the mean-field description to describe the thermodynamics of the system in $d = 2$ does not challenge the validity of the mean-field description in higher dimensions.

The robust mean-field account of the transition line in $d = 3$ could suggest that glassy systems are well described in the absence of bias, as far as the thermodynamic aspects involving the overlap order parameter are concerned, by the mean-field approximation. However standard phenomenological arguments applied to obtain predictions on the dynamics of finite-dimensional systems (to go beyond the mean-field artifact of a dynamical transition occurring at T_d) are not able to capture the true relaxation time of plaquette spin models. An account of the dynamical events allowing the relaxation of finite-dimensional plaquette models from first-principle calculation at the level of the mean-field approximation would be required.

Chapter 5

Space-time fluctuations in Arrhenius systems

Contents

The work of this chapter is still in progress.

5.1 Introduction

In section 1.1.1 we presented the notion of dynamical heterogeneities; see [40] for a reviewing book. They can be characterized by a dynamical correlation length $\xi_d(t)$ through the 4-point space-time correlation function $g_4(r,t)$, $\xi_d(t)$ describing how far the motion of particles is correlated during an elapsed time t. The "nonlinear dynamic susceptibility" $\chi_4(t)$ gives access to the maximal value of $\xi_d(t)$ which corresponds to a time of order of the α-relaxation time.

The measure of the two above quantities requires a "tracking" of all the particle positions. This is easy in simulations, but impossible in real experiments. In the latter case one prefers the use of "response functions" which quantify how the system reacts to some external, well-controlled, perturbation. Unfortunately, nor $g_4(r,t)$ or $\chi_4(t)$ are directly linked to a response function.

They are however indirectly related to the "three-point" dynamic susceptibility χ_T. It gives the response of the auto-correlation function $C(t)$ to a change of temperature,

$$\chi_T(t) \equiv \frac{\partial C(t)}{\partial T} \,. \tag{5.1}$$

For a system with deterministic Hamiltonian dynamics and closed volume V, all the "histories" of the N particles in positions $x_i(t)$ at time t are encoded in the possible initial configurations $\{x_i(0)\}$ of the system. The statistic average of an observable $\mathcal{O}$ can then be computed exactly by weighting the initial configurations by their respective Boltzmann weights, as $\langle \mathcal{O}(t) \rangle = (Z(t=0))^{-1} \int_{\{x_i(0)\}} \mathcal{O}(\{x_i(t)\})\, e^{-\beta \mathcal{H}[\{x_i(0)\}]}$. The total Hamiltonian can also be expressed as a sum of its elementary degrees of freedom $\mathcal{H}[\{x_i(0)\}] = \int_{\vec{y}} h[\{x_i(0)\}; \vec{y}]$. Then the auto-correlation function $C(t) = N^{-1} \sum_{j=1}^{N} \left\{ \langle x_j(t) x_j(0) \rangle - \langle x_j(0) \rangle^2 \right\}$ becomes:

$$C(t) = \frac{1}{Z(0)} \frac{1}{N} \sum_{j=1}^{N} \int_{\{x_i(0)\}} x_j(t) x_j(0) e^{-\beta \int_{\vec{y}} h[\{x_i(0)\};\vec{y}]} - \frac{1}{Z(0)^2} \frac{1}{N^2} \left[\sum_{j=1}^{N} \int_{\{x_i(0)\}} x_j(0) e^{-\beta \int_{\vec{y}} h[\{x_i(0)\};\vec{y}]} \right]^2 . \tag{5.2}$$

We can compute its derivative with respect to the inverse temperature $\beta = (k_B T)^{-1}$. The figures shown all along this chapter have been done for $k_B = 1$. Using $\langle h[\{x_i(0)\}; \vec{y}] \rangle = h_0(\vec{y})$ and $\frac{\partial \beta}{\partial T} = -(k_B T^2)^{-1}$, χ_T becomes

$$\chi_T(t) = \frac{1}{k_B T^2} \frac{1}{N} \sum_{j=1}^{N} \int_{\vec{y}} \langle [x_j(t) - x_0][x_j(0) - x_0][h[\{x_i(0)\}; \vec{y}] - h_0(\vec{y})] \rangle \,. \tag{5.3}$$

The integrand is a two-time and two-space-point function and can give rise to a dynamical length scale, be it trivial or not.

Evaluating the square of $\chi_T(t)$ and using the Cauchy-Schwarz relation, one finds an inequality (or bound) between $\chi_T^2(t)$ and $\chi_4(t)$, that must be valid in systems where the energy is conserved, [189, 190] and in particular if we consider the NVE ensemble (where the energy is fixed and the temperature varies), this inequality reads:

$$\chi_T(t)^2 \leq \frac{1}{(k_B\, T^2)^2} \left\langle \delta H^2 \right\rangle \chi_4(t) \,. \tag{5.4}$$

The quantity $\left\langle (\delta H = \mathcal{H}[\{\vec{x_i}(0)\}] - \mathcal{H}_0)^2 \right\rangle$ represents the average energy fluctuations. It is equal to $N\, c_V\, k_B T^2$ in the NVT ensemble, with c_V the *intensive* heat capacity at constant volume V which is equal to $3/2\, k_B$ for a monatomic gas.

The above dynamical length scale, $\xi_d(t)$, and the static point-to-set length scale are often seen as evidences of the emergence of cooperativity in supercooled liquids. One does not know to what extent these two length scales are two facets of the same physical phenomenon. In this respect, we will study the dynamical correlations emerging in Arrhenius systems. On the one hand these systems can be seen as a collection of independent degrees of freedom, with no static correlations whatsoever, and no cooperative glassy dynamics (at least in the usual sense). On the other hand, Arrhenius systems can be viewed as a collection of independent two-level systems that relax on a typical time $\tau \propto e^{\Delta/T}$, where Δ is some constant energy barrier. The auto-correlation function has a simple behavior $C(t) \propto e^{-t/\tau(T)}$, which directly yields an expression for the dynamical susceptibility, $\chi_T(t) \propto 1/T^2 (t/\tau)^2 e^{-t/\tau}$. This function is non-monotonous with a maximum at time $t = \tau$ which increases as $1/T^2$. Then, there exists a $\chi_4(t)$ that must satisfy the bound and eventually has a maximum, which would be associated to the presence of a growing dynamical correlation length which diverges at $T = 0$ and at least as $1/T^2$.

Finding this dynamic length scale for Arrhenius systems could allow one to pinpoint the mechanisms responsible for it. These non-glassy mechanisms could occur in supercooled liquids that also present Arrhenius, or super-Arrhenius, dynamics. They should then not be identified erroneously as a marker of glassiness and the related dynamical length scale as an evidence of the emergence of cooperativity in glassy systems. Their knowledge would allow to discriminate between trivial (Arrhenius-like) and nontrivial (glassy) properties of the dynamical heterogeneities of glasses.

One can then ask for the possible physical mechanisms yielding to such a dynamical correlation in simple Arrhenius systems, and the most reasonable hypothesis seems to be that the dynamical correlation is mediated by the thermal bath. Indeed, the jump of an Arrhenius particle above the energy barrier Δ could generate a perturbation of order Δ that can be very large compared to $k_B\,T$, the typical thermal energy of the degrees of freedom of the bath, if we choose to work at low enough temperature such that the thermal fluctuations are negligible, $\Delta \gg k_B T$. This mechanism could give rise to some nontrivial dynamical correlation. Since the bound given by equation (5.4) is valid in the NVE ensemble, we want to dive the Arrhenius systems in a thermal bath that allow for conservation of the total energy of the system and that is "complex" enough such that it can mediate dynamical correlations.

In the following, we will try to compute the two dynamical susceptibilities, χ_T and χ_4. To do this, we first present the model and the modelisation of the thermal bath by an assembly of harmonic oscillators [191, 192], then we will derive generalized Langevin equations for the Arrhenius systems following [43, 191, 44, 193, 194, 195] and we will transform these differential equations with stochastic noise into deterministic differential equations following the Martin-Siggia-Rose-De Dominicis-Janssen formalism [196, 197, 198]. Since we are interesting in the finding of eventual dynamical length scales that should diverge at $T = 0$, we will restrict our calculations to the limit of low temperatures and will present instantons calculations that one can then perform (see also chapter 2).

5.2 The model: system {particles + bath}

The model is defined on a square lattice in dimension $d = 3$, with linear size L and volume V, containing N sites separated by a lattice spacing a, hence $N = (L/a)^3$. Each site is the equilibrium position of a harmonic oscillator of mass m, which is connected to its $2d$ nearest neighbors by springs of stiffness K_0. It has been shown that an assembly of harmonic oscillators can play the role of a heat bath. [191]

Then, we distribute Arrhenius systems, which are modeled by a collection of N_{dw} independent particles of mass $M > m$, living in one-dimensional double-well (dw) potentials at fixed random positions in space. The center of the double well i is *fixed* at position $\vec{R}_i$ and $X_i(t)$ represents the coordinate of the particle inside the double well i relative to its center. To be concrete, we take the following form of the potential, with two symmetric minima in ± 1,

$$V(X) = \frac{\Delta}{4}(X^2 - 1)^2\,. \tag{5.5}$$

The probability to jump from one minimum to the other follow an Arrhenius law, namely the relaxation time of one particle is $\tau = \tau_0 e^{\beta\,\Delta/4}$, where $\beta = (k_B T)^{-1}$, $\Delta/4$ is the height of the potential barrier and τ_0 is some microscopic relaxation time. The thermodynamic limit is taken in such a way that $N \to \infty$ and $N_{dw} \to \infty$ with $N_{dw}/N = \rho =$ finite but small, ρ being the density of double wells.

In addition, each particle particle i is coupled to its nearest oscillator of the bath by a spring of stiffness g, and the quadratic coupling between the particle in the double well and the oscillator in the bath is such that the force is zero when the oscillator is at its equilibrium position and the particle on

the top of the barrier of V. A pictorial representation of the model projected in one dimension is shown in figure 5.1.

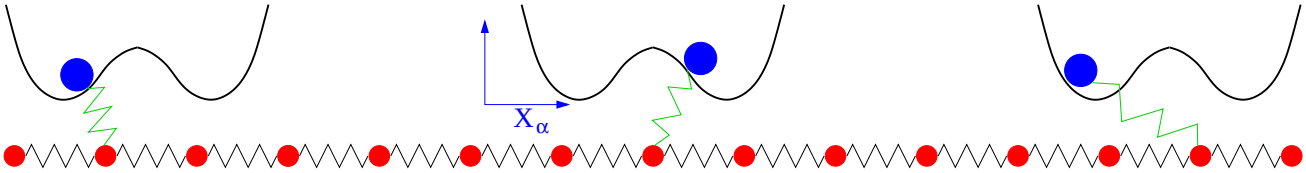

Figure 5.1: Pictorial sketch of the model in one dimension.

$\delta\vec{x}_j(t)$ is the distance of the j-th oscillator with respect to its equilibrium position $\delta\vec{x}_j(t) = \vec{x}_j(t) - \vec{l}_j$, with $\vec{l}_j = (l_j^x, l_j^y, l_j^z)$ and $l_j^\varepsilon \in a\{1, ..., L/a\}$ for $\varepsilon = \{x, y, z\}$. We suppose that the whole system {bath + particles} is isolated such that the total energy is conserved,

$$H[\{\vec{X}\}, \{\delta\vec{x}\}, \{\dot{\vec{X}}\}, \{\delta\dot{\vec{x}}\}] = E_c^P[\{\dot{\vec{X}}\}] + E_c^B[\{\delta\dot{\vec{x}}\}] + E_p[\{\vec{X}\}, \{\delta\vec{x}\}] = \text{cst}\,. \tag{5.6}$$

The total kinetic energies of the particles (P) and of the bath (B) are given by:

$$E_c^P[\{\dot{\vec{X}}\}] = \frac{M}{2}\sum_{i=1}^{N_{dw}} \dot{\vec{X}}_i(t)^2\,, \tag{5.7}$$

$$E_c^B[\{\delta\dot{\vec{x}}\}] = \frac{m}{2}\sum_{j=1}^{N} \delta\dot{\vec{x}}_j(t)^2\,. \tag{5.8}$$

The total potential energy of the ensemble bath plus N_{dw} particles can be written as a sum of subcomponents,

$$E_p[\{\vec{X}\}, \{\delta\vec{x}\}] = E_p^P[\{\vec{X}\}] + E_p^B[\{\delta\vec{x}\}] + E_p^I[\{\vec{X}\}, \{\delta\vec{x}\}]\,, \tag{5.9}$$

corresponding to the total double-well potential energy of particles and to the total elastic potential energy of the bath, respectively given by,

$$E_p^P[\{\vec{X}\}] = \sum_{i=1}^{N_{dw}} \sum_{\varepsilon=x,y,z} V(X_{i,\varepsilon})\,, \tag{5.10}$$

$$E_p^B[\{\delta\vec{x}\}] = \frac{K_0}{2}\sum_{j=1}^{N} \left(\delta\vec{x}_{j+1}(t) - \delta\vec{x}_j(t)\right)^2\,, \tag{5.11}$$

and a elastic potential energy of interaction (I) between bath and particles,

$$E_p^I[\{\vec{X}\}, \{\delta\vec{x}\}] = \frac{g}{2}\sum_{i=1}^{N_{dw}} \left(\vec{X}_i(t) - \delta\vec{x}_{R_i}(t)\right)^2\,, \tag{5.12}$$

where we have introduced $\delta\vec{x}_{R_i}(t) = \sum_{j=1}^{N} \delta\vec{x}_j(t)\delta(\vec{l}_j - \vec{R}_i)$.

5.3 From a deterministic Hamiltonian to Langevin equations

In this section, we are going to derive generalized Langevin equations for our double-well systems interacting with a heat bath formed by the three-dimensional assembly of harmonic oscillators. Then, we will give the statistic properties of the heat bath. [43, 191, 44, 193, 194, 195]

5.3.1 Normal modes

It is well known that the motion of an ensemble of harmonic oscillators in euclidean lattices can be described in terms of normal modes, *i.e.*, standing waves with the same wave number and frequency. [199] For periodic boundary conditions, the wave number values must respect that:

$$e^{i(k_\mu \mu)} = e^{i\, k_\mu (\mu + L)} \Rightarrow k_\mu = \pm \frac{2\pi}{L} p_\mu \quad \text{with} \quad \mu = x, y, z\,, \tag{5.13}$$

with p_x, p_y, p_z integers. The wave number that can be taken in one direction depends on the linear size of the system L, or, equivalently, on the linear number of harmonic oscillators L/a, and is such that $(k_x, k_y, k_z) = (2\pi/L)\,(p_x, p_y, p_z)$, with $(p_x, p_y, p_z) \in \{0; \pm 1; ...; \pm L/(2a)\}$, and with increment of $2\pi/L$ between two nearest wave vectors.

The distance $\delta\vec{x}_j(t)$ of a harmonic oscillator j with respect to its equilibrium position $\vec{l}_j$ is, using the notation $\sum_{\vec{k}} \equiv \sum_{(k_x,k_y,k_z)=-\pi/a}^{\pi/a}$,

$$\delta\vec{x}_j(t) = \frac{1}{\sqrt{N}} \sum_{\vec{k}} \vec{u}_{\vec{k}}(t) e^{i\vec{k}\cdot\vec{l}_j}\,. \tag{5.14}$$

The $\vec{u}_{\vec{k}}$ are complex numbers, and $\overline{\vec{u}_{\vec{k}}}$ their complex conjugate. To ensure that $\delta\vec{x}_j(t)$ is real we have to impose that $\vec{u}_{\vec{k}} = \overline{\vec{u}_{-\vec{k}}}$, from which ensues the following property: $\vec{u}_{\vec{k}}\vec{u}_{-\vec{k}} = \vec{u}_{\vec{k}}\overline{\vec{u}_{\vec{k}}} = |\vec{u}_{\vec{k}}|^2$. We finally introduce the Fourier transform of the Kronecker delta function in discrete space:

$$\delta_{\vec{k},-\vec{k}'} = \frac{1}{N} \sum_{j=1}^{N} e^{i(\vec{k}+\vec{k}')\cdot\vec{l}_j}\,. \tag{5.15}$$

5.3.2 Expressing the Hamiltonian in terms of the normal modes

The different terms of the Hamiltonian can be rewritten in terms of the normal modes.

Kinetic energy

The kinetic energy of the bath of oscillators becomes:

$$E_c^B = \frac{m}{2} \sum_{\vec{k},\vec{k}'} \dot{\vec{u}}_{\vec{k}} \dot{\vec{u}}_{\vec{k}'} \delta_{\vec{k},-\vec{k}'} = \frac{m}{2} \sum_{\vec{k}} |\dot{\vec{u}}_{\vec{k}}(t)|^2\,. \tag{5.16}$$

Potential energy

The total potential energy $E_p^P + E_p^B + E_p^I$ is going to be rewritten like $\widetilde{E}_p^P + \widetilde{E}_p^B + \widetilde{E}_p^I$, the two being equal. The first term, expression (5.11), becomes:

$$E_p^B = \frac{1}{2} \sum_{\vec{k}} \lambda_{\vec{k}}^2 |\vec{u}_{\vec{k}}(t)|^2\,. \tag{5.17}$$

We have introduced λ_k^2, $\lambda_{\vec{k}}^2 = K_0 \sum_{\vec{k}'} N^{-1} \sum_{j=1}^{N} e^{i(\vec{k}+\vec{k}')\cdot\vec{l}_j} \left(1 - e^{i\vec{k}\cdot(\vec{l}_{j+1}-\vec{l}_j)}\right)\left(1 - e^{i\vec{k}'\cdot(\vec{l}_{j+1}-\vec{l}_j)}\right)$, the k-dependent coupling between phonons that propagate within the bath of harmonic oscillators. In dimension $d = 3$ when $||\vec{k}|| \ll 1$, with $\vec{k}^2 = ||\vec{k}||^2 = k$ and $K = K_0/d$ (see appendix C.1), it reads

$$\lambda_k^2 = K a^2 k^2 + o(\vec{k}^2)\,. \tag{5.18}$$

The third term, expression (5.12), can be reexpressed as

$$E_p^I = \frac{g}{2} \sum_{j=1}^{N_{dw}} \left(\vec{X}_j(t) - \frac{1}{\sqrt{N}} \sum_{\vec{k}} \vec{u}_{\vec{k}}(t) e^{i\vec{k}\vec{R}_j} \right)^2\,, \tag{5.19}$$

and developed into three distinct contributions:
1) One depending only on the $\vec{X}_i(t)$.
2) A term depending only on the degrees of freedom of the bath, that can be written, with $\rho = N_{dw}/N$ the density of double wells,

$$\frac{1}{N}\frac{g}{2}\sum_{k,k'}\vec{u}_{\vec{k}}(t)\vec{u}_{\vec{k}'}(t)\sum_{j=1}^{N_{dw}}e^{i(\vec{k}+\vec{k}')\vec{R}_j} = \frac{1}{2}\rho\, g\sum_{k,k'}\vec{u}_{\vec{k}}(t)\vec{u}_{\vec{k}'}(t)\delta_{\vec{k},-\vec{k}'} = \frac{1}{2}\rho\, g\sum_{k}|\vec{u}_{\vec{k}}(t)|^2\,. \tag{5.20}$$

3) And a term coupling the normal modes to the double-well particles.
The above three contributions can be distributed into the following redefinitions of the potential energies:

$$\widetilde{E}_p^P = E_p^P + \sum_{i=1}^{N_{dw}}\sum_{\varepsilon=x,y,z}\frac{g}{2}X_{i,\varepsilon}(t)^2 = \sum_{i=1}^{N_{dw}}\sum_{\varepsilon=x,y,z}\left(V(X_{i,\varepsilon}) + \frac{g}{2}X_{i,\varepsilon}(t)^2\right)\,, \tag{5.21}$$

$$\widetilde{E}_p^B = E_p^B + \frac{1}{2}\sum_{\vec{k}}\frac{g}{2}\rho|\vec{u}_{\vec{k}}(t)|^2 = \frac{1}{2}\sum_{\vec{k}}\widetilde{\lambda}_k^2|\vec{u}_{\vec{k}}(t)|^2\,, \tag{5.22}$$

$$\widetilde{E}_p^I = -\frac{g}{\sqrt{N}}\sum_{j=1}^{N_{dw}}\vec{X}_j(t)\sum_{\vec{k}}\vec{u}_{\vec{k}}(t)e^{i\vec{k}\vec{R}_j}\,, \tag{5.23}$$

where we have introduced a modified phonon coupling,

$$\widetilde{\lambda}_k^2 = \lambda_k^2 + g\,\rho\,. \tag{5.24}$$

In the following, we further manipulate the expression of the potential energy. The sum $\widetilde{E}_p^B + \widetilde{E}_p^I$ can be rewritten as a factorized square, with $\vec{R}_{mn} = \vec{R}_m - \vec{R}_n$,

$$\widetilde{E}_p^B + \widetilde{E}_p^I = \widetilde{E}_p^{B+I} - \frac{1}{2}\frac{g^2}{N}\sum_{m,n=1}^{N_{dw}}\vec{X}_m(t)\vec{X}_n(t)\sum_{\vec{k}}\frac{e^{i\vec{k}\vec{R}_{mn}}}{\widetilde{\lambda}_k^2}\,. \tag{5.25}$$

The first term is given by:

$$\widetilde{E}_p^{B+I} = \frac{1}{2}\sum_{\vec{k}}\left\{\widetilde{\lambda}_k^2\left(\vec{u}_{\vec{k}}(t) - \frac{g}{\sqrt{N}}\frac{1}{\widetilde{\lambda}_k^2}\sum_{j=1}^{N_{dw}}\vec{X}_j(t)e^{-i\vec{k}\vec{R}_j}\right)\left(\vec{u}_{-\vec{k}}(t) - \frac{g}{\sqrt{N}}\frac{1}{\widetilde{\lambda}_k^2}\sum_{j=1}^{N_{dw}}\vec{X}_j(t)e^{i\vec{k}\vec{R}_j}\right)\right\}\,. \tag{5.26}$$

The second term gives rise to a local contribution when $m = n$ and to a nonlocal contribution when $m \neq n$. The local part is $-\frac{1}{2}g^2\alpha\sum_{n=1}^{N_{dw}}\vec{X}_n(t)^2$ (in the thermodynamic limit $N \to \infty$), with

$$\alpha = (2\pi K)^{-1}\left[1 - \pi^{-1}\sqrt{\frac{\rho g}{K}}\arctan\left(\pi\sqrt{\frac{K}{\rho g}}\right)\right]\,. \tag{5.27}$$

Together with $\widetilde{E}_p^P$ in equation (5.21), it allows us to define an effective "free" double-well potential $U_{N_{dw}}$ for the particles,

$$U_{N_{dw}}\left(\{\vec{X}_i\}\right) = \sum_{i=1}^{N_{dw}}\sum_{\varepsilon=x,y,z}\left[V(X_{i,\varepsilon}) + \frac{g}{2}\left(1 - g\alpha\right)X_{i,\varepsilon}^2\right] = \sum_{i=1}^{N_{dw}}\sum_{\varepsilon=x,y,z}V_1\left(X_{i,\varepsilon}\right) + \mathrm{cst}\,, \tag{5.28}$$

where cst denotes an irrelevant constant that will be neglected. V_1 is the new effective local potential for each particle (in direction ε),

$$V_1\left(X_{i,\varepsilon}\right) = \frac{\Delta}{4}\left(X_{i,\varepsilon}^2 - X_0^2\right)^2 , \tag{5.29}$$

and X_0 is a redefinition of the minimum of V in equation (5.5), defined if $1 > (g/\Delta)\,(1-\alpha\, g)$,

$$X_0^2 = 1 - \frac{g}{\Delta}\,(1-\alpha\, g) . \tag{5.30}$$

The nonlocal part, yielding a total effective interaction energy

$$I_{N_{dw}}\left(\{X_{i,\varepsilon}\}\right) = \sum_{\varepsilon=x,y,z} \sum_{\substack{m,n=1 \\ m<n}}^{N_{dw}} V_2\left(X_{m,\varepsilon}, X_{n,\varepsilon}\right) , \tag{5.31}$$

gives rise to an effective ferromagnetic pair interaction mediated by the bath, as it can be found for instance in [200] for Brownian particles. This comes from the fact that when two particles in two double wells are, say, respectively in $+1$ and in -1, the harmonic oscillators of the bath are either "compressed" or "elongated", and this gives rise to an elastic cost. For two particles at dimensionless distance $\hat{R}_{mn} = R_{mn}/a$ (a being the lattice spacing), the effective ferromagnetic pair potential reads

$$V_2\left(X_{m,\varepsilon}, X_{n,\varepsilon}\right) = -X_{m,\varepsilon}\, X_{n,\varepsilon}\, Y(\hat{R}_{mn}) , \tag{5.32}$$

whose interaction is asymptotically given by a Yukawa potential:

$$Y(\hat{R}_{mn}) \simeq \frac{g^2}{4\pi K}\frac{1}{\hat{R}_{mn}} \exp\left[-\sqrt{\frac{\rho g}{K}}\hat{R}_{mn}\right] . \tag{5.33}$$

The constant α and the function $Y(\hat{R}_{mn})$ are computed in appendix C.3.1.

This effective ferromagnetic interaction gives rise to a static length scale that can eventually be large. We want to be in a regime where the dynamical length scale(s) are large compared to this static length scale, and this will be so if we impose to the effective energy of interaction of the ferromagnetic state to be small compared to the total thermal-energy fluctuations, $N\, k_B\, T \gg |I_{N_{dw}}\left(\{X_{i,\varepsilon}\} = \{+1\} \text{ or } \{-1\}\right)|$. This energy is computed in appendix C.2 and yields the following condition, where constants of order one have been discarded,

$$T \gg \rho\, g\, . \tag{5.34}$$

Before going to the next section, we set the Hamiltonian of the system to be written as

$$H[\{\vec{X}\},\{\vec{u}\},\{\dot{\vec{X}}\},\{\dot{\vec{u}}\}] = E_c^P[\{\dot{\vec{X}}\}] + U_{N_{dw}}[\{\vec{X}\}] + I_{N_{dw}}[\{\vec{X}\}] + E_c^B[\{\dot{\vec{u}}\}] + E_1^{B+I}[\{\vec{X}\},\{\vec{u}\}] . \tag{5.35}$$

and we finally define the effective potential energy of the particles, or generalized potential, as

$$W_{N_{dw}} = U_{N_{dw}} + I_{N_{dw}} . \tag{5.36}$$

5.3.3 Generalized Langevin equations

We suppose that the time dependence of the $\vec{X}_j(t)$ is known. Dynamical equations are computed from Hamilton's equations for both bath and particles degrees of freedom, which are, in each of the three directions of space denoted by ε, with $b_{\vec{k},\varepsilon} = \vec{b}_{\vec{k},\varepsilon} \cdot \vec{e}_\varepsilon$,

$$\left\{ \frac{\partial H}{\partial u_{\vec{k},\varepsilon}}(t) = -m\ddot{u}_{\vec{k},\varepsilon}(t)\,;\; \frac{\partial H}{\partial (m\dot{u}_{\vec{k},\varepsilon})}(t) = \dot{u}_{\vec{k},\varepsilon}(t) \right\} , \tag{5.37}$$

$$\left\{ \frac{\partial H}{\partial X_{j,\varepsilon}}(t) = -M\ddot{X}_{j,\varepsilon}(t)\,;\; \frac{\partial H}{\partial (M\dot{X}_{j,\varepsilon})}(t) = \dot{X}_{j,\varepsilon}(t) \right\}. \tag{5.38}$$

Using the expression of the Hamiltonian in equation (5.35), we obtain the equations of motion for the particles and for the bath degrees of freedom:

$$m\ddot{u}_{\vec{k},\varepsilon}(t) + \widetilde{\lambda}_k^2 u_{\vec{k},\varepsilon}(t) = \frac{g}{\sqrt{N}} \sum_{j=1}^{N_{dw}} X_{j,\varepsilon}(t) e^{-i\vec{k}\vec{R}_j}\,, \tag{5.39}$$

$$M\ddot{X}_{j,\varepsilon}(t) = -\frac{\partial W_{N_{dw}}}{\partial X_{j,\varepsilon}} + \frac{g}{\sqrt{N}} \sum_{\vec{k}} u_{\vec{k},\varepsilon}(t) e^{i\vec{k}\vec{R}_j} - g^2 \sum_n X_{n,\varepsilon}(t) \frac{1}{N} \sum_{\vec{k}} \frac{1}{\widetilde{\lambda}_k^2} \cos\left[\vec{k}\left(\vec{R}_n - \vec{R}_j\right)\right]. \tag{5.40}$$

They are coupled differential equations, nonlinear in space and nonlocal both in space and time. The solution of the equation of motion of one of the bath's degrees of freedom $u_{\vec{k},\varepsilon}$ in equation (5.39), with initial position and velocity $u_{\vec{k},\varepsilon}(0)$ and $\dot{u}_{\vec{k},\varepsilon}(0)$, can be formally written as

$$u_{\vec{k},\varepsilon}(t) = u_{\vec{k},\varepsilon}(0)\cos(\omega t) + \frac{\dot{u}_{\vec{k},\varepsilon}(0)}{\omega_k}\sin(\omega_k t) + \frac{g/m}{\sqrt{N}} \sum_{j=1}^{N_{dw}} e^{-i\vec{k}\vec{R}_j} \int_0^t dt'\, X_{j,\varepsilon}(t') \frac{\sin[\omega_k(t-t')]}{\omega_k}\,, \tag{5.41}$$

where we defined the phonon frequency $\omega_k = \sqrt{\widetilde{\lambda}_k^2/m}$. Inserting equation (5.41) in equation (5.40), we obtain an equation of motion for the particles that depends on the bath only through its initial condition:

$$\begin{aligned} M\ddot{X}_{j,\varepsilon}(t) = &-\frac{\partial W_{N_{dw}}}{\partial X_{j,\varepsilon}} - g^2 \sum_n X_{n,\varepsilon}(t) \frac{1}{N} \sum_{\vec{k}} \frac{1}{\widetilde{\lambda}_k^2} \cos\left[\vec{k}\left(\vec{R}_n - \vec{R}_j\right)\right] \\ &+ \frac{g}{\sqrt{N}} \sum_{\vec{k}} e^{i\vec{k}\vec{R}_j} \left[u_{\vec{k},\varepsilon}(0)\cos(\omega_k t) + \frac{\dot{u}_{\vec{k},\varepsilon}(0)}{\omega_k}\sin(\omega_k t) \right] \\ &+ \frac{g^2}{m} \sum_n \frac{1}{N} \sum_{\vec{k}} e^{i\vec{k}(\vec{R}_j - \vec{R}_n)} \int_0^t dt'\, X_{n,\varepsilon}(t') \frac{\sin[\omega_k(t-t')]}{\omega_k}\,. \end{aligned} \tag{5.42}$$

We integrate by part the last term, this yields a memory kernel that couples to the velocity of the particle:

$$\int_0^t dt'\, X_{n,\varepsilon}(t') \frac{\sin[\omega_k(t-t')]}{\omega_k} = \frac{1}{\omega_k^2}\left[X_{n,\varepsilon}(t) - X_{n,\varepsilon}(0)\cos(\omega_k t)\right] - \int_0^t dt' \dot{X}_{n,\varepsilon}(t') \frac{\cos(\omega_k(t-t'))}{\omega_k^2}\,. \tag{5.43}$$

After a distribution of the above leftmost term (into brackets), the equation (5.42) becomes:

$$\begin{aligned} M\ddot{X}_{j,\varepsilon}(t) = &-\frac{\partial W_{N_{dw}}}{\partial X_{j,\varepsilon}} + g^2 \sum_n X_{n,\varepsilon}(t) \frac{1}{N} \sum_{\vec{k}} \frac{1}{\widetilde{\lambda}_k^2} \left(e^{i\vec{k}(\vec{R}_n - \vec{R}_j)} - \cos\left[\vec{k}\left(\vec{R}_n - \vec{R}_j\right)\right] \right) \\ &+ \frac{g}{\sqrt{N}} \sum_{\vec{k}} e^{i\vec{k}\vec{R}_j} \left[\left(u_{\vec{k},\varepsilon}(0) - \frac{g}{m} \sum_n \frac{1}{\sqrt{N}} \frac{e^{-i\vec{k}\vec{R}_n}}{\omega_k^2} X_{n,\varepsilon}(0) \right) \cos(\omega_k t) + \frac{\dot{u}_{\vec{k},\varepsilon}(0)}{\omega_k}\sin(\omega_k t) \right] \\ &- \frac{g^2}{m} \sum_n \frac{1}{N} \sum_{\vec{k}} e^{i\vec{k}(\vec{R}_j - \vec{R}_n)} \int_0^t dt' \dot{X}_{n,\varepsilon}(t') \frac{\cos(\omega_k(t-t'))}{\omega_k^2}\,. \end{aligned} \tag{5.44}$$

Since $e^{i\vec{k}(\vec{R}_n-\vec{R}_j)} - \cos\left[\vec{k}\left(\vec{R}_j-\vec{R}_n\right)\right] = 1/2\left(e^{i\vec{k}(\vec{R}_n-\vec{R}_j)} - e^{-i\vec{k}(\vec{R}_n-\vec{R}_j)}\right)$, the rightmost term of the above equation vanishes. [1] This last equation is a generalized Langevin equation for the particle j

$$M\delta\ddot{X}_{j,\varepsilon}(t) = -\frac{\partial W_{N_{dw}}}{\partial X_{j,\varepsilon}} + F_{j,\varepsilon}(t) - \sum_{n=1}^{N_{dw}}\int_0^t dt'\,\dot{X}_{n,\varepsilon}(t')K_{jn}(t-t')\,, \tag{5.45}$$

living in the generalized potential $W_{N_{dw}}$, with a memory kernel $K_{jn}(t-t')$ non local in space and time acting as a time-dependent dissipation term, and subject to a random force $F_{j,\varepsilon}$ coming from the bath.

5.3.4 Random force, generalized potential and memory kernel

The random force is given by the expression:

$$F_{j,\varepsilon}(t) = \frac{g}{\sqrt{N}}\sum_{\vec{k}} e^{i\vec{k}\vec{R}_j}\left[\left(u_{\vec{k},\varepsilon}(0) - \frac{g}{m}\sum_n \frac{1}{\sqrt{N}}\frac{e^{-i\vec{k}\vec{R}_n}}{\omega_k^2}X_{n,\varepsilon}(0)\right)\cos(\omega_k t) + \frac{\dot{u}_{\vec{k},\varepsilon}(0)}{\omega_k}\sin(\omega_k t)\right], \tag{5.46}$$

and the two contributions of $W_{N_{dw}}$ are given by:

$$\begin{aligned} U_{N_{dw}}\left(\{X_i\}\right) &= \sum_{\varepsilon=x,y,z} U^{(\varepsilon)}_{N_{dw}}\left(\{X_{i,\varepsilon}\}\right) = \sum_{\varepsilon=x,y,z}\sum_{i=1}^{N_{dw}} V_1\left(X_{i,\varepsilon}\right)\,, \\ I_{N_{dw}}\left(\{X_i\}\right) &= \sum_{\varepsilon=x,y,z} I^{(\varepsilon)}_{N_{dw}}\left(\{X_{i,\varepsilon}\}\right) = \sum_{\varepsilon=x,y,z}\sum_{\substack{i,j=1\\ i<j}}^{N_{dw}} V_2\left(X_{i,\varepsilon},X_{j,\varepsilon}\right)\,. \end{aligned} \tag{5.47}$$

They can be respectively rewritten as a sum over all local potentials $V_1\left(X_{i,\varepsilon}\right)$, defined in equation (5.29), and all pair interaction potentials $V_2\left(X_{i,\varepsilon},X_{j,\varepsilon}\right)$, defined in equation (5.32).

The memory kernel of dissipation, nonlocal in time, reads:

$$K_{jn}(t-t') = \frac{g^2}{m}\frac{1}{N}\sum_{\vec{k}} e^{i\vec{k}\vec{R}_{jn}}\frac{\cos[\omega_k(t-t')]}{\omega_k^2}\,. \tag{5.48}$$

The kernel is symmetric in $t\to -t$, $K_{np}(t) = K_{np}(-t)$. It is *estimated* using arguments of continuity in appendix C.3.2. The different expression then obtained are compared to the above exact expression in figure 5.2. The expressions found are: a local (in space) one when $n=p$, with $R_{np} = ||\vec{R}_n - \vec{R}_p||$ and $\hat{R} = R/a$,

$$K_{nn}(t) \simeq g^2\,\alpha\,\frac{\sin\left(\sqrt{\frac{K}{m}}\pi\,t\right)}{\sqrt{\frac{K}{m}}\pi\,t}\,, \tag{5.49}$$

and a nonlocal (in space) asymptotic expression when $n\neq p$

$$K_{np}(t) \simeq \frac{1}{\pi}Y(\hat{R}_{np})\left(\text{SinIntegral}\left[\pi\left(\hat{R}_{np}-\sqrt{\frac{K}{m}}t\right)\right] + \text{SinIntegral}\left[\pi\left(\hat{R}_{np}+\sqrt{\frac{K}{m}}t\right)\right]\right) + O(\rho g\hat{R}_{np})\,. \tag{5.50}$$

One can go further and make a very crude approximation of the above expressions. It consists in replacing $\frac{\sin(Ax)}{Ax}$ by $\delta(x)$ and $\frac{1}{\pi}\left(\text{SinIntegral}\left[A(B+Ct)\right] + \text{SinIntegral}\left[A(B-Ct)\right]\right)$ by

[1] We have used that the sum $N^{-1}\sum_{\vec{k}}\left(\widetilde{\lambda}_k\right)^{-2}\left(e^{\vec{k}\vec{z}} - e^{-\vec{k}\vec{z}}\right)$ evaluates to zero, as $\vec{k}\in\mathbb{Z}^3$.

$[\Theta(t+B/C)-\Theta(t-B/C)]$ (both exact when $A\to\infty$). The interest of this crudest approximation is to perform analytically time integrals where the dissipation kernels appear. This approximation makes sense if the details of $K_{nj}(t)$ do not influence (much) the particles dynamics, as one can see on figure 5.2. We thus introduce the following simplified memory kernels: the local one,

$$K_{nn}(t)\simeq\sigma\,\delta(t)\,, \tag{5.51}$$

and the nonlocal one,

$$K_{np}(t-t')\simeq Y(\hat{R}_{np})\left[\Theta\left(\nu(t-t')+\hat{R}_{np}\right)-\Theta\left(\nu(t-t')-\hat{R}_{np}\right)\right]\,. \tag{5.52}$$

For simplicity of notation we have introduced the frequency $\nu=\sqrt{K/m}$ and the constant $\sigma=g^2\,\alpha$.

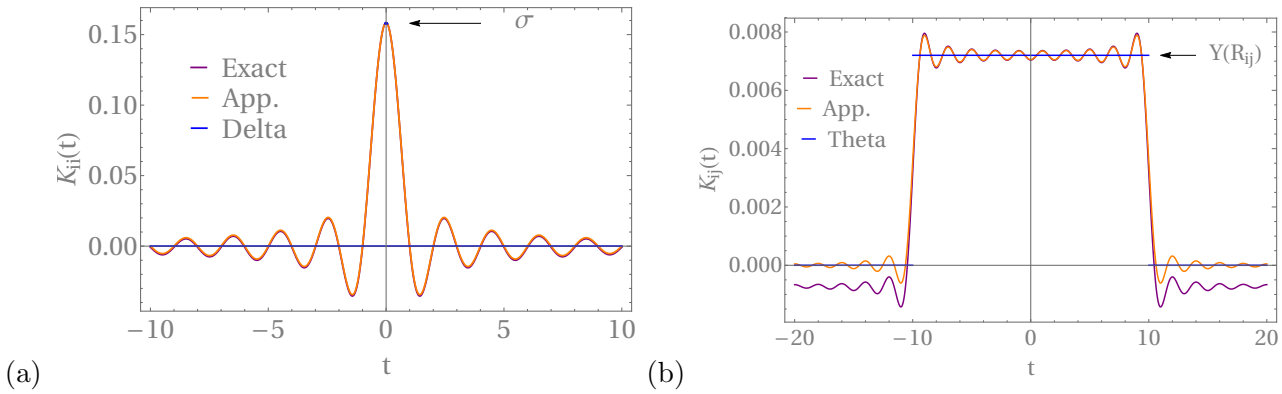

Figure 5.2: Memory kernels of dissipation $K_{ij}(t)$ for $i=j$ (a) and $i\neq j$ (b) (here $R_{ij}\equiv\hat{R}_{ij}$). The different curves are obtained either: from their exact expression (5.48) (purple), from their estimations (5.49) and (5.50) (orange), and from their crudest analytic approximations (5.51) and (5.52) (blue). The parameters are such that: $K=1$, $m=1$, $\rho g=0.0001$, $\hat{R}_{ij}=10$. We observe an error of order $O(\rho g\hat{R}_{ij})\simeq 0.001$ between the purple and the orange curves of $K_{ij}(t)$ when $i\neq j$, that we suppose (at least for the moment) does not spoil our calculations.

The local and the nonlocal kernels are represented on figure 5.2. The above estimation (orange) and the crude approximation (blue) are compared to the numerical values (purple) obtained from the expression in equation (5.48). The estimation of $K_{nj}(t)$ with $n\neq j$ in equation (5.50) presents a deviation of order $O(\rho g\hat{R}_{np})$ (see figure 5.2 (b)) that we do not take into account for the moment, supposing that it does not spoil our calculations.

5.3.5 Properties of the stochastic noise generated by the bath

Suppose that at $t=0$ the bath is equilibrated in presence of the particles. Hence, its possible initial configurations follow a Gibbs distribution with probability $p_0=(Z_0(\beta))^{-1}\,e^{-\beta E_{0;N_{dw}}}$, with $\beta=(k_BT)^{-1}$. The quantities $E_{0;N_{dw}}$ and $Z_0(\beta)$ are, respectively, the energy of the bath for a particular configuration of the system {particles + bath} and the partition function of the system, both at time $t=0$. The

expression of $E_{0;N_{dw}}$ is, from equation (5.35),

$$
\begin{aligned}
&E_{0;N_{dw}} = \\
&\frac{1}{2}\sum_{\vec{k}}\left\{ m|\dot{\vec{u}}_{\vec{k}}(0)|^2 + \widetilde{\lambda}_k^2 \left(\vec{u}_{\vec{k}}(0) - \frac{g}{\sqrt{N}}\frac{1}{\widetilde{\lambda}_k^2}\sum_{j=1}^{N_{dw}} X_j(0)\,\vec{e}_x e^{-i\vec{k}\vec{R}_j} \right)\left(\vec{u}_{-\vec{k}}(0) - \frac{g}{\sqrt{N}}\frac{1}{\widetilde{\lambda}_k^2}\sum_{j=1}^{N_{dw}} X_j(0)\,\vec{e}_x e^{i\vec{k}\vec{R}_j} \right) \right\} \\
&= \frac{1}{2}\sum_{\vec{k}}\left\{ m|\dot{\vec{u}}_{\vec{k}}(0)|^2 + \widetilde{\lambda}_k^2 \left| \vec{u}_{\vec{k}}(0) - \frac{g}{\sqrt{N}}\frac{1}{\widetilde{\lambda}_k^2}\sum_{j=1}^{N_{dw}} X_j(0)\,\vec{e}_x e^{-i\vec{k}\vec{R}_j} \right|^2 \right\} .
\end{aligned}
\tag{5.53}
$$

$Z_0(\beta)$ is the sum over all the initial configurations $\left\{\{\vec{u}_{\vec{k}}(0)\};\{\dot{\vec{u}}_{\vec{k}}(0)\}\right\}$ of the Boltzmann weight:

$$
Z_0(\beta) = \sum_{\{\vec{u}_{\vec{k}}(0)\},\{\dot{\vec{u}}_{\vec{k}}(0)\}} e^{-\beta E_{0;N_{dw}}} . \tag{5.54}
$$

Knowing the initial probability p_0, we can determine the stochastic properties of the bath noise, in the light of [192, 201]. It consists in computing the moments of the probability distribution of the stochastic force $F_{j,\varepsilon}(t)$, which depends on the stochastic variables $u_{\vec{k},\varepsilon}(0)$ and $\dot{u}_{\vec{k},\varepsilon}(0)$, as we can see in equation (5.46). We therefore introduce the average over the initial configurations of the bath, $\langle\,.\,\rangle_0 = (Z_0(\beta))^{-1}\sum_{\{\vec{u}_{\vec{k}}(0)\},\{\dot{\vec{u}}_{\vec{k}}(0)\}} .\, e^{-\beta E_{0;N_{dw}}}$. From standard properties of Gaussian distributions, we determine the mean and the variance of the stochastic variables composing p_0 directly looking at the expression of $E_{0;N_{dw}}$. In each space direction ε we have the means,

$$
\begin{aligned}
&\left\langle \dot{u}_{\vec{k},\varepsilon}(0) \right\rangle_0 = 0 , \\
&\left\langle u_{\vec{k},\varepsilon}(0) - \frac{g}{\sqrt{N}}\frac{1}{\widetilde{\lambda}_k^2}\sum_{j=1}^{N_{dw}} X_{j,\varepsilon}(0) e^{-i\vec{k}\vec{R}_j} \right\rangle_0 = 0 ,
\end{aligned}
\tag{5.55}
$$

and the variances,

$$
\left\langle \dot{u}_{\vec{k},\varepsilon}(0)\dot{u}_{\vec{k}',\varepsilon'}(0) \right\rangle_0 = \frac{k_B T}{m}\delta_{\vec{k},-\vec{k}'}\delta_{\varepsilon,\varepsilon'} , \tag{5.56}
$$

$$
\left\langle \left(u_{\vec{k},\varepsilon}(0) - \frac{g}{\sqrt{N}}\frac{1}{\widetilde{\lambda}_k^2}\sum_{j=1}^{N_{dw}} X_{j,\varepsilon}(0) e^{-i\vec{k}\vec{R}_j} \right)\left(u_{\vec{k}',\varepsilon'}(0) - \frac{g}{\sqrt{N}}\frac{1}{\widetilde{\lambda}_k^2}\sum_{j=1}^{N_{dw}} X_{j,\varepsilon'}(0) e^{-i\vec{k}'\vec{R}_j} \right) \right\rangle_0 = \frac{k_B T}{\lambda_k^2}\delta_{\vec{k},-\vec{k}'}\delta_{\varepsilon,\varepsilon'} , \tag{5.57}
$$

and the covariance,

$$
\left\langle u_{\vec{k},\varepsilon}(0)\dot{u}_{\vec{k}',\varepsilon'}(0) \right\rangle_0 = 0 . \tag{5.58}
$$

The above relations yield the following properties of the stochastic noise coming from the bath. The means immediately imply that

$$
\langle F_{j,\varepsilon}(t)\rangle_0 = 0 , \tag{5.59}
$$

and the variances and the covariance allow us to compute the time-correlation of the stochastic force,

$$
\begin{aligned}
\left\langle F_{j,\varepsilon}(t)F_{j',\varepsilon'}(t') \right\rangle_0 &= \frac{g^2 k_B T}{m}\frac{1}{N}\sum_{\vec{k},\vec{k}'}\frac{e^{i\vec{k}\vec{R}_j + i\vec{k}'\vec{R}_{j'}}}{\omega_k\omega_{k'}}\delta_{\vec{k},-\vec{k}'}\delta_{\varepsilon,\varepsilon'}\left[\cos(\omega_k t)\cos(\omega_{k'}t') + \sin(\omega_k t)\sin(\omega_{k'}t')\right] \\
&= \frac{g^2 k_B T}{m}\delta_{\varepsilon,\varepsilon'}\frac{1}{N}\sum_{\vec{k}} e^{i\vec{k}(\vec{R}_j - \vec{R}_{j'})}\frac{\cos[\omega_k(t-t')]}{\omega_k^2} = k_B T\delta_{\varepsilon,\varepsilon'}K_{jj'}(t-t') ,
\end{aligned}
\tag{5.60}
$$

where we have recognized the expression of the memory kernel $K_{jj'}(t-t')$ given in equation (5.48).

5.4 Deterministic field theory for particles with stochastic dynamics

We use the Martin-Siggia-Rose-De Dominicis-Janssen formalism to integrate over the bath noise and obtain a deterministic field theory. [196, 197, 198] The partition function of the system {particles + bath} is defined as a path integral over all possible time-trajectories $X_i(t)$ of all the particles i (i from 1 to N_{dw}) and over the time-configurations of the noise force $\vec{F}_i(t)$ acting on particle i.

The noise is a sum of independent Gaussian variables, hence it is also a Gaussian variable. Its probability distribution is therefore fully determined by its average (5.59) and its variance (5.60),

$$P\left[\{\vec{F}\};t\right] \propto \exp\left\{-\frac{1}{2}\sum_{i,j}\sum_{\varepsilon,\varepsilon'}\int_0^t dt_1\, dt_2 F_{i,\varepsilon}(t_1)\left[k_BT\delta_{\varepsilon,\varepsilon'}K_{ij}(t_1-t_2)\right]^{-1}F_{j,\varepsilon'}(t_2)\right\} \tag{5.61}$$

We compute the partition function $Z\left[\{\vec{h}\};t\right]$ adding particle dependent external fields $\vec{h}_i$ in order to compute thermodynamic quantities from field derivatives with respect to the external fields. It will be useful to compute correlations. The particles positions have to be solution of the Langevin equation (5.45) at all times $0 < t_1 < t$, this is imposed as a constraint by introducing a Dirac delta function. The partition function is then given by:

$$\begin{aligned} Z\left[\{\vec{h}\};t\right] = \int \prod_{i=1}^{N_{dw}}\prod_{\varepsilon}\left(\mathcal{D}X_{i,\varepsilon}\,\mathcal{D}F_{i,\varepsilon}\right) P\left[\{\vec{F}\};t\right] \exp\left\{\sum_i\sum_\varepsilon\int_0^t dt'\, h_{i,\varepsilon}(t')F_{i,\varepsilon}(t')\right\} \\ \prod_{t_1=0}^{t}\delta\left[\sum_j\sum_\varepsilon\left(M\ddot{X}_{j,\varepsilon}(t_1)+\frac{\partial W_{N_{dw}}}{\partial X_{j,\varepsilon}}(t_1)+\sum_{n=1}^{N_{dw}}\int_0^{t_1}dt_2\,\dot{X}_{n,\varepsilon}(t_2)K_{jn}(t_1-t_2)-F_{j,\varepsilon}(t_1)\right)\right]. \end{aligned} \tag{5.62}$$

The integral representation of the δ-function, $\delta(\vec{x}) = (2\pi)^{-3}\int_{-\infty}^{\infty}d\vec{y}\,e^{-i\vec{x}\vec{y}}$, requires the introduction of conjugate variables, $\vec{y}$. We call these conjugate variables $\hat{X}_{j,\varepsilon}(t)$. After introducing the probability distribution of the bath force given in equation (5.61) in the above equation, we obtain:

$$\begin{aligned} &Z\left[\{\vec{h}\};t\right] \propto \prod_\varepsilon\left[\int\prod_{j=1}^{N_{dw}}\left[\mathcal{D}X_{j,\varepsilon}\mathcal{D}\hat{X}_{j,\varepsilon}\times\right.\right. \\ &\exp\left\{-i\int_0^t dt_1\hat{X}_{j,\varepsilon}(t_1)\left(M\ddot{X}_{j,\varepsilon}(t_1)+\frac{\partial W_{N_{dw}}}{\partial X_{j,\varepsilon}}(t_1)+\sum_{n=1}^{N_{dw}}\int_0^{t_1}dt_2\,\dot{X}_{n,\varepsilon}(t_2)K_{jn}(t_1-t_2)\right)\right\} \\ &\left.\left.\int\mathcal{D}F_{j,\varepsilon}\exp\left\{-\frac{1}{2}\sum_n\int_0^t dt_1\,dt_2F_{n,\varepsilon}(t_1)\left[k_BTK_{nj}(t_1-t_2)\right]^{-1}F_{j,\varepsilon}(t_2)+\int_0^t dt'\,\left[h_{j,\varepsilon}(t')+i\hat{X}_{j,\varepsilon}(t')\right]F_{j,\varepsilon}(t')\right\}\right]\right]. \end{aligned} \tag{5.63}$$

The partition function can be written as a product of three partition functions in each space direction, $Z\left[\{\vec{h}\};t\right] = z_x[\{h\};t]z_y[\{h\};t]z_z[\{h\};t]$. Since the moves of the particles in the three space directions should be independent, we can equivalently restrict the study of the particle displacement to one direction of space. In the following, we will therefore rename the different ε-dependent variables as

$X_{i,\varepsilon} \to X_i$. To compute $z[\{h\};t] \equiv z_x[\{h\};t]$, we have to integrate over the stochastic force. This gives rise to a functional Gaussian integral,

$$\int \prod_i \mathcal{D}F_i \exp\left\{-\frac{1}{2}\sum_{n,j}\int_0^t dt_1\, dt_2 F_n(t_1)\left[k_B T K_{nj}(t_1-t_2)\right]^{-1} F_j(t_2) + \sum_j \int_0^t dt' \left[h_j(t') + i\hat{X}_j(t')\right] F_j(t')\right\}. \tag{5.64}$$

We use the notation $\vec{F} = (F_1, ..., F_{N_{dw}})$, the same for $\vec{\phi} = \vec{h} + i\vec{\hat{X}}$ and the $N_{dw} \times N_{dw}$ matrix $\mathbb{M} = k_B T\, \mathbb{K}(t-t')$. The above functional Gaussian integral then becomes

$$\int \mathcal{D}\vec{F} \exp\left\{-\frac{1}{2}\int_0^t dt_1\, dt_2 \vec{F}^t(t_1)\mathbb{M}(t_1-t_2)^{-1}\vec{F}(t_2) + \int_0^t dt_1\, \vec{\phi}^t(t_1)\vec{F}(t_1)\right\}, \tag{5.65}$$

and once the integration over the stochastic forces have been performed, reads

$$\frac{1}{\sqrt{\det \mathbb{K}}} \exp\left\{\frac{k_B T}{2}\int_0^t dt_1\, dt_2 \vec{\phi}^t(t_1)\mathbb{K}(t_1-t_2)\vec{\phi}(t_2)\right\}. \tag{5.66}$$

This expression can be used to compute the expression in equation (5.64),

$$\frac{1}{\sqrt{\det \mathbb{K}}} \exp\left\{\frac{k_B T}{2}\sum_{n,j=1}^{N_{dw}}\int_0^t dt_1\, dt_2 \left[h_j(t_1) + i\hat{X}_j(t_1)\right] K_{jn}(t_1-t_2)\left[h_n(t_2) + i\hat{X}_n(t_2)\right]\right\}. \tag{5.67}$$

This allows us to introduce an action $S[\{X\},\{\hat{X}\};t]$ entering in the definition of the partition function $z[\{h\};t]$,

$$z[\{h\};t] \propto \int \prod_{j=1}^{N_{dw}} \left(\mathcal{D}X_j \mathcal{D}\hat{X}_j\right) \frac{1}{\sqrt{\det \mathbb{K}}}\, e^{-\beta S\left[\{X\},\{\hat{X}\},\{h\};t\right]}. \tag{5.68}$$

The conjugate variables are redefined as $\hat{X}_j \to i k_B T \hat{X}_j$. The action obtained is fully deterministic, the price to pay is however to deal with the hard-to-interpret conjugate variables $\hat{X}_j$,

$$\begin{aligned} S[\{X\},\{\hat{X}\},\{h\};t] = &-\frac{1}{2}\sum_{n,j=1}^{N_{dw}}\int_0^t dt_1\, dt_2 [k_B T\, h_j(t_1) + \hat{X}_j(t_1)] K_{jn}(t_1-t_2)[k_B T\, h_n(t_2) + \hat{X}_n(t_2)] \\ &+ \sum_{j=1}^{N_{dw}}\int_0^t dt_1 \hat{X}_j(t_1)\left(M\ddot{X}_j(t_1) + \frac{\partial W_{N_{dw}}}{\partial X_j}(t_1) + \sum_{n=1}^{N_{dw}}\int_0^{t_1} dt_2\, \dot{X}_n(t_2) K_{jn}(t_1-t_2)\right). \end{aligned} \tag{5.69}$$

The potential appearing above is $W^{(\varepsilon)}_{N_{dw}}$, with $\sum_{\varepsilon=x,y,z} W^{(\varepsilon)}_{N_{dw}} = W_{N_{dw}}$, that we have renamed $W^{(\varepsilon)}_{N_{dw}} \to W_{N_{dw}}$. From the expression of S, one can compute correlation functions taking derivatives with respect to external sources. In general computing correlation functions from the action above is a hard task. However, simplifications arise if one works at very low temperature.

5.5 Low-T calculations: saddle points and instantons

At present, our aim is to compute the statistically relevant time-trajectories $\left\{\{X(t)\},\{\hat{X}(t)\}\right\}$ of the N_{dw} particles. These trajectories may dominate the partition function in equation (5.68) at very low T. At low temperature (when $S/T \ll 1$), they are easily accessible through a saddle-point method

onto the action $S[\{X\},\{\hat{X}\};t]$ found by setting $h_n(t)=0$ for all n in equation (5.69). The solutions found, $\Big\{\{X^\star(t)\},\{\hat{X}^\star(t)\}\Big\}$, correspond to the lowest energy-cost trajectories. There are generically two kinds of solutions: the trivial constant profiles ones, and the nontrivial ones called instantons, corresponding to sharp jumps between the trivial solutions. See also section 2.1 speaking about the method of instantons.

5.5.1 Saddle point and non-linear coupled-differential equations

The instantons solutions are found by minimizing the action $S[\{X\},\{\hat{X}\};t]$ with respect to the trajectories $\Big\{\{X(t)\},\{\hat{X}(t)\}\Big\}$. This is technically doable by taking functional derivatives of $S[\{X\},\{\hat{X}\};t]$, and gives a system of $2N_{dw}$ coupled differential equations:

$$\begin{cases} \dfrac{\delta S[\{X\},\{\hat{X}\};t]}{X_j(t')}\Big|_{X_j^\star,\hat{X}_j^\star}=0 \\ \dfrac{\delta S[\{X\},\{\hat{X}\};t]}{\delta\hat{X}_j(t')}\Big|_{X_j^\star,\hat{X}_j^\star}=0\,. \end{cases} \tag{5.70}$$

The above equations read, more precisely,

$$\begin{cases} 0=M\ddot{\hat{X}}_j^\star(t')+\hat{X}_j^\star(t')\dfrac{\partial^2 W_{N_{dw}}}{\partial(X_j^\star)^2}(t')-\displaystyle\sum_n\int_{t'}^t dt_1\,\hat{X}_n^\star(t_1)\partial_{t'}K_{nj}(t_1-t')+\sum_n\hat{X}_n^\star(t')K_{nj}(0) \\ 0=M\ddot{X}_j^\star(t')+\dfrac{\partial W_{N_{dw}}}{\partial X_j^\star}(t')+\displaystyle\sum_n\left[\int_0^{t'}dt_1\,\dot{X}_n^\star(t_1)K_{nj}(t'-t_1)-\int_0^t dt_1\,\hat{X}_n^\star(t_1)K_{nj}(t'-t_1)\right]. \end{cases} \tag{5.71}$$

Different integrations by parts are performed, yielding boundary terms (BT) that have to be evaluated. In equation (5.71) (top), two BT appear, $\Big[\hat{X}_j(t_1)\partial_{t_1}\delta(t_1-t')\Big]_0^t$ and $\Big[\partial_{t_1}\hat{X}_j(t_1)\delta(t_1-t')\Big]_0^t$ with t' fixed, which are zero for $0\ll t'\ll t$. Another BT, $\big[\delta(t'-t_2)K_{jj'}(t_1-t_2)\big]_0^{t_1}=\delta(t'-t_1)K_{jj'}(0)$, yields the following condition on the times appearing above: $0\leq t'\leq t_1$. In equation (5.71) (bottom), a term $K_{nj}(t_1)\delta(t'-0)$ appears, which is null for the same reason as above.

The mass of each particle is such that $M\gg m$, we can therefore neglect the inertial part of the Langevin equations, $\ddot{X}_j(t)\simeq 0$ and $\ddot{\hat{X}}_j^\star(t)\simeq 0$, going in the over-damped limit.

5.5.2 Simplest nontrivial solutions: general kernel

The constant profile $\hat{X}_j^\star(t)=0$ and $X_{j'}^\star(t)=0$ is the most trivial solution of the system composed by equations (5.71); we are interested in nontrivial ones. Below, we will deal with two kind of instantonic solutions for the particles in the double wells that will be characterized by the different energetic costs they yield. At very low temperature, the trajectories are a sequence of time lapses where the particles stay static in one of the two minima, followed by dynamical jumps across the potential energy barrier which corresponds to an instanton. This instanton can be decomposed in two parts, namely, the "descent" of the potential energy barrier which will be characterized by a zero energetic cost, and the "climb" of the potential energy barrier which will have a finite (and obviously positive) energetic cost.

Descent

The most simple nontrivial and non-constant solution one finds corresponds to the one with all the $\hat{X}_j^\star(t)=0$, for all $j=\{1,....,N_{dw}\}$. This immediately verifies equation (5.71) (top). Replacing the

$\hat{X}_j^\star(t)$ by 0 in equation (5.71) (bottom), we obtain a set of coupled dynamical equations for the particles $X_j^\star$, for all $j \in \{1, \cdots, N_{dw}\}$,

$$\left\{ \begin{array}{c} \hat{X}_j^\star(t') = 0 \\ \displaystyle\int_0^{t'} dt_1\, \dot{X}_j^\star(t_1) K_{jj}(t'-t_1) = -\frac{\partial W_{N_{dw}}}{\partial X_j^\star}(t') - \sum_{n\neq j} \int_0^{t'} dt_1\, \dot{X}_n^\star(t_1) K_{nj}(t'-t_1) \end{array} \right. . \tag{5.72}$$

They correspond to a particle X_j living in a generalized potential $W_{N_{dw}}$ and creating a time dissipation $K_{nj}(t-t')$ on the other particles $X_n^\star$ with $n \neq j$, and $K_{jj}(t-t')$ on itself. The static solutions of the above system of equations correspond to $\dot{X}_j^\star = 0$ for all j, and obviously correspond to stationary points of the generalized potential $W_{N_{dw}}$, that can be minima, maxima and saddle points. In the instanton method, these static solutions are joined by instantonic trajectories involving $1, 2, \cdots, N_{dw}$ particles that can be found by searching for solutions of the above differential equations with $\dot{X}_j^\star \neq 0$ for all the j's.

We can evaluate the energetic cost associated to such an instantonic trajectory, injecting the differential equation (5.72) in the effective action (5.69) for $\{h(t) = 0\}$. The fact that $\hat{X}_j^\star(t') = 0$, for all j and t', immediately provides that the trajectory has a zero energy cost,

$$S[\{X^\star\}, \{\hat{X}^\star\}; t] = 0\,, \tag{5.73}$$

and that this instantonic trajectory then corresponds to the "descent" trajectory of, say, n particles, from a saddle point A of $W_{N_{dw}}$ to a minimum B of $W_{N_{dw}}$ (corresponding to a stable state), that are such that $W_{N_{dw}}(A) > W_{N_{dw}}(B)$.

Climb

Another simple solution consists in fixing $\hat{X}_j^\star(t) = \dot{X}_j^\star(t)$. It transforms equation (5.71) (bottom) in the time-reversal of the bottom equation of the system (5.72),

$$\left\{ \begin{array}{c} \hat{X}_j^\star(t') = \dot{X}_j^\star(t') \\ \displaystyle -\int_{t'}^{t} dt_1\, \dot{X}_j^\star(t_1) K_{jj}(t'-t_1) = -\frac{\partial W_{N_{dw}}}{\partial X_j^\star}(t') + \sum_{n\neq j} \int_{t'}^{t} dt_1\, \dot{X}_n^\star(t_1) K_{nj}(t'-t_1)\,. \end{array} \right. \tag{5.74}$$

In addition, injecting $\hat{X}_j^\star(t) = \dot{X}_j^\star(t)$ into equation (5.71) (top) gives the time derivative of the bottom expression of the system (5.74) just obtained. One finds back that the static solutions are given by the stationary point of $W_{N_{dw}}$, and that the instantonic trajectory can be found by searching for non-static solutions.

If the system of equations (5.72) encodes the descent trajectory of particles within $W_{N_{dw}}$, the system of equations (5.74) which formally corresponds to its time-reverse trajectory then encodes the "climbing" one. We can compute the related energy cost, and obtain that it is finite, and can indeed describe the jump of particles over an energy barrier,

$$\begin{aligned} S[\{X^\star\}, \{\hat{X}^\star\}; t] &= \sum_{j=1}^{N_{dw}} \int_0^t dt_1 \dot{X}_j(t_1) \left[M\ddot{X}_j(t_1) + \frac{\partial W_{N_{dw}}}{\partial X_j}(t_1) \right] = \int_0^t dt_1 \left[\frac{M}{2} \sum_{j=1}^{N_{dw}} \partial_{t_1} \left(\dot{X}_j(t_1)^2 \right) + \partial_{t_1} W_{N_{dw}} \right] \\ &= E_c^P(t) - E_c^P(t=0) + W_{N_{dw}}(t) - W_{N_{dw}}(t=0)\,. \end{aligned} \tag{5.75}$$

The details of this computation are given in appendix C.4. Despite of the complex structure of the differential equations giving the instantonic solution, the finite action of the climb is simply given by the difference between final and initial energy values, irrespective to the details of the instantonic trajectory.

5.5.3 Simplest nontrivial solutions: approximated kernel

The expressions of the instantonic solutions simplify if we replace the local and nonlocal memory kernels by their crudest approximations, given in equations (5.51) and (5.52), respectively. The integrals then are exactly computable and we will use that $\int_0^t dt'\,\delta(t-t') = 1/2$. The potential $W_{N_{dw}}$ is expressed in terms of a free $U_{N_{dw}}$ and a interaction $I_{N_{dw}}$ contributions, expression (5.47) projected in one direction (for example $\varepsilon = x$), the latter verifying that $\partial I_{N_{dw}}/(\partial X_i)(t) = -\sum_{j\neq i} X_j(t)\, Y(\hat{R}_{12})$.

The descent solution then has a "delay" term, with $t_{ij}^d = \min\left(t' - \hat{R}_{ij}/\nu; 0\right)$,

$$\begin{cases} \hat{X}_i^\star(t') = 0 \\ \dfrac{\sigma}{2}\dot{X}_i^\star(t') = -\dfrac{\partial U_{N_{dw}}}{\partial X_i^\star}(t') + \displaystyle\sum_{j\neq i} Y(\hat{R}_{ij}) X_j^\star(t_{ij}^d) \end{cases} \quad \text{for} \quad i \in \{1, \cdots, N_{dw}\}\,, \tag{5.76}$$

and the climb solution has an "advance" term, with $t_{ij}^c = \min\left(t' + \hat{R}_{ij}/\nu; t\right)$,

$$\begin{cases} \hat{X}_i^\star(t') = \dot{X}_i^\star(t') \\ \dfrac{\sigma}{2}\dot{X}_i^\star(t') = +\dfrac{\partial U_{N_{dw}}}{\partial X_i^\star}(t') - \displaystyle\sum_{j\neq i} Y(\hat{R}_{ij}) X_j^\star(t_{ij}^c) \end{cases} \quad \text{for} \quad i \in \{1, \cdots, N_{dw}\}\,, \tag{5.77}$$

5.5.3.1 Low-density expansion

In the following, we want to compute the two dynamical susceptibilities presented in the introduction of this chapter, $\chi_T(t)$ and $\chi_4(t)$. In order to compute them, we are going to make expansions in the density ρ, that should be correct if ρ is low enough.

χ_T - We have seen in section 5.1 that for a system with Hamiltonian dynamics, χ_T could be defined by the expression in equation (5.3). In our case, the three point dynamic susceptibility of the double well reads

$$\chi_T(t) = \frac{1}{k_B T^2}\frac{1}{N_{dw}} \sum_{j=1}^{N_{dw}} \left\langle [X_j(t) - \langle X_j\rangle_0][X_j(0) - \langle X_j\rangle_0] E_{0;N_{dw}} \right\rangle_0 . \tag{5.78}$$

where the statistical average $\langle\,.\,\rangle_0$ is computed with respect to the initial bath-configuration distribution defined in section 5.3.5 and $E_{0;N_{dw}}$ is the energy of the thermal bath in presence of the N_{dw} particles at $t = 0$ for a particular initial configuration of the system {particles + bath}, given in equation (5.53). We have used that its average over all the initial bath configurations is $\langle E_{0;N_{dw}}\rangle_0 = 0$. To compute χ_T, we consider that each term of the sum, corresponding to a particle j, has a dominant contribution (of order 1) coming from the correlation of the particle j *in the absence* of the $N_{dw} - 1$ other particles of the bath, and then the effect of the presence of $N_{dw} - 1$ other particles in the bath contributes as a correction term of order ρ. We can also use that, in the case where there is only one particle in the bath, the mean position of that particle is equal to zero, $\langle X\rangle_{0,1} = 0$, since this particle does not feel the effective ferromagnetic pair interaction that would be generated by the other particles, and the problem of one free particle (submitted to thermal noise) in a double well is symmetric. The average $\langle\,.\,\rangle_{0,1}$ is computed for a bath containing only one particle ($j = 1$), whose initial energy is given by $E_{0;N_{dw}=1}$. In equation, this means that each term of the above sum can be rewritten as

$$\left\langle [X_j(t) - \langle X_j\rangle_0][X_j(0) - \langle X_j\rangle_0] E_{0;N_{dw}} \right\rangle_0 = \langle X_1(t) X_1(0) E_{0;1}\rangle_{0,1} + O(\rho)\,, \tag{5.79}$$

and that the quantity of interest, χ_T, can be computed for a bath containing only one particle at leading order, plus sub-leading corrections of order ρ,

$$\chi_T(t) = \frac{1}{k_B T^2}\,\langle X_1(t) X_1(0) E_{0;1}\rangle_{0,1} + O(\rho)\,. \tag{5.80}$$

χ_4 - The four-point susceptibility was introduced in section 5.1, and for the double-well particles it is defined as

$$\begin{aligned}\chi_4(t) = \tfrac{1}{N_{dw}^2}\textstyle\sum_{i,j=1}^{N_{dw}} \Big\{ &\big\langle [X_i(t)-\langle X_i\rangle_0][X_i(0)-\langle X_i\rangle_0][X_j(t)-\langle X_j\rangle_0][X_j(0)-\langle X_j\rangle_0]\big\rangle_0 \\ &- \big\langle [X_i(t)-\langle X_i\rangle_0][X_i(0)-\langle X_i\rangle_0]\big\rangle_0 \big\langle [X_j(t)-\langle X_j\rangle_0][X_j(0)-\langle X_j\rangle_0]\big\rangle_0 \Big\} .\end{aligned} \tag{5.81}$$

We are going to use the same argument than above, that is that one-particle quantities can be estimated by their leading order, such that the "self" part (when $i=j$) of the expression of χ_4 is given by

$$\begin{aligned}&\big\langle [X_i(t)-\langle X_i\rangle_0]^2[X_i(0)-\langle X_i\rangle_0]^2\big\rangle_0 - \big\langle [X_i(t)-\langle X_i\rangle_0][X_i(0)-\langle X_i\rangle_0]\big\rangle_0^2 \\ &= \big\langle X_1(t)^2X_1(0)^2\big\rangle_{0,1} - \big\langle X_1(t)X_1(0)\big\rangle_{0,1}^2 + O(\rho) ,\end{aligned} \tag{5.82}$$

and also the connected part of the nonlocal contribution of χ_4 (when $i\neq j$)

$$\big\langle [X_i(t)-\langle X_i\rangle_0][X_i(0)-\langle X_i\rangle_0]\big\rangle_0 \big\langle [X_j(t)-\langle X_j\rangle_0][X_j(0)-\langle X_j\rangle_0]\big\rangle_0 = \big\langle X_1(t)X_1(0)\big\rangle_{0,1}^2 + O(\rho) . \tag{5.83}$$

The effect of the $N_{dw}-1$ other particles that yields a correction of order ρ in the self part of χ_4, whose ρ-expansion is given in equation (5.82), acts as a small field on particle 1 which modifies slightly the stationary positions of X_1 (see below), and should therefore be trivial and not be responsible for the existence of dynamical correlations in $\chi_4(t)$. For this reason we neglect this correction of $O(\rho)$ in the following.

Similarly, two-particle quantities appearing in the sum giving χ_4 are computed, at leading order, for a bath containing only two particles, and the effect of the presence of the $N_{dw}-2$ other particles are encoded in a correction term of order ρ. Introducing the average $\langle\,.\,\rangle_{0,2}$, computed for a bath containing two double wells whose initial energy is given by $E_{0;N_{dw}=2}$, we obtain that the two-particle terms are given by, with $i\neq j$,

$$\big\langle [X_i(t)-\langle X_i\rangle_0][X_i(0)-\langle X_i\rangle_0][X_j(t)-\langle X_j\rangle_0][X_j(0)-\langle X_j\rangle_0]\big\rangle_0 = \big\langle X_1(t)X_1(0)X_2(t)X_2(0)\big\rangle_{0,2} + O(\rho) . \tag{5.84}$$

(Notice that the approximation in equation (5.83) can be a source of error. This is discussed in the conclusion of this chapter.) Within this low-ρ approximation and using translation invariance for the particle that are indiscernible, the four-point susceptibility is given by:

$$\begin{aligned}\chi_4(t) = &\frac{1}{N_{dw}}\Big(\big\langle X_1(t)^2X_1(0)^2\big\rangle_{0,1} - \big\langle X_1(t)X_1(0)\big\rangle_{0,1}^2\Big) \\ &+ \frac{1}{N_{dw}}\sum_{j=2}^{N_{dw}}\Big\{\big\langle X_1(t)X_1(0)X_j(t)X_j(0)\big\rangle_{0,2} - \big\langle X_1(t)X_1(0)\big\rangle_{0,1}^2 + O(\rho)\Big\} .\end{aligned} \tag{5.85}$$

We have seen with the above density expansion that, at leading order, the two dynamic susceptibilities that we want to compute can be fully characterized by quantities calculated with baths containing only one or two particles. Therefore, in the following we focus on these two situations. We will drop the $\star$ to simplify the notations.

5.5.3.2 One particle

For a single particle "1" in a double-well potential, the effect of the other particles is absent in the expression of $U_{N_{dw}}$ and the potential is simply given by:

$$U_1(X) = V_1(X) = \frac{\Delta}{4}\left(X^2 - X_0^2\right)^2 , \tag{5.86}$$

with X_0 defined in equation (5.30). The differential equations giving the instantonic solutions become (with "−" standing for the descent and "+" for the climb):

$$\left\{\begin{array}{l} \hat{X}_-(t') = 0 \\ \frac{\sigma}{2}\dot{X}_-(t') = -\frac{\partial V_1}{\partial X_-}(t') \end{array}\right. , \quad \left\{\begin{array}{l} \hat{X}_+(t') = \dot{X}_+(t') \\ \frac{\sigma}{2}\dot{X}_+(t') = +\frac{\partial V_1}{\partial X_+}(t') \end{array}\right. . \tag{5.87}$$

There are two kind of solutions verifying the above equations: constant profiles $\pm X_0$, costing zero energy, and instantons linking the constant profiles. Their energetic cost is given by the action of the climb (the descent costing zero energy) in equation (5.75), for one particle whose climb occurs between $t = -\infty$ and $t = 0$, $S\left[X_+, \hat{X}_+\right] = \frac{M}{2}\left(\dot{X}_+(0)^2 - \dot{X}_+(-\infty)^2\right) + V_1\left(X_+(0)\right) - V_1\left(X_+(-\infty)\right)$. Each instanton then costs a finite energy $S_\star$ which is given by

$$S_\star = V_1(0) = \Delta X_0^4/4\,, \tag{5.88}$$

if $X_+(t=-\infty) = \pm X_0$, $X_+(0) = 0$ and $\dot{X}_+(t=-\infty) = \dot{X}_+(t=0) = 0$.

The instantonic solutions verify the following equation:

$$\dot{X}_\pm(t) = \pm 2\frac{\Delta}{\sigma} X_\pm(t)\left(X_\pm(t)^2 - X_0^2\right)\,, \tag{5.89}$$

which can be solved analytically for both descent and climb: a typical solution has been represented on figure 5.3. This is rather well known [202], and one finds that the time spent at the top of the barrier is of duration $\delta t \sim -\log T$, and is very short compared to the typical time separating two consecutive instantons, $\tau = e^{\beta S_\star}$.

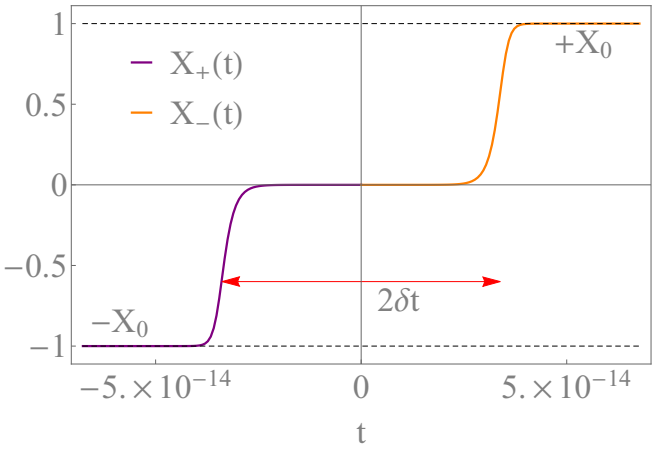

Figure 5.3: Instanton solutions for one independent particle linking the constant profiles $\pm X_0$. $X_+(t)$ and $X_-(t)$ correspond respectively to the "climb" and to the "descent" solutions. The "width" of the instanton is $\delta t \sim -\log T$ and is small compared to the distance between consecutive instantons, $\tau = e^{\beta S_\star}$.

5.5.3.3 Two particles

We solve numerically the coupled differential equations in (5.76) and (5.77), for a system of two particles at mutual (dimensionless) distance $\hat{R}_{12}$ on a time interval $[0; t]$. The free potential $U_{N_{dw}}$ in this case is equal to:

$$U_2(X_1, X_2) = V_1(X_1) + V_1(X_2) = \frac{\Delta}{4}\left(X_1^2 - X_0^2\right)^2 + \frac{\Delta}{4}\left(X_2^2 - X_0^2\right)^2\,, \tag{5.90}$$

with X_0 and $Y(\hat{R}_{12})$ defined in equations (5.30) and (5.33), respectively.

The coupled equations are different depending if we consider the descent solution $(-)$, with $t_d = \min\left(t' - \hat{R}_{12}/\nu; 0\right)$,

$$\begin{cases} \frac{\sigma}{2}\dot{X}_{1,-}(t') = -\frac{\partial U_2}{\partial X_{1,-}}(t') + Y(\hat{R}_{12})X_{2,-}(t_d) \quad \hat{X}_{1,-}(t') = 0 \\ \frac{\sigma}{2}\dot{X}_{2,-}(t') = -\frac{\partial U_2}{\partial X_{2,-}}(t') + Y(\hat{R}_{12})X_{1,-}(t_d) \quad \hat{X}_{2,-}(t') = 0\,, \end{cases} \tag{5.91}$$

or the climb solution $(+)$, with $t_c = \min\left(t' + \hat{R}_{12}/\nu; t\right)$,

$$\begin{cases} \frac{\sigma}{2}\dot{X}_{1,+}(t') = +\frac{\partial U_2}{\partial X_{1,+}}(t') - Y(\hat{R}_{12})X_{2,+}(t_c) \quad \hat{X}_{1,+}(t') = \dot{X}_{1,+}(t') \\ \frac{\sigma}{2}\dot{X}_{2,+}(t') = +\frac{\partial U_2}{\partial X_{2,+}}(t') - Y(\hat{R}_{12})X_{1,+}(t_c) \quad \hat{X}_{2,+}(t') = \dot{X}_{2,+}(t')\,. \end{cases} \tag{5.92}$$

The solutions of the above systems of differential equations are either constant profiles (X_1^c, X_2^c) or finite-energetic cost instantons linking them. We find the constant profiles by solving, for all j, $\dot{X}_{j,\pm}(t) = 0$ and setting $X_j(t) = X_j^c$ for all t, this gives:

$$\begin{cases} \frac{\partial U_2}{\partial X_1^c} = Y(\hat{R}_{12})X_2^c \\ \frac{\partial U_2}{\partial X_2^c} = Y(\hat{R}_{12})X_1^c \end{cases}. \tag{5.93}$$

The system has nine solutions (X_1^c, X_2^c), which, of course, correspond to stationary points of the potential $W_2(X_1, X_2)$. The solutions are: the global maximum in $(0,0)$, the minima in $\simeq (\pm X_0, \pm X_0)$ noted $(+,+)$, $(-,-)$, $(+,-)$, $(-,+)$, and the saddle points in $\simeq (0, \pm X_0)$ or $\simeq (\pm X_0, 0)$ (saddle points) noted $(0,+)$, $(0,-)$, $(+,0)$, $(-,0)$. Introducing $\psi_\pm(n) = \sqrt{1 \pm n\, Y(\hat{R}_{12})/(\Delta\, X_0^2)}$ with $\psi_+ > 1$ and $\psi_- < 1$, the static solutions are given by:

$$\begin{aligned} (X_1^c\,;\, X_2^c) = (\pm,\pm) &\equiv (\pm X_0\,\psi_+(1)\,;\, \pm X_0\,\psi_+(1)) \quad ; \quad (\pm,\mp) \equiv (\pm X_0\,\psi_-(1)\,;\, \mp X_0\,\psi_-(1))\,; \\ (0,\pm) &\equiv \left(\mp\frac{X_0}{\sqrt{2}}\sqrt{1-\psi_+(2)\psi_-(2)}\,;\, \pm\frac{X_0}{\sqrt{2}}\sqrt{1+\psi_+(2)\psi_-(2)}\right)\,; \\ (\pm,0) &\equiv \left(\pm\frac{X_0}{\sqrt{2}}\sqrt{1+\psi_+(2)\psi_-(2)}\,;\, \mp\frac{X_0}{\sqrt{2}}\sqrt{1-\psi_+(2)\psi_-(2)}\right)\,; \\ (0,0) &\equiv (0\,;\,0)\,. \end{aligned} \tag{5.94}$$

The respective potential energies of the stationary states are, with $S_\star$ the action of the instanton of an independent particle (see above),

$$\begin{aligned} W_2(\pm,\pm) &= -X_0^2\, Y\left(\hat{R}_{12}\right) - \frac{Y\left(\hat{R}_{12}\right)^2}{2\,\Delta} \quad ; \quad W_2(\pm,\mp) = +X_0^2\, Y\left(\hat{R}_{12}\right) - \frac{Y\left(\hat{R}_{12}\right)^2}{2\,\Delta} \\ W_2(0,\pm) &= W_2(\pm,0) = S_\star + \frac{Y\left(\hat{R}_{12}\right)^2}{2\,\Delta} \quad ; \quad W_2(0,0) = 2\,S_\star\,. \end{aligned} \tag{5.95}$$

The instantons are found in two steps: [2] First solving the system of differential equations which gives the descent part of the instanton. Then, since the climb system of equations is formally identical

[2] We previously considered a perturbative treatment of $Y(\hat{R}_{12}) \ll 1$ around the one particle solution found above. However this yielded diverging contributions and we abandoned it.

to the time reverse of the descent system of equations (forgetting about the auxiliary variables), we find the climb solution by taking the time reverse of the descent solution.

Simple instanton

We search the instanton for one particle, say X_1, while the other, X_2, stays in the same minimum. The descent solution is found by solving equations (5.91) with an initial condition taken among the saddle points of W_2, $(\pm, 0)$ and $(0, \pm)$. The width (in time) δt of the kink is small compared to $\hat{R}_{12}/\nu$. Then, supposing that the particle was static a time $\hat{R}_{12}/\nu$ before the kink, we can consider the delayed positions, $X_{1,-}(t_d)$ and $X_{2,-}(t_d)$ with $t_d = t - \hat{R}_{12}/\nu$ as constant and equal to the initial condition $(\pm, 0)$ or $(0, \pm)$ on the interval $t' \in [0; n\,\delta t]$, where $t = 0$ is the initial time of the kink and n is an integer. The system should at $t = 0$ is at a stationary point of W_2. Then, in order to find a dynamical solution one has to slightly perturb the initial condition away from the maximum, $X_{1,-}(0) \to X_{1,-}(0) \pm \varepsilon$, with $\varepsilon > 0$ small.

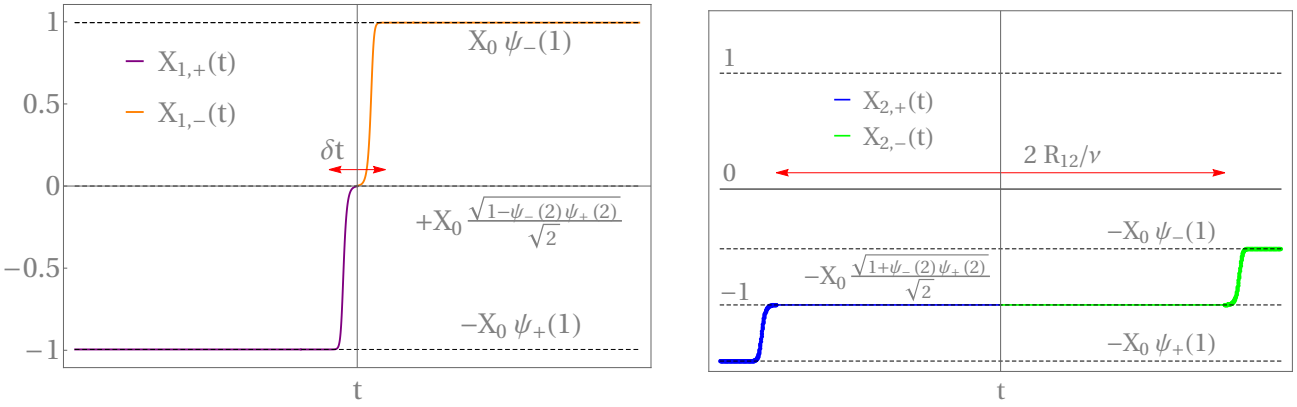

Figure 5.4: Sketch of the simple instanton solutions for two coupled particles, $X_{1/2,+}(t)$ and $X_{1/2,-}(t)$, corresponding respectively to the "climb" and to the "descent". The stationary points of $W_2(X_1, X_2)$ by which the solutions pass are represented. Here $R_{12} \equiv \hat{R}_{12}$.

As an example, in figure 5.4 we show a sketch of the descent solutions, $X_{1,-}(t)$ in orange and $X_{2,-}(t)$ in green, for $t \geq 0$ and for the initial condition: $(X_{1,-}(0), X_{2,-}(0)) \equiv (0 + \varepsilon, -)$. A time $\hat{R}_{12}/\nu$ after the beginning of the descent kink, the solution $X_{2,-}(t)$ begins to feel a contribution from the delayed term $X_{1,-}(t_d)$ which varies of $O(1)$ on a time $O(\delta t)$. This creates a small "kink" on $X_{2,-}(t)$, as one can see on figure 5.4. The height of this kink is of order $O\left[Y\left(\hat{R}_{12}\right) \Delta X_{1,-}\right]$, where $\Delta X_{1,-} = O(1)$ gives the difference between final and initial positions during the precedent kink.The system then ends in an "approximate" stable state $(+, -)$.

Indeed, one can see that after an other time interval $\hat{R}_{12}/\nu$, the particle $X_{1,-}(t)$ will feel a contribution from $X_{2,-}(t_d)$, creating a kink of order $O\left[Y\left(\hat{R}_{12}\right) \Delta X_{2,-}\right] = O\left[Y\left(\hat{R}_{12}\right)^2\right]$, since $\Delta X_{2,-} = O\left[Y\left(\hat{R}_{12}\right)\right]$. The stable state will be reached when the above serie will have converged, and that happens exponentially fast in $\hat{R}_{12}/\nu$.

On can obtain an other descent solution with initial condition : $(X_{1,-}(0), X_{2,-}(0)) = (0 - \varepsilon, -)$. Its time reverse gives the climb solution shown in figure 5.4, in purple for $X_{1,+}(t)$ and blue for $X_{2,+}(t)$. Joining the two at $t = 0$ gives the simple instanton at leading order for the two coupled particles.

The effective ferromagnetic interaction between X_1 and X_2 yields different finite energetic cost if the climb begins from a ferromagnetic initial state, $(\pm, \pm)$, or from an anti-ferromagnetic one, $(\pm, \mp)$.

The former costs more energy than the latter:

$$\begin{aligned} S\left[(\pm,\pm)\to(0,\pm)\right] &= W_2(0,\pm) - W_2(\pm,\pm) = S_\star + X_0^2\, Y\left(\hat{R}_{12}\right) + \frac{Y\left(\hat{R}_{12}\right)^2}{\Delta} > S_\star\,, \\ S\left[(\mp,\pm)\to(0,\pm)\right] &= W_2(0,\pm) - W_2(\mp,\pm) = S_\star - X_0^2\, Y\left(\hat{R}_{12}\right) + \frac{Y\left(\hat{R}_{12}\right)^2}{\Delta} < S_\star\,. \end{aligned} \tag{5.96}$$

In the computation of the energetic costs we have considered the initial and final states as stable states of W_2, hence neglecting sub-leading corrections of the exponential convergence (in $\hat{R}_{12}/\nu$) of the instanton toward a stable state. This approximation will be kept in the following of this chapter.

Double instanton

Besides the instantonic solutions during which only one particles overcomes the barrier (and whose energy cost is of order $S_\star$), there is another class of possible solutions, that we will call the "double instanton": it corresponds to two particles jumping together over the barrier. These solutions will turn out to cost an energy of order $2\,S_\star$, and one could generically expect that only yield a sub-leading contribution. Yet, as we will discuss below, they might be relevant for the computation of the dynamical susceptibilities.

In order to find the double instanton solution, we perform the same analysis than above with the initial condition $(0,0)$. The initial position $X_{1,-}(0)$ is slightly perturbed by ε, hence X_1 makes the first descent kink. It is shown in figure 5.5 for the initial condition $(\varepsilon,0)$. After a time $\hat{R}_{12}/\nu$, the second particle feels a contribution from $X_{1,-}(t_d)$ and begins to move toward a stable state of W_2, as shown on figure 5.5. If one does not apply at hand an ε-perturbation on $X_{2,-}(0)=0$ the final state will always be ferromagnetic. As in the case of the simple instanton, the climb solution is taken as the time reverse of the descent solution with initial condition $(-\varepsilon,0)$.

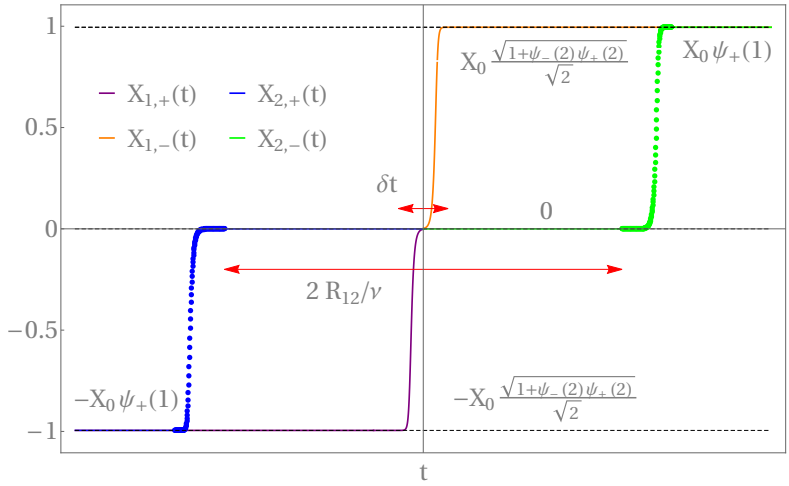

Figure 5.5: Double instanton solutions for two coupled particles, $X_{1/2,+}(t)$ and $X_{1/2,-}(t)$, corresponding respectively to the "climb" and to the "descent". Here $R_{12}\equiv\hat{R}_{12}$.

The finite energetic cost of the double instanton depends on the initial state of the climb, ferromag-

netic or anti-ferromagnetic. The former will cost more energy than the latter:

$$\begin{aligned} S\left[(\pm,\pm)\to(0,0)\right] &= W_2(0,0) - W_2(\pm,\pm) = 2\,S_\star + X_0^2\,Y\left(\hat{R}_{12}\right) + \frac{Y\left(\hat{R}_{12}\right)^2}{2\,\Delta} > 2\,S_\star\,, \\ S\left[(\mp,\pm)\to(0,0)\right] &= W_2(0,0) - W_2(\mp,\pm) = 2\,S_\star - X_0^2\,Y\left(\hat{R}_{12}\right) + \frac{Y\left(\hat{R}_{12}\right)^2}{2\,\Delta} < 2\,S_\star\,, \end{aligned} \tag{5.97}$$

where we have also considered that initial and final states can be taken as stable states of W_2. The instantonic solution form $(\mp,\pm)$ to $(0,0)$ has a smaller energetic cost than two independent instantons and might be physically relevant.

5.6 Three-point susceptibility

We have seen in section 5.5.3.1 that the three-point susceptibility is given by the equation (5.80), for which we have to compute $\langle X_1(t)X_1(0)E_{0;1}\rangle_{0,1}$ for a bath containing only one particle.

$E_{0;1}$ contains a kinetic and a potential parts, $E_{0;1} = E_{0;1}^{(c)} + E_{0;1}^{(p)}$, that, we suppose for the moment, contribute identically to the expression of χ_T. We use the expression in equation (5.46) at $t = 0$ (in one particular space direction ε), with $F_1(t=0) = \sum_{\vec{k}} F_{1,\vec{k}}(0)$, to write

$$E_{0;1}^{(p)} = \frac{1}{2}\sum_{\vec{k}} \widetilde{\lambda}_k^2 \left| \vec{u}_{\vec{k}}(0) - \frac{g}{\sqrt{N}}\frac{1}{\widetilde{\lambda}_k^2} X_1(0)\,\vec{e}_x e^{-i\vec{k}\vec{R}_1} \right|^2 = \frac{1}{2}\frac{N}{g^2}\sum_{\vec{k},\vec{k}'} \widetilde{\lambda}_k^2\, e^{-i(\vec{k}+\vec{k}')\vec{R}_1}\, F_{1,\vec{k}}(0)\, F_{1,\vec{k}'}(0)\, \delta_{\vec{k},-\vec{k}'}\,. \tag{5.98}$$

Using the equation (5.15) to reintroduce the lattice spacing in the above expression, the quantity to compute becomes:

$$\left\langle X_1(t)X_1(0)E_{0;1}^{(p)}\right\rangle_{0,1} = \frac{1}{2}\frac{1}{g^2}\sum_{j=1}^{N}\sum_{\vec{k},\vec{k}'} e^{i(\vec{k}+\vec{k}')\cdot(\vec{l}_j-\vec{R}_1)}\,\widetilde{\lambda}_k\,\widetilde{\lambda}_{k'}\left\langle X_1(t)\,X_1(0)\,F_{1,\vec{k}}(0)\,F_{1,\vec{k}'}(0)\right\rangle_{0,1}\,. \tag{5.99}$$

The dynamical correlation $\left\langle X_1(t)X_1(0)E_{0;1}^{(p)}\right\rangle_{0,1}$, and probably also the three-point dynamical susceptibility $\chi_T(t)$, is composed of small correlations $\left\langle X_1(t)\,X_1(0)\,F_{1,\vec{k}}(0)\,F_{1,\vec{k}'}(0)\right\rangle_{0,1}$ that are of order g^2, since we know from the equation (5.60) that the time-correlation of the stochastic force is of order g^2. This correlation propagates *via* phonons of wavelength $\vec{k}$, and when one sums over all wavelengths and over all space points one finds a correlation $\left\langle X_1(t)X_1(0)E_{0;1}^{(p)}\right\rangle_{0,1}$ which is of order 1, as well as the three-point dynamic susceptibility $\chi_T(t)$.

We can use the field theory obtained via the Martin-Siggia-Rose-De Dominicis-Janssen formalism to compute this correlation function. Indeed, we remark that field derivatives of the partition function in equation (5.62) (in one fixed direction ε) with respect to the sources $h_{1,\vec{k}}(t')$ and evaluated in zero field give rise to the connected correlation functions of the stochastic force, with $\left\langle F_{1,\vec{k}}(0)\right\rangle_{0,1} = 0$,

$$\frac{1}{z[\{h=0\}]}\frac{\delta z[\{h\}]}{\delta h_{1,\vec{k}}(0)\delta h_{1,\vec{k}'}(0)}\Big|_{\{h_{1,\vec{k}}=0\}} = \left\langle F_{1,\vec{k}}(0)\,F_{1,\vec{k}'}(0)\right\rangle_{0,1}\,. \tag{5.100}$$

Therefore the average of equation (5.99) can be computed *via*:

$$\left\langle X_1(t)X_1(0)\,F_{1,\vec{k}}(0)\,F_{1,\vec{k}'}(0)\right\rangle_{0,1} = \frac{\delta\left\langle X_1(t)X_1(0)\right\rangle_{0,\{h\}}}{\delta h_{1,\vec{k}}(0)\delta h_{1,\vec{k}'}(0)}\Big|_{\{h_{1,\vec{k}}=0\}}\,. \tag{5.101}$$

We can compute an estimation of the above quantity from the expression in equation (5.68) of the partition function. This is an estimation because all the terms that would be generated by the field derivative with respect to the fields are not displayed, however we can suppose that they would yield the same conclusion as the one we give at the end of this section. One of the terms generated by the computation of the correlation $\left\langle X_1(t)X_1(0)\,F_{1,\vec{k}}(0)\,F_{1,\vec{k}'}(0)\right\rangle_{0,1}$ is given by:

$$\begin{aligned}&\frac{1}{z[\{h=0\};t]}\int_0^t dt_1\,dt_2\,K_{11}(t_1;\vec{k})K_{11}(t_2;\vec{k}')\int \mathcal{D}X_1\mathcal{D}\hat{X}_1\,X_1(t)X_1(0)\,\hat{X}_1(t_1)\hat{X}_1(t_2)\,e^{-\beta S\left[X_1,\hat{X}_1,\{h=0\};t\right]}\\&=\int_0^t dt_1\,dt_2\,K_{11}(t_1;\vec{k})K_{11}(t_2;\vec{k}')\left\langle X_1(t)X_1(0)\,\hat{X}_1(t_1)\hat{X}_1(t_2)\right\rangle_{0,1}\,,\end{aligned} \tag{5.102}$$

with $K_{11}(t_1)=\sum_{\vec{k}}K_{11}(t_1;\vec{k})$.

This quantity is not easy to compute. However, in the limit of low temperatures we can make use of the instanton method, exact in the limit $T\to 0$ (see section 2.1). The system is then dominated by trajectories which minimize the action $S\left[X_1,\hat{X}_1,\{h=0\};t\right]$. From section 5.5.3.2 we know that these trajectories are composed by constant profiles $\pm X_0$ linked by localized (in time) instantonic jumps. The energetic cost of the former is zero, and of the latter is $S_\star=\Delta X_0^4/4$. A trajectory of duration t and composed by n instantons has therefore a probability $e^{-n\,\beta S_\star}$. In the following we make the hypothesis that the instantons width is negligible compared to the distance between two consecutive instantons. Since subsequent instantons are uncorrelated, we suppose that they arrive at Poissonian times. As a consequence, the entropic factor coming from the location of the n instantons is simply given by this integral

$$\int_0^t dt_1\int_{t_1}^t dt_2\cdots\int_{t_{n-1}}^t dt_n=\frac{t^n}{n!}\,. \tag{5.103}$$

The probability for a particle to go from, say, $X_1(0)=-X_0$ to $X_1(t)=-X_0$ is then given by a sum over all possible even values of $n=2k$,

$$P(-X_0\to -X_0)=\frac{1}{M}\sum_{k=0}^{\infty}e^{-2k\,\beta S_\star}\frac{t^{2k}}{(2k)!}=2\,\cosh\left(t/\tau\right)\quad\text{with}\quad\tau=e^{\beta S_\star}\,, \tag{5.104}$$

with M some normalization constant, and becomes a sum over odd values if initial and final states are different. Summing over all possible initial and final states, we can compute easily the autocorrelation function of a system of N_{dw} particles,

$$C(t)=\langle X_1(t)X_1(0)\rangle_{0,1}-\langle X_1\rangle_{0,1}^2+O(\rho)=X_0^2\,e^{-2t/\tau}+O(\rho)\,. \tag{5.105}$$

We now turn to compute the quantity of interest which is given in equation (5.102). From equation (5.87), $\hat{X}_1(t')$ is nonzero only if t' is evaluated during an instantonic event which are assumed to have a zero width. Therefore we add the constraint that at time t_1 occurs the m_1-th instanton and at time $t_2>t_1$ occurs the (m_1+m_2)-th instanton, obliging us to consider at least $n=2$ instantons to have a nonzero expression. Then we can also estimate that, at the "middle" of the kink/anti-kink, when $X_1(t)\simeq\pm X_0/2$, the auxiliary variables are given by $\hat{X}_1=\dot{X}_1=(2/\sigma)\,(\partial_{X_1}U_1)\,(X_1\simeq\mp X_0/2)\propto\pm\Delta\,X_0^3/\sigma$, with $\sigma=g^2\,\alpha$. Then the expression becomes, supposing that $X_1(0)=-X_0$,

$$\begin{aligned}&\left\langle X_1(t)X_1(0)\,\hat{X}_1(t_1)\hat{X}_1(t_2)\right\rangle_{0,1}\propto X_0^8\,\frac{\Delta^2}{\sigma^2}\sum_{n=2}^{\infty}(-1)^n e^{-n\,\beta S_\star}\\&\sum_{m_1=1}^{\infty}\sum_{m_2=1}^{\infty}\sum_{m_3=0}^{\infty}\delta(m_1+m_2+m_3-n)\,(-1)^{m_1-1}\frac{t_1^{m_1-1}}{(m_1-1)!}(-1)^{m_2}\frac{(t_2-t_1)^{m_2-1}}{(m_2-1)!}\frac{(t-t_2)^{m_3}}{m_3!}\,.\end{aligned} \tag{5.106}$$

The factor $(-1)^n$ account for the fact that $X_1(0)X_1(t) = \pm X_0^2$ depending if the number n of instanton is even or odd, respectively. The factor $(-1)^{m_1-1}$ (or $(-1)^{m_2}$) takes into account that $\hat{X}_1(t_1)$ (or $\hat{X}_1(t_2)$) does not have the same sign if m_1 (or m_2) is a kink or an anti-kink. The sums over m_1, m_2 and m_3 can be performed by shifting m_1 and m_2 by minus one, this yields: $-[t-2(t_2-t_1)]^{n-2}/((n-2)!)$. This expression can be injected into equation (5.106) and gives, after summing over n,

$$\left\langle X_1(t)X_1(0)\,\hat{X}_1(t_1)\hat{X}_1(t_2)\right\rangle_{0,1} \propto -\left(\frac{4\,S_\star}{\tau\,\sigma}\right)^2 \exp\left(-[t-2\,(t_2-t_1)]/\tau\right)\,. \tag{5.107}$$

If the trajectory begins from $X_1(0) = +X_0$, one has to consider factors $(-1)^{m_1}$ and $(-1)^{m_2-1}$ instead, and one obtains exactly the same contribution. We have also considered the case where the times t_1 and t_2 fall into the same instantonic event, $t_1 = t_2$, this yields a similar expression. Injecting all the ingredients into equation (5.99) we obtain an estimation of $\left\langle X_1(t)X_1(0)E^{(p)}_{0;1}\right\rangle_{0,1}$:

$$-8\,\frac{g^2\,S_\star^2}{\tau^2\,\sigma^2}\,e^{-t/\tau}\sum_{j=1}^{N}\left\{\tau\int_0^t dt_1\,[f_j\,(t_1)]^2 + 4\int_0^t dt_2\int_0^{t_2} dt_1\,f_j\,(t_1)\,f_j\,(t_2)\,e^{2\,(t_2-t_1)/\tau}\right\}\,, \tag{5.108}$$

where we have introduced the function $f_j\,(t_1)$, with $K_{11}(t_1;\vec{k})$ from equation (5.48),

$$f_j\,(t_1) = \sum_{\vec{k}} e^{i\vec{k}(\vec{l}_j-\vec{R}_1)}\,\widetilde{\lambda}_k\,\frac{1}{g^2}K_{11}(t_1;\vec{k}) = \frac{1}{N}\sum_{\vec{k}} e^{i\vec{k}(\vec{l}_j-\vec{R}_1)}\,\frac{\cos(\omega_k\,t_1)}{\widetilde{\lambda}_k}\,. \tag{5.109}$$

This function can be rewritten as $f_j(t_1) = (2\pi)^{-2}\,K^{-1/2}\,a^2/d_j^2\,\phi_j\left(\sqrt{K/m}\,t_1\,a/d_j\right)$, with a the lattice spacing and the length $d_j = ||\vec{l}_j - \vec{R}_1||$. The scaling function ϕ_j contains a unique dynamical length scale d_j, the distance between the double well and site j, over which phonons propagate with a constant velocity $c = a\,\sqrt{K/m}$. The computation of ϕ_j is performed in appendix C.5. We can make a change of variable to reexpress the equation (5.108), replacing the time variables t_1 over which the integrals are performed by $t_1 \to x\,t_j$, x being without dimension and $t_j = d_j/c$ a time scale, and this gives a new expression for equation (5.108),

$$-\frac{8\,g^2\,S_\star^2\,a^4\,e^{-t/\tau}}{(2\pi)^4K^2}\sum_{j=1}^{N}\frac{1}{(\tau\,d_j)^2}\left\{\frac{\tau}{t_j}\int_0^{t/t_j} dx\,[\phi_j\,(x)]^2 + 4\int_0^{t/t_j} dx\int_0^x dy\,\phi_j\,(x)\,\phi_j\,(y)\,e^{2\,(x-y)/(\tau/t_j)}\right\}\,. \tag{5.110}$$

This estimation is informative since it implies that $\left\langle X_1(t)X_1(0)E^{(p)}_{0;1}\right\rangle_{0,1}$ is composed of small contributions that propagate in a ballistic way: they cover distances d_j with constant velocity c. If the other terms composing the dynamical correlation $\left\langle X_1(t)X_1(0)E^{(p)}_{0;1}\right\rangle_{0,1}$ behave in the same fashion and if $E^{(p)}_{0;1}$ and $E^{(c)}_{0;1}$ contribute identically to χ_T, we can estimate that the maximal dynamical correlation that arises from the maximum of χ_T at $t \sim \tau$ has a ballistic dynamical length scale $c\,\tau$. Physically, the jump of an Arrhenius particle over its potential energy barrier creates a perturbation of order Δ which is large compared to the thermal fluctuations of the bath k_BT, this perturbation propagates within the bath and generates small-amplitude dynamical correlations that spread on a ballistic length scale of order $c\,\tau$: the jump of an Arrhenius particle dynamically correlates to a volume $(c\,\tau)^3$ of the bath around it. After a time of order τ, the Arrhenius particles makes a new jump and the dynamical correlation begins to vanish.

5.7 Four-point susceptibility

We have seen in section 5.5.3.1 that the four-point susceptibility is given by the equation (5.85), for which we have to compute $\langle X_1(t)^2 X_1(0)^2 \rangle_{0,1}$, $\langle X_1(t) X_1(0) \rangle_{0,1}$ and $\langle X_1(t) X_1(0) X_2(t) X_2(0) \rangle_{0,2}$. We introduce the four-point correlation function as

$$g_4(\hat{R}_{12}, t) = \langle X_1(t) X_1(0) X_2(t) X_2(0) \rangle_{0,2} - \langle X_1(t) X_1(0) \rangle_{0,1}^2 \,, \tag{5.111}$$

where $\hat{R}_{12}$ is the dimensionless distance between particles 1 and 2. We can transform the sum appearing in the expression of χ_4 in an integral, using that the double-wells are separated by a typical distance $\Delta\hat{r} = \rho^{-1/3} \to d\hat{r}$, then

$$\sum_{j=2}^{N_{dw}} g_4(\hat{R}_{1j}, t) \simeq \rho \int_{(\tau\,\nu)^3} d^3\hat{r}\, g_4(\hat{r}, t) \,. \tag{5.112}$$

The integral is over a dimensionless volume of radius $\tau\,\nu$ (with $\nu = \sqrt{K/m} = c/a$) because two particles at distance $\hat{r} > \tau\,\nu$ cannot be correlated since they would have relaxed before the ballistic signal or correlation would arrive (see also section 5.6), and $g_4(\hat{r} > \tau\,\nu, t) \simeq 0$. The four-point susceptibility can then be rewritten as

$$\chi_4(t) \simeq \frac{1}{N_{dw}} \left\{ \langle X_1(t)^2 X_1(0)^2 \rangle_{0,1} - \langle X_1(t) X_1(0) \rangle_{0,1}^2 + \rho \int_{(\tau\,\nu)^3} d^3\hat{r}\, g_4(\hat{r}, t) + O(\rho^2) \right\} . \tag{5.113}$$

We want to compute $g_4(\hat{r}, t)$, with $\hat{r} \geq 1$. In order to proceed we use again the method of instantons, valid in the low temperature limit. Then, we know that the time-trajectories of our two particles, $X_1(t)$ and $X_2(t)$, are dominated by constant profiles, $(\pm, \pm)$ and $(\pm, \mp)$, costing almost no energy, and instanton trajectories linking them, given by either a simple $O(1)$ jump or two, called respectively the "simple" and "double" instantons. To compute statistic averages one has to sum over all possible trajectories of this kind, akin to what was done to compute χ_T.

However it is slightly more involved here as one is confronted to four constant profiles (instead of two for χ_T) and to four different instantons, or four different energy costs, from the left state to the right state,

$$(\pm, \pm) \to (0, \pm)\,;\ (\mp, \pm) \to (0, \pm)\,;\ (\pm, \pm) \to (0, 0)\,;\ (\mp, \pm) \to (0, 0)\,. \tag{5.114}$$

The energy costs of the above instantons are fully determined by the initial and final states, as one can see in equations (5.96) and (5.97). Since the instantons are diluted enough in time, typically separated by a time of order of the relaxation time of one Arrhenius particle, it should then be possible to compute the averages by means of transition rates between steady states and a master equation.

5.7.1 Master equation

General considerations

We are interested on the statistics of the dynamical jumps, that requires the knowledge of the time-dependent probability $P_\alpha(t)$ to find the system in state α.

The Master equation gives a differential equation for the probability $P_\alpha(t)$ to be in the steady state α at time t. It requires the knowledge of the ensemble of steady states, Ω, and of the transition rates from state β to state α, $r_{\beta\to\alpha} = r_{\alpha\beta}$. The probability then verifies:

$$\frac{dP_\alpha(t)}{dt} = \sum_{\beta\in\Omega} r_{\alpha\beta} P_\beta(t) \,, \tag{5.115}$$

which can be expressed in a matrix form $\frac{d\vec{P}(t)}{dt} = \mathbb{r}\vec{P}(t)$, with $\mathbb{r}$ the transfer matrix, such that $(\mathbb{r})_{\alpha\beta} = r_{\alpha\beta}$. The transfer matrix contains the probability to go from any state β to any state α on a time interval dt. It must satisfy some properties. Since the total probability must be conserved, $\sum_\alpha P_\alpha(t) = 1$, the diagonal elements of the transfer matrix are constrained,

$$\sum_{\alpha\in\Omega} \frac{dP_\alpha(t)}{dt} = \sum_{\alpha\beta\in\Omega} r_{\alpha\beta}P_\beta(t) = 0 \quad \Rightarrow \quad \sum_{\alpha\in\Omega} r_{\alpha\beta} = 0 \quad \Rightarrow \quad r_{\alpha\alpha} = -\sum_{\beta\neq\alpha} r_{\alpha\beta}\,. \tag{5.116}$$

Then, in order for equilibrium to be reachable, the detailed balance must be satisfied,

$$r_{\alpha\beta}P_\beta = r_{\beta\alpha}P_\alpha\,. \tag{5.117}$$

One can find a formal solution for the probability, for all $\alpha \in \Omega$,

$$P_\alpha(t) = \sum_{\beta\in\Omega} (e^{\mathbb{r}t})_{\alpha\beta} P_\beta(0)\,, \tag{5.118}$$

with $P_\beta(0)$ the initial probability of state β. In order to find explicit solutions one has to diagonalize the transfer matrix. It is not doable directly as the matrix is not symmetric and one has to "symmetrize" it. One constructs a new ratio matrix, symmetric, $\widetilde{r}_{\alpha\beta} = P_\alpha^{-1/2}(0)\, r_{\alpha\beta}\, P_\beta^{1/2}(0)$. This yields a master equation for a new probability, $\widetilde{P}_\alpha(t) = P_\alpha(t)/\sqrt{P_\alpha(0)}$, whose explicit solutions can be computed. Introducing the eigenvalues of $\widetilde{\mathbb{r}}$, λ_i, and $\mathbb{M} = \{\vec{v}_i\}$ the matrix of eigenvectors, $\vec{v}_i$, the probability can be computed *via*:

$$\widetilde{P}_\alpha(t) = \sum_{\beta\gamma\in\Omega} M_{\alpha\gamma}\, e^{\lambda_\gamma t}\, (M^{-1})_{\gamma\beta}\, \widetilde{P}_\beta(0)\,. \tag{5.119}$$

The initial probability is then recovered using $P_\alpha(t) = \sqrt{P_\alpha(0)}\widetilde{P}_\alpha(t)$. From the expression of $P_\alpha(t)$, any average of a time-dependent observable $O(t)O(0)$ can be computed as:

$$\langle O(t)O(0)\rangle = \frac{1}{Z(t)} \sum_{\alpha\beta\gamma\in\Omega} O_\alpha(t)\sqrt{P_\alpha(0)}\, M_{\alpha\gamma}\, e^{\lambda_\gamma t}\, \left(M^{-1}\right)_{\gamma\beta}\, O_\beta(0)\sqrt{P_\beta(0)}\,, \tag{5.120}$$

with $Z(t)$ the partition function, $Z(t) = \sum_{\alpha\in\Omega} P_\alpha(t)$, and $P_\alpha(0)$ the initial probability of state α at thermal equilibrium.

Our problem

In our case, Arrhenius systems, the transition rate to go from one state α to another state γ is proportional to $e^{-\beta\Delta E}$, with ΔE some finite energy barrier and β the inverse temperature. Here the transitions between states occur through instantonic trajectories whose energy barriers are given by the action of the corresponding instanton.

System of two coupled particles

For the case of two coupled particles (*i.e.* $g > 0$) at distance $\hat{R}_{12}$ the instantons have a width of $\delta t = 2\,\hat{R}_{12}/\nu$. If $\delta t \ll \tau$, *i.e.* $\hat{R}_{12} \ll \tau\,\nu$, one can define the transition rates on a time span δt like follows. As soon as $\hat{R}_{12} \gg \tau\,\nu$ the particles decorrelate faster than the ballistic wave would propagate and the particles are *independent*. In the former case the transfer matrix is given by, in the basis $\Omega = \{(+,+)\,,\,(-,-)\,,\,(+,-)\,,\,(-,+)\}$, with $\tau = e^{\beta\, S_\star}$, $\zeta = e^{\beta\, Y\left(\hat{R}_{12}\right)^2/(2\,\Delta)} > 1$ and $\mu = e^{\beta\, X_0^2\, Y\left(\hat{R}_{12}\right)} > 1$,

$$\mathbb{r} = \begin{pmatrix} r_{11} & \tau^{-2}\,\zeta^{-1}\,\mu^{-1} & \tau^{-1}\,\zeta^{-2}\mu & \tau^{-1}\,\zeta^{-2}\,\mu \\ \tau^{-2}\,\zeta^{-1}\,\mu^{-1} & r_{22} & \tau^{-1}\,\zeta^{-2}\,\mu & \tau^{-1}\,\zeta^{-2}\,\mu \\ \tau^{-1}\,\zeta^{-2}\,\mu^{-1} & \tau^{-1}\,\zeta^{-2}\,\mu^{-1} & r_{33} & \tau^{-2}\,\zeta^{-1}\,\mu \\ \tau^{-1}\,\zeta^{-2}\,\mu^{-1} & \tau^{-1}\,\zeta^{-2}\,\mu^{-1} & \tau^{-2}\,\zeta^{-1}\,\mu & r_{44} \end{pmatrix}. \tag{5.121}$$

The diagonal elements r_{ii} verify equation (5.116). Since $Y\left(\hat{R}_{12}\right) \ll 1$, the following holds $\mu > \mu/\zeta > \mu/\zeta^2 > 1$, and some transitions are more probable than the others.

The initial probability of the steady state α is given by $\propto e^{-\beta W_2(\alpha)}$. From equation (5.95), we have that:

$$P_{(+,+)}(0) = P_{(-,-)}(0) = \frac{1}{Z(0)}\,\mu\,\zeta \quad ; \quad P_{(+,-)}(0) = P_{(-,+)}(0) = \frac{1}{Z(0)}\,\mu^{-1}\,\zeta\,, \tag{5.122}$$

with $Z(0)$ the normalization, $Z(0) = \sum_{\alpha\in\Omega} P_\alpha(0)$. One can check easily that detailed balance is then satisfied.

The two quantities to compute are expressed with the expression (5.120), replacing the observable O by $X_1\,X_2$. Using that the eigenvalues of the matrix $\widetilde{\mathbb{r}}$ and the matrix $\mathbb{M}$ are given by:

$$\{\lambda_i\} = \left\{0, -\frac{2(\zeta+\tau)}{\mu\zeta^2\tau^2}, -\frac{2\mu(\zeta+\tau)}{\zeta^2\tau^2}, -\frac{2\left(\mu^2+1\right)}{\mu\zeta^2\tau}\right\} \quad , \quad \mathbb{M} = \begin{pmatrix} \mu & -1 & 0 & -\mu^{-1} \\ \mu & 1 & 0 & -\mu^{-1} \\ 1 & 0 & -1 & 1 \\ 1 & 0 & 1 & 1 \end{pmatrix}, \tag{5.123}$$

we determine the following expression, with $Z(t) = 1$,

$$\langle X_1(t)X_1(0)X_2(t)X_2(0)\rangle_{0,2} = \frac{X_0^4}{\left(1+\mu^2\right)^2}\left(\left[\mu^2\psi_+(1)^2 - \psi_-(1)^2\right]^2 + \mu^2\left[\psi_-(1)^2 + \psi_+(1)^2\right]^2 e^{-\frac{2\left(\mu^2+1\right)}{\mu\zeta^2\tau}\,t}\right). \tag{5.124}$$

System of one particle

In this case the transfer matrix in the basis $\{X_0, -X_0\} = \{+,-\}$ and the initial probability are simply given by:

$$\mathbb{r} = \begin{pmatrix} -\tau^{-1} & \tau^{-1} \\ \tau^{-1} & -\tau^{-1} \end{pmatrix} \quad , \quad P_+(0) = P_-(0) = \frac{1}{2}\,. \tag{5.125}$$

The eigenvalues of $\widetilde{\mathbb{r}}$ and the matrix $\mathbb{M}$ are then given by:

$$\{\lambda_i\} = \left\{-\frac{2}{\tau}, 0\right\} \quad , \quad \mathbb{M} = \begin{pmatrix} -1 & 1 \\ 1 & 1 \end{pmatrix}, \tag{5.126}$$

from which we compute the following, with $Z(t) = 1$,

$$\left\langle X_1(t)^2X_1(0)^2\right\rangle_{0,1} = X_0^4 \quad , \quad \langle X_1(t)X_1(0)\rangle_{0,1} = X_0^2\,e^{-2\,t/\tau}\,. \tag{5.127}$$

We find back the auto-correlation function of equation (5.105) since $C(t) = \langle X_1(t)X_1(0)\rangle_{0,1} + O(\rho)$, from which we obtain back $\chi_T \equiv \partial_T C(t)$. This yields:

$$\chi_T(t) = -\frac{1}{k_B T^2}\frac{\Delta\,X_0^6}{2}\frac{t}{\tau}\,e^{-2\,t/\tau} + O(\rho)\,. \tag{5.128}$$

5.7.2 Four-point correlation function and susceptibility

The approach described above gives access to the self part of χ_4 and to the function $g_4(\hat{r},t)$, that appear in the expression (5.113). Using that $\left[\psi_-(1)^2 + \psi_+(1)^2\right] = 2$, we find that they are given by

$$\begin{aligned} &\left\langle X_1(t)^2X_1(0)^2\right\rangle_{0,1} - \langle X_1(t)X_1(0)\rangle_{0,1}^2 = X_0^4\left(1 - e^{-4\,t/\tau}\right), \\ &g_4(\hat{r},t) = X_0^4\left(\frac{\left[\mu^2\psi_+(1)^2 - \psi_-(1)^2\right]^2 + 4\,\mu^2\,e^{-\frac{2\left(\mu^2+1\right)}{\mu\zeta^2\tau}\,t}}{\left(1+\mu^2\right)^2} - e^{-4\,t/\tau}\right) \quad \text{with} \quad \hat{r} > 1\,. \end{aligned} \tag{5.129}$$

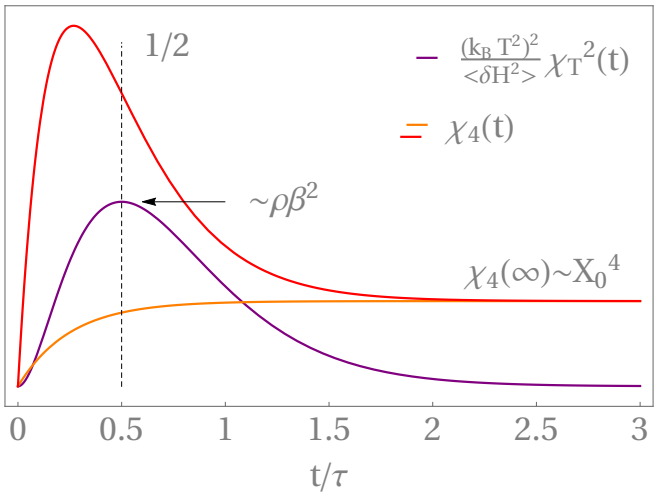

Figure 5.6: Schematic left and right sides of the bound $N_{dw}(k_BT^2)^2\,\chi_T^2(t)/\langle\delta H^2\rangle \leq N_{dw}\chi_4(t)$ (the overall N_{dw} factors are not reported on the figure to alleviate the legend). The left term is non-monotonous with a maximum at $t=\tau/2$. Then, if $N_{dw}\chi_4(\infty) < N_{dw}(k_BT^2)^2\,\chi_T^2(\tau/2)/\langle\delta H^2\rangle$, which is equivalent to $X_0^4 < \rho\,\beta^2$ for our problem (see main text), $\chi_4(t)$ must also be a non-monotonous function of t in order to satisfy the bound at all times.

When the particles are decorrelated, $g=0$, then $(\zeta,\mu,\psi_+(1),\psi_-(1))=1$ and one finds that all the contributions to χ_4 are zero, except the "self" part. The nonlocal part of χ_4, $g_4(\hat{r},t)$, begins near 0 at $t=0$ and converges toward the square of the static two-point correlation function, $C_{stat}(\hat{r})=\langle X_1X_2\rangle_{0,2}$, when $t\to\infty$. $C_{stat}(\hat{r})$ can be determined by evaluating the square root of the infinite-time limit of $g_4(\hat{r},t)$, and is a strictly increasing function of the inverse temperature β:

$$C_{stat}(\hat{r}) = \left(\lim_{t\to\infty} g_4(\hat{r},t)\right)^{1/2} = \frac{X_0^2}{1+\mu^2}\left(\mu^2\psi_+(1)^2-\psi_-(1)^2\right) = X_0^2\,\tanh\left[\beta\,X_0^2\,Y\left(\hat{R}_{12}\right)\right] + \frac{Y\left(\hat{R}_{12}\right)}{\Delta}\,. \tag{5.130}$$

Between the two above limits, $g_4(\hat{r},t)$ and $\chi_4(t)$ can eventually present a non-monotonous behavior. [3] $\chi_4(t)$ must be non-monotonous in order to satisfy the bound given in equation (5.4) at all times t if we satisfy a condition that is pictorially represented on figure 5.6, and corresponds to impose that the long-time limit of χ_4, $\lim_{t\to\infty}\chi_4(t)=\chi_4(\infty)$, is lower than $(k_BT^2)^2\,\chi_T^2(\tau/2)/\langle\delta H^2\rangle$. From the generic expression of the bound in equation (5.4) and using that $\langle\delta H^2\rangle_0 = N\,c_V\,k_BT^2$ and that $\chi_T(t)$ is given by the equation (5.128), the bound can be rewritten as

$$\chi_4(t) \geq \beta^2\,k_B\,(N\,c_V)^{-1}\left(\frac{X_0^6\Delta}{2}\right)^2\left(\frac{t}{\tau}\right)^2 e^{-4\,t/\tau} + O(\rho)\,. \tag{5.131}$$

We can then express the condition to have a non-monotonous behavior of $\chi_4(t)$ (and $g_4(\hat{r},t)$) for our problem, demanding to $\chi_4(\infty)$ to be smaller than the right-hand side of the above inequality evaluated in $t=\tau/2$. $\chi_4(t)$ in the infinite-time limit is usually dominated by the static susceptibility to the square, $\rho\int d^3\hat{r}\,C_{stat}(\hat{r})^2$. In our case, the self part of χ_4 dominates the long time limit since we are in the low-ρ and low-g regime, and forms a plateau whose height is $\chi_4(\infty)\sim X_0^4/N_{dw}$. This plateau must be lower than the peak of the right-hand side of the inequality in equation (5.131) evaluated for

[3] $\chi_4(t)$ is given by a sum of positive contributions, $g_4(\hat{r},t)$, for different values of $\hat{r}$ and can present a non-monotonous behavior with t only if $g_4(\hat{r},t)$ also in non-monotonous with t.

$t = \tau/2$, using that $N_{dw}/N = \rho$ it gives:

$$X_0^4/N_{dw} \leq \beta^2 \frac{k_B}{N\, c_V} \left(\frac{X_0^6 \Delta}{2}\right)^2 (1/2)^2\, e^{-2} \Rightarrow T \ll \rho^{1/2}\,. \tag{5.132}$$

If the above condition is verified we should be in a regime where the bound is not trivially satisfied by the self part and the static correlations of χ_4. In the meantime, we remember that the condition given in equation (5.34) must be respected otherwise the correlations would be dominated by the static length scale, this condition is recalled here: $T \gg \rho\, g$.

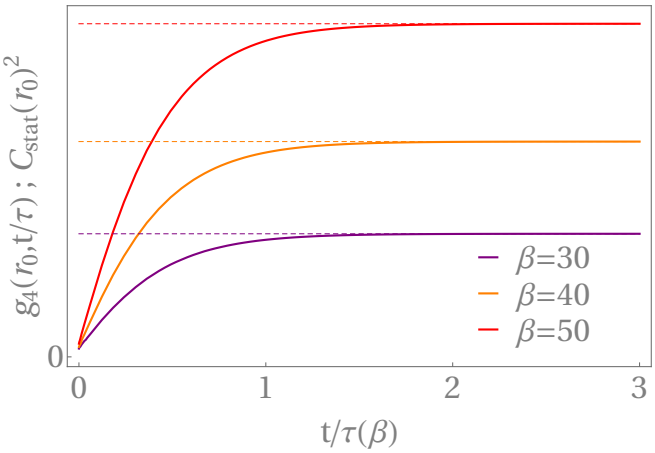

Figure 5.7: Representation of $g_4(\hat{r}_0, t)$ (here $r_0 \equiv \hat{r}_0$), $\hat{r}_0 > 1$, as a function of t for various values of the inverse temperature β. The static average $C_{stat}(\hat{r}_0)^2$ is also represented. The parameters are fixed such that: $\hat{r}_0 = \hat{R}_{12} = 1$, $g = 0.001$, $\rho = 0.1$, $\Delta = 1$, $K_0 = 1$.

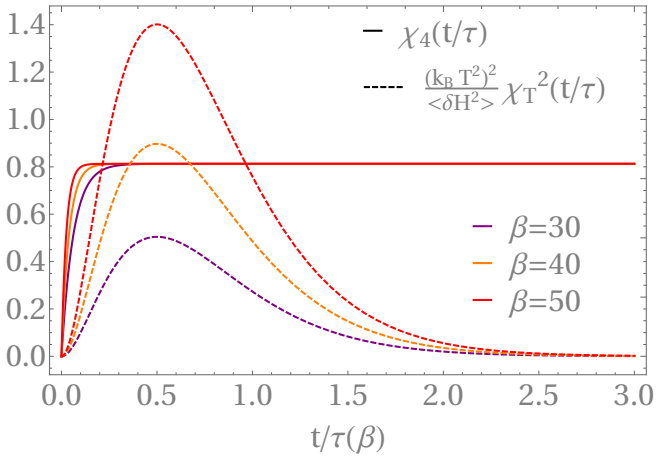

Figure 5.8: Representation of the left and right sides of the bound $N_{dw}\,\chi_4(t) > N_{dw}\,(k_B T^2)^2\,\chi_T^2(t)/\left\langle \delta H^2 \right\rangle$ for different values of β (the overall N_{dw} factors are not reported on the figure to alleviate the legend). All quantities are computed with the master equation formalism. We clearly see that for times of order τ and when the the bound is not trivially satisfied, *i.e.* by the self part of $\chi_4(t)$, the right term $N_{dw}\,(k_B T^2)^2\,\chi_T^2(t)/\left\langle \delta H^2 \right\rangle$, dashed lines, is larger than the left term $N_{dw}\,\chi_4(t)$, plain lines, hence violating the said bound.

However, even in respecting these two conditions, *i.e.* $\rho\, g \ll T \ll \rho^{1/2}$, g_4 (and χ_4) is a strictly monotonous (and increasing) function of t, as it can be viewed on figure 5.7. [4]

[4] Actually it can be non-monotonous in the limit of high temperatures, with a maximum at a time $t_0 = \tau/2\,\mu\zeta^2/(1+$

As expected from the above argument, the bound given in equation (5.131) is then found to be not satisfied at all times. Even if it is trivially satisfied when $t \gg \tau$ since the self part of $\chi_4(t)$ is always larger than the long time limit of $\chi_T(t)$, indeed $N_{dw} \lim_{t\gg\tau} \chi_4(t) \simeq X_0^4$ is always larger than $N_{dw} \lim_{t\gg\tau} \chi_T(t) \simeq 0$, this is not so at times of order of the relaxation time τ as one can see on figure 5.8.

Since the physical bound is violated, our result for χ_4 and g_4 are clearly wrong, and we are obviously unable to determine a dynamical length scale from their behaviors. At present we have to understand what are the possible sources that could have yield an error; the different possibilities are exposed in more details in the conclusion.

5.8 Conclusion and perspectives

From a simple implementation of the Cauchy-Schwarz theorem one finds that the four-point susceptibility, $\chi_4(t)$, is bounded by below by a term depending on the three-point susceptibility squared, $\chi_T(t)^2$. In glassy systems the two above quantities have been efficiently used to determine a nontrivial dynamical length scale that characterizes how far can be two correlated events occurring at distinct times t_1 and t_2. This length scale is maximal when $|t_1 - t_2|$ is of order τ, the relaxation time of the system, and can be related to the maximum of χ_4. This dynamical length scale as well as the static point-to-set length scale are two of the strongest candidates that could characterize the relevant fluctuations responsible for the relaxation occurring in supercooled liquids. One does not know if they can be considered as different evidences of the same physical phenomenon. If it is the case, is the physical mechanism generating them linked to the glassy properties of supercooled liquids and can the associated dynamical length scale be viewed as concomitant to the emergence of some cooperativity in the system? Or, does the underlying physical mechanism have a non-glassy origin?

In this chapter we studied a model of independent Arrhenius systems coupled via a conservative bath of harmonic oscillators for which the three-point susceptibility is known to be non-monotonous in time, with a maximum at time of order τ which increases with the inverse temperature squared, T^{-2}. Since the bound should be satisfied in these systems, one eventually expects a non-monotonous $\chi_4(t)$ from which could be extracted a nontrivial dynamical length scale going at least as T^{-2}. In parallel, one knows from the beginning that the static of these systems is trivial, at least in the range of parameters where the effective ferromagnetic coupling generated by the interaction with the bath can be neglected. Hence, characterizing the dynamical length scale existing in such Arrhenius systems could allow one to understand the non-glassy mechanisms at the origin of its existence. Such knowledge could be used as a benchmark to distinguish the trivial, non-glassy, and nontrival, glassy, generators of this dynamical length scale in supercooled liquids.

In Arrhenius systems at low T, a fluctuation of the order of the Arrhenius barrier ($O(1)$) is huge compared to the thermal fluctuations, $k_B T$. We found that these fluctuations of order 1 excite phonons that propagate in the bath, each one carrying a correlation proportional to the square of the (small) coupling between Arrhenius systems and the bath. These phonons propagate ballistically (with a constant velocity c depending on the parameters of the bath) and the dynamical correlation that arises from the peak of χ_T at times of order τ spreads on a dynamical length scale $c\,\tau$ and over a volume of order $(c\,\tau)^3$ in dimension three. Here we have studied a simplified version of thermal bath with

$\mu^2 - 2\mu\zeta^2) \log\left(2\mu\zeta^{-1}/(1+\mu^2)\right)$. This t_0 is positive only when $\zeta^{-2} < (1+\mu^2)/(2\,\mu) < \zeta^2 \Rightarrow \exp\left(-\beta\, Y\,(\hat{r})^2/\Delta\right) < \cosh\left(\beta\, X_0^2\, Y\,(\hat{r})\right) < \exp\left(\beta\, Y\,(\hat{r})^2/\Delta\right)$, then only if $\beta\, Y\,(\hat{r})^2 \ll \beta\, Y\,(\hat{r}) \ll 1$. We can then make three expansions that yield a supplementary condition for the temperature, $\beta < 2/(\Delta\, X_0^4)$. This is in contradiction with our primary assumption for validity of the instanton method, $\beta\, S_\star \gg 1$, and cannot be considered as the relevant mechanism for non-monotonicity.

quadratic couplings and this is why we have found a simple ballistic propagation of the phonons. In a more realistic case, the couplings are not simply quadratic and the ballistic regime, that would exist for short times, would be rapidly replaced by a diffusive regime. [203]

Then we have computed $\chi_4(t)$ using a master equation formalism, however we obtained an inconsistent result since the bound evoked above is "violated" for times of order τ. We have therefore been unable to go further in the characterization of the dynamical length scale(s) existing in our "simple" problem.

To bypass this unsatisfactory situation, we have tried to understand the possible sources of error that could arise from our study.

First, we could have neglected other important instantonic solutions that give rise to dynamical correlations in $\chi_4(t)$. To this respect, we have performed numerical computer simulations of the exact generalized Langevin equations with the approximate nonlocal memory kernel of dissipation for a bath containing two Arrhenius particles and yet, we have not been able to see any sign of the existence of a peak in g_4. A first possibility is that the approximations for the kernel were maybe too violent and not valid. Then, if the existence of very small dynamical correlations that spread over a length scale $c\,\tau$ is the sole source of dynamical correlation, the jump of one particle would create a signal that would propagate through phonons and would change a little the potential barrier of the other particle. Such effect would therefore be invisible in g_4 obtained from computer simulations, since their amplitude would be exponentially small and smeared by the statistic noise. However once integrated over the relevant volume $(c\,\tau)^3$, which is exponentially large, they would have satisfied the bound. Another possible explanation for the failure of these simulations could be that the instanton involving the mutual jump of two particles over an Arrhenius barrier is responsible for the dynamical correlations, and that it would not have been present in our result with the correct statistics since it requires quite long times of simulation to happen.

Second, the error could come from one of the approximations made in this chapter. There are several of them, but the most important one is the low-density expansion. It allowed us to compute correlations existing in a bath containing N_{dw} particles at leading order *via* correlations existing in bathes containing only one or two particles. Carrying too far this expansion, we could have simplified a correlation that should have been computed for a bath containing two particles, *i.e.* $\langle X_1(0)X_1(t)X_2(0)X_2(t)\rangle$, in a product of correlations computed for a bath containing only one particle, *i.e.* $\langle X_1(0)X_1(t)\rangle^2$. For example, if we did so in a regime where the two particles can effectively be dynamically correlated, their mutual correlation cannot be factorized; it is the case if the distance separating them is smaller than $c\,\tau$, the ballistic length that phonons can cover in a time span equal to the Arrhenius relaxation time after which the two particles totally decorrelate. This would mean in particular that all the dynamical correlations mediated by the bath are trivial and propagate *via* phonons on ballistic length scales.

We have tried to go beyond the low-density expansion, which would change some of the equations of this chapter. This seems to yield a non-monotonous behavior of χ_4 that could satisfy the bound and from which a length scale could be extracted. However, all this is still very preliminary and begs for a deeper understanding.

Chapter 6

Critical behavior of the Ising spin-glass below six dimensions

Contents

The results of this chapter are under preparation to be published.

6.1 Introduction

In this chapter, we consider a different type of glassy systems than those studied above: the Ising spin glass, which we have briefly introduced and reviewed in chapter 1. Our goal is to extend the formalism of the nonperturbative renormalization group (NPRG) presented in chapter 2 to such a system in order to investigate the long-distance behavior. As we will see, there are serious technical difficulties to achieve this, mostly related to the nature of the order parameter field, but our hope is to be able to tackle unsettled problems concerning the role fluctuations in spin glasses by a novel approach.

As discussed in the introductory chapter, the main open issues in spin glasses theory concern the nature of the low-temperature (spin-glass ordered) phase and the existence of a transition in presence of an applied magnetic field. In this work we consider as a first step a simpler question, that of critical behavior associated with the transition between the paramagnetic and the spin-glass phases in zero applied field.

We first recall the field theoretical description of the spin-glass transition point. The first treatment to go from the microscopic EA Hamiltonian (1.26) to a continuous Ginzburg-Landau-Wilson field theory was proposed by Harris and Lubensky [139, 204] in their RG treatment of the critical behavior in zero applied field. A similar derivation was given shortly after in [205], who constructed a field

theoretical Lagrangian up to cubic order using a Hubbard-Stratonovich transformation [206]. The use of this transformation and the generic cubic field theory, with all possible terms generated during a field expansion (argued to be necessary to study the transition in a field), can also be found in [207].

When performing the Hubbard-Stratonovich transformation, the replica trick is used to formally integrate the disorder (see section 1.1.3.2). The collective overlap variables are defined as $Q_{ab}(i) = S_i^a S_i^b (1 - \delta_{ab})$ (hence $Q_{aa} = 0$ and $Q_{ab} = Q_{ba}$), where a and b refer to replicas and i to a site of the lattice. Their average gives back the EA order parameter (see section 1.2.3).

The Hamiltonian is then expanded in powers of the field Q_{ab} around zero (to study the critical behavior) and the continuum limit is taken. This gives at order $O(Q^4)$

$$H[\{Q_{ab}\}] = \int d^d x \left\{ \frac{1}{2} \sum_{(ab)} (\partial_x Q_{ab}(x))^2 + \frac{m_1}{2} \sum_{(ab)} Q_{ab}^2(x) + w_1 \sum_{(abc)} Q_{ab}(x) Q_{bc}(x) Q_{ca}(x) \right.$$
$$\left. + u_1 \sum_{(abcd)} Q_{ab}(x) Q_{bc}(x) Q_{cd}(x) Q_{da}(x) + u_2 \sum_{(ab)} Q_{ab}^4(x) + u_3 \sum_{(abc)} Q_{ab}^2(x) Q_{bc}^2(x) + u_4 \sum_{(abcd)} Q_{ab}^2(x) Q_{cd}^2(x) \right\}, \tag{6.1}$$

where $\sum_{(ab)} \equiv \sum_{a<b}$, $\sum_{(abc)} \equiv \sum_{a<b<c}$, *etc.*

This effective Hamiltonian has an important symmetry that it inherits from the original Edwards-Anderson Hamiltonian through the replica method: if for one replica index, say a, one changes $Q_{ab}(x)$ in $-Q_{ab}(x)$ for all space points x and all other replica indices b, the Hamiltonian is left invariant. As a result in each polynomial term, a given replica index must appear an even number of times. This is easily generalized to higher order terms not present in equation (6.1).

6.2 Ising spin glass in zero field: previous results

6.2.1 Mean-field critical exponents and beyond with perturbative RG

Within the mean-field description, the critical exponents are given by the classical values

$$\begin{aligned} \nu^{MF} &= 1/2, \\ \eta^{MF} &= 0, \end{aligned} \tag{6.2}$$

which are valid above an upper critical dimension $d_u = 6$. [59, 15, 139]

The first RG study of the critical behavior was performed by Harris and Lubensky [139]. They computed, in perturbation around the mean field solution in $d = 6 - \varepsilon$, the critical exponents of the spin glass transition at order $O(\varepsilon)$.

The ε expansion was extended to order $O(\varepsilon^2)$ in [208]. The coefficients of the $O(\varepsilon^3)$ of the serie were first computed in [209] but were found to be erroneous and were corrected in [210]. In practice, the perturbative RG can involve a very high number of diagrams (going to $O(\varepsilon^p)$ generates all the p-loop diagrams) and the computation of their contributions rapidly becomes tedious. No calculation beyond $O(\varepsilon^3)$ has been carried out. The three-loop critical exponents of the spin glass transition are given by

$$\begin{aligned} \nu(\varepsilon) &= \frac{1}{2} + \frac{5}{12}\varepsilon - 1.6574\,\varepsilon^2 - 1.2597\,\varepsilon^3 + O(\varepsilon^4), \\ \eta(\varepsilon) &= -\frac{\varepsilon}{3} + 1.2593\,\varepsilon^2 + 0.7637\,\varepsilon^3 + O(\varepsilon^4). \end{aligned} \tag{6.3}$$

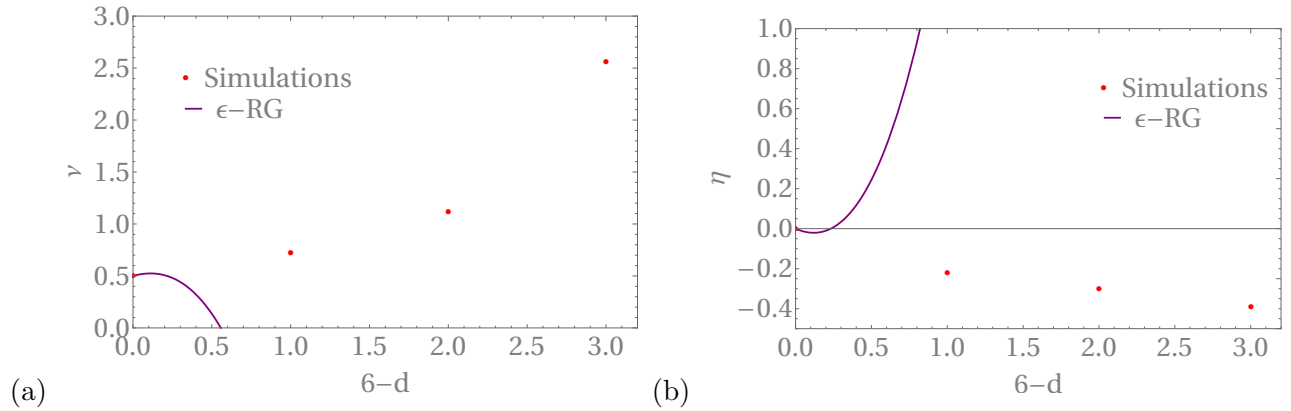

(a) (b)

Figure 6.1: Critical exponents (a) ν and (b) η from both computer simulations and from the RG ε-expansion. The ε-expansion is very far from the computer simulations results as soon as the dimension is $d \lesssim 5.9 - 5.8$.

They are shown in figure 6.1 together with results of computer simulations. Except extremely close to $d = 6$, the predictions from the ε-expansion are strikingly poor, being complete nonsense below $d \simeq 5.9$ or 5.8. This rather unusual feature may also explain why no one attempted to go to the next order in the perturbation in ε. We will see that a much better and simpler result can be reached with a nonperturbative RG approach.

6.2.2 Critical exponents from computer simulations and lower critical dimension

The most accurate determination of the critical exponents of the zero field transition of the EA Ising spin glass known to date are listed in the following table. They are computed for a Gaussian distribution of the random couplings. The values for dimensions $d = 3$, 4, 5 and $d \geq 6$ are respectively collected from [211, 212, 213].

Table 6.1: Critical exponents of the Ising spin glass from simulations in various dimensions d. The mean field (MF) values are also given.

d	$d \geq 6$	5	4	3
ν	1/2	0.720(5)	1.113(1)	2.562(42)
η	0	-0.22(2)	-0.30(5)	-0.3900(36)

The other exponents can be deduced from the standard scaling relations, given in equation (2.53).

We recall that the transition in the Ising spin glass remains down to a lower critical dimension d_l between 2 and 3 (see also section 1.2.2).

6.3 Approximation scheme for the nonperturbative RG for the Ising spin glass

We saw in chapter 2 that the derivative expansion provides a powerful approximation scheme to solve the exact functional RG equation for the effective average action. In the context of the critical behavior of the Ising spin glass with field theoretical description based on the Hamiltonian (or "bare action")

given in equation (6.1), the order ∂^2 of the expansion of the effective average action reads

$$\Gamma_k[\{Q_{ab}\}] = \int d^dx \left\{ \frac{1}{2} \sum_{(cd),(ef)} Z_{k;cd,ef}\left(\{Q_{ab}(x)\}\right) \partial_x Q_{cd}(x) \partial_x Q_{ef}(x) + U_k\left(\{Q_{ab}(x)\}\right) \right\}, \tag{6.4}$$

As previously discussed, an important symmetry of the problem (in zero applied magnetic field) is that when changing $Q_{ab}(x)$ to $-Q_{ab}(x)$ for a given replica index a for all space points x and all other replica indices $b \neq a$, the effective action should be left invariant. This also constrains the form of the quadratic infrared (IR) regulator used to suppress long wavelength fluctuations of the overlap field, which can be chosen as

$$\Delta S_k\left[\{Q_{ab}\}\right] = \frac{1}{2} \sum_{(ab)} \int\int d^dx\, d^dx'\, R_k\left(|x-x'|\right)\, Q_{ab}(x)\, Q_{ab}(x')\,. \tag{6.5}$$

The flow of the effective average action Γ_k is described by the exact RG equation

$$\partial_t \Gamma_k\left[\{Q_{ab}\}\right] = \frac{1}{2} \sum_{(ab)} \int_q \partial_t R_k(q^2) \left[\left(\Gamma_k^{(2)} + R_k\, \mathbb{1} \right)^{-1} \right]^{ab,ab}_{q,-q} \tag{6.6}$$

where $\int_q = \int \frac{d^dq}{(2\pi)^d}$, $\sum_{(ab)} \equiv \sum_{a<b}$, and $\Gamma_k^{(2)}$ is the matrix of the second derivatives, *i.e.*,

$$\Gamma^{(2)}_{k;x,cd,x',ef}\left[\{Q_{ab}\}\right] = \frac{\delta^2}{\delta Q_{cd}(x) \delta Q_{ef}(x')} \Gamma_k\left[\{Q_{ab}\}\right], \tag{6.7}$$

with $c < d$ and $e < f$.

One immediately sees from equation (6.6) that there is a severe difficulty for deriving RG flow equations for functions of this order $O(\partial^2)$ as done for the simpler problem of the φ^4 theory discussed in chapter 2. Indeed, even if one considers spatially uniform configurations of the overlap field, $Q_{ab}(x) = Q_{ab}$, there is *a priori* no way to properly invert the matrix $\Gamma_k^{(2)} + R_k \mathbb{1}$ in replica indices: either one keeps generic configurations in replica space and the inversion is not possible in general (in the absence of a procedure generalizing the expansion in free replica sums used to derive the nonperturbative RG theory of the RFIM [214]) or one chooses configurations with a specific symmetry in replica indices, *e.g.*, a replica symmetric configuration with $Q_{ab} = Q$ for all a and b different, and one cannot obtain a *closed* set of functional equations.

An alternative is then to further expand the functions Z_k and U_k around a nontrivial configuration, as also often employed in nonperturbative RG studies. [25] A choice that has been proven efficient for retaining the nonperturbative character of the RG method is to expand around one of the (nonzero) minima of the running potential U_k. [25] (This implies before all that fluctuations are accounted for, the system is in the symmetry-broken phase with a nontrivial minimum different from zero.) In what follows, for studying the critical point of the Ising spin glass in zero field, we choose a replica symmetric minimum of $U_k\left(\{Q_{ab}\}\right)$, *i.e.*,

$$U^{(1)}_{k;cd}\left(\{Q_k\}\right) = \frac{\delta}{\delta Q_{cd}} U_k\left(\{Q_{ab}\}\right)\Big|_{Q_{ab}=Q_k} = 0 \tag{6.8}$$

for all $c < d$. For convenience, we will use in the following the short-hand notation $|_{Q_k}$ to indicate that a function or its derivatives are evaluated for all Q_{ab}'s equal to the minimum Q_k.

For the kinetic (gradient) term of the effective average action, we will consider the lowest-order approximation,

$$Z_{k;cd,ef}\left(\{Q_{ab}\}\right) \simeq Z_k\, \delta_{ec}\, \delta_{fd} \tag{6.9}$$

where $Z_k \equiv Z_{k;ab,ab}(\{Q_k\})$ is given by

$$Z_k = \frac{1}{\delta^{(d)}(0)} \frac{d}{dq^2} \left(\frac{\delta^2 \Gamma_k}{\delta Q_{ab}(q) \delta Q_{ab}(-q)} \Big|_{Q_k} \right) \Big|_{q^2=0} \tag{6.10}$$

with $\delta^{(d)}(0) = (2\pi)^{-d} V$ and V the volume of the system.

More care is needed for the expansion around Q_k of the potential $U_k(\{Q_{ab}\})$. Indeed we would like to work with an expansion that when truncated does not break the symmetry of the effective action already mentioned and in which the definition of the coupling constants (evaluated at the minimum) does not depend on the order of the truncation. Let us illustrate these considerations with a (much) simpler problem, that of the standard φ^4 theory with $\mathbb{Z}_2$ inversion symmetry. The theory has an unique invariant (for the $\mathbb{Z}_2$ symmetry), $\rho(x) = 1/2\,\phi(x)^2$. The potential can then be expanded around the nontrivial minimum $\rho_k = 1/2\,\phi_k^2$ as

$$U_k(\phi) \equiv U_k(\rho) = \sum_{i=2}^{\infty} \frac{\lambda_{k;2i}}{i!} (\rho - \rho_k)^i \ . \tag{6.11}$$

This form of the potential, when truncated at any order $i = p$, encodes by construction the $\mathbb{Z}_2$ symmetry. The coupling constants $\lambda_{k,2i}$ for $i \leq p$ can be defined in a way that does not depend on the level p of the truncation. An obvious choice is

$$\lambda_{k;2i} = \frac{\partial^i}{\partial \rho^i} U_k(\rho) \Big|_{\rho_k} , \tag{6.12}$$

as the contribution of the terms of higher order than i vanishes when evaluated at the minimum. This choice however relies on the uniqueness of the invariant ρ and will not be of any use when considering the spin-glass problem in which the number of invariants is infinite. One can instead make use of derivatives with respect to the original ϕ field and a proper definition can still be found by obtaining the coupling constants $\lambda_{k;4}, \lambda_{k;6}, \cdots, \lambda_{k;2p}$ from the derivatives with respect to ϕ up to order p evaluated in the minimum ϕ_k. For instance, $U_k^{(1)}(\phi_k)$ defines ϕ_k; adding $U_k^{(2)}(\phi_k) = \lambda_{k;4}\,\phi_k^2$ then defines $\lambda_{k;4}$; adding $U_k^{(3)} = 3\,\lambda_{k;4}\,\phi_k + \lambda_{k;6}\,\phi_k^3$ defines $\lambda_{k;6}$; *etc.* At the level p, truncating the potential at any order strictly larger than p does not change the expressions of the coupling constants up to $\lambda_{k;2p}$.

6.4 Expansion in invariants of the potential around the minimum and definition of the coupling constants

In this section we detail how to expand the effective average potential U_k around the replica symmetric minimum configuration Q_k while keeping track at each order of the symmetry of the effective action, *i.e.*, the invariance for any given replica index a under the change $Q_{ab}(x) \to -Q_{ab}(x)$ for all other replica indices b and all space points x. Invariants here refer to combinations of the overlap fields that satisfy this symmetry. There is a list of such quantities in appendix D.1.

To achieve our goal, we do not expand the potential in mere powers of the overlap fluctuations $\delta Q_{ab} = Q_{ab} - Q_k$ as done, *e.g.*, in [215, 207]. As a first step, one can reorganize the expansion in Q_{ab}'s similar to that given in equation (6.1) with the help of invariants that vanish when evaluated at the minimum Q_k (meaning that all the overlaps Q_{ab} are set equal to Q_k) and, apart from the lowest order are such that their first derivatives also vanish when evaluated at Q_k.

We define a variable $\rho_{ab}^{(2)}$ written in terms of the unique invariant of $O(Q^2)$,

$$\rho_{ab}^{(2)} = \frac{1}{2}(Q_{ab}^2 - Q_k^2) \,, \tag{6.13}$$

and the higher-order terms up to $p = 5$ (the replica indices are distinct, $a, b, c, d, e \neq$) are defined as follows:

$$\begin{aligned}
\mu^{(3)}_{abc} &= Q_{ab}Q_{bc}Q_{ca} - Q_k^3 - Q_k\left(\rho^{(2)}_{ab} + \rho^{(2)}_{bc} + \rho^{(2)}_{ca}\right), \\
\mu^{(4)}_{abcd} &= Q_{ab}Q_{bc}Q_{cd}Q_{da} - Q_k^4 - Q_k^2\left(\rho^{(2)}_{ab} + \rho^{(2)}_{bc} + \rho^{(2)}_{cd} + \rho^{(2)}_{da}\right), \\
\lambda^{(4)}_{ab} &= \rho^{(2)}_{ab}\rho^{(2)}_{ab}, \qquad \lambda^{(4)}_{abc} = \rho^{(2)}_{ab}\rho^{(2)}_{bc}, \qquad \lambda^{(4)}_{abcd} = \rho^{(2)}_{ab}\rho^{(2)}_{cd}, \\
\mu^{(5)}_{abcde} &= Q_{ab}Q_{bc}Q_{cd}Q_{de}Q_{ea} - Q_k^5 - Q_k^3\left(\rho^{(2)}_{ab} + \rho^{(2)}_{bc} + \rho^{(2)}_{cd} + \rho^{(2)}_{de} + \rho^{(2)}_{ea}\right), \\
\nu^{(5)}_{abc} &= \rho^{(2)}_{ab}\mu^{(3)}_{abc}, \qquad \nu^{(5)}_{abcd} = \frac{1}{2}\rho^{(2)}_{ab}\left(\mu^{(3)}_{acd} + \mu^{(3)}_{bcd}\right), \qquad \nu^{(5)}_{abcde} = \rho^{(2)}_{ab}\mu^{(3)}_{cde}.
\end{aligned} \tag{6.14}$$

The terms of order $O(Q^6)$ are given in appendix D.2. Each of the above term is such that replica indices appear an even number of times, as desired. The expansion of the potential can then be reexpressed as

$$\begin{aligned}
U_k(\{Q_{ab}\}) = W_{k,1}(Q_k)\sum_{(abc)}\mu^{(3)}_{abc} + U_{k,1}(Q_k)\sum_{(abcd)}\mu^{(4)}_{abcd} + U_{k,2}(Q_k)\sum_{(ab)}\lambda^{(4)}_{ab} \\
+ U_{k,3}(Q_k)\sum_{(abc)}\lambda^{(4)}_{abc} + U_{k,4}(Q_k)\sum_{(abcd)}\lambda^{(4)}_{abcd} \\
+ V_{k,1}(Q_k)\sum_{(abcde)}\mu^{(5)}_{abcde} + V_{k,2}(Q_k)\sum_{(abc)}\nu^{(5)}_{abc} \\
+ V_{k,3}(Q_k)\sum_{(abcd)}\nu^{(5)}_{abcd} + V_{k,4}(Q_k)\sum_{(abcde)}\nu^{(5)}_{abcde} + \cdots .
\end{aligned} \tag{6.15}$$

The terms of order Q^6 are given in equations (D.1), (D.2)and (D.3). The above expression of U_k is not satisfying yet, although the invariance is now manifest at each order. Indeed, as explained in the simple example of the ϕ^4 theory treated above, we also require that the coupling constants (*i.e.*, the parameters in front of the various invariants) be defined through derivatives evaluated at the minimum Q_k in such a way that the expression does not depend on the order of the truncation of the expansion.

As can be seen with the help of the tables in appendix D.3, second-order derivatives of U_k evaluated at the minimum, for instance, may involve terms of the expansion in equation (6.15) up to arbitrarily high orders (contrarily to what found above for the ϕ^4 theory). One should therefore proceed to an additional resummation and reorganization of all the terms so that the newly defined coupling constants up to a given order, say p, can be defined through derivatives of order p or less in a way that is independent on the level q of the truncation, provided of course that $q \geq p$.

The procedure has unfortunately to be implemented order by order explicitly. We use the derivatives of the various terms of the expansion in equation (6.15) evaluated at the minimum Q_k, which are listed up to $O(Q^5)$ and to fourth-order derivatives in tables D.3 to D.5 of appendix D. One then has to consider a term by term approach to ensure that all new coupling constants up to order p are exactly defined from derivatives of order up to $n \leq p$ evaluated at Q_k, irrespective of the order $q \geq p$ of the truncation. (This implies that these derivatives when applied to any term of order larger than q gives exactly zero.) We have checked the construction explicitly up to order $q = 6$. However, the number of derivatives growing with the order more rapidly than the number of possible invariants (hence, of coupling constants), the problem appears underconstrained and one expects that it is always possible to find a solution. [1] The solution however is not unique and the coupling constants may therefore be

[1] At any order p the number of derivatives is given by the number of possible multigraphs with an infinite set of nodes and with p edges where the loops are forbidden [216, 217, 218] and the number of invariants is given by the number of *Euler* multigraphs with the same property [219, 220].

defined through different sets of derivatives. In an exact treatment this has of course no consequences, but it does when considering an approximation where the potential is truncated at given order.

Let us now illustrate the procedure at the lowest orders. We introduce for convenience the variables $X_i^{(p)}$ (p is the order of the term, i the label of the associated coupling constant) defined by:

$$\begin{aligned} &X_1^{(3)} = \sum_{(abc)} \mu_{abc}^{(3)}\,, \quad X_1^{(4)} = \sum_{(abcd)} \mu_{abcd}^{(4)}\,, \quad X_2^{(4)} = \sum_{(ab)} \lambda_{ab}^{(4)}\,, \quad X_3^{(4)} = \sum_{(abc)} \lambda_{abc}^{(4)}\,, \quad X_4^{(4)} = \sum_{(abcd)} \lambda_{abcd}^{(4)}\,, \\ &X_1^{(5)} = \sum_{(abcde)} \mu_{abcde}^{(5)}\,, \quad X_2^{(5)} = \sum_{(abc)} \nu_{abc}^{(5)}\,, \quad X_3^{(5)} = \sum_{(abcd)} \nu_{abcd}^{(5)}\,, \quad X_4^{(5)} = \sum_{(abcde)} \nu_{abcde}^{(5)}\,, \quad \textit{etc.}\,, \end{aligned} \tag{6.16}$$

and we look for an expansion of the potential U_k in the form

$$U_k(\{Q_{ab}\}) = \widetilde{W}_{k,1} X_1^{(3)} + \sum_{i=1}^{4} \widetilde{U}_{k,i}\, \widetilde{X}_i^{(4)} + \sum_{i=1}^{4} \widetilde{V}_{k,i}\, \widetilde{X}_i^{(5)} + O(Q^6)\,, \tag{6.17}$$

which corresponds to a rearrangement of the expression in equation (6.15) with new coupling constants and new invariants distinguished by a tilde.

At the lowest order, we require that one exactly has

$$\widetilde{W}_{k,1} = \frac{\delta^3 U_k}{\delta Q_{ab}\delta Q_{bc}\delta Q_{ca}}\,, \tag{6.18}$$

where a, b, c are all distinct (one can, *e.g.*, choose $a < b < c$). This condition is satisfied at each subsequent order of a truncation of the expansion of U_k if order by order, the third derivative involved in equation (6.18) gives zero when acting on any invariant $\widetilde{X}_i^{(p)}$ with $p \geq 4$. These invariants are linear combinations of the original $X_i^{(q)}$'s with $q \leq p$. (By construction, $\widetilde{X}_1^{(3)} = X_1^{(3)}$.)

From table D.3, one can check that $\delta^3/(\delta Q_{ab}\delta Q_{bc}\delta Q_{ca})$ acting on any $X_i^{(4)}$ is zero when evaluated at the minimum. Hence, $\widetilde{X}_i^{(4)} = X_i^{(4)}$. For the $O(Q^5)$ terms, the solution is of the form

$$\widetilde{X}_i^{(5)} = X_i^{(5)} - \sum_{j=1}^{4} b_{ij}\, Q_k\, X_j^{(4)} - c_i\, Q_k^2\, X_1^{(3)} \tag{6.19}$$

where the coefficients b_{ij} and c_i must be chosen such that $\delta^3 \widetilde{X}_i^{(5)}/(\delta Q_{ab}\delta Q_{bc}\delta Q_{ca})|_{Q_k} = 0$. This requirement is easily satisfied considering that there are 20 unknowns for only 4 constraints.

At the next order, *i.e.*, $O(Q^4)$, one has to choose the protocol to define the coupling constants $\widetilde{U}_{k,i}$, $i = 1, \cdots, 4$, knowing that $\widetilde{W}_{k,1}$ is defined by equation (6.18). As detailed in appendix D.2, one can come up with two different acceptable sets of conditions using all three derivatives of second order and one derivative of third order, all evaluated at the minimum Q_k. One finds

$$\begin{aligned} \frac{\delta^2 U_k}{\delta Q_{ab}^2}\Big|_{Q_k} &= -(n-2) Q_k\, \widetilde{W}_{k,1} - (n-2)(n-4) Q_k^2\, \tilde{U}_{k,1} + \frac{1}{3} Q_k^2 \tilde{U}_{k,2} \\ \frac{\delta^2 U_k}{\delta Q_{ab}\delta Q_{bc}}\Big|_{Q_k} &= Q_k\, \widetilde{W}_{k,1} + (n-3) Q_k^2\, \widetilde{U}_{k,1} + Q_k^2 \tilde{U}_{k,3} \\ \frac{\delta^2 U_k}{\delta Q_{ab}\delta Q_{cd}}\Big|_{Q_k} &= 2 Q_k^2\, \widetilde{U}_{k,1} + Q_k^2 \widetilde{U}_{k,4} \\ \frac{\delta^3 U_k}{\delta Q_{ab}\delta Q_{bc}\delta Q_{ca}}\Big|_{Q_k} &= \widetilde{W}_{k,1}\,, \end{aligned} \tag{6.20}$$

and either (later called choice (A))

$$\frac{\delta^3 U_k}{\delta Q_{ab}^2 \delta Q_{cd}}\Big|_{Q_k} = Q_k \, \widetilde{U}_{k,4} \, , \tag{6.21}$$

or (and choice (B))

$$\frac{\delta^3 U_k}{\delta Q_{ab} \delta Q_{bc} \delta Q_{cd}}\Big|_{Q_k} = Q_k \, \widetilde{U}_{k,1} \, . \tag{6.22}$$

It is possible to define the invariants $\widetilde{X}_i^{(5)}$ such that they do not contribute to these derivatives evaluated at Q_k (see appendix D.2). We expect that this is also possible for higher-order terms because the system of linear equations to solve has many more unknowns than the number of constraints. In principle the procedure can be generalized to consider higher orders. In practice we have only studied the two orders presented above.

In what follows we show how to implement the nonperturbative RG by using the above considerations.

6.5 Implementing the nonperturbative RG with the chosen approximation scheme

We can now insert the chosen ansatz for the effective average action,

$$\Gamma_k \left[\{Q_{ab}\} \right] = \int d^d x \left\{ \frac{1}{2} Z_k \sum_{(cd)} \left(\partial_x Q_{cd}(x) \right)^2 + U_k \left(\{Q_{ab}(x)\} \right) \right\} , \tag{6.23}$$

where U_k is expanded in invariants around the minimum Q_k as in equation (6.17), into the exact RG equation, equation (6.6).

At the lowest order of the expansion of U_k, one has to consider the RG flow of 3 parameters, Z_k, Q_k, and $\widetilde{W}_{k,1}$. The corresponding equations can be derived from the definitions of the three quantities, equation (6.10) for the field renormalization constant Z_k, equation (6.8) for the nontrivial minimum of the potential Q_k, and equation (6.18) for the coupling constant $\widetilde{W}_{k,1}$, by differentiating the exact RG equation in equation (6.23) and evaluating the final expression for a uniform configuration of the field overlaps with $Q_{ab} = Q_k$ for all distinct pairs (a, b) of replica indices. When proceeding to these manipulations, the ansatz in equation (6.23) with U_k truncated at the lowest order is inserted in the right-hand side of the functional RG flow equation.

For spatially uniform field configurations and the ansatz in equation (6.23), one has

$$\Gamma^{(2)}_{k;ab,cd}(q, q') = \delta^{(d)}(q + q') \, \Gamma_{k;ab,cd}(q^2) \tag{6.24}$$

with

$$\Gamma^{(2)}_{k;ab,cd}(q^2) = Z_k q^2 \delta_{ac} \delta_{bd} + U^{(2)}_{k;ab,cd} \, , \tag{6.25}$$

where we have taken $a < b$ and $c < d$, and for the proper (1-particle irreducible) vertices of order $n \geq 3$,

$$\Gamma^{(n)}_{k;a_1 b_1, \cdots, a_n b_n}(q_1, \cdots, q_n) = \delta^{(d)}(q_1 + \cdots q_n) \, U^{(n)}_{k;a_1 b_1, \cdots, a_n b_n} \, . \tag{6.26}$$

After differentiating the exact functional RG equation for Γ_k and evaluating the result at the minimum Q_k of the potential, one obtains expressions of the form

$$\partial_t U^{(1)}_{k;ab}\Big|_{Q_k} = \frac{1}{2} \widetilde{\partial}_t D^{(3)}_{ab}(0)\Big|_{Q_k} \, , \tag{6.27}$$

$$\partial_t \Gamma^{(2)}_{k;ab,cd}(q^2)\Big|_{Q_k} = \frac{1}{2}\widetilde{\partial}_t \left\{ E^{(4)}_{ab,cd}(0) - E^{(3),(3)}_{ab,cd}(q^2) \right\}\Big|_{Q_k} , \tag{6.28}$$

and

$$\partial_t U^{(3)}_{k;ab,cd,ef} = \frac{1}{2}\widetilde{\partial}_t \left\{ 2\, F^{(3),(3),(3)}_{ab,cd,ef}(0) - F^{(4),(3)}_{ab,cd;ef}(0) - F^{(4),(3)}_{ab,ef;cd}(0) - F^{(4),(3)}_{cd,ef;ab}(0) + F^{(5)}_{ab,cd,ef}(0) \right\}\Big|_{Q_k} . \tag{6.29}$$

etc., where the operator $\widetilde{\partial}_t$ acts only on the IR cutoff function $R_k(q^2)$, and the expressions of the various quantities $D^{(3)}_{ab}(0)$, $E^{(4)}_{ab,cd}(0)$, $\cdots$, $F^{(5)}_{ab,cd,ef}(0)$ are given in appendix D.4. These expressions involve the proper vertices obtained from equation (6.26) as well as the propagators $P_{k;ab,cd}(q^2)$ evaluated for spatially uniform overlap fields (in practice here all chosen equal to Q_k):

$$P_{k;ab,cd}(q^2) = \left[\left(\mathbb{\Gamma}^{(2)}(q^2) + R_k(q^2)\mathbb{1} \right)^{-1} \right]_{ab,cd} , \tag{6.30}$$

where $a < b$ and $c < d$. For the replica-symmetric minimum configuration, $Q_{ab} = Q_k$, one has

$$\begin{aligned} \Gamma^{(2)}_{k;ab,cd}(q^2) = (1-\delta_{a,b})(1-\delta_{c,d}) \Big(& \Gamma^{(2)}_{k;1}(q^2)[\delta_{a,c}\delta_{b,d} + \delta_{a,d}\delta_{b,c}] \\ & + \Gamma^{(2)}_{k;2}(q^2)[\delta_{a,d}(1-\delta_{b,c}) + \delta_{b,c}(1-\delta_{a,d}) + \delta_{a,c}(1-\delta_{b,d}) + \delta_{b,d}(1-\delta_{a,c})] \\ & + \Gamma^{(3)}_{k;2}(q^2)(1-\delta_{a,c})(1-\delta_{a,d})(1-\delta_{b,c})(1-\delta_{b,d}) \Big) , \end{aligned} \tag{6.31}$$

with (distinct a, b, c, d)

$$\begin{aligned} \Gamma^{(2)}_{k;1}(q^2) &= \Gamma^{(2)}_{k;ab,ab}(q^2) = q^2 Z_k + U^{(2)}_{k;1} , \\ \Gamma^{(2)}_{k;2}(q^2) &= \Gamma^{(2)}_{k;ab,bc}(q^2) = U^{(2)}_{k;2} , \\ \Gamma^{(2)}_{k;3}(q^2) &= \Gamma^{(2)}_{k;ab,cd}(q^2) = U^{(2)}_{k;3} . \end{aligned} \tag{6.32}$$

It is easy to check that the matrix $P_{k;ab,cd}(q^2)$ has the same form as that of $\Gamma^{(2)}_{k;ab,cd}(q^2)$ in equation (6.31) with

$$\begin{aligned} P_{k,1}(q^2) &= \frac{2}{n(n-1)} \left[\frac{\frac{1}{2}n(n-3)}{\Gamma^{(2)}_{k;R}(q^2) + R_k(q^2)} + \frac{n-1}{\Gamma^{(2)}_{k;A}(q^2) + R_k(q^2)} + \frac{1}{\Gamma^{(2)}_{k;L}(q^2) + R_k(q^2)} \right] , \\ P_{k,2}(q^2) &= \frac{2}{n(n-1)(n-2)} \left[-\frac{\frac{1}{2}n(n-3)}{\Gamma^{(2)}_{k;R}(q^2) + R_k(q^2)} + \frac{\frac{1}{2}(n-4)(n-1)}{\Gamma^{(2)}_{k;A}(q^2) + R_k(q^2)} + \frac{n-2}{\Gamma^{(2)}_{k;L}(q^2) + R_k(q^2)} \right] , \\ P_{k,3}(q^2) &= \frac{2}{n(n-1)(n-2)} \left[\frac{n}{\Gamma^{(2)}_{k;R}(q^2) + R_k(q^2)} - \frac{2(n-1)}{\Gamma^{(2)}_{k;A}(q^2) + R_k(q^2)} + \frac{n-2}{\Gamma^{(2)}_{k;L}(q^2) + R_k(q^2)} \right] , \end{aligned} \tag{6.33}$$

where we have introduced the eigenvalues of $\mathbb{\Gamma}^{(2)}_k$, $\Gamma_{k;R,A,L}(q^2) = Z_k\, q^2 + U^{(2)}_{k;R,A,L}$, with the "masses" given by

$$\begin{aligned} U^{(2)}_{k;R} &= U^{(2)}_{k;1} - 2\, U^{(2)}_{k;2} + U^{(2)}_{k;3} , \\ U^{(2)}_{k;A} &= U^{(2)}_{k;1} + (n-4)\, U^{(2)}_{k;2} - (n-3)\, U^{(2)}_{k;3} , \\ U^{(2)}_{k;L} &= U^{(2)}_{k;1} + 2(n-2)\, U^{(2)}_{k;2} + \frac{1}{2}(n-2)(n-3)\, U^{(2)}_{k;3} . \end{aligned} \tag{6.34}$$

and corresponding to the "replicon" (R), "anomalous" (A), and "longitudinal" (L) sectors of the $\frac{n(n-1)}{2} \times \frac{n(n-1)}{2}$ matrix. [6] In the limit $n \to 0$, one can see that the anomalous and longitudinal masses are degenerate, with their difference going to 0 linearly in n. When $n \to 0$, it is then convenient to introduce the quantity

$$U^{(2)}_{k;AL} = \frac{U^{(2)}_{k;A} - U^{(2)}_{k;L}}{n} = -U^{(2)}_{k;2} - \frac{(n-3)}{2} U^{(2)}_{k;3} \,. \tag{6.35}$$

In this limit the propagators $P_{k,1}$, $P_{k,2}$, $P_{k,3}$ become

$$\begin{aligned}
P_{k,1}(q^2)\Big|_{n=0} &= 3\, P_R(q^2) - 2\, P_A(q^2) - 2\, U^{(2)}_{k;AL}\, P^2_A(q^2)\Big|_{n=0} \,, \\
P_{k,2}(q^2)\Big|_{n=0} &= \frac{3}{2}\, P_R(q^2) - \frac{3}{2}\, P_A(q^2) - 2\, U^{(2)}_{k;AL}\, P^2_A(q^2)\Big|_{n=0} \,, \\
P_{k,3}(q^2)\Big|_{n=0} &= P_R(q^2) - P_A(q^2) - 2\, U^{(2)}_{k;AL}\, P^2_A(q^2)\Big|_{n=0} \,,
\end{aligned} \tag{6.36}$$

with

$$\begin{aligned}
P_R(q^2)\Big|_{n=0} &= \frac{1}{q^2 Z_k + R_k(q^2) + U^{(2)}_{k;R}}\Big|_{n=0} \,, \\
P_A(q^2)\Big|_{n=0} &= \frac{1}{q^2 Z_k + R_k(q^2) + U^{(2)}_{k;A}}\Big|_{n=0} \,.
\end{aligned} \tag{6.37}$$

Finally, from equation (6.27) we obtain the flow of Q_k. By deriving equation (6.28) with respect to q^2 (which therefore only involves $E^{(3),(3)}_{ab,cd}(q^2)$) and evaluating the result in $q^2 = 0$ we obtain the flow of Z_k and from equation (6.29) specified to $U_{k;ab,bc,ca}(Q_k)$ (distinct a, b, c) we obtain the flow of $\widetilde{W}_{k,1}$. In all cases, we have to use the identity that for any function f_k, $\partial_t f_k(Q_k) = \partial_t f_k|_{Q_k} + \sum_{(cd)} f_{k;cd}(Q_k)\, \partial_t Q_k$.

When studying the next order of the truncation, one also needs the flow of the 4 coupling constants $\widetilde{U}_{k,i}$, or equivalently the flow of the 4 derivatives in equations (6.20) and (6.21) or (6.22) evaluated in Q_k: the flow of the 3 second-order derivatives is obtained from equation (6.28) and that of the additional third-order derivative from equation (6.29).

In the practical implementation of this nonperturbative RG, we have used the so-called optimized regulator proposed by Litim, which is given by the expression

$$R_k(q^2) = Z_k(k^2 - q^2)\Theta(k^2 - q^2) \,. \tag{6.38}$$

It gives a mass equal to $Z_k\,(k^2 - q^2)$ to the field fluctuations with $q^2 \leq k^2$, hence freezing them, and does not affect the ones with $q^2 > k^2$ as it vanishes in this range, see also section 2.2.2.1.

6.6 Nonperturbative RG equations in dimensionless form

In order to search for the fixed point controlling the critical point of the Ising spin glass in zero applied field, one needs to cast the RG flow equations derived in the preceding section into a dimensionless form. This can be done by introducing scaling dimensions and dimensionless quantities (which will be denoted by lowercase letters while their dimensionful counterpart are denoted by capital letters):

$$\begin{aligned}
U_k &= k^d\, u_k \,, \\
Q &= k^{d/2-1} Z_k^{-1/2}\, q \,, \\
U^{(n)}_k &= k^{d+n(1-d/2)} Z_k^{n/2}\, u^{(n)}_k \,.
\end{aligned} \tag{6.39}$$

We also introduce dimensionless momentum, regulator and propagator,

$$\begin{aligned} q &= k\,\hat{q}\,, \\ R_k(q^2) &= Z_k k^2\, r_k\left(\hat{q}^2\right)\,, \\ P_{k;ab,cd}(q^2) &= Z_k^{-1/2} k^{-2}\, p_{k;ab,cd}\left(\hat{q}^2\right)\,. \end{aligned} \tag{6.40}$$

A running anomalous dimension η_k is also defined from the flow equation of Z_k,

$$\eta_k = -\partial_t \log Z_k\,, \tag{6.41}$$

which, by using the definition of Z_k and the flow equation in equation (6.28) can be rewritten as

$$\eta_k = \frac{1}{2}\frac{d}{d\hat{p}^2}\left(\widetilde{\partial}_t e^{(3),(3)}_{ab,ab}\left(\hat{p}^2\right)\Big|_{q_k}\right)\Big|_{\hat{p}^2=0}\,, \tag{6.42}$$

where $e^{(3),(3)}$ is the dimensionless counterpart of $E^{(3),(3)}$. In deriving equation (6.42) we have used the fact that $E^{(4)}$ does not depend on $\hat{p}^2$ and that similarly $\Gamma^{(3)}_{k;ac,cd,ef} = U^{(3)}_{k;ac,cd,ef}$ does not depend on $\hat{p}^2$ in the present approximation. The explicit expression of $e^{(3),(3)}_{ab,ab}\left(\hat{p}^2\right)$ is for instance

$$e^{(3),(3)}_{ab,ab}(\hat{p}^2) = \sum_{\substack{(ef),(gh),\\(ij),(lm)}} \int_{\hat{q}} u^{(3)}_{k;ab,ef,gh}\, p_{k;gh,ij}(\hat{q}^2)\, u^{(3)}_{k;ab,ij,lm}\, p_{k;lm,ef}\left(|\vec{\hat{q}}+\vec{\hat{p}}|^2\right)\,. \tag{6.43}$$

The flow of the needed derivatives of the potential evaluated in the minimum in dimensionless form is obtained from equations (6.28), (6.29) and generically read

$$\begin{aligned} \partial_t u^{(n)}_{k;a_1b_1,\ldots,a_nb_n}(q_k) = &\left[-d+\frac{n}{2}(d-2+\eta_k)\right] u^{(n)}_{k;a_1b_1,\ldots,a_nb_n}(q_k) + \partial_t u^{(n)}_{k;a_1b_1,\ldots,a_nb_n}\Big|_{q_k} \\ &+ \delta q_k \sum_{(a_{n+1}b_{n+1})} u^{(n+1)}_{k;a_1b_1,\ldots,a_nb_n,a_{n+1}b_{n+1}}(q_k) \end{aligned} \tag{6.44}$$

where we have defined

$$\delta q_k = \dot{q}_k + \frac{1}{2}(-2+d+\eta_k)\, q_k\,. \tag{6.45}$$

The notation $\dot{x} = dx/dt$ is used when there is no ambiguity. From equation (6.44) one easily obtains that

$$\delta q_k = \frac{1}{2}\frac{\widetilde{\partial}_t d^{(3)}_{ab}(0)|_{q_k}}{\sum_{(cd)} u^{(2)}_{k;ab,cd}}\,, \tag{6.46}$$

where $d^{(3)}_{ab}$ again denotes the dimensionless counterpart of $D^{(3)}_{ab}$ and the denominator can be simply rewritten as

$$\begin{aligned} \sum_{(cd)} u^{(2)}_{k;ab,cd}(q_k) &= u^{(2)}_{k;1}(q_k) + 2(n-2)\, u^{(2)}_{k;2}(q_k) + \frac{1}{2}(n-2)(n-3)\, u^{(2)}_{k;3}(q_k) \\ &= u^{(2)}_{k;L}(q_k)\,, \end{aligned} \tag{6.47}$$

where $u^{(2)}_{k;L}(q_k)$'s is the dimensionless longitudinal mass evaluated in q_k.

6.7 Lowest-order $O(Q^3)$ truncation

We consider now the lowest-order approximation in which the expansion of the potential U_k in equation (6.17) is truncated at the first nonzero term:

$$U_k(\{Q_{ab}\}) = \widetilde{W}_{k,1} X_1^{(3)} \tag{6.48}$$

where $\widetilde{W}_{k,1}$ is defined by equation (6.18). This approximation of the nonperturbative RG which we will refer to as "NPRG-0" has already been discussed in section 6.5.

The different field derivatives of U_k appearing in the flow equations can be expressed in this truncation as

$$\begin{aligned}
&U^{(2)}_{k;ab,ab}\Big|_{Q_k} = -(n-2)Q_k\,\widetilde{W}_{k,1} && U^{(3)}_{k;ab,bc,ca}\Big|_{Q_k} = \widetilde{W}_{k,1} && U^{(3)}_{k;ab,bc,cd}\Big|_{Q_k} = 0 \\
&U^{(2)}_{k;ab,bc}\Big|_{Q_k} = Q_k\,\widetilde{W}_{k,1} && U^{(3)}_{k;ab,ab,ab}\Big|_{Q_k} = 0 && U^{(3)}_{k;ab,ac,ad}\Big|_{Q_k} = 0 \\
&U^{(2)}_{k;ab,cd}\Big|_{Q_k} = 0 && U^{(3)}_{k;ab,ab,bc}\Big|_{Q_k} = 0 && U^{(3)}_{k;ab,ac,de}\Big|_{Q_k} = 0 \\
& && U^{(3)}_{k;ab,ab,cd}\Big|_{Q_k} = 0 && U^{(3)}_{k;ab,cd,ef}\Big|_{Q_k} = 0
\end{aligned} \qquad U^{(i)}_k\Big|_{Q_k} = 0 \text{ for } i \geq 4 \tag{6.49}$$

with distinct a, b, c, d, e, f. (We recall that the equation $U^{(3)}_{k;ab,bc,ca}\Big|_{Q_k} = \widetilde{W}_{k,1}$ is true beyond the present truncation.)

The three coupled dimensionless flow equations read

$$\begin{aligned}
\eta_k &= \frac{1}{2} w_{k,1}^2 \frac{d}{d\hat{p}^2}\left(\widetilde{\partial}_t \widetilde{e}^{(3),(3)}_{ab,ab}\left(\hat{p}^2\right)\Big|_{q_k}\right)\Big|_{\hat{p}=0}, \\
\dot{q}_k &= -\frac{1}{2}(-2+d+\eta_k)\,q_k + \frac{1}{2(n-2)\,q_k}\widetilde{\partial}_t \widetilde{d}^{(3)}_{ab}(0)\Big|_{q_k},
\end{aligned} \tag{6.50}$$

as $u^{(2)}_{k;L}(q_k) = (n-2)\,q_k\,w_{k,1}$ from equation (6.34), and

$$\dot{w}_{k,1} = \frac{1}{2}(-6+d+3\eta_k)\,w_{k,1} + w_{k,1}^3\,\widetilde{\partial}_t \widetilde{f}^{(3),(3),(3),(3)}_{ab,bc,ca}(0)\Big|_{q_k}. \tag{6.51}$$

We have defined the dimensionless coupling constant $w_{k,1}$ associated with $\widetilde{W}_{k,1}$ and we introduced the tilde quantities as $\widetilde{e}^{(3),(3)}_{ab,ab}\left(\hat{p}^2\right)\Big|_{q_k} = w_{k,1}^{-2}\, e^{(3),(3)}_{ab,ab}\left(\hat{p}^2\right)\Big|_{q_k}$, $\widetilde{d}^{(3)}_{ab}(0)\Big|_{q_k} = w_{k,1}^{-1}\, d^{(3)}_{ab}(0)\Big|_{q_k}$ and $\widetilde{f}^{(3),(3),(3),(3)}_{ab,bc,ca}(0)\Big|_{q_k} = w_{k,1}^{-3}\, f^{(3),(3),(3),(3)}_{ab,bc,ca}(0)\Big|_{q_k}$ to make the coupling constant $w_{k,1}$ apparent in the flow equations. The definitions of the dimensionless diagrams are given with dimensions in: $e^{(3),(3)}_{ab,ab}(\hat{p})$ (D.20), $d^{(3)}_{ab}(0)$ (D.19) and $f^{(3),(3),(3),(3)}_{ab,bc,ca}(0)$ (D.21). After having performed the sums over replica indices, we

find

$$\begin{aligned}
\widetilde{d}^{(3)}_{ab}(0)\Big|_{q_k} &= 2(n-2)\int_{\hat{q}} p_{k,2}\left(\hat{q}^2\right)\Big|_{q_k},\\
\widetilde{e}^{(3),(3)}_{ab,ab}(\hat{p}^2)\Big|_{q_k} &= 2(n-2)\int_{\hat{q}} \left[p_{k,1}\left(\hat{q}^2\right)\, p_{k,1}\left(|\hat{q}+\hat{p}|^2\right)\right.\\
&\quad \left.+(n-2)\, p_{k,2}\left(\hat{q}^2\right)\, p_{k,2}\left(|\hat{q}+\hat{p}|^2\right)+(n-3)\, p_{k,3}\left(\hat{q}^2\right)\, p_{k,3}\left(|\hat{q}+\hat{p}|^2\right)\right]\Big|_{q_k},\\
\widetilde{f}^{(3),(3),(3)}_{ab,bc,ca}(0)\Big|_{q_k} &= \int_{\hat{q}} \left\{(n-2)\, p^3_{k,1}\left(\hat{q}^2\right)+3(n-2)\, p_{k,1}\left(\hat{q}^2\right)\, \left[(n-2)\, p^2_{k,2}\left(\hat{q}^2\right)+(n-3)\, p^2_{k,3}\left(\hat{q}^2\right)\right]\right.\\
&\quad +\left[n((n-9)n+54)-104\right] p^3_{k,2}\left(\hat{q}^2\right)+6(n-3)(3n-10)\, p^2_{k,2}\left(\hat{q}^2\right)\, p_{k,3}(\hat{q},-\hat{q})\\
&\quad \left.+3(n-4)(n-3)(n+2)\, p_{k,2}\left(\hat{q}^2\right)\, p^2_{k,3}\left(\hat{q}^2\right)+4(n-5)(n-4)(n-3)\, p^3_{k,3}\left(\hat{q}^2\right)\right\}\Big|_{q_k}.
\end{aligned} \tag{6.52}$$

The first and last equations of (6.52) involve $\hat{q}$-integrations of products of propagators $\prod_{i=1}^{m} p_{a_i}\left(\hat{q}^2\right)$ for $m = 1, 3$ with the a_i's $\in \{1, 2, 3\}$. Using equation (6.36), the propagators $p_{1,2,3}$ are rewritten in terms of the diagonal propagators $p_{R,A}$. As a consequence, we have to compute only one kind of integral in the flow equations of q_k and $w_{k,1}$; it is given by:

$$j(R, n_R; A, n_A) = v_d\, \widetilde{\partial}_t \int_0^\infty d\hat{q}\, \hat{q}^{d-1}\, p_R\left(\hat{q}^2\right)^{n_R}\, p_A\left(\hat{q}^2\right)^{n_A}\Big|_{q_k}, \tag{6.53}$$

with n_R and n_A integers such that $1 \leq n_R + n_A \leq 2\,m$. The computation of this integral can be performed using the expressions of $p_{R,A}\left(\hat{q}^2\right)$, $r_k\left(\hat{q}^2\right)$ and the Litim regulator in equation (6.38), and gives in the limit $n \to 0$:

$$j(R, n_R; A, n_A) = -v_d\, \frac{2}{d}\, \frac{\left(1-\frac{\eta_k}{d+2}\right)}{\left(1+u^{(2)}_{k;R}(q_k)\right)^{n_R}\left(1+u^{(2)}_{k;A}(q_k)\right)^{n_A}} \left(\frac{n_R}{1+u^{(2)}_{k;R}(q_k)}+\frac{n_A}{1+u^{(2)}_{k;A}(q_k)}\right), \tag{6.54}$$

with v_d a factor coming from the integration over angular variables,

$$v_d = \frac{\Omega_d}{(2\pi)^d}, \qquad \text{with} \qquad \Omega_d = \frac{2\pi^{d/2}}{\Gamma(d/2)}. \tag{6.55}$$

The equation for η_k requires to compute an other integral, slightly more involved, whose general expression is

$$jz(R, n_R; A, n_A) = v_d \left(\frac{d}{d\hat{p}^2}\, \widetilde{\partial}_t \int_0^\infty d\hat{q}\, \hat{q}^{d-1}\, p_R\left(\hat{q}^2\right)^{n_R}\, p_A\left(|\hat{q}+\hat{p}|^2\right)^{n_A}\right)\Big|_{q_k;\hat{p}=0}. \tag{6.56}$$

The computation of this integral can also be performed, with the result in the limit $n \to 0$:

$$jz(R, n_R; A, n_A) = v_d \frac{2}{d}\, \frac{n_R\, n_A}{\left(1+u^{(2)}_{k;R}(q_k)\right)^{n_R+1}\left(1+u^{(2)}_{k;A}(q_k)\right)^{n_A+1}}. \tag{6.57}$$

The physics at criticality is obtained by finding the fixed point of the system formed by equations (6.50) and (6.51) in the limit $n \to 0$, with the knowledge of η_k as a function of q_k and $w_{k,1}$. In addition to the Gaussian fixed point $\{q^\star = 0, w_1^\star = 0\}$, we find below $d = 6$ a nontrivial solution $\{q^\star, w_1^\star\}$ which is plotted in figure 6.2 (a) and (b) as a function of the distance from the upper critical

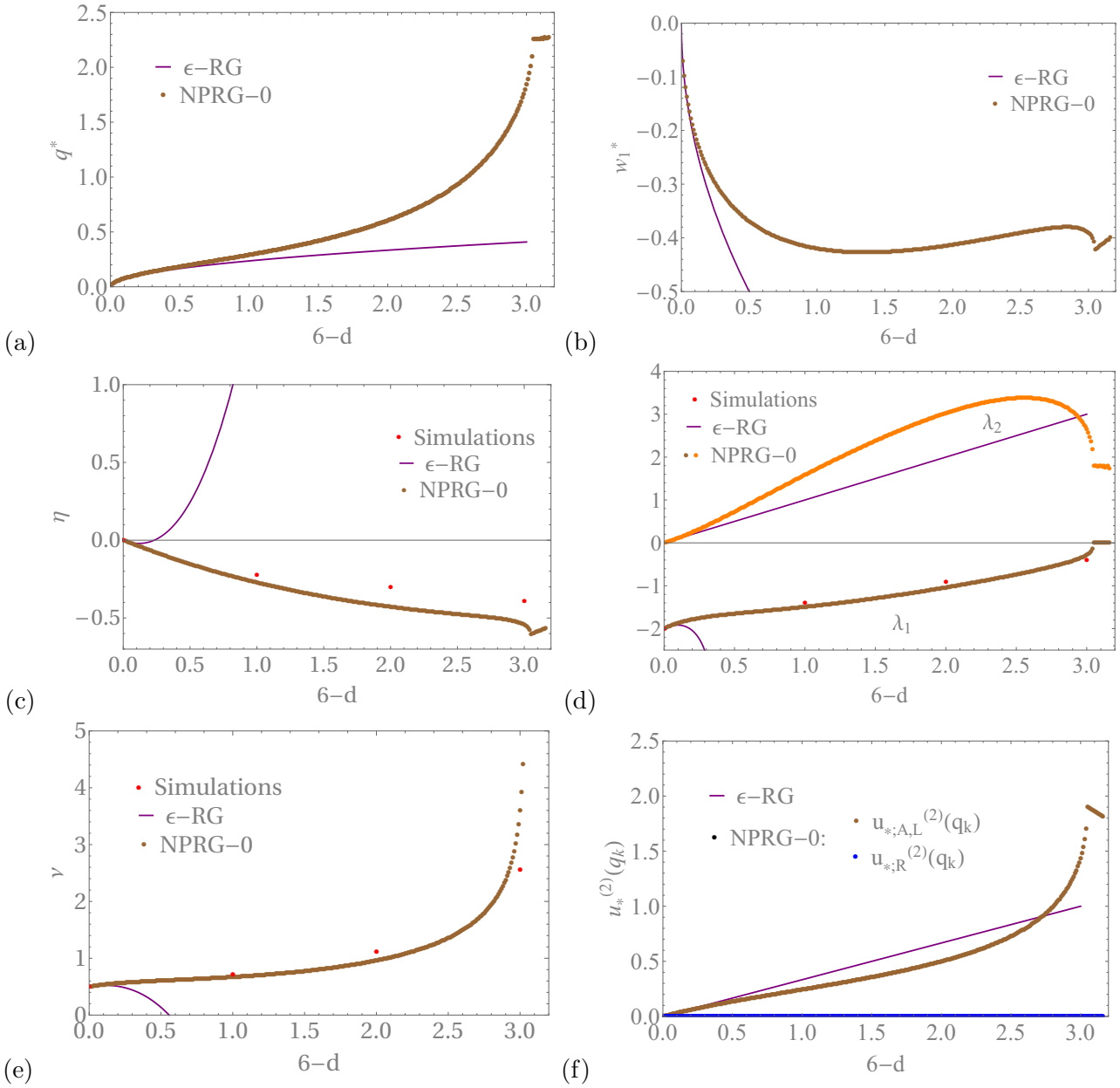

Figure 6.2: Fixed point solution for the critical point of the Ising spin glass at the lowest order NPRG-0 of the nonperturbative RG approach (in brown) versus $6-d$. We also show the perturbative ε expansion to order ε^3 (purple) and results from computer simulations (red points): (a) Dimensionless minimum $q^\star$; (b) dimensionless cubic coupling constant $w_1^\star$; (c) anomalous dimension η; (d) relevant (λ_1) and irrelevant eigenvalues of the stability matrix around the fixed point; (e) correlation length exponent ν; and (f) dimensionless anomalous and longitudinal masses $u^{(2)}_{\star;A,L} = -2\,q^\star\,w_1^\star$ (in brown) and replicon mass $u^{(2)}_{\star;R} = 0$ (in blue).

dimension, $6-d$. In figure 6.2 (c) we also plot the anomalous dimension η obtained at the fixed point. By studying the linear stability of the RG flow equations around the fixed point, we have determined the relevant eigenvalue, $\lambda_1 < 0$, and the irrelevant one, $\lambda_2 > 0$, also shown as a function of dimensions: see figure 6.2 (d). From the relevant eigenvalue one can obtain the correlation length exponent ν as

$$\nu = \frac{1}{|\lambda_1|} \tag{6.58}$$

and it is plotted in figure 6.2 (e).

The critical fixed point is found from $d_u = 6$ down to some lower critical dimension less than 3, $d_l \simeq 2.97$. When approaching this lower critical dimension from above, both the value of the dimensionless minimum $q^\star$ and the correlation length exponent ν diverge (see figures 6.2 (a),(e)) in agreement with theoretical predictions. [221]

In figures 6.2 (a)-(e) we have also plotted the results of the perturbative RG up to 3 loops [209] as well as the results from state-of-the-art computer simulations [211, 212, 213]. The comparison clearly shows that while the ε expansion even at order ε^3 fails when $\varepsilon \gtrsim 0.1 - 0.2$, as already mentioned in section 6.2, the present nonperturbative RG is quantitatively correct for a larger domain of dimensions and is still semi-quantitatively good in $d = 3$ (the predicted anomalous dimension η is about -0.5 to be compared with the simulation result $\eta \simeq -0.4$).

Near $d = 6$, the present NPRG-0 approximation exactly reproduces the 1-loop perturbative calculation, with

$$\begin{aligned} q^\star &= \sqrt{\varepsilon}/(3\sqrt{2})\,(1 + O(\varepsilon))\ , \\ w_1^\star &= -\sqrt{\varepsilon/2}\,(1 + O(\varepsilon))\ , \\ \lambda_1 &= -2 + \frac{5}{3}\varepsilon, \quad \lambda_2 = \varepsilon + O(\varepsilon^2)\,, \end{aligned} \tag{6.59}$$

in agreement with [139, 215]. However, it represents a drastic improvement over the perturbative RG when dimension is lowered.

All in all, the success of the NPRG-0 approximation for describing the critical behavior of the Ising spin glass suggests that the nonperturbative RG may prove a very promising approach. A shortcoming of the present truncation is that the dimensionless replicon mass $u^{(2)}_{\star;R}$ is exactly zero by construction (see also figure 6.2 (f)). It would be interesting to check whether it becomes negative in an improved truncation. In simpler cases, such as the ϕ^4 theory, the *dimensionless* potential at the critical fixed point has a shape that resembles the shape of a *dimensionful* potential in the symmetry broken phase of a finite-size system: in some sense it gives some indication of the symmetry-breaking scenario. One knows that for spin glasses, a negative *dimensionful* replicon mass may signal an instability toward replica symmetry breaking. [6] Knowing whether the *dimensionless* replicon mass is negative or not at the critical point would then provide a nontrivial piece of information. We therefore consider below the next order of the NPRG truncation scheme.

6.8 Next-order $O(Q^4)$ truncation

The potential is now truncated at order $O(Q^4)$, *i.e.*

$$U_k(\{Q_{ab}\}) = \widetilde{W}_{k,1}[Q_k]\widetilde{X}_1^{(3)} + \sum_{i=1}^{4} \widetilde{U}_{k,i}\,\widetilde{X}_i^{(4)}\,, \tag{6.60}$$

and the independent flowing parameters of the theory, in addition to the field renormalization constant Z_k, are Q_k, $\widetilde{W}_{k,1}$, $\widetilde{U}_{k,1}$, $\widetilde{U}_{k,2}$, $\widetilde{U}_{k,3}$, and $\widetilde{U}_{k,4}$, which are defined from derivatives of the potential U_k as explained in section 6.4. Note that there are two possible choices denoted (A) and (B) that depend on which specific third-order derivative is considered in addition to that defining $\widetilde{W}_{k,1}$. The different field derivatives of U_k at this level of the truncation are, with $(a, b, c, d, e, f \neq)$ and evaluated in $\{Q_{ab}\} = \{Q_k\}$,

$$\begin{aligned}
U^{(2)}_{k;ab,ab}\Big|_{Q_k} &= -(n-2)Q_k\,\widetilde{W}_{k,1} - (n-2)(n-3)Q_k^2\widetilde{U}_{k,1} + \frac{1}{3}Q_k^2\widetilde{U}_{k,2}\,,\\
U^{(2)}_{k;ab,bc}\Big|_{Q_k} &= Q_k\,\widetilde{W}_{k,1} + (n-3)Q_k^2\widetilde{U}_{k,1} + Q_k^2\widetilde{U}_{k,3}\,,\\
U^{(2)}_{k;ab,cd}\Big|_{Q_k} &= 2Q_k^2\widetilde{U}_{k,1} + Q_k^2\widetilde{U}_{k,4}\,,
\end{aligned} \tag{6.61}$$

$$\begin{aligned}
&U^{(3)}_{k;ab,bc,ca}\Big|_{Q_k} = \widetilde{W}_{k,1}\,, && U^{(3)}_{k;ab,bc,cd}\Big|_{Q_k} = Q_k\widetilde{U}_{k,1}\,, && U^{(4)}_{k;ab,bc,cd,da}\Big|_{Q_k} = U_{k,1}\,,\\
&U^{(3)}_{k;ab,ab,ab}\Big|_{Q_k} = Q_k\widetilde{U}_{k,2}\,, && U^{(3)}_{k;ab,ac,ad}\Big|_{Q_k} = 0\,, && U^{(4)}_{k;ab,ab,ab,ab}\Big|_{Q_k} = U_{k,2}\,,\\
&U^{(3)}_{k;ab,ab,bc}\Big|_{Q_k} = Q_k\widetilde{U}_{k,3}\,, && U^{(3)}_{k;ab,ac,de}\Big|_{Q_k} = 0\,, && U^{(4)}_{k;ab,ab,bc,bc}\Big|_{Q_k} = U_{k,3}\,,\\
&U^{(3)}_{k;ab,ab,cd}\Big|_{Q_k} = Q_k\widetilde{U}_{k,4}\,, && U^{(3)}_{k;ab,cd,ef}\Big|_{Q_k} = 0\,, && U^{(4)}_{k;ab,ab,cd,cd}\Big|_{Q_k} = U_{k,4}\,,
\end{aligned} \tag{6.62}$$

$$\begin{aligned}
U^{(4)}_{k;others}\Big|_{Q_k} &= 0\,,\\
U^{(i)}_{k}\Big|_{Q_k} &= 0 \;\text{ for }\; i \geq 5\,.
\end{aligned} \tag{6.63}$$

The above expressions of the derivatives of the potential enter in the right-hand side of the flow equations (the "beta functions") of Z_k, Q_k and the 5 coupling constants. As explained above, these coupling constants are defined from a *restricted* set of derivatives, which we write below in a dimensionless form (as before the dimensionless quantities are written without a tilde to alleviate the notation):

$$\begin{aligned}
u^{(2)}_{k;ab,ab}\Big|_{q_k} &= -(n-2)q_k\,w_{k,1} - (n-2)(n-3)q_k^2u_{k,1} + \frac{1}{3}q_k^2u_{k,2}\,,\\
u^{(2)}_{k;ab,bc}\Big|_{q_k} &= q_k\,w_{k,1} + (n-3)q_k^2u_{k,1} + q_k^2u_{k,3}\,,\\
u^{(2)}_{k;ab,cd}\Big|_{q_k} &= 2q_k^2u_{k,1} + q_k^2u_{k,4}\,,\\
u^{(3)}_{k;ab,bc,ca}\Big|_{q_k} &= w_{k,1}\,,
\end{aligned} \tag{6.64}$$

and either one of two choices,

$$\begin{aligned}
(A)\;\; u^{(3)}_{k;ab,ab,cd}\Big|_{q_k} &= q_ku_{k,4}\,,\\
(B)\;\; u^{(3)}_{k;ab,bc,cd}\Big|_{q_k} &= q_ku_{k,1}\,.
\end{aligned} \tag{6.65}$$

One can invert the two above systems (A) and (B) to obtain the explicit expressions of the constants as functions of the field derivatives of u_k; this simple inversion is done in appendix D.5.1. The dimensionless flow equations of η_k and q_k are given by equations (6.42) and (6.46), with the longitudinal mass

$$u^{(2)}_{k;L}(q_k) = (n-2)\,q_kw_{k,1} + q_k^2\left(2(n-3)(n-2)u_{k,1} + \frac{1}{3}u_{k,2} + \frac{(n-2)}{2}\left(4u_{k,3} + (n-3)u_{k,4}\right)\right)\,. \tag{6.66}$$

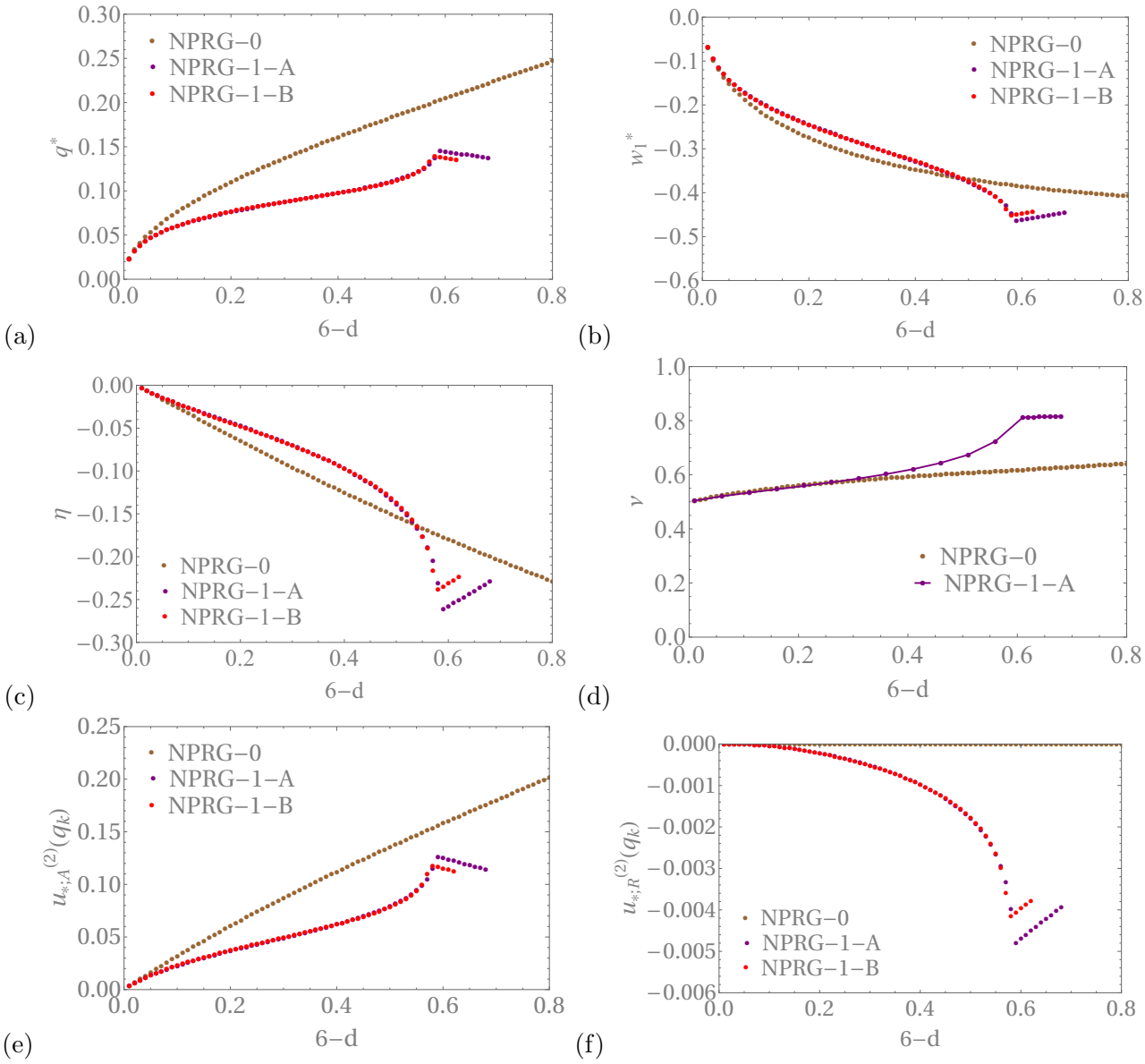

Figure 6.3: Critical fixed point properties of the Ising spin glass at the next order $O(Q^4)$ NPRG-1 (A) and (B) versus $6-d$. We also display in brown the results of the NPRG-0. (a) Dimensionless minimum $q^\star$; (b) dimensionless cubic coupling constant $w_1^\star$; (c) anomalous dimension η; (d) correlation length exponent ν (we expect ν to behave similarly for the choice (B) but we did not perform the calculation); (e) dimensionless anomalous/longitudinal mass $u^{(2)}_{k;A/L}(q_k)$; and (f) dimensionless replicon mass $u^{(2)}_{k;R}(q_k)$.

The five dimensionless RG flow equations $\{\dot{w}_{k,1}, \dot{u}_{k,1}, \dot{u}_{k,2}, \dot{u}_{k,3}, \dot{u}_{k,4}\}$ are directly obtained from the expressions given in appendix D.5.1, D.5.2.

The physics at criticalitity is obtained by finding the critical fixed point $\{q^\star, w_1^\star, u_1^\star, u_2^\star, u_3^\star, u_4^\star\}$ of the system of RG flow equations, η_k being determined as a function of the independent couplings. The cases (A) and (B) give almost the same results. The dimensionless dependence of $q^\star$ and $w_1^\star$ are given in figures 6.3 (a) and (b), that of the anomalous dimension η and of the correlation length exponent ν in figures 6.3 (c) and (d). We also show the predictions of the NPRG-0. The results of the NPRG-1 (A) or (B) are clearly not as good as those of the lower approximation NPRG-0, except possibly close to the upper critical dimension $d_u = 6$. Strinkingly, one finds that the critical fixed point no longer extends continuously down to a dimension between 2 and 3. The fixed point emerging from the Gaussian one below $d = 6$ indeed disappears at a dimension $d \simeq 5.4$ where it seems to merge with another (unstable) fixed point (and a new, probably unphysical, fiwed point then emerges): see figure 6.3 and the square-root like behavior of the various quantities when approaching $d \simeq 5.4$ from above, a behavior that is typical of the collapse of two fixed points. This scenario of an accidental collapse with spurious fixed points is found in other theories like the $O(N)$ model studied by the nonperturbative RG with a truncated expansion around a nontrivial minimum [Delamotte, private communications]: whereas the lowest-order approximation is well behaved, the higher order generates spurious unstable fixed points that at some (unphysical) dimension come to collapse with the (physical) critical fixed point. This occurs even at quite high orders (even as high as 16 [Delamotte, private communications]) and is cured by considering a functional approach where, *e.g.*, one derives and solves the RG flow for the effective average potential as a function of the order parameter field. We seem to encounter the same problem for the Ising spin-glass critical behavior.

The interesting piece of information that we nonetheless obtain from this NPRG-1 truncation concerns the dimensionless replicon mass expressed (when $n \to 0$) as

$$u^{(2)}_{k;R}(q_k) = \frac{1}{3} q_k^2 \, (6u_{k,1} + u_{k,2} - 6\, u_{k,3} + 3\, u_{k,4}) \; . \tag{6.67}$$

Over the range of dimensions where a reasonable critical fixed point exists, this dimensionless mass is negative (see figure 6.3 (f)).

6.9 One-loop-improved approximation

A possible solution for avoiding the generation of spurious fixed points as one increases the number of coupling constants is to treat the new coupling constants not as independent parameters determined from additional flow equations but as "slave" parameters explicitly determined in terms of lower-order terms. This is what is achieved by a mixed approximation scheme to the nonperturbative RG equation known as the one-loop improved approximation [222]. The couplings are therefore divided in primary ones that follow nonperturbative RG flow equations (in which other couplings may also appear) and secondary ones that are expressed in terms of 1-PI vertices obtained from a one-loop-like approximation involving the nonperturbative propagator calculated from the nonperturbative RG flow for the primary parameters.

The rationale for this approximation scheme is that higher-order 1-PI vertices are more easily approximated in the infrared (IR) regularized theory at scale k, even *via* a one-loop-like formula [222]. As we will see, the implementation of this approximation scheme in the spin-glass problem is however not as straightforward as for the φ^4 theory, again due to the nature of the order parameter and of the invariants. This will require an additional approximation. We now give the main steps of the procedure. More details are given in appendix D.6.

We start from the expression in invariants of the potential given in equation (6.17), which we recall here:

$$U[\{Q_{ab}\}] = \tilde{W}_1 X_1^{(3)} + \sum_{i=1}^{4} \tilde{U}_i \, X_i^{(4)} + \sum_{i=1}^{4} \tilde{V}_i \left(X_i^{(5)} - \sum_{j=1}^{4} b_{ij} \, Q_k \, X_j^{(4)} - c_i \, Q_k^2 \, X_1^{(3)} \right) + O(Q^6) \tag{6.68}$$

and where the constants $\{b_{ij}, c_i\}$ for $i = 1, ..., 4$ and $j = 1, ..., 4$ have two possible solutions, which are given in the equations (D.12) for (A) and (D.13) for (B) (see appendix D.6).

The RG equations for η_k and q_k are the same as in equations (6.42) and (6.46), and the RG flow equation for $w_{k,1}$ is (with distinct a, b, c):

$$\begin{aligned} \dot{w}_{k,1} = \frac{1}{2}(-6 + d + 3\eta_k) \, w_{k,1} + \frac{1}{2} \widetilde{\partial}_t \left\{ 2 \, f^{(3),(3),(3)}_{ab,bc,ca}(0) - 3 \, f^{(4),(3)}_{ab,bc;ca}(0) + f^{(5)}_{ab,bc,ca}(0) \right\} \Big|_{q_k} \\ + \delta q_k \sum_{(gh)} u^{(4)}_{k;ab,bc,ca,gh} \Big|_{q_k} , \end{aligned} \tag{6.69}$$

with the definitions of $f^{(3),(3),(3)}_{ab,bc,ca}(0)$, $f^{(4),(3)}_{ab,bc;ca}(0)$ and $f^{(5)}_{ab,bc,ca}(0)$ given in (D.21).

All the 1-PI vertices, *i.e.* field derivatives of the effective average action, $\gamma^{(n)}_{k;a_1 b_1,...,a_n b_n}$ for $n = 2, 3, 4, 5$ that are nonzero are listed in appendix D.6.1. These field derivatives are potentially functions of *all* the couplings of the expansion of the potential in equation (6.68). For simplicity, we will use a truncation of the exact potential (6.68) at order $O(Q^5)$; hence all the dependence on the couplings of higher order is neglected.

One-loop-improved prescription

The secondary couplings $\{u_{k,1}, u_{k,2}, u_{k,3}, u_{k,4}, v_{k,1}, v_{k,2}, v_{k,3}, v_{k,4}\}$ are computed as slave functions of the independent parameters $\{q_k, w_{k,1}\}$. Namely, they are determined from the one-loop-improved prescription of the $\gamma^{(n)}$ for $n = 4, 5$. This method is justified if the corrections to the flow equations of the independent primary couplings brought by the secondary couplings are small and can be seen as perturbations.

The one-loop improved prescription provides an expression for the field derivatives of Γ_k (the 1-PI vertices) in terms of the independent parameters q_k and $w_{k,1}$ only:

$$U^{(n)}_{k;a_1 b_1,...,a_n b_n} \Big|_{Q_k} = \frac{1}{2} \frac{\delta^n}{\delta Q_{a_1 b_1} ... \delta Q_{a_n b_n}} \mathrm{Tr} \log \left[\overline{\Gamma}^{(2)}_k + R_k \, \mathbb{1} \right] \Big|_{Q_k} , \tag{6.70}$$

where the Tr log term is the one-loop approximation and the effective action $\overline{\Gamma}_k$ is the $O(Q^3)$ truncation of Γ_k given by:

$$\overline{\Gamma}_k[\{Q_{ab}\}] = \int_x \left\{ \frac{1}{2} Z_k \sum_{(ab)} (\partial_x Q_{ab}(x))^2 + W_{k,1} \sum_{(abc)} \mu^{(3)}_{abc} \right\} . \tag{6.71}$$

The different nonzero field derivatives of $\overline{U}_k$ (the local piece of $\overline{\Gamma}_k$) are listed in equation (6.49). The one-loop-improved prescription of the $\gamma^{(5)}$'s and $\gamma^{(4)}$'s, and the expressions of the secondary couplings $u_{k,i}$'s and $v_{k,i}$'s in terms of them are given in appendix D.6.2. These expressions of the $u_{k,i}$'s and $v_{k,i}$'s thus obtained are injected into the different 1-PI vertices $\gamma^{(p)}$ listed from (D.44) to (D.47) that appear into the three dimensionless flow equations.

Critical fixed-point solution

All the results of this section have been obtained for the choice (A) of the potential. The same study has been performed for the choice (B), the results obtained are almost identical with that obtained with the choice (A) and for this reason they are not represented.

We search for the critical fixed-point solution $\{q^\star, w_1^\star\}$ of the RG flow equations with η_k and the secondary couplings $\{u_{k,1}, u_{k,2}, u_{k,3}, u_{k,4}, v_{k,1}, v_{k,2}, v_{k,3}, v_{k,4}\}$ fully determined as functions of q_k and $w_{k,1}$.

The critical fixed-point solution seems to depend on the maximal number of distinct replicas n_{max} that we consider in the indices $\{a_1, b_1, ..., a_p, b_p\}$ of the different vertices $\gamma^{(p)}_{k;a_1b_1,...,a_pb_p}$ listed in (D.44) to (D.47). Indeed, the Trace present in the flow equations generates sums over replica indices, and distinct replicas generates factors like $(n-3)(n-4)(n-5)$ that can potentially be large and violate the assumed perturbative character of the terms containing the secondary couplings $u_{k,i}$ and $v_{k,i}$.

We study the critical fixed point for various n_{max}, beginning with $n_{max} = 3$ (the minimal number required to define $w_{k,1}$ as it comes from $\gamma^{(3)}_{k;ab,bc,ca}$, with $a, b, c \neq$). The definition of the secondary couplings in equations (D.49) and (D.48) imply a dependence on n_{max}. For a given value of n_{max}, the only nonzero coupling constants are

$$\begin{aligned} n_{max} = 3 &\rightarrow u_{k,2}\,,\ u_{k,3}\,,\ v_{k,2}\,, \\ n_{max} = 4 &\rightarrow u_{k,2}\,,\ u_{k,3}\,,\ v_{k,2}\,;\ u_{k,1}\,,\ u_{k,4}\,,\ v_{k,3}\,, \\ n_{max} \geq 5 &\rightarrow u_{k,2}\,,\ u_{k,3}\,,\ v_{k,2}\,;\ u_{k,1}\,,\ u_{k,4}\,,\ v_{k,3}\,;\ v_{k,1}\,,\ v_{k,4}\,. \end{aligned} \tag{6.72}$$

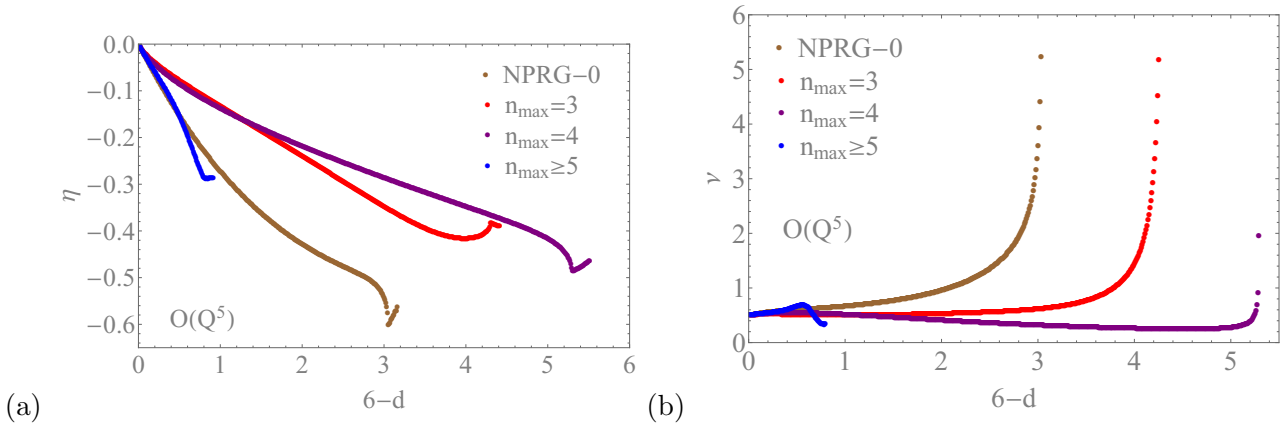

Figure 6.4: Fixed point solution for the critical point of the Ising spin glass at the $O(Q^5)$ truncation of the potential in one-loop-improved approximation of the nonperturbative RG versus $6-d$. We compare three situations where the maximal number of replicas n_{max} appearing in the vertices is varied: $n_{max} = 3$ (red/gray), $n_{max} = 4$ (purple/pink) and $n_{max} = 5$ (blue/black). We also display the results of the NPRG-0 (in brown/orange). (a) Anomalous dimension η; and (b) correlation length critical exponent ν.

The critical exponents of the critical fixed-point solutions are represented as a function of the distance $6-d$ to the upper critical dimension in figure 6.4 for each case of n_{max}. In this case there are no spurious fixed points that come to collapse the critical fixed point but the lower critical dimension is now found to be too small compared to expected values (d_l is supposed to be between dimensions 2 and 3). In particular for $n_{max} = 4$, the exponent ν diverges for a dimension d between 0 and 1, which is unphysical.

We also studied the one-loop improved scheme when the truncation for the primary parameters is carried out at the next order to see the influence of the truncation on the results. The case $n_{max} = 4$ is slightly better for the $O(Q^5)$ truncation of U_k, plotted here, than for the $O(Q^4)$ truncation whose results are shown in appendix D.6.4. In the latter the exponent ν is found to diverge for $d = 0$ only, hence *no* lower critical dimension is found. This can be linked to the fact that at fixed n_{max}, the order of truncation of U_k has to be such that not too many derivatives are missed in the lists (D.44)

and (D.47). One can note indeed that the more reasonable behavior is obtained in the case $n_{max} = 3$ for both truncations to $O(Q^4)$ and $O(Q^5)$.

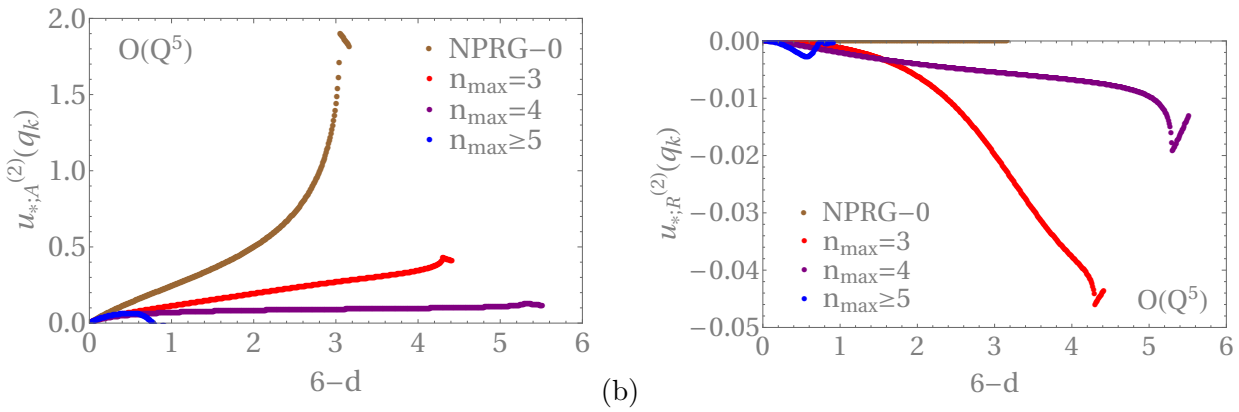

Figure 6.5: Fixed point solution for the critical point of the Ising spin glass at the $O(Q^5)$ truncation of the potential in one-loop improved approximation of the nonperturbative RG versus $6-d$. We compare three situations where the maximal number of replicas n_{max} appearing in the vertices is varied: $n_{max} = 3$ (red/gray), $n_{max} = 4$ (purple/pink) and $n_{max} = 5$ (blue/black). We also display the results of the NPRG-0 (in brown/orange). (a) Dimensionless anomalous/longitudinal mass $u^{(2)}_{\star;A}(q_k)$; and (b) dimensionless replicon mass $u^{(2)}_{\star;R}(q_k)$.

We obtain in each case a positive dimensionless anomalous/longitudinal dimensionless mass and a negative dimensionless replicon mass, as plotted in figure 6.5 for the $O(Q^5)$ truncation of U_k (the $O(Q^4)$ plots can be found in appendix D.6.4 and display the same behavior). The masses are given by expressions in terms of secondary couplings in equations (6.66) (for $n \to 0$) and (6.67).

6.10 Conclusion

In this chapter, we have developed a nonperturbative RG approach to study the critical behavior associated with the phase transition of the Ising spin glass in zero applied field. To get around the methodological difficulties due to the nature of the order parameter (a $n \times n$ matrix with $n \to 0$) we have devised an approximation scheme based on an expansion around a nontrivial minimum of the potential that keeps explicitly into account the symmetry of the theory at each order of the truncation.

Whereas we find that the lowest-order approximation is very successful compared to the ε expansion in describing the critical physics from the upper critical dimension $d_u = 6$ down to $d = 3$, problems arising from the generation of spurious fixed points appear at higher orders and are only partly solved by another, mixed, approximation scheme known as one-loop improved.

One could then try to expand around a minimum of the potential with a more complex structure, *i.e.*, a Parisi full-RSB solution. This would considerably increase the complexity of the algebra for deriving flow equations (see *e.g.* [141]) and there is no guarantee that spurious fixed points would not be generated at high-enough order of the truncation. It seems that any further progress by means of the nonperturbative RG will have to retain the functional character of the method and avoid field expansions.

Conclusion and perspectives

Understanding glassy systems, such as structural glasses and spin glasses, in two and three dimensions still represents a challenge for physicists. Mean-field approximations for both systems have been known for some time and proven exact (quite recently for glass-forming liquids) when the dimension is infinite. These mean-field scenarios are quite intricate and involve complex free-energy landscapes, multitude of pure states, and metastability, all phenomena that may be fragile in the presence of spatial fluctuations which are ubiquitous in finite-dimensional systems. In this work we have tackled this problem of the effect of fluctuations in glassy systems. The task being arduous, we have studied a set of relatively simple, yet finite-dimensional, models and for this purpose we have used and developed a variety of theoretical tools.

Below, we briefly summarize the main conclusions of this work and sketch some perspectives. The interested reader can go back to the conclusion section that closes each chapter for more details.

In chapter 3, we have considered the role of nonperturbative fluctuations in a one-dimensional toy model in which these fluctuations destroy the phase transition found at the mean-field level. The extent of the fluctuations can be restricted either by considering a finite-size system or by introducing an infrared cutoff in the renormalization group formalism. We have shown how one can extract information on the parameters of the underlying theory from finite-size studies of systems of small to moderate sizes and how to build from this an effective theory. This provides a guide for computer-simulation studies of glass-forming liquid models that for practical reasons can only access limited system sizes. We have also studied how various approximation schemes of the nonperturbative renormalization group fail on describing strong fluctuations and rare events in the simple (and otherwise well known) example of the one-dimensional φ^4 theory.

In chapter 4, we have investigated the thermodynamic properties of plaquette spin models of glass-forming systems that have been described in terms of kinetically-constrained motion of localized defects [27] and taken as a paradigm for the theory of dynamical facilitation [11]. Both "short-range" fluctuations associated with the local environment on Bethe lattice and "long-range" fluctuations that distinguish Euclidean from Bethe lattices with the same local environment have been considered. Surprisingly, we have found that what was considered as singular thermodynamic properties characteristic of the three-dimensional (Euclidean) models are reproduced on a Bethe lattice, provided one chooses the same local environment. The long-range fluctuations therefore seem to have a week influence on these properties, contrary to short-range fluctuations. In two dimensions however, long-range fluctuations have a more drastic effect as they destroy the phase transition predicted from the Bethe lattice calculation.

In chapter 5, we have investigated analytically the spatial correlations in the dynamics of a simple finite-dimensional system whose relaxation is thermally activated yet trivial in the sense that it is described by a single constant activation energy and an Arrhenius law. These correlations are usually associated with the development of dynamical heterogeneities in glassy systems and characterized by a length scale that can be extracted from multi-body (beyond two) space-time correlation functions. [40] We have found that such a "dynamical" length does grow in the system under study in spite of the absence of any cooperativity in the relaxation. However, the nature of this length in the present model appears rather trivial and not directly related to the kind of dynamical heterogeneities observed in glass-forming liquids. The study is still in progress to determine whether there is or not an additional characteristic length at play in the behavior of the four-point space-time correlation function.

Finally, in chapter 6 we have considered the critical behavior associated with the phase transition of

the Edwards-Anderson Ising spin-glass model [59] in the absence of an applied magnetic field. We have developed an approximation scheme of the nonperturbative renormalization group that preserves the original symmetry of the model. We have found that the lowest order of our scheme provides a good description of the critical behavior down to the dimension three, which must be contrasted with the poor performance of the perturbative renormalization group treatment. However, at the higher orders the situation deteriorates due to the presence of spurious fixed points that may annihilate the critical fixed point in (unphysical) dimensions larger than three. In the range of dimensions where the critical fixed point exists, the *dimensionless* replicon mass is negative at the fixed point (the dimensionful mass is of course zero), which may be tentatively interpreted as indicating that replica symmetry must be broken in the spin-glass phase for all finite sizes. [58] (Nothing can be said for the thermodynamic limit or equivalently the limit where the infrared cutoff is zero.) The goal of this study was not the description of the critical behavior *per se* (as the existence of a transition in dimension three is well established and large-scale computer simulations provide accurate estimates of the critical properties) but rather to provide a first implementation of the nonperturbative renormalization group for glassy systems characterized by an overlap order parameter field. [16, 12] The difficulties encountered in the present study suggest that the next step to make progress within this framework is to develop a *functional* approximation scheme that avoids field expansions.

Despite progress made by several authors and the insight provided by phenomenological approaches, a description from first principles of the effect of the spatial fluctuations on the properties of glassy systems is clearly a daunting task. We have emphasized in several places of this manuscript the obstacles on the way to a full-blown implementation of a nonperturbative renormalization group and pointed out that a functional approach would likely be necessary to make further progress. Another potentially useful approach, more specifically for the case of glass-forming liquids and (structural) glasses, is to devise a proper *effective theory* in which the already nontrivial effect of the short-range fluctuations have been incorporated. As found from previous work [7, 95, 105, 86, 102, 89] (for a differing view see [110]) a good candidate is some variant of the random-field Ising model [90, 94] or its field-theoretical version. The parameters of this effective theory could be systematically extracted from finite-size computer-simulation studies of realistic glass-forming models (as proposed in chapter 3). The long-distance physics of this effective theory could then be determined either by numerical simulations or renormalization group analysis. Whether or not this leads to a complete description of both the statistics and the dynamics of glassy systems in three dimensions is yet to be seen.

Appendix A

Non-perturbative fluctuations in a simple model with metastability

A.1 Computation of the combinatorial factors for the gas of instantons

The combinatorial coefficients $I_{2n}(L)$ are configuration integrals of $2n$ domain walls of width σ on a ring of size L. This problem is equivalent to the computation of the partition function of $2n$ (discernible) hard spheres of size σ on a ring of size L in $D = 1$. As done in the main text, we define x_i, $i = 1, \ldots, 2n$, as the lengths of the regions with constant $\phi = \pm 1$ (*i.e.*, the gaps between the spheres). These variables must satisfy the constraint $\sum_{i=1}^{2n} x_i + 2n\sigma = L$.

One then has

$$I_{2n}(L) = \frac{L}{n} \int_0^{L-2n\sigma} \mathrm{d}x_{2n-1} \int_0^{L-2n\sigma-x_{2n-1}} \mathrm{d}x_{2n-2} \cdots \int_0^{L-2n\sigma-(x_{2n-1}+x_{2n-2}+\cdots+x_2)} \mathrm{d}x_1 \,,$$

where the factor L comes from translational invariance and the factor $1/n$ accounts for the number of ways one can choose the first kink/anti-kink pair. In the following, we will determine the expression of I_{2n} by recurrence. In order to do this, it is convenient to introduce the functions

$$g_n(y) = \int_0^{y} \mathrm{d}x_{n-1} \int_0^{y-x_{n-1}} \mathrm{d}x_{n-2} \cdots \int_0^{y-(x_{n-1}+x_{n-2}+\cdots+x_2)} \mathrm{d}x_1 \,, \tag{A.1}$$

in terms of which the combinatorial factors can be expressed as

$$I_{2n}(L) = \frac{L}{n}\, g_{2n}(L - 2n\sigma) \,. \tag{A.2}$$

From the definition in equation (A.1), one can write $g_{n+1}(y)$ in terms of $g_n(y)$,

$$g_{n+1}(x) = \int_0^{y} \mathrm{d}x_n\, g_n(y - x_n) = \int_0^{y} \mathrm{d}x_n\, g_n(x_n) \,, \tag{A.3}$$

which, from $g_2(y) = \int_0^y \mathrm{d}x_1 = y$ and by recurrence, immediately leads to

$$g_n(y) = \frac{y^{n-1}}{(n-1)!} \,. \tag{A.4}$$

Finally, after plugging equation (A.4) into (A.2), one obtains equation (3.13) of the main text.

In order to compute the combinatorial factors $J_{2n}(M, L)$ one has to impose that the gaps x_i satisfy the two following constraints:

$$\begin{cases} \displaystyle\sum_{i=1}^{2n} x_i = L - 2n\sigma \,, \\ \displaystyle\sum_{i=1}^{n} (x_{2i-1} - x_{2i}) = M \,, \end{cases}$$

which can be rewritten as

$$\begin{cases} \displaystyle\sum_{i=1}^{n} x_{2i-1} = \frac{L - 2k\sigma + M}{2}\,, \\ \displaystyle\sum_{i=1}^{n} x_{2i} = \frac{L - 2k\sigma - M}{2}\,. \end{cases}$$

As a result, the integrals over the variables x_i can be divided into separate integrations over even and odd gaps, which can be written in terms of the functions $g_n(y)$ defined above. This yields

$$J_{2n}(M,L) = \frac{L}{2n}\, g_n\!\left(\frac{L - 2n\sigma - M}{2}\right) g_n\!\left(\frac{L - 2n\sigma + M}{2}\right).$$

The extra $1/2$ factor comes from the fact that only half of the configurations, namely, those with the first domain wall joining $\varphi = -1$ to $\varphi = +1$, contribute to magnetization $+M$, whereas the others contribute to $-M$. After using the exact expression in equation (A.1), one finally finds

$$J_{2n}(M,L) = \frac{L}{2n}\, \frac{\left[(L-2n\sigma)^2 - M^2\right]^{n-1}}{2^{2(n-1)}(n-1)!^2}\,, \tag{A.5}$$

which, with the help of the intensive variables $\phi = M/L$ and $\alpha = \sigma/L$, leads to equation (3.18) of the main text.

In the following we show that $P_L(\phi)$ given in equation (3.18) is properly normalized to 1. We start by computing the integrals over ϕ of the terms of the sum separately. By changing variable to $x = \phi/(1-2n\alpha)$ one gets

$$\begin{aligned} \Upsilon_{2n}(L) &= 2\left(\frac{\zeta}{2}\right)^{2n} \int_{-(1-2n\alpha)}^{+(1-2n\alpha)} \mathrm{d}\phi\, \frac{\left[(1-2n\alpha)^2 - \phi^2\right]^{n-1}}{n!(n-1)!} \\ &= 2\,\frac{(\zeta/2)^{2n}}{n!(n-1)!}\,(1-2n\alpha)^{2(n-1)}(1-2n\alpha)\int_{-1}^{+1} \mathrm{d}x\,(1-x^2)^{n-1}\,. \end{aligned}$$

The integral over $\mathrm{d}x$ can be computed as

$$\int_{-1}^{+1} \mathrm{d}x\,(1-x^2)^{n-1} = 2\int_0^{\pi/2} \mathrm{d}\theta\,(\cos\theta)^{2n-1} = \sqrt{\pi}\,\frac{\Gamma(n)}{\Gamma(n+1/2)}\,,$$

where $\Gamma(n+1/2) = 2^{-n}(2n-1)!!\,\sqrt{\pi}$. By using the fact that

$$(2n-1)!! = \frac{(2n)!}{(2n)!!} = \frac{(2n)!}{2^n n!}\,,$$

one then finds

$$\Upsilon_{2n}(L) = 2\zeta^{2n}\,\frac{(1-2n\alpha)^{2n-1}}{(2n)!}\,. \tag{A.6}$$

From equations (3.18), (3.14) and (A.6), one ends up with

$$\begin{aligned} \int_{-1}^{+1} \mathrm{d}\phi\, P_L(\phi) &= \frac{1}{Z_L(\zeta,\alpha)}\left[\int_{-1}^{+1} d\phi\,\left(\delta(\phi-1)+\delta(\phi+1)\right) + \sum_{n=1}^{1/(2\alpha)} 2\zeta^{2n}\,\frac{(1-2n\alpha)^{2n-1}}{(2n)!}\right] \\ &= \frac{1}{Z_L(\zeta,\alpha)}\sum_{n=0}^{1/(2\alpha)} 2\zeta^{2n}\,\frac{(1-2n\alpha)^{2n-1}}{(2n)!} = 1\,. \end{aligned} \tag{A.7}$$

The expression of $P_L(\phi)$ for the one-dimensional Ising model [168] can be recovered as a particular case of equation (3.18) in the limit $\sigma \to 0$ (*i.e.*, for infinitely sharp domain walls) and for $\tilde{S}^\star = 2J$. In particular one then has

$$Z_L(\zeta, \alpha = 0) = 2\sum_{n=0}^{\infty} \frac{\zeta^{2n}}{(2n)!} = 2\cosh\zeta\,,$$

and

$$P_L(\phi) = \frac{1}{2\cosh\zeta}\left[(\delta(\phi-1)+\delta(\phi+1)) + \sum_{n=1}^{\infty} 2(\zeta/2)^{2n}\frac{(1-\phi^2)^{n-1}}{n!(n-1)!}\right].$$

These expressions coincide with the results of reference [168].

A.2 Instanton calculation for the one-dimensional Ising model

As stated in the main text, we consider the one-dimensional Ising model with periodic boundary condition which is described by the Hamiltonian

$$H[\{\sigma_i\}] = -J\sum_{i=1}^{L}\sigma_i\sigma_{i+1} - h\sum_{i=1}^{L}\sigma_i \tag{A.8}$$

where $\sigma_{L+1} \equiv \sigma_1$, the lattice spacing which is as unity, and, contrary to the case studied in section 3.2, only the thermodynamic limit $L \to \infty$ is considered.

We summarize the main (known) results about the model. The partition function can be computed using the transfer matrix method.[223] The transfer matrix is given by

$$\mathbf{V} = \begin{pmatrix} e^{\tilde{h}+\tilde{J}} & e^{-\tilde{J}} \\ e^{-\tilde{J}} & e^{-\tilde{h}+\tilde{J}} \end{pmatrix} \tag{A.9}$$

where $\tilde{h} = \beta h$ and $\tilde{J} = \beta J$ and the partition function is obtained as $Z_N = \mathrm{Tr}\mathbf{V}^N$. One can easily diagonalize the transfer matrix with the rotation

$$\mathbf{U} = \begin{pmatrix} \cos\theta & -\sin\theta \\ \sin\theta & \cos\theta \end{pmatrix} \tag{A.10}$$

where $1/\tan(2\theta) = e^{2\tilde{J}}\sinh\tilde{h}$. The eigenvalues are given by

$$\lambda_\pm = e^{\tilde{J}}\cosh\tilde{h} \pm \sqrt{e^{2\tilde{J}}\cosh^2\tilde{h} - 2\sinh(2\tilde{J})}\,. \tag{A.11}$$

The average magnetization $m =< \sigma_i >$ is then

$$m = \frac{e^{\tilde{J}}\sinh\tilde{h}}{\sqrt{e^{2\tilde{J}}\cosh^2\tilde{h} - 2\sinh(2\tilde{J})}} \tag{A.12}$$

and the two-point connected correlation function

$$G_c^{(2)}(|i-j|) = \langle\sigma_i\sigma_j\rangle - m^2 = \sin^2(2\theta)\left(\frac{\lambda_-}{\lambda_+}\right)^{|i-j|}, \tag{A.13}$$

which can be rewritten as

$$G_c^{(2)}(r) = \sin^2(2\theta)e^{-r/\xi} \tag{A.14}$$

where $\xi = \left[\ln\left(\frac{\lambda_-}{\lambda_+}\right)\right]^{-1}$. These expressions provide the magnetization and the two-point function at fixed external magnetic field h. However we would like to have the magnetization instead of the external field as the primary variable since we want to work with the effective action defined by the Legendre transform.

One can thus invert the relation in equation (A.12) to obtain

$$\frac{\lambda_+}{\lambda_-} = \frac{\sqrt{1-m^2(1-e^{-4\tilde{J}})}+e^{-2\tilde{J}}}{\sqrt{1-m^2(1-e^{-4\tilde{J}})}-e^{-2\tilde{J}}}\,, \tag{A.15}$$

so that, in the limit of very low temperature, one gets

$$\xi(m)^{-1} \simeq \frac{2e^{-2\tilde{J}}}{\sqrt{1-m^2}} \tag{A.16}$$

and

$$G_c^{(2)}(r) = (1-m^2)e^{-r/\xi(m)}\,. \tag{A.17}$$

These results are used in section A.3.1.

A.3 Nonperturbative renormalization group

See section 2.2 for an introduction on the nonperturbative renormalization group (NPRG).

A k-dependent cutoff function is added to the microscopic (bare) action $S[\varphi]$ ($S[\varphi]$ is equal to the Hamiltonian $H_L[\varphi]$ of equation (3.1)) that freezes all fluctuations with $k' < k$:

$$S[\varphi] \to S_k[\varphi] = S[\varphi] + \frac{1}{2}\int_q \varphi(q)R_k(q)\varphi(-q)\,, \tag{A.18}$$

where $\int_q \equiv \int d^dq/(2\pi)^d$ with d the space dimension. The function $R_k(q)$ is the regulator.

The effective average action $\Gamma_k[\phi]$ can be constructed, and an exact evolution equation of $\Gamma_k[\phi]$ under the variation of k can be written. The k-dependent magnetization $\phi_k(x) = \langle\varphi(x)\rangle_k$ is introduced, where the average $\langle\,.\,\rangle_k$ is taken by using the modified action $S_k[\varphi]$. The k subscript in is then omitted and $\phi_k(x) \equiv \phi(x)$. In particular the exact flow equation for $\Gamma_k[\phi]$ writes, from equation (2.25):

$$\frac{\partial\Gamma_k[\phi]}{\partial k} = \frac{\beta}{2}\int_{xy} R_k(x-y)\left[\left(\Gamma_k^{(2)}+\beta R_k\right)^{-1}\right]_{xy} \tag{A.19}$$

with the initial condition $\Gamma_\Lambda[\phi] = \beta S[\phi]$ and $\Gamma_k^{(n)}(x_1,\ldots,x_n) \equiv \delta^n\Gamma_k/\delta\phi(x_1)\ldots\delta\phi(x_n)$. The whole equation is multiplied by β such that $\Gamma_k[\phi]$ has no dimension; we have used the notation $\int_x \equiv \int d^dx$.

By differentiation, this functional flow equation is equivalent to an infinite hierarchy of coupled flow equations for the running effective potential, $U_k(\phi) = \Gamma_k[\phi]/L^d$, and the running field derivatives $\Gamma_k^{(n)}(x_1,\ldots,x_n)$ (then all evaluated for uniform field configurations).

A.3.1 Running effective action and instantons in the limit $T \to 0$ ($\xi \to \infty$)

We first compute the expression of the running effective potential, $U_k(\phi) = \Gamma_k[\phi]/L$ with ϕ a uniform field, by using the instanton technique in the low-temperature regime where the correlation length is large (see also section 3.2).

For the one-dimensional φ^4 theory under study, the k-dependent regularized action (A.18) reads

$$\begin{aligned} S_k[\varphi] = &\int_0^L \mathrm{d}x \left[\frac{c}{2}(\partial_x\varphi)^2 + V(\varphi(x))\right] + \frac{1}{2}\int_0^L \mathrm{d}x \int_0^L \mathrm{d}y\, \phi(x) R_k(x-y)\phi(y) \\ &- L\left[V(\phi_{0,k}) + \frac{1}{2}R_k(0)\phi_{0,k}^2\right] \end{aligned} \tag{A.20}$$

where $S[\varphi]$ have been replaced by the Hamiltonian $H_L[\varphi]$ of equation (3.1) and $V(\varphi)$ is given in equation (3.2),

$$\phi_{0,k} = \mathrm{argmin}_\varphi \left[V(\varphi) + \frac{1}{2}R_k(0)\varphi^2\right], \tag{A.21}$$

and we have added the last term in equation (A.20) for convenience, so that $S_k[\phi_{0,k}] = 0$. Contrary to the previous section on the finite-size effective potential, we take here the thermodynamic limit and let $L \to \infty$. The restriction to the spatial extent of the fluctuations is now provided by the IR regulator $R_k(q)$.

A very simple regulator is the Callan-Symanzik one, $R_k(q) = k^2$, which amounts to adding a conventional mass term to the bare action $S[\varphi]$ (A.18). (Note that in this case the running effective action is equal to the bare action only in the limit $\Lambda \to \infty$ but this has no consequences for the physics at intermediate and small momentum scales.) It is then possible to see that there exists a threshold $k = k_c$ such that $\phi_{0,k} \neq 0$ for all $k \geq k_c$. This threshold corresponds to the moment along the RG flow where the running modified potential $V(\varphi) + \frac{1}{2}k^2\varphi^2$ develops two minima and has a double-well shape. One can expect that this qualitative evolution is very general and does not depend on the details of the regulator. The precise form of $R_k(q)$ changes only the point k_c where the double-well shape first appears.

For $k > k_c$ we can thus evaluate the probability of finding a particular magnetization in the system by using the instanton method, much like in section 3.2.2. This probability is given by

$$P_k(\phi = M/L) = \mathcal{N}\sum_{n\geq 1} e^{-2n\beta S_k^\star} \int_0^\infty \left(\prod_{i=1}^{2n}\mathrm{d}z_i\right) \delta\left(\sum_{i=1}^{2n} z_i - L - 2n\sigma_k\right) \delta\left[\sum_{i=1}^{n}(z_{2i-1} - h_{2i}) - \frac{M}{\phi_{0,k}}\right] \tag{A.22}$$

where z_i is the length of the ith interval separated by two domain walls, $\mathcal{N}$ is a normalization constant, $S_k^\star$ is the action evaluated on an single instanton profile and σ_k is the instanton width. By exponentiating the Dirac delta functions and passing from a discrete sum to a continuum one so that $\alpha L = 2n$, we get

$$\begin{aligned} P_k(\phi) = &\mathcal{N}' \int_0^\infty \mathrm{d}\alpha\, \mathrm{e}^{-\alpha L\beta S_k^\star} \int_{-i\infty}^{i\infty} \mathrm{d}\mu\mathrm{d}\nu \int_0^\infty \left(\prod_{i=1}^{2n}\mathrm{d}z_i\right) \times \\ &\exp\left[\mu L(1+\alpha\sigma_k) + L\nu\frac{\phi}{\phi_{0,k}} - \sum_{i=1}^{n}\left[(\mu+\nu)z_{2i-1} + (\mu-\nu)z_{2i}\right]\right] \end{aligned} \tag{A.23}$$

where $\mathcal{N}'$ is another normalization constant. Integration over the variables z_i then leads to

$$P_k(\phi) = \mathcal{N}' \int_0^\infty \mathrm{d}\alpha e^{-\alpha L\beta S_k^\star} \int_{-i\infty}^{i\infty} \mathrm{d}\mu\mathrm{d}\nu \exp\left[L\left(\mu + \alpha\mu\sigma_k + \nu\frac{\phi}{\phi_{0,k}} - \frac{\alpha}{2}\ln(\mu^2-\nu^2)\right)\right]. \tag{A.24}$$

For large L we can use a saddle point evaluation of the integrals over μ and ν, which gives

$$P_k(\phi) = \mathcal{N}' \int_0^\infty \mathrm{d}\alpha \exp\left[-\alpha L\beta S_k^\star + L\left(\alpha - \alpha\ln\alpha + \frac{\alpha}{2}\ln[(1+\alpha\sigma_k)^2 - (\frac{\phi}{\phi_{0,k}})^2]\right)\right]. \tag{A.25}$$

Finally the integral over α can also be evaluated with the saddle point method and the value of α at the saddle point is found to be

$$\alpha = \sqrt{1 - \frac{\phi^2}{\phi_{0,k}^2}} \mathrm{e}^{-\beta S_k^\star} \tag{A.26}$$

where the range of magnetizations is limited to $\phi < \phi_{0,k}$. The low-temperature regime corresponds to $\beta S_k^\star$ large and the system is then described by a dilute instanton gas. The running effective potential U_k is just $-1/(\beta L)$ times $\ln P_k(\phi)$, to which one subtracts the contribution of the IR regulator, and it is given by

$$\begin{aligned} U_k(\phi) &= -\frac{1}{\beta L} \ln P_k(\phi) - \frac{1}{2} R_k(0) \left(\phi^2 - \phi_{0,k}^2\right) + V(\phi_{0,k}) \\ &= -\frac{1}{\beta} \sqrt{1 - \frac{\phi^2}{\phi_{0,k}^2}} \mathrm{e}^{-\beta S_k^\star} - \frac{1}{2} R_k(0) \left(\phi^2 - \phi_{0,k}^2\right) + V(\phi_{0,k}) \,, \end{aligned} \tag{A.27}$$

which is valid for $\phi < \phi_{0,k}$ and is asymptotically exact when the temperature goes to zero. The associated flow equation reads

$$\frac{\partial U_k(\phi)}{\partial k} = \frac{\partial}{\partial k} \left[-\frac{1}{\beta} \sqrt{1 - \frac{\phi^2}{\phi_{0,k}^2}} \mathrm{e}^{-\beta S_k^\star} \right] + \frac{1}{2} \frac{\partial R_k(0)}{\partial k} \left(\phi_{0,k}^2 - \phi^2\right) \tag{A.28}$$

To go further and find the asymptotic low-temperature expressions for the $\Gamma_k^{(n)}(x_1, \ldots, x_n)$ vertices at scale k, we use a short-cut provided by an approximate mapping when $T \to 0$ between the φ^4 theory and the Ising model. The latter is described by the Hamiltonian

$$H[\{\sigma_i\}] = -J \sum_{i=1}^{L} \sigma_i \sigma_{i+1} - h \sum_{i=1}^{L} \sigma_i \tag{A.29}$$

where $\sigma_{L+1} \equiv \sigma_1$ if periodic boundary conditions are used and we have set the lattice spacing to one. The thermodynamic limit with $L \to \infty$ is considered here. This calculation for the one-dimensional Ising model is rather standard[223] and the details are given in appendix A.2.

In the low-temperature limit, the long-distance properties of both theories are described in the continuum. The expressions of their pair correlation function are respectively: for the Ising case

$$G_c^{(2)}(r; m) \simeq (1 - m^2) e^{-r/\xi(m)} \quad \text{with} \quad \xi(m) \simeq \frac{1}{2} \sqrt{1 - m^2} \,, e^{2\beta J} \tag{A.30}$$

$\xi(m)$ being the correlation length and m the magnetization per site, and for the (modified) φ^4 theory (from the instanton calculation)

$$G_c^{(2)}(r; \phi) \simeq (\phi_{0,k}^2 - \phi^2) e^{-r/\xi(\phi)} \quad \text{with} \quad \xi(\phi) \simeq \frac{1}{2} \sqrt{1 - \frac{\phi^2}{\phi_{0,k}^2}} e^{\beta S_k^\star} \,. \tag{A.31}$$

From the comparison between (A.30) and (A.31), one can see that the two theories map onto each other with the following formal replacements when $T \to 0$:

$$2J \to S_k^\star \quad \text{and} \quad (1 - m^2) \to (\phi_{0,k}^2 - \phi^2) \tag{A.32}$$

and $S_k^\star$, the instanton action, is identified with the domain-wall energy when $T \to 0$.

At low temperature, the two-leg vertex can be written as

$$\frac{1}{\beta}\Gamma_k^{(2)}(p;\phi) \simeq \frac{1}{2\beta(\phi_{0,k}^2-\phi^2)}\xi(\phi)\left[p^2+\xi^{-2}(\phi)\right] - R_k(0) \tag{A.33}$$

where the last term is due to the definition of the running effective action from the modified Legendre transform (2.24). This expression can be put in the form

$$\beta^{-1}\Gamma_k^{(2)}(p;\phi) = Z_k(\phi)p^2 + U_k''(\phi) \tag{A.34}$$

where $Z_k(\phi)$ can be obtained as

$$Z_k(\phi) = \lim_{p\to 0}\frac{1}{2\beta}\frac{\partial^2}{\partial p^2}\Gamma_k^{(2)}(p,\phi) = \frac{1}{2\beta(\phi_{0,k}^2-\phi^2)}\xi(\phi)\,. \tag{A.35}$$

In addition, we can check that

$$U_k''(\phi) + R_k(0) = \frac{1}{\beta}\frac{1}{\phi_{0,k}^2-\phi^2}\frac{e^{-\beta S_k}}{\sqrt{1-\phi^2/\phi_{0,k}^2}}\,, \tag{A.36}$$

in complete agreement with equation (A.27).

By using the mapping with the one-dimensional Ising model, we can also obtain low-temperature expressions for the higher-order 1PI correlation functions, $\Gamma_k^{(3)}$, $\Gamma_k^{(4)}$, $\cdots$, at the scale k. With the results given in appendix A.4 we obtain

$$\Gamma_k^{(3)}(p_1,p_2,p_3;\phi) = (2\pi)\delta(p_1+p_2+p_3)\frac{c(\phi)s(\phi)^2}{2\xi(\phi)}\left[3-\xi(\phi)^2\left(p_1p_2+p_1p_3+p_2p_3\right)\right] \tag{A.37}$$

$$\begin{aligned}\Gamma_k^{(4)}(p_1,p_2,p_3,p_4;\phi) = \frac{(2\pi)\delta(p_1+p_2+p_3+p_4)}{2\xi(\phi)s(\phi)^6}\big(&-[c(\phi)^2+s(\phi)^2]\xi(\phi)^4p_1p_2p_3p_4\\ &-[3c(\phi)^2+s(\phi)^2]\xi(\phi)^2(p_1p_2+p_1p_3+p_1p_4+p_2p_3+p_2p_4+p_3p_4)+3[5c(\phi)^2+s(\phi)^2]\big)\end{aligned} \tag{A.38}$$

where $c(\phi)=\phi$ and $c(\phi)^2+s(\phi)^2=\phi_{0,k}^2$ (c should not be confused with the notation also used for the prefactor of the derivative term in the bare action). More generally the running 1PI correlation function can be cast in the form $\Gamma_k^{(n)}(p_1,\cdots,p_n;\phi) = (2\pi)\delta(p_1+\cdots+p_n)\xi(\phi)^{-1}g_n(\xi(\phi)p_1,\cdots,\xi(\phi)p_n;\phi)$ where the remaining ϕ dependence in g_n does not contain exponential terms involving $\exp(\beta S_k^\star)$.

A.3.2 Approximation schemes

Having obtained the exact expressions for the running effective potential and the running 1PI correlation functions in the low-temperature limit, we can now test approximation schemes for the exact NPRG equation in equation (A.19). Among the several approximation schemes so far proposed, we will focus first on the most popular one, the so-called derivative expansion. In this approximation, the running effective action at the scale k is expanded in gradients of the field,

$$\Gamma_k[\phi] = \beta\int_x\left[U_k(\phi(x)) + \frac{1}{2}Z_k(\phi(x))\left(\frac{\partial\phi(x)}{\partial x}\right)^2+\cdots\right] \tag{A.39}$$

where the higher-order terms involve 4, 6, etc., derivatives of the field. We will show that finite truncations of the derivative expansion are unable to reproduce the exact features of the low-temperature physics.

A.3.2.1 LPA

The Local potential Approximation (LPA) is the lowest order of the derivative equation. It corresponds to (2.33)

$$\Gamma_k[\phi] = \beta \int_x \left[U_k(\phi(x)) + \frac{1}{2} \left(\frac{\partial \phi(x)}{\partial x} \right)^2 \right] , \tag{A.40}$$

where the coefficient of the gradient term is constant and is not renormalized. Plugging this ansatz into equation (A.19), computing it for a uniform field ϕ and choosing the simple regulator $R_k(q) = b_k k^2$ with b_k constant (taken to 1) lead to the following differential equation for the running effective potential $U_k(\phi)$:

$$\partial_k U_k(\phi) = \frac{1}{4\beta} \frac{1}{\sqrt{U_k''(\phi) + k^2}} \partial_k(k^2) \, . \tag{A.41}$$

It is easily verified that the exact expression in equation (A.27) does not satisfy the above equation. The latter is actually unable to reproduce the correct scaling of the correlation length, with, *e.g.*, $U_k'' + k^2 \propto \exp(-\beta S_k^\star)$ [see equation (A.36)].

In figure 3.1 (b), we have plotted the running effective potential $U_k(\phi)$ at several values of k, as obtained from the LPA with the Litim regulator (2.22): $R_k(p) = (k^2 - p^2)\Theta(k^2 - p^2)$. The curves illustrate the return to convexity of the potential. However, as also known from previous attempts,[169, 170, 172] if the LPA provides a good description for values of T higher than the energy barrier of the double well, or more precisely than the instanton energy cost $S^\star$, they fail to reproduce the low-temperature result with a thermally activated dependence of the correlation length, $\propto \exp(\beta S^\star)$. For instance, the curvature of the effective potential in zero, $\kappa_{k=0} = U_{k=0}''(0)$, which should vanish exponentially when $T \to 0$ as $\exp(-\beta S^\star)$ (see also section 3.2) is generically found to vanish as a power law of T instead. The nonperturbative regime associated with the rare localized events, which is captured by the instanton calculation, is therefore completely missed.

A.3.2.2 Second order of the derivation expansion

The next order corresponds to the following ansatz (from (2.34) setting $Y_k(\phi(x)) = 0$), sometimes called LPA':

$$\Gamma_k[\phi] = \beta \int_x \left[U_k(\phi(x)) + \frac{1}{2} Z_k(\phi) \left(\frac{\partial \phi}{\partial x} \right)^2 \right] . \tag{A.42}$$

When inserted in the exact RG flow equation, this ansatz leads to two coupled differential equations for the functions $U_k(\phi)$ and $Z_k(\phi)$ [the latter is obtained from the exact flow equation for the second vertex $\Gamma_k^{(2)}$ with the use of the prescription given in the first equality of equation (A.35)]:

$$\partial_k U_k(\phi) = \frac{1}{4\beta} \partial_k(b_k k^2) \left[Z_k(\phi) \left(U_k''(\phi) + b_k k^2 \right) \right]^{-1/2} \tag{A.43}$$

$$\begin{aligned} \partial_k Z_k(\phi) = \frac{1}{\beta} \partial_k(b_k k^2) \times \\ \left[-\frac{5}{64} U_k'''(\phi)^2 Z_k(\phi)^{1/2} \left(U_k''(\phi) + b_k k^2 \right)^{-7/2} + \frac{9}{32} Z_k'(\phi) U_k'''(\phi) Z_k(\phi)^{-1/2} \left(U_k''(\phi) + b_k k^2 \right)^{-5/2} \right. \\ \left. + \frac{7}{64} Z_k'(\phi)^2 Z_k(\phi)^{-3/2} \left(U_k''(\phi) + b_k k^2 \right)^{-3/2} - \frac{1}{8} Z_k''(\phi) Z_k(\phi)^{-1/2} \left(U_k''(\phi) + b_k k^2 \right)^{-3/2} \right] \end{aligned} \tag{A.44}$$

where the IR cutoff function is of the same form as above (and a residual k-dependence is allowed in b_k).

When inserting the exact expression for $U_k(\phi)$ and $Z_k(\phi)$ given in equations (A.27), (A.35), and (A.36), one can see that equation (A.43) is now satisfied at leading order in $\exp(-\beta S_k^\star)$ but not equation (A.44). The exact expressions indeed generate terms of order $\exp(2\beta S_k^\star)$ in the right-hand side of equation (A.44) which do not cancel and have no counterparts in the left-hand side [which is itself essentially of order $\exp(\beta S_k^\star)$]. The problem found at the LPA level can be formally cured at the level of the effective average potential but at the expense of an inconsistency at the level of the function $Z_k(\phi)$.

A.3.2.3 Fourth order of the derivative expansion

To check whether the results found above correspond to a more systematic pattern, we have considered the fourth order, which corresponds to taking (2.34), called the leading approximation:

$$\Gamma_k[\phi] = \int_x \left[U_k(\phi(x)) + \frac{1}{2} Z_k(\phi(x)) (\partial\phi(x))^2 + \frac{1}{4!} Y_k(\phi(x)) \, (\partial\phi(x))^4 \right] . \tag{A.45}$$

The equation for the running effective potential in equation (A.43) is unchanged but that for $Z_k(\phi)$ is now obtained as

$$\begin{aligned} \partial_k Z_k(\phi) = \frac{1}{\beta} \partial_k (b_k k^2) \Big[& -\frac{5}{64} U_k'''(\phi)^2 Z_k(\phi)^{1/2} \left(U_k''(\phi) + b_k k^2 \right)^{-7/2} \\ & + \frac{9}{32} Z_k'(\phi) U_k'''(\phi) Z_k(\phi)^{-1/2} \left(U_k''(\phi) + b_k k^2 \right)^{-5/2} + \frac{7}{64} Z_k'(\phi)^2 Z_k(\phi)^{-3/2} \left(U_k''(\phi) + b_k k^2 \right)^{-3/2} \\ & - \frac{1}{8} Z_k''(\phi) Z_k(\phi)^{-1/2} \left(U_k''(\phi) + b_k k^2 \right)^{-3/2} - \frac{1}{8} Y_k(\phi) Z_k(\phi)^{-3/2} \left(U_k''(\phi) + b_k k^2 \right)^{-1/2} \Big] . \end{aligned} \tag{A.46}$$

An equation for $Y_k(\phi)$ is also derived by considering the flow of the 4-point 1PI vertex but it is too long to be given here.

When inserting the exact low-temperature expressions for $U_k(\phi)$, $Z_k(\phi)$, and $Y_k(\phi)$ [the latter can be obtained from equations (A.37,A.38)] in the three flow equations corresponding to the present ansatz, one finds that both the equation for U_k and that for Z_k in equation (A.46) are satisfied. For the latter, the term involving $Y_k(\phi)$ in the right-hand side of equation (A.46) now exactly cancels the term in $\exp(2\beta S_k^\star)$ that led to an inconsistency in the second-order approximation (see above). On the other hand, one can check that the approximate equation for $Y_k(\phi)$ is not satisfied by the exact expression because of the presence of terms of order $\exp(4\beta S_k^\star)$ in the right-hand side [while Y_k itself behaves as $\exp(3\beta S_k^\star)$].

A.3.2.4 General scheme and further approximations

Guided by the above results, it is now easy to infer the general pattern. The prefactors of the terms with $2l$ derivatives of the field in the derivative expansion of the running effective action $\Gamma_k[\phi]$ are of order $\exp[(2l-1)\beta S_k^\star]$ in the low-temperature regime [and $U_k''(\phi) + R_k(0)$ is itself of order $\exp(-\beta S_k^\star)$]. This dominant behavior when $\beta S_k^\star \to \infty$ emerges from the exact NPRG hierarchy of equations for the 1PI vertices because terms that would naively lead to a higher power in $\exp(\beta S_k^\star)$ in the right-hand side of the equations (the "beta functions") exactly cancel out. This cancelation effect is however lost if

one truncates the expansion, whatever the order of the truncation. We conjecture that the appropriate ansatz of $\Gamma_k[\phi]$ that reproduces the low-temperature physics of the model is instead

$$\Gamma_k[\phi] = \int_x \left[U_k(\phi(x)) + \sum_{l=1}^{\infty} \frac{1}{(2l)!} Y_{k,2l}(\phi(x)) (\partial\phi(x))^{2l} \right] \tag{A.47}$$

with, to make contact with the previous notations, $Y_{k,2}(\phi) \equiv Z_k(\phi)$ and $Y_{k,4}(\phi) \equiv Y_k(\phi)$. Note that the above form of Γ_k is *not* the most general one: in the derivative expansion, the term of order ∂^{2l} is actually a combination of terms involving $(\partial\phi)^{2l}$, $\partial^2\phi(\partial\phi)^{2l-2}$, $\cdots$, $\partial^{2l}\phi$ which even after integration by part cannot in general be reduced to a single contribution as in equation (A.47). The specific form in equation (A.47) results from the rather simple momentum dependence of the 1PI correlation functions in the one-dimensional Ising model and φ^4 theory at low temperature.

The above finding allows us to discuss another approximation of the NPRG called BMW.[224] It corresponds to a closure of the exact NPRG hierarchy at the level of the equation for the 1PI two-point function $\Gamma_k^{(2)}(p,\phi)$:

$$\partial_k \Gamma_k^{(2)}(p,\phi) = \beta \int \frac{\mathrm{d}q}{2\pi} \partial_k R_k(q) \left[G_k(q,\phi)^2 G_k(p+q,\phi) \Gamma_k^{(3)}(p,q,-p-q;\phi)^2 - \frac{1}{2} G_k(q,\phi)^2 \Gamma_k^{(4)}(p,-p,q,-q;\phi) \right] \tag{A.48}$$

where $G_k(p,\phi) = [\Gamma_k^{(2)}(p,\phi) + R_k(p)]^{-1}$. The BMW closure consists in setting to zero the internal momentum q appearing in the 3- and 4- point vertices in the right-hand side. After using the consistency relations, $\Gamma_k^{(3)}(p,0,-p;\phi) = \partial\Gamma_k^{(2)}(p;\phi)/\partial\phi$ and $\Gamma_k^{(4)}(p,-p,0,0;\phi) = \partial^2\Gamma_k^{(2)}(p;\phi)/\partial\phi^2$, one obtains a closed equation

$$\partial_k \Gamma_k^{(2)}(p,\phi) = \beta \int \frac{\mathrm{d}q}{2\pi} \partial_k R_k(q) \left[G_k(q,\phi)^2 G_k(p+q,\phi) \left[\frac{\partial\Gamma_k^{(2)}(p;\phi)}{\partial\phi} \right]^2 - \frac{1}{2} G_k(q,\phi)^2 \frac{\partial^2\Gamma_k^{(2)}(p;\phi)}{\partial\phi^2} \right] \tag{A.49}$$

which can be combined with the equation for the running effective potential $U_k(\phi)$. It is easily checked that equation (A.49) is not compatible with the exact low-temperature expressions of U_k and $\Gamma_k^{(2)}$ given in section A.3.1: after scaling the momenta by $\xi(\phi)$ (see section A.3.1), the left-hand side of equation (A.49) scales as ξ^{-1} whereas the right-hand side has a term in ξ^0 that does *not* cancel out. Just like truncations of the derivative expansion, the BMW closure is therefore unable to properly describe the nonperturbative physics of the one-dimensional φ^4 at low temperature.

The alternative to the existing approximation schemes of the NPRG is to start from the exact low-temperature ansatz in equation (A.47). This however leads to an infinite set of differential equations that cannot be treated with standard methods. We have tried another route which amounts to considering the running effective action as being local in the two variables $\phi(x)$ and $\partial\phi(x)$ and introduce an auxiliary field $\hat{\phi}(x)$ to decouple $\partial\phi(x)$ from $\phi(x)$. This procedure however is highly ambiguous. In addition, say we end up with a running effective action of the form $\Gamma_k[\phi,\hat{\phi}] = \int_x \mathcal{V}_k(\phi(x),\hat{\phi}(x))$, it is not clear that standard approximations on this ansatz will correctly capture the expected low-temperature physics. Actually we have tried an LPA approximation at the level of the two fields ϕ and $\hat{\phi}$ and it completely misses the nonperturbative regime.

A.3.3 Higher dimensions

In a sense, the one-dimensional case is harder than the situation in higher dimensions. There, the transition associated with a spontaneous symmetry breaking is not destroyed by the fluctuations and the return to convexity has been shown to be properly described through simple approximations of the NPRG. [225, 226, 25]

Consider for instance the 3-dimensional φ^4 theory. As far as the finite-size effective potential $U_L(\phi)$ is concerned, one can repeat and adapt the qualitative arguments developed in section 3.2.1. At low enough temperature, the bare potential has two minima in, say, $\phi = \pm 1$ and the relevant excitations above the uniform ground states are system-spanning domain walls or interfaces between regions of essentially constant positive and negative magnetization. When the system size L becomes larger than the interface width (which is of the order of the correlation length[227]), the system can accommodate one system-spanning interface: $U_L(\phi)$ should then have, on top of the two symmetric minima for $\phi \simeq \pm 1$, a plateau for intermediate values of the field; the height of the plateau compared to the bottom of the minima is given by Υ/L where Υ is the surface tension. As L increases, this height decreases and goes to zero in the thermodynamic limit. The effective potential is convex with a flat intermediate portion corresponding to phase coexistence. The evolution with L of $U_L(\phi)$ is schematically depicted in figure A.1. In this case, studying finite-size systems should allow one to extract two physical quantities, the surface tension and the correlation length which corresponds to the interface width.

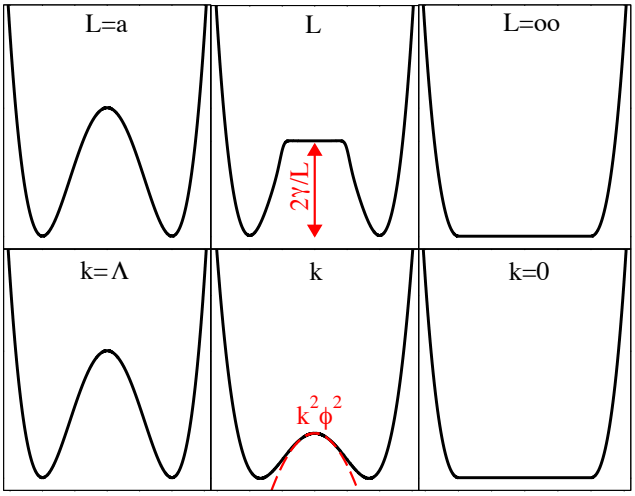

Figure A.1: Schematic plot of the evolution of the shape of the finite-size effective potential $U_L(\phi)$ (top) and of the running effective potential $U_k(\phi)$ (bottom) with either system size L or running IR momentum scale k for the φ^4 theory in 3 dimensions.

This 3-dimensional φ^4 theory in the symmetry-broken region [1] has also been studied in detail within the NPRG framework.[225, 226, 25] Although influenced by domain walls as in one dimension, the long-distance physics is nonetheless different as these nonperturbative fluctuations are not strong enough to destroy the phase transition. As a result, simple approximation schemes of the running effective action properly capture the effect of these fluctuations. The running effective potential $U_k(\phi)$ evolves with decreasing k from the bare double-well potential to a convex effective potential when $k = 0$: see the schematic plot in figure A.1. Provided one chooses an appropriate class of IR regulator,[25] the intermediate "inner" part of $U_k(\phi)$ displays at small k a parabolic shape $\propto k^2\phi^2$ that comes in addition to the two symmetric minima in $\phi = \pm\,\phi_{0,k}$. This parabolic dependence corresponds to the expected exact behavior obtained by considering the nonuniform configurations of the field involving domain walls. The remarkable feature is that this behavior is recovered by using approximations of the NPRG, such as the first orders of the derivative expansion, which only consider expansions about uniform fields.[226] This is in stark contrast with the situation encountered in one dimension.

[1] The return to convexity of the running effective potential has also been studied in the $O(N)$ model with $N > 2$. In this case, the excitations above the ground state take the form of spin waves: see Refs. [[228],[226]].

A.4 Derivation of $\Gamma_k^{(3)}$ and $\Gamma_k^{(4)}$ from the one-dimensional Ising model

We start from the calculation of the 3-point correlation function in the Ising model. We need to compute

$$\langle \sigma_i \sigma_{i+r_1} \sigma_{i+r_1+r_2} \rangle \,. \tag{A.50}$$

It is given by

$$\langle \sigma_i \sigma_{i+r_1} \sigma_{i+r_1+r_2} \rangle = \frac{1}{\lambda_+^N + \lambda_-^N} \mathrm{Tr}\left[\mathcal{S}\mathbf{V}^{r_1} \mathcal{S}\mathbf{V}^{r_2} \mathcal{S}\mathbf{V}^{N-r_1-r_2} \right] \tag{A.51}$$

where

$$\mathcal{S} = \begin{pmatrix} 1 & 0 \\ 0 & -1 \end{pmatrix} \,. \tag{A.52}$$

After diagonalizing the transfer matrix (see appendix A.2) and using that

$$\mathbf{U}^{-1} \mathcal{S} \mathbf{U} = \begin{pmatrix} \cos(2\theta) & -\sin(2\theta) \\ -\sin(2\theta) & -\cos(2\theta) \end{pmatrix} \,, \tag{A.53}$$

one obtains in the thermodynamic limit

$$\langle \sigma_i \sigma_{i+r_1} \sigma_{i+r_1+r_2} \rangle = c^3 + cs^2 \left(\left(\frac{\lambda_-}{\lambda_+} \right)^{r_1} + \left(\frac{\lambda_-}{\lambda_+} \right)^{r_2} - \left(\frac{\lambda_-}{\lambda_+} \right)^{r_1+r_2} \right) \tag{A.54}$$

where $c = \cos(2\theta) = m$ and $s = \sin(2\theta) = 1 - m^2$ (c should not be confused with the notation also used for the prefactor of the derivative term in the bare action). The connected 3-point correlation function is then given by

$$\langle \sigma_i \sigma_{i+r_1} \sigma_{i+r_1+r_2} \rangle_c = \langle (\sigma_i - \langle \sigma_i \rangle)(\sigma_{i+r_1} - \langle \sigma_{i+r_1} \rangle) \left(\sigma_{i+r_1+r_2} - \langle \sigma_{i+r_1+r_2} \rangle \right) \rangle = -2cs^2 \left(\frac{\lambda_-}{\lambda_+} \right)^{r_1+r_2} \,. \tag{A.55}$$

If we call $x_1 = i$, $x_2 = i + r_1$, $x_3 = i + r_1 + r_2$, the above result translates into

$$W^{(3)}(x_1 < x_2 < x_3) = -2cs^2 \left(\frac{\lambda_-}{\lambda_+} \right)^{x_3 - x_1} \,, \tag{A.56}$$

so that the 3-point connected correlation function for generic arguments can be written as

$$\begin{aligned} W^{(3)}(x_1, x_2, x_3) = -2cs^2 \Bigg[& \left(\frac{\lambda_-}{\lambda_+} \right)^{x_3 - x_1} \Theta(x_3 - x_2)\Theta(x_2 - x_1) + \left(\frac{\lambda_-}{\lambda_+} \right)^{x_1 - x_3} \Theta(x_1 - x_2)\Theta(x_2 - x_3) \\ & + \left(\frac{\lambda_-}{\lambda_+} \right)^{x_2 - x_1} \Theta(x_2 - x_3)\Theta(x_3 - x_1) + \left(\frac{\lambda_-}{\lambda_+} \right)^{x_1 - x_2} \Theta(x_1 - x_3)\Theta(x_3 - x_2) \\ & + \left(\frac{\lambda_-}{\lambda_+} \right)^{x_2 - x_3} \Theta(x_2 - x_1)\Theta(x_1 - x_3) + \left(\frac{\lambda_-}{\lambda_+} \right)^{x_3 - x_2} \Theta(x_3 - x_1)\Theta(x_1 - x_2) \Bigg] \,, \end{aligned} \tag{A.57}$$

where $\Theta(x)$ is the Heaviside step function. Neglecting the underlying lattice and performing the Fourier transform lead to

$$W^{(3)}(p_1, p_2, p_3) = (2\pi)\delta(p_1 + p_2 + p_3) \frac{4cs^2\xi^{-2}\left((p_1p_2 + p_1p_3 + p_2p_3) - 3\xi^{-2} \right)}{\left(p_1^2 + \xi^{-2} \right)\left(p_2^2 + \xi^{-2} \right)\left(p_3^2 + \xi^{-2} \right)} \,. \tag{A.58}$$

We now use the mapping between the Ising model and the φ^4 theory at low temperature and the relation between the connected 3-point correlation function and the 1PI 3-point vertex. [149] We finally obtain

$$\begin{aligned}\Gamma_k^{(3)}(p_1,p_2,p_3) &= -\tilde{\Gamma}_k^{(2)}(p_1)\tilde{\Gamma}_k^{(2)}(p_2)\tilde{\Gamma}_k^{(2)}(p_3)W^{(3)}(p_1,p_2,p_3) \\ &= (2\pi)\delta(p_1+p_2+p_3)\frac{cs^2}{2}\xi(\phi)\left[3\xi^{-2}(\phi)-(p_1p_2+p_1p_3+p_2p_3)\right]\end{aligned} \tag{A.59}$$

where $c=\phi$ and $s^2=\phi_{0,k}^2-\phi^2$. Note that it is $\tilde{\Gamma}_k^{(2)}(p)\equiv G_{c,k}^{(2)}(p)^{-1}$, obtained from $\tilde{\Gamma}_k[\phi]=\Gamma_k[\phi]+\frac{\beta}{2}\int \mathrm{d}q R_k(q)\phi(q)\phi(-q)$, which appears in equation (A.59) and not $\Gamma_k^{(2)}(p)$. The calculation of $\Gamma_k^{(4)}$ can be done in an analogous way and leads to equation (A.38). Although a cumbersome derivation, the higher orders can also be obtained along the same lines.

Appendix B

Short- and long-range fluctuations in glassy plaquette spin models

B.1 Universality class of the terminal critical points

If present the terminal critical points take place for nonzero values of the coupling ε and therefore nonzero values of the mean overlap q. As a result, one can expand the effective Hamiltonian for the overlap variables in the region around the critical point. It is convenient to move on to a soft-spin description by replacing the hard constraint $q_i = \pm 1$ by an additional term in the Hamiltonian $V(q_i) = (\lambda/8)(q_i^2 - 1)^2$ and let the q_i's take any real value. The annealed and quenched Hamiltonians for the overlap variables become [see equations (4.15) and (4.11) of the main text]

$$\mathcal{H}_\varepsilon^{an}[\{q_i\}] = -\frac{\tilde{J}}{2}\sum_\mu \prod_{\alpha=1}^{p} q_{\mu\alpha} - \varepsilon \sum_i q_i + \sum_i V(q_i)\,, \tag{B.1}$$

$$\mathcal{H}_\varepsilon^{qu}[\{q_i\}|\mathcal{C}_0] = -\frac{J}{2}\sum_\mu S_\mu^0 \prod_{\alpha=1}^{p} q_{\mu\alpha} - \varepsilon \sum_i q_i + \sum_i V(q_i)\,, \tag{B.2}$$

with $\tilde{J} = (1/\beta)\ln[\cosh(\beta J)]$ and the S_μ^0's independently distributed variables with $\overline{S_\mu^0} = \tanh(\beta J/2)$, $\overline{S_\mu^0 S_\nu^0} = \tanh^2(\beta J/2) + \delta_{\mu\nu}[1 - \tanh^2(\beta J/2)]$, etc. (see the main text).

For the annealed case, we simply expand around the saddle-point solution q_*: $q_i = q_* + \phi_i$, with q_* solution of

$$-p\frac{\tilde{J}}{2}q_*^{p-1} - \varepsilon + V'(q_*) = 0\,. \tag{B.3}$$

One then obtains

$$\mathcal{H}_\varepsilon^{an}[\{q_i\}] - \mathcal{H}_\varepsilon^{an}[q_*] = -\frac{\tilde{J}}{2}q_*^{p-2}\sum_{<ij>}\phi_i\phi_j + \frac{\lambda}{8}\sum_i[2(3q_*^2 - 2)\phi_i^2 + 4q_*\phi_i^3 + \phi_i^4] + \cdots\,, \tag{B.4}$$

where $< ij >$ is a sum over distinct nearest-neighbor pairs on the lattice and the ellipsis denote 3-body and higher-order ferromagnetic interactions. These interactions are known to be subdominant near the critical point if the pair interactions do not vanish, which is the case if $\varepsilon_c > 0$, and consequently $q_* > 0$ (note that q_* is the mean-field or saddle-point value and is different from the exact q_c, but this is irrelevant for the argument). The effective Hamiltonian in equation (B.4) has no Z_2 inversion symmetry, but as for the gas-liquid critical point of a fluid this is also known to be irrelevant at criticality (the Z_2 symmetry is asymptotically restored at the underlying renormalization-group fixed point). The critical point of the annealed model is therefore expected to be in the universality class of the Ising model.

For the quenched setting, the argument is slightly more involved. One expand the overlap variable as before, $q_i = q_* + \phi_i$; however, q_* is the saddle-point solution not for the Hamiltonian in equation (B.2), which would be site-dependent due to the quenched disorder, but for the replicated theory,

$$\mathcal{H}_{\varepsilon,\mathrm{rep}}^{qu}[\{q_i^a\}] = -\frac{1}{\beta}\sum_\mu \ln\left[\frac{\cosh[(\beta J/2)(1 + \sum_a \prod_{\alpha=1}^{p} q_{\mu\alpha}^a)]}{\cosh(\beta J/2)}\right] - \varepsilon\sum_a\sum_i q_i^a + \sum_a\sum_i V(q_i^a)\,, \tag{B.5}$$

where $a = 1, \cdots, n$ is the replica index. Looking for a replica-symmetric and spatially uniform saddle-point solution leads to the following equation for q_* when $n \to 0$:

$$-p\frac{J}{2}\tanh(\beta J/2)q_*^{p-1} - \varepsilon + V'(q_*) = 0\,. \tag{B.6}$$

The effective hamiltonian can then be rewritten as

$$\begin{aligned}\mathcal{H}_\varepsilon^{qu}[\{q_i\}|\mathcal{C}_0] - \mathcal{H}_\varepsilon^{qu}[q_*|\mathcal{C}_0] = &-\frac{J}{2}q_*^{p-2}\overline{S_\mu^0}\sum_{<ij>}\phi_i\phi_j - \frac{J}{2}q_*^{p-1}\sum_i\sum_{\mu/i}(S_\mu^0 - \overline{S_\mu^0})\phi_i \\ &- \frac{J}{2}q_*^{p-2}\sum_{<ij>}\sum_{\mu/<ij>}(S_\mu^0 - \overline{S_\mu^0})\phi_i\phi_j + \frac{\lambda}{8}\sum_i[2(3q_*^2-2)\phi_i^2 + 4q_*\phi_i^3 + \phi_i^4] + \cdots\,,\end{aligned} \tag{B.7}$$

where $\overline{S_\mu^0} = \tanh(\beta J/2)$, the sum on μ/i is over all plaquettes attached to site i and that on $\mu/ < ij >$ is over all plaquettes sharing the edge (ij); the ellipsis denotes 3-body and higher-order interactions. The Hamiltonian is therefore that of a lattice scalar-field theory with random fields, $(J/2)q_*^{p-1}\sum_{\mu/i}(S_\mu^0 - \overline{S_\mu^0})$, and random bonds, $(J/2)q_*^{p-2}\sum_{\mu/<ij>}(S_\mu^0 - \overline{S_\mu^0})$. Provided $q_* > 0$, the dominant features at long distance are thus the ferromagnetic pair interactions and the random field, and the associated critical point is then expected to be in the universality class of the RFIM.

B.2 Cavity equations for the Bethe-lattice coupled plaquette spin models: free energy

In order to compute the free energy per site one starts with $p(c-1)$ sub-trees. As illustrated in figure B.1, one can either add a new plaquette μ and connect $(c-1)$ sub-trees to each site of the plaquette or add $(p - p/c)$ sites linked to c sub-trees.

Correspondingly, the average free energy per site can be computed as the difference between a "plaquette" (p) contribution and a "site" (s) contribution:

$$\begin{aligned}-\beta f = &\frac{c}{p}\sum_{S_\mu=\pm1} p[S_\mu]\int\prod_{j=1}^{c-1}\prod_{\nu=1}^{p}\left[dh_\nu^{(j)}P^*(h_\nu^{(j)})\right]\log Z_p^{(\mu)}(\{h_\nu^{(j)}\}, S_\mu) \\ &- (c-1)\int\prod_{j=1}^{c}\left[dh_\nu^{(j)}P^*(h_\nu^{(j)})\right]\log Z_s^{(j)}(\{h_\nu^{(j)}\})\end{aligned} \tag{B.8}$$

with $P^*(h)$ the sationnary probability distribution solution of equation (4.24).

The plaquette and site contributions $Z_p^{(\mu)}$ and $Z_s^{(j)}$ read respectively:

$$Z_p^{(\mu)}(\{h_\nu^{(j)}\}, S_\mu) = \sum_{\{q_\mu^{(1)},\ldots,q_\mu^{(p)}=\pm1\}}\exp\left[\frac{\beta J S_\mu}{2}\prod_{i\in\mu}q_\mu^{(i)} + \beta\sum_{i\in\mu}q_\mu^{(i)}(\varepsilon + H_\mu^{(i)})\right] \tag{B.9}$$

and

$$Z_s(\{h_\nu^{(j)}\}) = \sum_{q_j=\pm1}\exp\left[\beta q_j(\varepsilon + \sum_{\nu\ni j}h_\nu^{(j)})\right]. \tag{B.10}$$

In the annealed setting, the free energy is simply expressed as

$$-\beta f = \frac{c}{p}\log Z_p(h^*) - (c-1)\log Z_s(h^*) \tag{B.11}$$

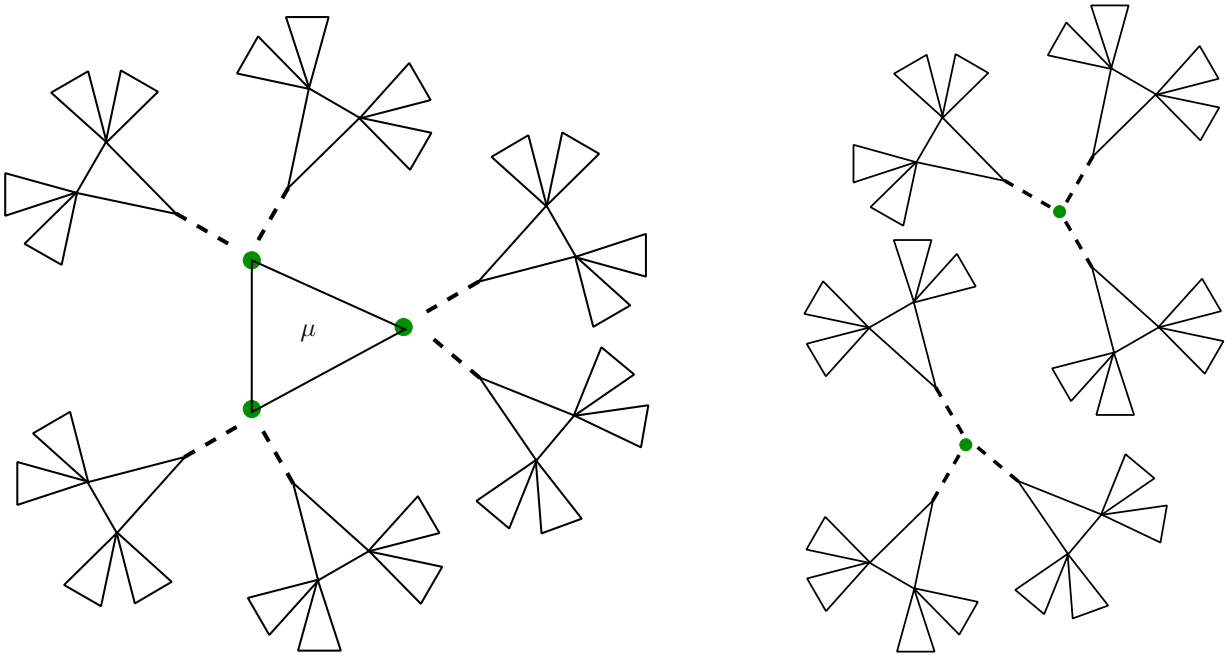

Figure B.1: One can merge $(p-1)(c-1)$ sub-trees of N sites either to one plaquette μ or to $(p-p/c)$ sites. In the former case, one has a new tree with $p(c-1)N+p$ sites and in the latter case, $(p-p/c)$ trees with $cN+1$ sites. We illustrate here the TPM where $c=p=3$.

with h^* the solution of equation (4.25) and

$$\begin{aligned} Z_p(h) &= \sum_{\{q_\mu^{(1)},\ldots,q_\mu^{(p)}=\pm 1\}} \exp\Big[\frac{\beta\widetilde{J}}{2}\prod_{i\in\mu} q_\mu^{(i)} + \beta(\varepsilon+h)\sum_{i\in\mu} q_\mu^{(i)}\Big] \\ Z_s(h) &= \sum_{q=\pm 1} \exp\big[\beta q(\varepsilon+h)\big]\,. \end{aligned} \tag{B.12}$$

Appendix C

Space-time fluctuations in Arrhenius systems

C.1 Normal modes

The internal energy (5.11) is modified by the introduction of normal modes,

$$E_p^B = \frac{K_0}{2}\sum_{\vec{k},\vec{k'}} \vec{u}_{\vec{k}}(t)\vec{u}_{\vec{k'}}(t)\,\frac{1}{N}\sum_{j=1}^{N} e^{i(\vec{k}+\vec{k'})\cdot\vec{l}_j}(1-e^{i\vec{k}\cdot(\vec{l}_{j+1}-\vec{l}_j)})(1-e^{i\vec{k'}\cdot(\vec{l}_{j+1}-\vec{l}_j)}) = \frac{1}{2}\sum_{\vec{k}}\lambda_{\vec{k}}^2|\vec{u}_{\vec{k}}(t)|^2\,, \quad \text{(C.1)}$$

where we introduced $\lambda_{\vec{k}}^2$, the coupling between phonons that propagate within the bath of harmonic oscillators. The rightmost term can be decomposed on each space direction ε,

$$\sum_{\varepsilon=\{x,y,z\}}\frac{1}{N}\sum_{\substack{j|\\(\vec{l}_{j+1}-\vec{l}_j)=\vec{e}_\varepsilon}} e^{i(\vec{k}+\vec{k'})\cdot\vec{l}_j}(1-e^{i\vec{k}\cdot(\vec{l}_{j+1}-\vec{l}_j)})(1-e^{i\vec{k'}\cdot(\vec{l}_{j+1}-\vec{l}_j)})$$

$$= \sum_{\varepsilon=\{x,y,z\}}(1-e^{i\vec{k}\cdot\vec{e}_\varepsilon})(1-e^{i\vec{k'}\cdot\vec{e}_\varepsilon})\frac{1}{N}\sum_{j=1}^{N/d} e^{i(\vec{k}+\vec{k'})\cdot\vec{l}_j} = \sum_{\varepsilon=\{x,y,z\}}(1-e^{ia\vec{k}\cdot\vec{e}_\varepsilon})(1-e^{ia\vec{k'}\cdot\vec{e}_\varepsilon})\frac{1}{d}\delta_{\vec{k},-\vec{k'}}\,,$$

where we have used that the difference $(\vec{l}_{j+1}-\vec{l}_j)$ can take three distinct values $a\{\vec{e}_x,\vec{e}_y,\vec{e}_z\}$, each of them in equal proportion $\frac{1}{d}$. The coupling is given by, with $k_\varepsilon = \vec{k}\cdot\vec{e}_\varepsilon$ and $K = K_0/d$,

$$\lambda_{\vec{k}}^2 = K\sum_{\varepsilon=x,y,z}(1-e^{ik_\varepsilon a})(1-e^{-ik_\varepsilon a}) = 4\,K\left[\sin^2\left(\frac{k_x a}{2}\right)+\sin^2\left(\frac{k_y a}{2}\right)+\sin^2\left(\frac{k_z a}{2}\right)\right]. \quad \text{(C.2)}$$

C.2 Effective ferromagnetic interaction energy

Our aim is to compute the following term

$$I_{N_{dw}}\left(\{X_i\}=\{+X_0\}\,\text{or}\,\{-X_0\}\right), \quad \text{(C.3)}$$

which is given by, using equations (5.31) and (5.32),

$$-\frac{X_0^2}{2}\sum_{\substack{m,n=1\\m\neq n}}^{N_{dw}} Y(\hat{R}_{mn})\,. \quad \text{(C.4)}$$

We can transform this double sum into a double integration, setting $\hat{R}_{mn} = ||\vec{x}-\vec{y}||/a$, $\vec{x}$ and $\vec{y}$ being the positions of the particles equilibrium positions. The integration must be done in respect to an

"exclusion" radius lower cutoff corresponding to the minimal radius separating two nearest neighbors particles $R^\star$. Hence the sum becomes, with the dimensionless variables $\hat{x} = x/a$, $\hat{y} = y/a$, $\hat{R}^\star = R^\star/a$,

$$\begin{aligned}\sum_{\substack{m,n=1\\m\neq n}}^{N_{dw}} Y(\hat{R}_{mn}) &= \int_{-N_{dw}^{1/3}R^\star/2}^{N_{dw}^{1/3}R^\star/2} \frac{d^3x}{(R^\star)^3} \int_{-N_{dw}^{1/3}R^\star/2}^{N_{dw}^{1/3}R^\star/2} \frac{d^3y}{(R^\star)^3}\, Y\left(||\vec{x}-\vec{y}||/a\right)\Theta\left(||\vec{x}-\vec{y}||-R^\star\right)\\ &= \frac{a^6}{(R^\star)^6}\int_{-N_{dw}^{1/3}\hat{R}^\star/2}^{N_{dw}^{1/3}\hat{R}^\star/2} d^3\hat{x}\int_{-N_{dw}^{1/3}\hat{R}^\star}^{N_{dw}^{1/3}\hat{R}^\star} d^3\hat{z}\, Y\left(||\hat{\vec{z}}||\right)\Theta\left(||\hat{\vec{z}}||-\hat{R}^\star\right)\\ &\sim \frac{a^6}{(R^\star)^6}\left(N_{dw}^{1/3}\hat{R}^\star\right)^3\int_{\hat{R}^\star}^{N_{dw}^{1/3}\hat{R}^\star} d\hat{z}\hat{z}^2\, Y\left(\hat{z}\right) \sim \frac{a^6}{(R^\star)^6}N_{dw}\left(\hat{R}^\star\right)^6\int_1^{N_{dw}^{1/3}} d\widetilde{z}\,\widetilde{z}^2\, Y\left(\hat{R}^\star\widetilde{z}\right),\end{aligned} \tag{C.5}$$

with $\widetilde{z} = \hat{z}/\hat{R}^\star$. The above expression is finally

$$\sum_{\substack{m,n=1\\m\neq n}}^{N_{dw}} Y(\hat{R}_{mn}) \sim N_{dw}\int_1^{N_{dw}^{1/3}} d\widetilde{z}\,\widetilde{z}^2\, Y\left(\hat{R}^\star\widetilde{z}\right). \tag{C.6}$$

The right function has the form $Y(\hat{z}) = A\frac{e^{-B\hat{z}}}{\hat{z}}$, with A and $B > 0$, thus its integration yields

$$A\int_1^{N_{dw}^{1/3}} d\hat{z}\hat{z}\, e^{-B\hat{z}} = \frac{A}{B^2}\left[e^{-B}\left(1+B\right) - e^{-BN_{dw}^{1/3}}\left(1+BN_{dw}^{1/3}\right)\right]. \tag{C.7}$$

As $A = \frac{g^2}{4\pi K}\frac{1}{\hat{R}^\star}$ and $B = \sqrt{\frac{\rho g}{K}}\hat{R}^\star$, we have $\frac{A}{B^2} = \frac{1}{\left(\hat{R}^\star\right)^3}\frac{g}{4\pi\rho}$. The volume is equivalently given by $V = a^3N$ and $V = (R^\star)^3N_{dw}$, hence $\frac{1}{\left(\hat{R}^\star\right)^3} = \left(\frac{a}{R^\star}\right)^3 = \frac{N_{dw}}{N} = \rho$, the density of double-wells. The effective interaction energy becomes

$$\begin{aligned}I_{N_{dw}}\left(\{+X_0\}\right) &\sim -\frac{X_0^2}{2}N_{dw}\frac{g}{4\pi}\left[e^{-\sqrt{\frac{\rho g}{K}}\hat{R}^\star}\left(1+\sqrt{\frac{\rho g}{K}}\hat{R}^\star\right) - e^{-\sqrt{\frac{\rho g}{K}}N_{dw}^{1/3}\hat{R}^\star}\left(1+\sqrt{\frac{\rho g}{K}}N_{dw}^{1/3}\hat{R}^\star\right)\right]\\ &\underset{N_{dw}\gg 1}{\sim} -\frac{X_0^2}{2}N_{dw}\frac{g}{4\pi}e^{-\sqrt{\frac{\rho g}{K}}\hat{R}^\star}\left(1+\sqrt{\frac{\rho g}{K}}\hat{R}^\star\right).\end{aligned} \tag{C.8}$$

C.3 Different sums over $\vec{k}$

In the following we will have to evaluate terms like $\frac{1}{N}\sum_{\vec{k}}$. Using that, for $L = V^{1/3}$ large, the sum can be transformed in an integral, of some function $f(\vec{k})$ becomes

$$\frac{1}{N}\sum_{\vec{k}} f(\vec{k}) = \frac{1}{N}\frac{L^3}{(2\pi)^3}\int_{-\frac{\pi}{a}}^{\frac{\pi}{a}} d\vec{k}\, f(\vec{k}) = \frac{1}{(2\pi)^3}\int_{-\pi}^{\pi} d\hat{\vec{k}}\, f(\hat{\vec{k}}), \tag{C.9}$$

as the number of sites is $N = \frac{V}{a^3}$ and where we have defined the dimensionless variable $\hat{\vec{k}} = a\vec{k}$. In addition the system under study is isotropic and all the functions we will encounter can be expressed in term of spherical coordinates (k,θ,ϕ). They all have the same form $f(\vec{k}) = \frac{l(\vec{k})}{\widetilde{\lambda}_k^2}$, where $\widetilde{\lambda}_k^2 = g\rho + K\hat{k}^2 + o(\hat{k}^2)$, where we have used $\rho = \frac{N_{dw}}{N}$ as the density of double-wells. Therefore the integrals all read

$$\frac{1}{(2\pi)^3}\int_{-\pi}^{\pi} d^3\hat{k}\,\frac{l(\hat{\vec{k}})}{g\rho + K\hat{k}^2} = \frac{1}{(2\pi)^3}\int_0^{2\pi} d\phi\int_0^{\pi} d\theta\sin\theta\int_0^{\pi} d\hat{k}\,\hat{k}^2\,\frac{l(\hat{k},\theta,\phi)}{g\rho + K\hat{k}^2}. \tag{C.10}$$

In the limit where $\rho g \ll 1$ and in dimension $d = 3$, the rightmost integral is dominated by the infra-red regime where $k \ll 1$.

C.3.1 Effective interaction between particles

We want to evaluate following sum which appears in the expression (5.25),

$$\frac{1}{N}\sum_{\vec{k}} \frac{e^{i\vec{k}(\vec{R}_m - \vec{R}_n)}}{\widetilde{\lambda}^2_{\vec{k}}}\,, \tag{C.11}$$

in the two possible cases, $n = m$ and $n \neq m$.

C.3.1.1 Case $m = n$

We have to compute

$$\alpha = \frac{1}{N}\sum_{\vec{k}} \frac{1}{\widetilde{\lambda}^2_{\vec{k}}} = \frac{1}{(2\pi)^3} 4\pi \int_0^\pi d\hat{k}\, \hat{k}^2\, \frac{1}{\widetilde{\lambda}^2_k}\,, \tag{C.12}$$

with $\widetilde{\lambda}^2_k = g\rho + Ka^2k^2 + o(\hat{k}^2)$ from (5.24), where we have used $\rho = \frac{N_{dw}}{N}$ as the density of double-wells. This reads, integrated over the dimensionless $\hat{k}$,

$$\alpha = \frac{1}{2\pi^2}\int_0^\pi d\hat{k}\, \hat{k}^2\, \frac{1}{g\rho + K\hat{k}^2} = \frac{1}{2\pi K}\left[1 - \frac{1}{\pi}\sqrt{\frac{\rho g}{K}}\arctan\left(\pi\sqrt{\frac{K}{\rho g}}\right)\right]. \tag{C.13}$$

C.3.1.2 Case $m \neq n$

We define

$$Y(\hat{R}_{mn}) = g^2\, h(\hat{R}_{mn})\,, \tag{C.14}$$

with the dimensionless variable $\hat{R}_{mn} = R_{mn}/a$, a being the lattice spacing, $R_{mn} = ||\vec{R}_{mn}||$. The function to compute, $h(\hat{R}_{mn})$ with $\hat{R}_{mn} \gg 1$, is given by

$$h(\hat{R}_{mn}) = \frac{1}{N}\sum_{\vec{k}} \frac{e^{i\vec{k}\vec{R}_{mn}}}{\widetilde{\lambda}^2_k}\,. \tag{C.15}$$

Changing variable for $\hat{\vec{R}}$, the term to compute becomes

$$h(\hat{R}_{mn}) = \frac{1}{(2\pi)^3}\int_{-\pi}^{\pi} d\hat{\vec{k}}\, \frac{e^{i\hat{\vec{k}}\hat{\vec{R}}_{mn}}}{\widetilde{\lambda}^2_{\hat{\vec{k}}}} = \frac{1}{(2\pi)^3}\int_0^{2\pi} d\phi \int_0^\pi d\hat{k}\, \frac{\hat{k}^2}{\widetilde{\lambda}^2_{\hat{\vec{k}}}} \int_0^\pi d\theta \sin\theta\, e^{i\hat{k}\hat{R}_{mn}\cos\theta} \tag{C.16}$$

$$= \frac{1}{(2\pi)^2}\frac{2}{\hat{R}_{mn}}\int_0^\pi d\hat{k}\, \hat{k}\, \frac{\sin(\hat{k}\hat{R}_{mn})}{K\hat{k}^2 + \rho g}\,, \tag{C.17}$$

which gives

$$h(\hat{R}_{mn}) = \frac{1}{2\pi^2}\frac{1}{\hat{R}_{mn}}\frac{1}{K}\left[\mathrm{SinIntegral}(\pi\hat{R}_{mn}) - \frac{\pi}{2}\sqrt{\frac{\rho g}{K}}\hat{R}_{mn} + O(g\rho)\right]. \tag{C.18}$$

Using that for values of $x \gg 1$, $\mathrm{SinIntegral}(2\pi x) \sim \frac{\pi}{2}\Theta(x)$, where $\Theta(x) = 1$ if $x > 0$ is the Heaviside function, $h(\hat{R}_{mn})$ can be expressed as

$$h(\hat{R}_{mn}) = \frac{1}{4\pi K}\frac{1}{\hat{R}_{mn}}\left(1 - \sqrt{\frac{\rho g}{K}}\hat{R}_{mn} + O(g\rho)\right) \underset{\rho g\hat{R}_{mn}\ll 1}{\simeq} \frac{1}{4\pi K}\frac{1}{\hat{R}_{mn}}\exp\left[-\sqrt{\frac{\rho g}{K}}\hat{R}_{mn}\right], \tag{C.19}$$

with both $\hat{R}_{mn} \gg 1$ and $\rho g\hat{R}_{mn} \ll 1$.

C.3.2 Memory kernel

We have to compute the equation 5.48, that we recall

$$K_{np}(t-t') = \frac{g^2}{m}\frac{1}{N}\sum_{\vec{k}} e^{i\vec{k}\vec{R}_{np}}\frac{\cos[\omega_k(t-t')]}{\omega_k^2}\,, \tag{C.20}$$

where $\vec{R}_{np} = \vec{R}_n - \vec{R}_p$ and $\omega_k^2 = \frac{\widetilde{\lambda}_{\vec{k}}^2}{m}$. We will determine an *estimation* for the above quantity by using continuity of different limits. As is said in the main text, this gives a quite reasonable description of the dissipation kernel for the parameters we are concerned in.

C.3.2.1 Case $n = p$

We have to determine:

$$K_{nn}(t-t') = \frac{g^2}{m}\frac{1}{N}\sum_{\vec{k}}\frac{\cos[\omega_k(t-t')]}{\omega_k^2}\,. \tag{C.21}$$

In the following limits the kernel is given the following expressions.
• $t = t'$, (C.20) evaluates to $g^2 \times$ (C.13), or

$$K_{nn}(0) = \frac{g^2}{2\pi K}\left[1 - \frac{1}{\pi}\sqrt{\frac{\rho g}{K}}\arctan\left(\pi\sqrt{\frac{K}{\rho g}}\right)\right]\,, \tag{C.22}$$

• $t \neq t'$ and $\rho g = 0$

$$K_{nn;0}(t-t') = g^2\frac{1}{2\pi^2}\int_0^\pi d\hat{k}\hat{k}^2\,\frac{\cos\left[\sqrt{\frac{K}{m}}(t-t')\hat{k}\right]}{K\hat{k}^2} = \frac{g^2}{2\pi^2}\frac{m}{K^{3/2}}\frac{\sin\left[\sqrt{\frac{K}{m}}\pi(t-t')\right]}{(t-t')}\,. \tag{C.23}$$

We find that the limits coincide, $\lim_{t\to t'} K_{nn;0}(t-t') = \lim_{\rho g\to 0} K_{nn}(0)$. Then we estimate the kernel of dissipation when $t \neq t'$ and $\rho g \neq 0$ by

$$K_{nn}(t-t') \simeq \frac{g^2}{2\pi^2}\frac{\sqrt{m}}{K^{3/2}}\left[1 - \frac{1}{\pi}\sqrt{\frac{\rho g}{K}}\arctan\left(\pi\sqrt{\frac{K}{\rho g}}\right)\right]\frac{\sin\left[\sqrt{\frac{K}{m}}\pi(t-t')\right]}{(t-t')}\,. \tag{C.24}$$

C.3.2.2 Case $n \neq p$

We have to determine, with $n \neq p$:

$$K_{np}(t-t') = \frac{g^2}{m}\frac{1}{N}\sum_{\vec{k}} e^{i\vec{k}\vec{R}_{np}}\frac{\cos[\omega_k(t-t')]}{\omega_k^2}\,. \tag{C.25}$$

The dimensionless variables are $\hat{\vec{k}} = a\vec{k}$ and $\hat{\vec{R}} = \vec{R}/a$, with $\hat{R}_{np} = ||\hat{\vec{R}}_{np}||$. The sum can be transformed as

$$\begin{aligned}\frac{1}{N}\sum_{\vec{k}} e^{i\vec{k}\vec{R}_{np}}\frac{\cos[\omega_k(t-t')]}{\omega_k^2} &= \frac{1}{(2\pi)^3}\int_0^{2\pi} d\phi\int_0^\pi d\hat{k}\,\hat{k}^2\,\frac{\cos[\omega_{\hat{k}}(t-t')]}{\omega_{\hat{k}}^2}\int_0^\pi d\theta\sin\theta\, e^{i\hat{k}\hat{R}_{np}\cos\theta}\\ &= \frac{1}{(2\pi)^2}\frac{2m}{\hat{R}_{np}}\int_0^\pi d\hat{k}\,\hat{k}^2\,\frac{\cos[\omega_{\hat{k}}(t-t')]}{\widetilde{\lambda}_{\hat{k}}^2}\frac{\sin\left(\hat{k}\hat{R}_{np}\right)}{\hat{k}}\end{aligned} \tag{C.26}$$

$$= \frac{1}{(2\pi)^2}\frac{2m}{\hat{R}_{np}}\int_0^\pi d\hat{k}\,\hat{k}\,\frac{\cos\left[(t-t')\sqrt{(K\hat{k}^2+\rho g)/m}\right]}{K\hat{k}^2+\rho g}\sin\left(\hat{k}\hat{R}_{np}\right). \quad \text{(C.27)}$$

Then in the following limits the kernel takes the expressions below.
• When $t = t'$, we recover the integral (C.17) which values is (C.19), hence the kernel at time $t = t'$ writes, for $\hat{R}_{np} \gg 1$ and $g\rho\hat{R}_{np} \ll 1$,

$$K_{np}(0) \simeq_{\rho g\ll 1} g^2\frac{1}{4\pi K}\frac{1}{\hat{R}_{np}}\exp\left[-\sqrt{\frac{\rho g}{K}}\hat{R}_{np}\right]. \quad \text{(C.28)}$$

• When $t \neq t'$ and $\rho g = 0$

$$\begin{aligned}K_{np;0}(t-t') &= g^2\frac{1}{2\pi^2}\frac{1}{\hat{R}_{np}}\int_0^\pi d\hat{k}\hat{k}^2\,\frac{\cos\left[\sqrt{\frac{K}{m}}(t-t')\hat{k}\right]}{K\hat{k}^2}\frac{\sin\left(\hat{k}\hat{R}_{np}\right)}{\hat{k}}\\ &= g^2\frac{1}{4\pi^2 K}\frac{1}{\hat{R}_{np}}\left(\text{SinIntegral}\left[\pi\left(\hat{R}_{np}-\sqrt{\frac{K}{m}}(t-t')\right)\right]+\text{SinIntegral}\left[\pi\left(\hat{R}_{np}+\sqrt{\frac{K}{m}}(t-t')\right)\right]\right).\end{aligned} \quad \text{(C.29)}$$

The limits coincide $\lim_{t\to t'} K_{np;0}(t-t') = \lim_{\rho g\to 0} K_{np}(0)$. Then we estimate the kernel of dissipation when $t \neq t'$ and $\rho g \neq 0$ by

$$\begin{aligned}K_{np}(t-t') &\simeq g^2\frac{1}{4\pi^2 K}\frac{1}{\hat{R}_{np}}\exp\left[-\sqrt{\frac{\rho g}{K}}\hat{R}_{np}\right]\\ &\left(\text{SinIntegral}\left[\pi\left(\hat{R}_{np}-\sqrt{\frac{K}{m}}(t-t')\right)\right]+\text{SinIntegral}\left[\pi\left(\hat{R}_{np}+\sqrt{\frac{K}{m}}(t-t')\right)\right]\right),\end{aligned} \quad \text{(C.30)}$$

with both $\hat{R}_{mn} \gg 1$ and $\rho g\hat{R}_{mn} \ll 1$.

C.4 Simplification for the action of the climb

The finite action of the climb, equation (5.75) of the main text, is computed using the following simplification:

$$\begin{aligned}&\sum_{n,j=1}^{N_{dw}}\int_0^t dt_1\,\dot{X}_j(t_1)\left[\int_0^{t_1} dt_2\,\dot{X}_n(t_2)K_{jn}(t_1-t_2)-\frac{1}{2}\int_0^t dt_2\,\dot{X}_n(t_2)K_{jn}(t_1-t_2)\right] =\\ &\frac{1}{2}\sum_{n,j=1}^{N_{dw}}\left[\int_0^t dt_1\,\dot{X}_j(t_1)\int_0^{t_1} dt_2\,\dot{X}_n(t_2)K_{jn}(t_1-t_2)-\int_0^t dt_1\,\dot{X}_j(t_1)\int_{t_1}^t dt_2\,\dot{X}_n(t_2)K_{jn}(t_1-t_2)\right] =\\ &\frac{1}{2}\sum_{n,j=1}^{N_{dw}}\left[\int_0^t dt_1\,\dot{X}_n(t_1)\int_{t_1}^t dt_2\,\dot{X}_j(t_2)K_{jn}(t_1-t_2)-\int_0^t dt_1\,\dot{X}_j(t_1)\int_{t_1}^t dt_2\,\dot{X}_n(t_2)K_{jn}(t_1-t_2)\right] =\\ &\frac{1}{2}\sum_{n,j=1}^{N_{dw}}\left[\int_0^t dt_1\,\dot{X}_j(t_1)\int_{t_1}^t dt_2\,\dot{X}_n(t_2)K_{jn}(t_1-t_2)-\int_0^t dt_1\,\dot{X}_j(t_1)\int_{t_1}^t dt_2\,\dot{X}_n(t_2)K_{jn}(t_1-t_2)\right] = 0\,.\end{aligned} \quad \text{(C.31)}$$

C.5 Scaling function appearing in the three-point susceptibility

We have introduced the function $f_j\,(t_1)$, with $K_{11}(t_1;\vec{k})$ from equation (5.48) and $\sigma = g^2\,\alpha$,

$$f_j\,(t_1) = \sum_{\vec{k}} e^{i\vec{k}(\vec{l}_j - \vec{R}_1)}\,\widetilde{\lambda}_k\,\frac{1}{g^2} K_{11}(t_1;\vec{k}) = \frac{1}{N}\sum_{\vec{k}} e^{i\vec{k}(\vec{l}_j - \vec{R}_1)}\,\frac{\cos(\omega_k\,t_1)}{\widetilde{\lambda}_k}\,. \tag{C.32}$$

We recall that $\omega_k = \widetilde{\lambda}_k/\sqrt{m} = \sqrt{K/m}\,ak + O(g\,\rho)$. Then the above can be rewritten, with $\vec{y} = a\vec{k}$ dimensionless,

$$\begin{aligned} f_j\,(t_1) &= (2\pi)^{-3}\int_{-\pi}^{\pi} d^3y\, e^{i\vec{y}(\vec{l}_j - \vec{R}_1)}\,\frac{\cos\left(\sqrt{\frac{K}{m}}y\,t_1\right)}{\sqrt{K}y} + O(\rho) \\ &= (2\pi)^{-2}K^{-1/2}\int_0^{\pi} dy y\,\cos\left(\sqrt{\frac{K}{m}}y\,t_1\right)\int_0^{\pi} d\theta\,\sin\theta\, e^{iy\,a^{-1}\,||\vec{l}_j - \vec{R}_1||\cos\theta} + O(\rho) \\ &= 2\,(2\pi)^{-2}K^{-1/2}\frac{a}{||\vec{l}_j - \vec{R}_1||}\int_0^{\pi} dy\,\cos\left(\sqrt{\frac{K}{m}}y\,t_1\right)\,\sin\left(ya^{-1}\,||\vec{l}_j - \vec{R}_1||\right) + O(\rho)\,. \end{aligned} \tag{C.33}$$

We change variable for $z = y\,a^{-1}\,||\vec{l}_j - \vec{R}_1||$, always dimensionless, and $||\vec{l}_j - \vec{R}_1|| = d_j$. Since $\sin Ay\,\cos By = 1/2\,\{\sin[y(A+B)] + \sin[y(A-B)]\}$, we obtain

$$f_j\,(t_1) = (2\pi)^{-2}K^{-1/2}\frac{a^2}{d_j^2}\int_0^{\pi\,d_j/a} dz\,\left\{\sin\left[z\left(1+\sqrt{\frac{K}{m}}\frac{a}{d_j}\,t_1\right)\right] + \sin\left[z\left(1-\sqrt{\frac{K}{m}}\frac{a}{d_j}\,t_1\right)\right]\right\} + O(\rho)\,. \tag{C.34}$$

The initial function can therefore be written

$$f_j(t) = (2\pi)^{-2}K^{-1/2}\frac{a^2}{d_j^2}\,\phi_j\left(\frac{t}{t_j}\right)\,, \tag{C.35}$$

with, $t_j = d_j/a\,\sqrt{\frac{m}{K}}$,

$$\begin{aligned} \phi_j\left(\frac{t_1}{t_j}\right) &= \int_0^{\pi\,d_j/a} dz\,\left\{\sin\left[z\left(1+\frac{t}{t_j}\right)\right] + \sin\left[z\left(1-\frac{t}{t_j}\right)\right]\right\} + O(\rho) \\ &= \frac{1}{1+t/t_j} + \frac{1}{1-t/t_j} - \frac{\cos\left[\pi K\,t_j\,(1+t/t_j)\right]}{1+t/t_j} - \frac{\cos\left[\pi K\,t_j\,(1-t/t_j)\right]}{1-t/t_j} + O(\rho)\,. \end{aligned} \tag{C.36}$$

The function ϕ, defined for $0 < t_1, t_j < t$, is such that $\phi_j(t_1/t_j) \to \pm t_j$ when $t_j \to t_1^{-/+}$.

Appendix D

Critical behavior of the Ising spin glass below six dimensions

D.1 Simple invariants of the Ising spin-glass theory built from the overlaps

The invariants of the Ising spin-glass theory are polynomials of the overlap field such that replica indices must appear an even number of times. They are listed in the two following tables up to order $O(Q^6)$.

Table D.1: Invariants of the Ising spin glass field theory up to $O(Q^5)$.

$O(Q^2)$	$O(Q^3)$	$O(Q^4)$	$O(Q^5)$
Q_{ab}^2	$Q_{ab}Q_{bc}Q_{ca}$	$Q_{ab}Q_{bc}Q_{cd}Q_{da}$	$Q_{ab}Q_{bc}Q_{cd}Q_{de}Q_{ea}$
		Q_{ab}^4	$Q_{ab}^2Q_{ab}Q_{bc}Q_{ca}$
		$Q_{ab}^2Q_{bc}^2$	$Q_{ab}^2Q_{bc}Q_{cd}Q_{db}$
		$Q_{ab}^2Q_{cd}^2$	$Q_{ab}^2Q_{cd}Q_{de}Q_{ec}$

Table D.2: Invariants of the Ising spin glass field theory at $O(Q^6)$.

$O(Q^6)$		
$Q_{ab}Q_{bc}Q_{cd}Q_{de}Q_{ef}Q_{fa}$	$Q_{ab}^2Q_{ac}^2Q_{ad}^2$	$Q_{ab}^2Q_{bc}Q_{ca}Q_{bd}Q_{da}$
Q_{ab}^6	$Q_{ab}^2Q_{bc}^2Q_{cd}^2$	$Q_{ab}^2Q_{bc}Q_{cd}Q_{de}Q_{eb}$
$Q_{ab}^4Q_{bc}^2$	$Q_{ab}^2Q_{ac}^2Q_{de}^2$	$Q_{ab}^2Q_{cd}Q_{de}Q_{ef}Q_{fc}$
$Q_{ab}^4Q_{cd}^2$	$Q_{ab}^2Q_{cd}^2Q_{ef}^2$	$Q_{ab}Q_{bc}Q_{ca}Q_{ad}Q_{de}Q_{ea}$
$Q_{ab}^2Q_{bc}^2Q_{ca}^2$	$Q_{ab}^3Q_{bc}Q_{cd}Q_{da}$	$Q_{ab}Q_{bc}Q_{ca}Q_{de}Q_{ef}Q_{fd}$

D.2 Expansion around the minimum in terms of invariants up to $O(Q^6)$

Each term of the expansion is chosen to be a function of the invariants of the same or lower order, having its first field derivative equal to zero in Q_k, and being itself zero in Q_k. The terms are listed below in increasing order of $O(Q^p)$. For orders up to $O(Q^5)$, they are given in the main text in equation (6.14). For order $O(Q^6)$, they are (with distinct replica indices $a, b, c, d, e, f \neq$),

$$\mu^{(6)}_{abcdef} = Q_{ab}Q_{bc}Q_{cd}Q_{de}Q_{ef}Q_{fa} - Q_k^6 - Q_k^4\left(\rho^{(2)}_{ab} + \rho^{(2)}_{bc} + \rho^{(2)}_{cd} + \rho^{(2)}_{de} + \rho^{(2)}_{ef} + \rho^{(2)}_{fa}\right), \tag{D.1}$$

$$
\begin{aligned}
\eta^{(6)}_{ab} &= \rho^{(2)}_{ab}\,\rho^{(2)}_{ab}\,\rho^{(2)}_{ab} & \eta^{(6)}_{abcd,2} &= \rho^{(2)}_{ab}\,\rho^{(2)}_{ac}\,\rho^{(2)}_{ad}\\
\eta^{(6)}_{abc,1} &= \frac{1}{2}\rho^{(2)}_{ab}\,\rho^{(2)}_{ab}\left(\rho^{(2)}_{ac}+\rho^{(2)}_{bc}\right) & \eta^{(6)}_{abcd,3} &= \rho^{(2)}_{ab}\,\rho^{(2)}_{bc}\,\rho^{(2)}_{cd}\\
\eta^{(6)}_{abc,2} &= \rho^{(2)}_{ab}\,\rho^{(2)}_{bc}\,\rho^{(2)}_{ca} & \eta^{(6)}_{abcde} &= \rho^{(2)}_{ab}\,\rho^{(2)}_{ac}\,\rho^{(2)}_{de}\\
\eta^{(6)}_{abcd,1} &= \rho^{(2)}_{ab}\,\rho^{(2)}_{ab}\,\rho^{(2)}_{cd} & \eta^{(6)}_{abcdef} &= \rho^{(2)}_{ab}\,\rho^{(2)}_{cd}\,\rho^{(2)}_{ef}\\
\sigma^{(6)}_{abcd} &= \rho^{(2)}_{ab}\,\mu^{(4)}_{abcd} & \tau^{(6)}_{abcd} &= \mu^{(3)}_{abc}\mu^{(3)}_{abd}\\
\sigma^{(6)}_{abcde} &= \frac{1}{2}\rho^{(2)}_{ab}\left(\mu^{(4)}_{acde}+\mu^{(4)}_{bcde}\right) & \tau^{(6)}_{abcde} &= \mu^{(3)}_{abc}\mu^{(3)}_{ade}\\
\sigma^{(6)}_{abcdef} &= \rho^{(2)}_{ab}\,\mu^{(4)}_{cdef} & \tau^{(6)}_{abcdef} &= \mu^{(3)}_{abc}\mu^{(3)}_{def}\,.
\end{aligned}
\tag{D.2}
$$

The sums are over distinct ordered replica indices $\sum_{(abc)} = \sum_{a<b<c}$, *etc.* The potential can thus be rewritten as (the dependence on Q_k of the coupling constants is not shown)

$$
\begin{aligned}
U_k(\{Q_{ab}\}) = {} & W_{k,1}\sum_{(abc)}\mu^{(3)}_{abc}\\
& + U_{k,1}\sum_{(abcd)}\mu^{(4)}_{abcd} + U_{k,2}\sum_{(ab)}\lambda^{(4)}_{ab} + U_{k,3}\sum_{(abc)}\lambda^{(4)}_{abc} + U_{k,4}\sum_{(abcd)}\lambda^{(4)}_{abcd}\\
& + V_{k,1}\sum_{(abcde)}\mu^{(5)}_{abcde} + V_{k,2}\sum_{(abc)}\nu^{(5)}_{abc} + V_{k,3}\sum_{(abcd)}\nu^{(5)}_{abcd} + V_{k,4}\sum_{(abcde)}\nu^{(5)}_{abcde}\\
& + T_{k,1}\sum_{(abcdef)}\mu^{(6)}_{abcdef} + T_{k,2}\sum_{(ab)}\eta^{(6)}_{ab} + T_{k,3}\sum_{(abc)}\eta^{(6)}_{abc,1} + T_{k,4}\sum_{(abc)}\eta^{(6)}_{abc,2}\\
& + T_{k,5}\sum_{(abcd)}\eta^{(6)}_{abcd,1} + T_{k,6}\sum_{(abcd)}\eta^{(6)}_{abcd,2} + T_{k,7}\sum_{(abcd)}\eta^{(6)}_{abcd,3} + T_{k,8}\sum_{(abcde)}\eta^{(6)}_{abcde}\\
& + T_{k,9}\sum_{(abcdef)}\eta^{(6)}_{abcdef} + T_{k,10}\sum_{(abcd)}\sigma^{(6)}_{abcd} + T_{k,11}\sum_{(abcde)}\sigma^{(6)}_{abcde} + T_{k,12}\sum_{(abcdef)}\sigma^{(6)}_{abcdef}\\
& + T_{k,13}\sum_{(abcd)}\tau^{(6)}_{abcd} + T_{k,14}\sum_{(abcde)}\tau^{(6)}_{abcde} + T_{k,15}\sum_{(abcdef)}\tau^{(6)}_{abcdef} + O(Q^7)\,.
\end{aligned}
\tag{D.3}
$$

As explained in the main text, this form is not yet satisfying, and some work remains to be done. It is explained below.

A a starting point, we rewrite equation (D.3) in a more compact form:

$$
U_k[\{Q_{ab}\}] = W_{k,1}\,X^{(3)}_1 + \sum_{i=1}^{4} U_{k,i}\,X^{(4)}_i + \sum_{i=1}^{4} V_{k,i}\,X^{(5)}_i + \sum_{i=1}^{15} T_{k,i}\,X^{(6)}_i + O(Q^7)\,. \tag{D.4}
$$

The $X^{(j)}_i$'s are expressed as sums of order $O(Q^j)$ of the terms of the invariant expansion listed in (6.14), (D.1), and (D.2). For example, $X^{(3)}_1 = \sum_{(abc)}\mu^{(3)}_{abc}$, $X^{(4)}_1 = \sum_{(abcd)}\mu^{(4)}_{abcd}$, *etc.*

As explained in the main text, our goal is to reorganize the above expression of the potential in such a way that one can define the (new) coupling constants *via* derivatives of the potential evaluated at the minimum Q_k whose expression does not depend on terms above a certain order of the expansion. We therefore rewrite U_k as

$$
U_k(\{Q_{ab}\}) = \widetilde{W}_{k,1}\,\widetilde{X}^{(3)}_1 + \sum_{i=1}^{4}\widetilde{U}_{k,i}\,\widetilde{X}^{(4)}_i + \sum_{i=1}^{4}\widetilde{V}_{k,i}\,\widetilde{X}^{(5)}_i + \sum_{i=1}^{15}\widetilde{T}_{k,i}\,\widetilde{X}^{(6)}_i + O(Q^7)\,, \tag{D.5}
$$

where the new invariants are expressed as linear combinations of the old ones:

$$\begin{aligned}
\widetilde{X}_1^{(3)} &= X_1^{(3)} \\
\widetilde{X}_i^{(4)} &= X_i^{(4)} - a_i\, Q_k\, X_1^{(3)} \\
\widetilde{X}_i^{(5)} &= X_i^{(5)} - \sum_{j=1}^{4} b_{ij}\, Q_k\, X_j^{(4)} - c_i\, Q_k^2\, X_1^{(3)} \\
\widetilde{X}_i^{(6)} &= X_i^{(6)} - \sum_{j=1}^{4} d_{ij}\, Q_k\, X_j^{(5)} - \sum_{j=1}^{4} e_{ij}\, Q_k^2\, X_j^{(4)} - f_i\, Q_k^3\, X_1^{(3)}
\end{aligned} \tag{D.6}$$

etc. We want $\widetilde{W}_{k,1}$ to be defined irrespective of $\widetilde{X}_i^{(4)}$, $\widetilde{X}_i^{(5)}$, ..., the $\widetilde{U}_{k,i}$'s to be defined irrespective of $\widetilde{X}_i^{(5)}$, $\widetilde{X}_i^{(6)}$, *etc.* We also require that any subtracted term of the right hand side of expressions (D.6) should not involve more distinct replica indices than the number of replicas involved in the definition of the left hand side. (If this was left to happen, factors $(n-p)^{-1}$ would be present in the right hand side and would cause divergences for a fixed number $n = p$ of replicas, whereas this should be valid whatever the number n of replicas is.)

To implement the procedure, we make use of the tables D.3 to D.5 given below.

For the lowest order $O(Q^3)$ truncation, we choose to use the third order derivative to define $\widetilde{W}_1$. In this case one has

$$\widetilde{W}_{k,1} = \frac{\delta^3 U_k}{\delta Q_{ab}\delta Q_{bc}\delta Q_{ca}}\Big|_{Q_k} . \tag{D.7}$$

The $X_i^{(4)}$'s all have their derivative with respect to $\delta Q_{ab}\delta Q_{bc}\delta Q_{ca}$ in Q_k equal to zero so that one has to consider the $X_i^{(5)}$'s to guarantee the exactness of equation (D.7), which leads to one constraint for each $X_i^{(5)}$. At the next order, we want to define the $\widetilde{U}_{k,i}$'s using the three second order derivatives and one third order derivative. The $X_i^{(5)}$'s have to be modified according to

$$\widetilde{X}_i^{(5)} = X_i^{(5)} - \sum_{j=1}^{4} b_{ij}\, Q_k\, X_j^{(4)} - c_i\, Q_k^2\, X_1^{(3)} . \tag{D.8}$$

The c_i's and b_{ij}'s are obtained by solving the following system of five equations (with $a, b, c, d \neq$), with the three conditions on the second-order derivatives evaluated in Q_k

$$\frac{\delta^2 \widetilde{X}_i^{(5)}}{\delta Q_{ab}\delta Q_{ab}}\Big|_{Q_k} = 0\,, \quad \frac{\delta^2 \widetilde{X}_i^{(5)}}{\delta Q_{ab}\delta Q_{bc}}\Big|_{Q_k} = 0\,, \quad \frac{\delta^2 \widetilde{X}_i^{(5)}}{\delta Q_{ab}\delta Q_{cd}}\Big|_{Q_k} = 0\,, \tag{D.9}$$

and two conditions on third-order derivatives evaluated in $Q_k$which must include the derivative used for the definition of $\widetilde{W}_{k,1}$,

$$(1) \quad \frac{\delta^2 \widetilde{X}_i^{(5)}}{\delta Q_{ab}\delta Q_{bc}\delta Q_{ca}}\Big|_{Q_k} = 0, \tag{D.10}$$

and a second one, which *a priori* can be one of the following four (the numbers (p) refers to the derivative number as in table D.3):

$$\begin{aligned}
&(2) \quad \frac{\delta^3 \widetilde{X}_i^{(5)}}{\delta Q_{ab}^3} = 0\Big|_{Q_k} \qquad &&(4) \quad \frac{\delta^3 \widetilde{X}_i^{(5)}}{\delta Q_{ab}^2\delta Q_{cd}} = 0\Big|_{Q_k} \\
&(3) \quad \frac{\delta^3 \widetilde{X}_i^{(5)}}{\delta Q_{ab}^2\delta Q_{bc}} = 0\Big|_{Q_k} \qquad &&(5) \quad \frac{\delta^3 \widetilde{X}_i^{(5)}}{\delta Q_{ab}\delta Q_{bc}\delta Q_{cd}} = 0\Big|_{Q_k} .
\end{aligned} \tag{D.11}$$

There are four $\widetilde{X}_i^{(5)}$'s and five equations for each $\widetilde{X}_i^{(5)}$: therefore we have a system of 20 equations and 20 unknowns to solve. The choices (2) and (3) of the equation (D.11) are not acceptable, because they force one to subtract terms with more replicas than $X_i^{(5)}$ itself. The other choices (4) and (5) have solutions which are given below: for (4) (called (A) in the main text)

$$\begin{aligned}\{&c_1 \to 0, c_2 \to 1, c_3 \to 0, c_4 \to 0, b_{1,1} \to 2(n-4), b_{1,2} \to 3(n-4)(n-3)(n-2), b_{1,3} \to -(n-4)(n-3),\\ &b_{1,4} \to 0, b_{2,1} \to 0, b_{2,2} \to 3(n-2), b_{2,3} \to -1, b_{2,4} \to 0, b_{3,1} \to 1, b_{3,2} \to 3(n-3)(n-2), b_{3,3} \to 3-n,\\ &b_{3,4} \to -2, b_{4,1} \to \frac{n-4}{2}, b_{4,2} \to \frac{3}{2}(n-4)(n-3)(n-2), b_{4,3} \to -\frac{1}{2}(n-4)(n-3), b_{4,4} \to 4-n\}\,,\end{aligned} \tag{D.12}$$

and for (5) (called (B) in the main text)

$$\begin{aligned}\{&c_1 \to 0, c_2 \to 1, c_3 \to 0, c_4 \to 0, b_{1,1} \to n-4, b_{1,2} \to 0, b_{1,3} \to 0, b_{1,4} \to 2(n-4), b_{2,1} \to 0,\\ &b_{2,2} \to 3(n-2), b_{2,3} \to -1, b_{2,4} \to 0, b_{3,1} \to 2, b_{3,2} \to 6(n-3)(n-2), b_{3,3} \to 6-2n, b_{3,4} \to -4,\\ &b_{4,1} \to 0, b_{4,2} \to 0, b_{4,3} \to 0, b_{4,4} \to 0\}\,.\end{aligned} \tag{D.13}$$

The potential is then given by

$$U[\{Q_{ab}\}] = \widetilde{W}_{k,1}\, X_1^{(3)} + \sum_{i=1}^{4} \widetilde{U}_{k,i}\, X_i^{(4)} + \sum_{i=1}^{4} \widetilde{V}_{k,i}\, \widetilde{X}_i^{(5)} + O(Q^6) \tag{D.14}$$

where the $\widetilde{X}_i^{(5)}$'s are given by one of the two solutions in (D.12) and (D.13).

The constants $\widetilde{W}_{k,1}$ and $\widetilde{U}_{k,i}$ are thus exactly defined through the following expressions, which do not involve higher order coupling constants:

$$\begin{aligned}\frac{\delta^2 U_k}{\delta Q_{ab}^2}\Big|_{Q_k} &= -(n-2)Q_k\,\widetilde{W}_{k,1} - (n-2)(n-4)Q_k^2\,\widetilde{U}_{k,1} + \frac{1}{3}Q_k^2\widetilde{U}_{k,2}\,,\\ \frac{\delta^2 U_k}{\delta Q_{ab}\delta Q_{bc}}\Big|_{Q_k} &= Q_k\,\widetilde{W}_{k,1} + (n-3)Q_k^2\,\widetilde{U}_{k,1} + Q_k^2\widetilde{U}_{k,3}\,,\\ \frac{\delta^2 U_k}{\delta Q_{ab}\delta Q_{cd}}\Big|_{Q_k} &= 2Q_k^2\,\widetilde{U}_{k,1} + Q_k^2\widetilde{U}_{k,4}\,,\\ \frac{\delta^3 U_k}{\delta Q_{ab}\delta Q_{bc}\delta Q_{ca}}\Big|_{Q_k} &= \widetilde{W}_{k,1}\,,\end{aligned} \tag{D.15}$$

and either (choice (A) in the main text)

$$(4) \quad \frac{\delta^3 U_k}{\delta Q_{ab}^2 \delta Q_{cd}}\Big|_{Q_k} = Q_k\,\widetilde{U}_{k,4}\,, \tag{D.16}$$

or (choice (B) in the main text)

$$(5) \quad \frac{\delta^3 U_k}{\delta Q_{ab}\delta Q_{bc}\delta Q_{cd}}\Big|_{Q_k} = Q_k\,\widetilde{U}_{k,1}\,. \tag{D.17}$$

The implicit assumption here is that one can generalize the construction given above for the $\widetilde{X}_i^{(5)}$ to the higher-order terms. As mentioned in the main text, this is supported by the fact that the system of linear equations to be solved is underconstrained, the number of possibilities for defining an acceptable set of new invariants increasing with the order. (This is easily verified at the order $O(Q^6)$ for the $\widetilde{X}_i^{(6)}$.)

D.3 Table of field derivatives of various invariants in U_k evaluated at the minimum

The definitions of the variables $X_i^{(p)}$ expressed in terms of the invariants are:

$$X_1^{(3)} = \sum_{(abc)} \mu_{abc}^{(3)}\,, \quad X_1^{(4)} = \sum_{(abcd)} \mu_{abcd}^{(4)}\,, \quad X_2^{(4)} = \sum_{(ab)} \lambda_{ab}^{(4)}, \quad X_3^{(4)} = \sum_{(abc)} \lambda_{abc}^{(4)}\,, \quad X_4^{(4)} = \sum_{(abcd)} \lambda_{abcd}^{(4)}\,,$$
$$X_1^{(5)} = \sum_{(abcde)} \mu_{abcde}^{(5)}\,, \quad X_2^{(5)} = \sum_{(abc)} \nu_{abc}^{(5)}\,, \quad X_3^{(5)} = \sum_{(abcd)} \nu_{abcd}^{(5)}\,, \quad X_4^{(5)} = \sum_{(abcde)} \nu_{abcde}^{(5)}\,, \; etc.\,, \tag{D.18}$$

and give, in the tables below, the derivatives of the variables $X_i^{(p)}$ (up to $O(Q^5)$) with respect to the overlap fields and evaluated in the minimum, $\{Q_{ab}\} = \{Q_k\}$.

Table D.3: Derivatives of $X_1^{(3)}$ and $X_i^{(4)}$ $(i = 1, 2, 3, 4)$ in $\{Q_{ab}\} = \{Q_k\}$

		$X_1^{(3)}$	$X_1^{(4)}$	$X_2^{(4)}$	$X_3^{(4)}$	$X_4^{(4)}$
1	δQ_{ab}^2	$-(n-2)\,Q_k$	$-(n-2)(n-3)Q_k^2$	$\frac{1}{3}Q_k^2$	0	0
2	$\delta Q_{ab}\delta Q_{bc}$	Q_k	$(n-3)Q_k^2$	0	Q_k^2	0
3	$\delta Q_{ab}\delta Q_{cd}$	0	$2\,Q_k^2$	0	0	Q_k^2
1	$\delta Q_{ab}\delta Q_{bc}\delta Q_{ca}$	1	0	0	0	0
2	δQ_{ab}^3	0	0	Q_k	0	0
3	$\delta Q_{ab}^2\delta Q_{bc}$	0	0	0	Q_k	0
4	$\delta Q_{ab}^2\delta Q_{cd}$	0	0	0	0	Q_k
5	$\delta Q_{ab}\delta Q_{bc}\delta Q_{cd}$	0	Q_k	0	0	0
6	$\delta Q_{ab}\delta Q_{ac}\delta Q_{ad}$	0	0	0	0	0
7	$\delta Q_{ab}\delta Q_{ac}\delta Q_{de}$	0	0	0	0	0
8	$\delta Q_{ab}\delta Q_{cd}\delta Q_{ef}$	0	0	0	0	0
1	$\delta Q_{ab}\delta Q_{bc}\delta Q_{cd}\delta Q_{da}$	0	1	0	0	0
2	δQ_{ab}^4	0	0	1	0	0
3	$\delta Q_{ab}^2\delta Q_{bc}^2$	0	0	0	1	0
4	$\delta Q_{ab}^2\delta Q_{cd}^2$	0	0	0	0	1

Table D.4: Derivatives of $X_i^{(5)}$ $(i = 1, 2, 3, 4)$ in $\{Q_{ab}\} = \{Q_k\}$

		$X_1^{(5)}$	$X_2^{(5)}$	$X_3^{(5)}$	$X_4^{(5)}$
1	δQ_{ab}^2	$-(n-2)(n-3)(n-4)Q_k^3$	0	0	0
2	$\delta Q_{ab}\delta Q_{bc}$	$(n-3)(n-4)Q_k^3$	0	0	0
3	$\delta Q_{ab}\delta Q_{cd}$	$4(n-4)Q_k^3$	0	0	0
1	$\delta Q_{ab}\delta Q_{bc}\delta Q_{ca}$	0	Q_k^2	0	0
2	δQ_{ab}^3	0	$-(n-2)Q_k^2$	0	0
3	$\delta Q_{ab}^2\delta Q_{bc}$	0	$\frac{1}{3}Q_k^2$	$-(n-3)Q_k^2$	0
4	$\delta Q_{ab}^2\delta Q_{cd}$	0	0	$-2Q_k^2$	$-(n-4)Q_k^2$
5	$\delta Q_{ab}\delta Q_{bc}\delta Q_{cd}$	$(n-4)Q_k^2$	0	$2Q_k^2$	0
6	$\delta Q_{ab}\delta Q_{ac}\delta Q_{ad}$	0	0	$3Q_k^2$	0
7	$\delta Q_{ab}\delta Q_{ac}\delta Q_{de}$	$2Q_k^2$	0	0	Q_k^2
8	$\delta Q_{ab}\delta Q_{cd}\delta Q_{ef}$	0	0	0	0

Table D.5: Derivatives of $X_i^{(5)}$ $(i = 1, 2, 3, 4)$ in $\{Q_{ab}\} = \{Q_k\}$

		$X_1^{(5)}$	$X_2^{(5)}$	$X_3^{(5)}$	$X_4^{(5)}$
1	$\delta Q_{ab}\delta Q_{bc}\delta Q_{cd}\delta Q_{da}$	0	0	0	0
2	δQ_{ab}^4	0	$-2(n-2)Q_k$	0	0
3	$\delta Q_{ab}^2\delta Q_{bc}^2$	0	$-\frac{2}{3}Q_k$	$-2(n-3)Q_k$	0
4	$\delta Q_{ab}^2\delta Q_{cd}^2$	0	0	$-4Q_k$	$-2(n-4)Q_k$
5	$\delta Q_{ab}^2\delta Q_{ac}\delta Q_{bc}$	0	Q_k	0	0
6	$\delta Q_{ab}\delta Q_{ac}\delta Q_{bc}\delta Q_{cd}$	0	0	Q_k	0
7	$\delta Q_{ab}\delta Q_{ac}\delta Q_{bc}\delta Q_{de}$	0	0	0	Q_k
8	$\delta Q_{ab}^3\delta Q_{bc}$	0	Q_k	0	0
9	$\delta Q_{ab}^3\delta Q_{cd}$	0	0	0	0
10	$\delta Q_{ab}^2\delta Q_{bc}\delta Q_{bd}$	0	0	Q_k	0
11	$\delta Q_{ab}^2\delta Q_{bc}\delta Q_{cd}$	0	0	Q_k	0
12	$\delta Q_{ab}^2\delta Q_{bc}\delta Q_{de}$	0	0	0	0
13	$\delta Q_{ab}^2\delta Q_{ac}\delta Q_{bd}$	0	0	0	0
14	$\delta Q_{ab}^2\delta Q_{cd}\delta Q_{ce}$	0	0	0	Q_k
15	$\delta Q_{ab}^2\delta Q_{cd}\delta Q_{ef}$	0	0	0	0
16	$\delta Q_{ab}\delta Q_{bc}\delta Q_{cd}\delta Q_{de}$	Q_k	0	0	0
17	$\delta Q_{ab}\delta Q_{bc}\delta Q_{cd}\delta Q_{ef}$	0	0	0	0
18	$\delta Q_{ab}\delta Q_{bc}\delta Q_{cd}\delta Q_{ce}$	0	0	0	0
19	$\delta Q_{ab}\delta Q_{ac}\delta Q_{ad}\delta Q_{ae}$	0	0	0	0
20	$\delta Q_{ab}\delta Q_{cd}\delta Q_{ce}\delta Q_{cf}$	0	0	0	0
21	$\delta Q_{ac}\delta Q_{ad}\delta Q_{be}\delta Q_{bf}$	0	0	0	0
22	$\delta Q_{ac}\delta Q_{bc}\delta Q_{de}\delta Q_{fg}$	0	0	0	0
23	$\delta Q_{ab}\delta Q_{cd}\delta Q_{ef}\delta Q_{gh}$	0	0	0	0

D.4 Terms appearing in the RG flow equations of the derivatives of the effective average action

The terms appear in the flow equations obtained by functional differentiation of the exact RG equation for Γ_k and are evaluated for a spatially uniform field configuration. A graphical representation (without replica indices) has been given in chapter 2. We obtain the following expressions:

$$D_{ab}^{(3)}(0) = \sum_{\substack{(cd),\\(ef)}} \int_q \Gamma^{(3)}_{k;ab,cd,ef}(0,q,-q)\, P_{k;ef,cd}(q^2)\,, \tag{D.19}$$

$$
\begin{aligned}
E^{(3),(3)}_{ab,cd}(p^2) &= \sum_{\substack{(ef),(gh),\\(ij),(lm)}} \int_q \Gamma^{(3)}_{k;ab,ef,gh}(p,q,-q-p)\, P_{k;gh,ij}(q^2)\, \Gamma^{(3)}_{k;cd,ij,lm}(-p,-q,q+p)\, P_{k;lm,ef}(|\vec{q}+\vec{p}|^2)\,, \\
E^{(4)}_{ab,cd}(0) &= \sum_{(ef),(gh)} \int_q \Gamma^{(4)}_{k;ab,cd,ef,gh}(0,0,q,-q)\, P_{k;ef,gh}(q^2)\,,
\end{aligned}
\tag{D.20}
$$

$$
\begin{aligned}
F^{(3),(3),(3)}_{ab,cd,ef}(0) = \sum_{\substack{(gh),(ij),(lt),\\(mn),(op),(rs)}} \int_q \Gamma^{(3)}_{k;ab,gh,ij}(0,q,-q)\, P_{k;ij,lt}(q^2)\, \Gamma^{(3)}_{k;cd,lt,mn}(0,q,-q)\, P_{mn,op}(q^2) \times \\
\Gamma^{(3)}_{k;ef,op,rs}(0,q,-q)\, P_{rs,gh}(q^2)\,, \\
F^{(4),(3)}_{ab,cd;ef}(0) = \sum_{\substack{(gh),(ij),\\(lp),(mn)}} \int_q \Gamma^{(4)}_{k;ab,cd,gh,ij}(0,0,q,-q)\, P_{k;ij,lp}(q^2)\, \Gamma^{(3)}_{k;ef,lp,mn}(0,q,-q)\, P_{mn,gh}(q^2), \\
F^{(5)}_{ab,cd,ef}(0) = \sum_{(gh),(ij)} \int_q \Gamma^{(5)}_{k;ab,cd,ef,gh,ij}(0,0,0,q,-q)\, P_{ij,gh}(q^2)\,.
\end{aligned}
\tag{D.21}
$$

By an abuse of notation, we have defined the proper vertices $\Gamma^{(n)}_k$ without the delta function $\delta^{(d)}(q_1 + \cdots + q_n)$.

D.5 Truncation of the expansion in invariants around the minimum at order $O(Q^4)$

D.5.1 Expressions of the coupling constants

The two systems of equations, (6.64) and (6.65) of the main text, can be inverted to obtain the expressions of the constants as functions of the field derivatives of u_k. For the choice (A), it gives

$$
\begin{aligned}
&w_{k,1} = u^{(3)}_{k;ab,bc,ca}\Big|_{q_k} \quad , \quad u_{k,1} = \frac{u^{(2)}_{k;ab,cd} - u^{(3)}_{k;ab,ab,cd} q_k}{2q_k^2}\Big|_{q_k} \quad , \quad u_{k,4} = \frac{u^{(3)}_{k;ab,ab,cd}}{q_k}\Big|_{q_k}\,, \\
(A) \qquad &u_{k,2} = \frac{3(n-2)\left(u^{(2)}_{k;ab,cd}(n-3) - u^{(3)}_{k;ab,ab,cd}(n-3)q_k + 2u^{(3)}_{k;ab,bc,ca}q_k\right) + 6u^{(2)}_{k;ab,ab}}{2q_k^2}\Big|_{q_k}\,, \\
&u_{k,3} = \frac{-u^{(2)}_{k;ab,cd}(n-3) + 2u^{(2)}_{k;ab,bc} + u^{(3)}_{k;ab,ab,cd}(n-3)q_k - 2u^{(3)}_{k;ab,bc,ca}q_k}{2q_k^2}\Big|_{q_k}\,,
\end{aligned}
\tag{D.22}
$$

and for the choice (B)

$$
\begin{aligned}
&w_{k,1} = u^{(3)}_{k;ab,bc,ca}\Big|_{q_k} \quad , \quad u_{k,1} = \frac{u^{(3)}_{k;ab,bc,cd}}{q_k}\Big|_{q_k} \quad , \quad u_{k,4} = \frac{u^{(2)}_{k;ab,cd} - 2u^{(3)}_{k;ab,bc,cd}q_k}{q_k^2}\Big|_{q_k}\,, \\
(B) \qquad &u_{k,2} = \frac{3\left(u^{(2)}_{k;ab,ab} + (n-2)q_k\left(u^{(3)}_{k;ab,bc,cd}(n-3) + u^{(3)}_{k;ab,bc,ca}\right)\right)}{q_k^2}\Big|_{q_k}\,, \\
&u_{k,3} = \frac{u^{(2)}_{k;ab,bc} - q_k\left(u^{(3)}_{k;ab,bc,cd}(n-3) + u^{(3)}_{k;ab,bc,ca}\right)}{q_k^2}\Big|_{q_k}\,.
\end{aligned}
\tag{D.23}
$$

D.5.2 Dimensionless flow equations

The five $\frac{d}{dt}\left(u^{(n)}_{k;a_1b_1,\dots,a_nb_n}\Big|_{q_k}\right)$ that we are susceptible to use are (with distinct a,b,c, and the three different cases $\{e,f\}=\{a,b\}$ or $\{b,c\}$ or $\{c,d\}$) read

$$\begin{aligned}
\frac{d}{dt}\left(u^{(2)}_{k;ab,ef}\Big|_{q_k}\right) &= (-2+\eta_k)\,u^{(2)}_{k;ab,ef}\Big|_{q_k} + \frac{1}{2}\widetilde{\partial}_t\left\{e^{(4)}_{ab,ef}(0) - e^{(3),(3)}_{ab,ef}(0)\right\}\Big|_{q_k} + \delta q_k \sum_{(gh)} u^{(3)}_{k;ab,ef,gh}\Big|_{q_k},\\
\frac{d}{dt}\left(u^{(3)}_{k;ab,bc,ca}\Big|_{q_k}\right) &= \frac{1}{2}(d-6+3\,\eta_k)\,u^{(3)}_{k;ab,bc,ca}\Big|_{q_k} + \frac{1}{2}\widetilde{\partial}_t\left\{2\,f^{(3),(3),(3)}_{ab,bc,ca}(0) - 3\,f^{(4),(3)}_{ab,bc;ca}(0)\right\}\Big|_{q_k}\\
&\quad + \delta q_k \sum_{(gh)} u^{(4)}_{k;ab,cd,ef,gh}\Big|_{q_k},
\end{aligned} \tag{D.24}$$

with in addition for the choice (A)

$$\begin{aligned}
(A)\qquad \frac{d}{dt}\left(u^{(3)}_{k;ab,ab,cd}\Big|_{q_k}\right) &= \frac{1}{2}(d-6+3\,\eta_k)\,u^{(3)}_{k;ab,ab,cd}\Big|_{q_k} + \delta q_k \sum_{(gh)} u^{(4)}_{k;ab,ab,cd,gh}\Big|_{q_k}\\
&\quad + \frac{1}{2}\widetilde{\partial}_t\left\{2\,f^{(3),(3),(3)}_{ab,ab,cd}(0) - f^{(4),(3)}_{ab,ab;cd}(0) - 2\,f^{(4),(3)}_{ab,cd;ab}(0)\right\}\Big|_{q_k},
\end{aligned} \tag{D.25}$$

and the choice (B)

$$\begin{aligned}
(B)\qquad \frac{d}{dt}\left(u^{(3)}_{k;ab,bc,cd}\Big|_{q_k}\right) &= \frac{1}{2}(d-6+3\,\eta_k)\,u^{(3)}_{k;ab,bc,cd}\Big|_{q_k} + \delta q_k \sum_{(gh)} u^{(4)}_{k;ab,bc,cd,gh}\Big|_{q_k}\\
&\quad + \frac{1}{2}\widetilde{\partial}_t\left\{2\,f^{(3),(3),(3)}_{ab,bc,cd}(0) - 2\,f^{(4),(3)}_{ab,bc;cd}(0) - f^{(4),(3)}_{ab,cd;bc}(0)\right\}\Big|_{q_k}.
\end{aligned} \tag{D.26}$$

The functions $d^{(3)}_{ab}(0)$, $e^{(4)}_{ab,cd}(\hat{p})$, $e^{(3),(3)}_{ab,cd}(0)$, $f^{(3),(3),(3)}_{ab,cd,ef}(0)$, and $f^{(4),(3)}_{ab,cd;ef}(0)$ for all values of $a,b,c,d,e,f \in \{1,\dots,n\}$ are coefficients which contain both sums over indices and integrals over momenta of the propagators. Their formal definition is given in (D.19), (D.20), and (D.21) respectively. Some of their expressions once the sums have been done can be found in the appendix D.5.3, the others are too long to be reproduced here.

D.5.3 Contributions to dimensionless beta functions

For simplicity of notation, we rename the different nonzero dimensionless field derivatives, in equations (6.61) and (6.62), of the dimensionless potential u_k (distinct a,b,c,d)

$$\begin{aligned}
u^{(3)}_{k;ab,bc,ca}\Big|_{q_k} &= w_1, & u^{(4)}_{k;ab,bc,cd,da}\Big|_{q_k} &= u_1,\\
u^{(3)}_{k;ab,ab,ab}\Big|_{q_k} &= w_2, & u^{(4)}_{k;ab,ab,ab,ab}\Big|_{q_k} &= u_2,\\
u^{(3)}_{k;ab,ab,bc}\Big|_{q_k} &= w_3, & u^{(4)}_{k;ab,ab,bc,bc}\Big|_{q_k} &= u_3,\\
u^{(3)}_{k;ab,ab,cd}\Big|_{q_k} &= w_4, & u^{(4)}_{k;ab,ab,cd,cd}\Big|_{q_k} &= u_4.\\
u^{(3)}_{k;ab,bc,cd}\Big|_{q_k} &= w_5,
\end{aligned} \tag{D.27}$$

The propagators $p_{k,i}(\hat{q}^2)$ below, with $i=1,2,3$, are also evaluated in q_k. Below, we give the not-too-long contributions to the dimensionless beta functions, and we precise which contributions are missing.

D.5.3.1 Equation for $\dot{q}_k$

$$d^{(3)}_{ab}(0)|_{q_k} = \frac{1}{4}\int_{\hat{q}} d\hat{q}\,\hat{q}^{d-1}\,\{2p_1\left((n-2)\left((n-3)w_4+4w_3\right)+2w_2\right)+(n-3)(n-2)p_3\left(4w_4+8w_5\right)$$
$$+4(n-2)p_2\left(4(n-3)w_5+2w_1+4w_3\right)\}\ .$$

D.5.3.2 Equations for η_k

$$\begin{aligned}
e^{(3),(3)}_{ab,ab}(\hat{p}^2)|_{q_k} = \frac{1}{4}\int_{\hat{q}} d\hat{q}\,\hat{q}^{d-1}\ \{&2(n-2)p_1\left[4p_2\left(n^2w_4^2+2nw_3^2+4nw_4w_3-7nw_4^2+4(n-3)(n-2)w_5^2\right.\right.\\
&\left.+8(n-3)\left(w_1+w_3+w_4\right)w_5+8w_1w_3+4w_2w_3-12w_4w_3+12w_4^2\right)\\
&+(n-3)p_3\left(8w_3\left((n-4)w_4+4w_5\right)+8(2n-7)w_5^2+w_4\left(\left((n-9)n+24\right)w_4+4w_2\right)+8w_3^2\right)\Big]\\
&+(n-2)\left(4p_2^2\left[n^2w_4^2+2(n-2)w_1^2+4w_1\left(2(n-2)w_3+(n-3)\left(nw_5+3w_4\right)+w_2\right)+18nw_3^2\right.\right.\\
&-7nw_4^2+2(n-3)(n(n+13)-50)w_5^2+12nw_3w_4+4(n-3)w_5\left(2(n+5)w_3+(8n-29)w_4+w_2\right)\\
&\left.-36w_3^2+12w_4^2+4w_2w_3-36w_3w_4\right]\\
&+16(n-3)p_3p_2\left[2w_3\left((n-2)w_4+2(3n-10)w_5\right)+(n-4)w_4^2+(n(3n-11)-2)w_5^2\right.\\
&+2w_5\left(\left((n-5)n+5\right)w_4+w_2\right)+w_1\left((n-4)w_4+2(n-2)w_5+4w_3\right)+2w_3^2\Big]\\
&+(n-3)p_3^2\left[8(n-4)\left(w_4+6w_5\right)w_1+8(n(11n-89)+181)w_5^2\right.\\
&+w_4\left(24(n-4)w_3+(n(7n-55)+112)w_4+4w_2\right)\\
&\left.+8w_5\left(4(2n-7)w_3+(n-4)(5n-21)w_4\right)+8w_1^2+8w_3^2\right]\Big)\\
&+2p_1^2\left[4(n-2)w_1^2+3(n-2)\left((n-3)\left(w_4^2+4w_5^2\right)+4w_3^2\right)+2w_2^2\right]\}\ .
\end{aligned} \tag{D.28}$$

D.5.3.3 Equation for $\frac{d}{dt}\left(u^{(2)}_{k;ab,ab}|_{q_k}\right)$

$$e^{(4)}_{ab,ab}(0)|_{q_k} = \int_{\hat{q}} d\hat{q}\,\hat{q}^{d-1}\left\{u_2+2(n-2)\,u_3+\frac{1}{2}(n-2)(n-3)\,u_4\right\}p_1\,, \tag{D.29}$$

$$\sum_{(cd)}\gamma^{(3)}_{ab,ab,cd}|_{q_k} = w_2+2(n-2)\,w_3+\frac{1}{2}(n-2)(n-3)w_4\,, \tag{D.30}$$

and the expression of $e^{(3),(3)}_{ab,ab}(0)|_{q_k}$ is obtained by evaluating equation (D.28) for $\hat{p}=0$.

D.5.3.4 Equation for $\frac{d}{dt}\left(u^{(2)}_{k;ab,bc}|_{q_k}\right)$

$$e^{(4)}_{ab,bc}(0)|_{q_k} = \int_{\hat{q}} d\hat{q}\,\hat{q}^{d-1}\,\{2\,u_3+2(n-3)\,u_1\}\,p_2\,, \tag{D.31}$$

$$\sum_{(ef)}\gamma^{(3)}_{ab,bc,ef}|_{q_k} = w_1+2\,w_3+2(n-3)\,w_5+(n-3)\,w_6+\frac{1}{2}(n-3)(n-4)w_7\,, \tag{D.32}$$

$$
\begin{aligned}
e^{(3),(3)}_{ab,bc}(0)|_{q_k} = \int_{\hat{q}} d\hat{q}\, \hat{q}^{d-1} \Big\{ & \frac{1}{2} p_1^2 \big[2nw_3^2 + 8w_1w_3 + 4w_2w_3 + 4nw_4w_3 - 12w_4w_3 + n^2w_4^2 - 7nw_4^2 + 12w_4^2 \\
& + 4(n-3)(n-2)w_5^2 + 8(n-3)\left(w_1 + w_3 + w_4\right) w_5 \big] \\
& + p_1 \big[2(n-3)p_3 \left(2w_3^2 + 2\left((n-2)w_4 + 2(3n-10)w_5\right) w_3 + (n-4)w_4^2 + (n(3n-11)-2)w_5^2 \right. \\
& \left. + 2\left(w_2 + ((n-5)n+5)w_4\right) w_5 + w_1\left(4w_3 + (n-4)w_4 + 2(n-2)w_5\right) \right) \\
& + p_2 \left(2(n-2)w_1^2 + 4\left(w_2 + 2(n-2)w_3 + (n-3)\left(3w_4 + nw_5\right)\right) w_1 + 18nw_3^2 - 36w_3^2 + n^2w_4^2 - 7nw_4^2 \right. \\
& \left. + 12w_4^2 + 2(n-3)(n(n+13)-50)w_5^2 + 4w_2w_3 + 12nw_3w_4 - 36w_3w_4 \right. \\
& \left. + 4(n-3)\left(w_2 + 2(n+5)w_3 + (8n-29)w_4\right) w_5 \right) \big] \\
& + \frac{(n-3)}{2} p_2p_3 \big[w_4^2n^3 + 5w_4^2n^2 + 16w_3w_4n^2 + 28w_3^2n - 78w_4^2n - 56w_3w_4n + 4(n-2)w_1^2 - 40w_3^2 + 168w_4^2 \\
& + 4(n(n(4n+17)-303)+702)w_5^2 - 8w_3w_4 + 8\left(2(n(4n-13)-3)w_3 + (n(n(n+3)-62)+139)w_4\right) w_5 \\
& + 4w_2\left(2w_3 + (n-4)w_4 + 2(2n-7)w_5\right) \\
& + 4w_1\left(2w_2 + 8(n-3)w_3 + ((n-4)n+6)w_4 + 2(n(2n-3)-16)w_5\right) \big] \\
& + \frac{1}{4}(n-3)p_3^2 \big[7w_4^2n^3 - 85w_4^2n^2 + 40w_3w_4n^2 + 52w_3^2n + 346w_4^2n - 312w_3w_4n + 8(n-4)w_1^2 - 192w_3^2 \\
& - 472w_4^2 + 8(n(14(n-12)n+687)-954)w_5^2 + 616w_3w_4 \\
& + 8\left(2(2n(5n-39)+153)w_3 + (n(n(7n-83)+334)-454)w_4\right) w_5 \\
& + 8w_1\left((2n-7)\left(2w_3 + (n-4)w_4\right) + 2(4(n-8)n+65)w_5\right) + 4w_2\left(2w_3 + (n-4)\left(w_4 + 4w_5\right)\right) \big] \\
& + p_2^2 \big[2(3n-8)w_1^2 + 12\left((3n-8)w_3 + (n-3)\left((n-4)w_4 + (3n-8)w_5\right)\right) w_1 + w_2^2 \\
& + 6w_2\left((n-2)w_3 + (n-3)\left(w_4 + 2w_5\right)\right) \\
& + 3\big((3(n-2)n-4)w_3^2 + 2(n-3)\left((5n-14)w_4 + 4(4n-11)w_5\right) w_3 \\
& + (n-3)\left(((n-5)n+7)w_4^2 + 4(2(n-6)n+19)w_5w_4 + 2(n(7n-33)+30)w_5^2\right)\big) \big] \Big\} \,.
\end{aligned}
\tag{D.33}
$$

D.5.3.5 Equation for $\frac{d}{dt}\left(u^{(2)}_{k;ab,cd}|_{q_k}\right)$

$$
e^{(4)}_{ab,cd}(0)|_{q_k} = \int_{\hat{q}} d\hat{q}\, \hat{q}^{d-1} \left\{ 2\, u_4 + 4\, u_1 \right\} p_3 \,, \tag{D.34}
$$

$$
\sum_{(ef)} \gamma^{(3)}_{ab,cd,ef}|_{q_k} = 2\, w_4 + 4\, w_5 + 4(n-4)\, w_7 + \frac{1}{2}(n-4)(n-5)w_8 \,, \tag{D.35}
$$

and we do not give the expression of $e^{(3),(3)}_{ab,bc}(0)|_{q_k}$.

D.5.3.6 Equation for $\frac{d}{dt}\left(u^{(3)}_{k;ab,bc,ca}|_{q_k}\right)$

$$
\begin{aligned}
f^{(4),(3)}_{ab,bc,ca}(0)|_{q_k} = & \frac{1}{2}\left((n-3)u_1 + u_3\right) \int_{\hat{q}} d\hat{q}\, \hat{q}^{d-1} \left\{ 16p_2p_1\left((n-3)w_5 + w_3\right) \right. \\
& + 4(n-3)p_2p_3\left((n-4)w_4 + 2(n-2)w_5 + 4w_3\right) + (n-3)p_3^2\left(2(n-4)\left(w_4 + 6w_5\right) + 4w_1\right) \\
& \left. + 4p_2^2\left((n-2)w_1 + 2(n-2)w_3 + (n-3)\left(nw_5 + 3w_4\right) + w_2\right) + 4p_1^2w_1 \right\} \,,
\end{aligned}
\tag{D.36}
$$

$$
\sum_{(ef)} \gamma^{(4)}_{ab,bc,ca,ef}|_{q_k} = 0 \,, \tag{D.37}
$$

and we do not give the expression of $f^{(3),(3),(3)}_{ab,bc,ca}(0)|_{q_k}$.

D.5.3.7 Choice (A): equation for $\frac{d}{dt}\left(u^{(3)}_{k;ab,ab,cd}|_{q_k}\right)$

$$
\begin{aligned}
f^{(4),(3)}_{ab,cd;ab}(0)|_{q_k} = \frac{1}{2}\int_{\hat{q}} d\hat{q}\,\hat{q}^{d-1}\ \{&u_1\left[4p_1\left(2p_3\left((n-4)w_5+w_3\right)+2p_2\left((n-3)w_5+w_1+w_3\right)\right)\right.\\
&+4p_2p_3\left(2(2n-7)w_3+(n-4)(n-1)w_4+2(n-4)nw_5+2w_1+2w_5\right)\\
&+p_3^2\left(4(n-4)w_1+2(n-5)(n-4)w_4+4(n(3n-23)+45)w_5\right)\\
&\left.+4p_2^2\left((n-4)w_1+2(n-1)w_3+n\left((n-3)w_5+2w_4\right)+w_2-5w_4+2w_5\right)+4p_1^2w_5\right]\\
&+u_4\left[2p_3p_1\left(4(n-4)w_3+((n-9)n+22)w_4+2w_2\right)\right.\\
&+p_3^2\left(4((n-7)n+13)w_4+8(n-4)(n-3)w_5\right)+16p_2^2\left((3n-11)w_5+w_1+w_3\right)\\
&+4p_2\left(2p_1\left((n-4)w_4+2w_3+2w_5\right)+p_3\left(2(n-4)w_1+4(n-3)w_3+n\left(4(n-7)w_5+2w_4\right)\right.\right.\\
&\left.\left.\left.-8w_4+52w_5\right)\right)+4p_1^2w_4\right]\Big\}\,,
\end{aligned}
\tag{D.38}
$$

$$
\begin{aligned}
f^{(4),(3)}_{ab,ab;cd}(0)|_{q_k} = \frac{1}{8}\int_{\hat{q}} d\hat{q}\,\hat{q}^{d-1}\ \{&4(n-2)u_3\left[4p_1\left(2(n-3)p_3w_5+2p_2\left((n-3)w_5+w_1+w_3\right)\right)\right.\\
&+4(n-3)p_2p_3\left((n-4)w_4+2(2n-7)w_5+2w_1+2w_3\right)+4p_2^2\left(3(n-2)w_3+3(n-3)\left(w_4+2w_5\right)\right.\\
&\left.\left.+w_2\right)+(n-3)p_3^2\left(2(n-4)\left(w_4+4w_5\right)+4w_3\right)+4p_1^2w_3\right]\\
&+(n-3)(n-2)u_4\left[(n-2)\left(8p_2^2\left((n-3)w_5+w_1+w_3\right)+8p_2\left(2(n-3)p_3w_5+2p_1w_3\right)\right.\right.\\
&\left.\left.+2(n-3)p_3\left(2p_1+p_3\right)w_4\right)+4p_1^2w_2\right]\\
&+2u_2\left[8p_2^2\left((n-4)w_4+2(2n-7)w_5+2w_1+2w_3\right)\right.\\
&+p_3^2\left(8(n-4)w_1+6(n-4)\left((n-5)\left(w_4+4w_5\right)+4w_3\right)+4w_2\right)\\
&\left.+8p_2\left(2p_3\left((n-4)\left(w_4+4w_5\right)+2w_3\right)+4p_1w_5\right)+4p_1^2w_4+8p_3p_1w_4\right]\Big\}\,,
\end{aligned}
\tag{D.39}
$$

$$
\sum_{(ef)}\gamma^{(4)}_{ab,ab,cd,ef}|_{q_k} = u_4\,,
\tag{D.40}
$$

and we do not give the expression of $f^{(3),(3),(3)}_{ab,ab,cd}(0)|_{q_k}$.

D.5.3.8 Choice (B): equation for $\frac{d}{dt}\left(u^{(3)}_{k;ab,bc,cd}|_{q_k}\right)$

$$
\begin{aligned}
f^{(4),(3)}_{ab,cd;bc}(0)|_{q_k} = \frac{1}{2}\int_{\hat{q}} d\hat{q}\,\hat{q}^{d-1}\ \{&u_4\left[4p_1\left(2p_3\left((n-4)w_5+w_3\right)+2p_2\left((n-3)w_5+w_1+w_3\right)\right)\right.\\
&+4p_2p_3\left(2(2n-7)w_3+(n-4)(n-1)w_4+2(n-4)nw_5+2w_1+2w_5\right)\\
&+p_3^2\left(4(n-4)w_1+2(n-5)(n-4)w_4+4(n(3n-23)+45)w_5\right)+4p_2^2\left((n-4)w_1+2(n-1)w_3\right.\\
&\left.\left.+n\left((n-3)w_5+2w_4\right)+w_2-5w_4+2w_5\right)+4p_1^2w_5\right]\\
&+u_1\left[2p_3p_1\left(4(n-4)w_3+((n-9)n+22)w_4+2w_2\right)+p_3^2\left(4((n-7)n+13)w_4+8(n-4)(n-3)w_5\right)\right.\\
&+16p_2^2\left((3n-11)w_5+w_1+w_3\right)+4p_2\left(2p_1\left((n-4)w_4+2w_3+2w_5\right)\right.\\
&\left.\left.\left.+p_3\left(2(n-4)w_1+4(n-3)w_3+n\left(4(n-7)w_5+2w_4\right)-8w_4+52w_5\right)\right)+4p_1^2w_4\right]\Big\}\,,
\end{aligned}
\tag{D.41}
$$

$$f^{(4),(3)}_{ab,bc;cd}(0)|_{q_k} = \frac{1}{2}\int_{\hat{q}} d\hat{q}\,\hat{q}^{d-1}\,\{u_3\,[2p_1\,(2p_3\,((n-3)w_5+w_3)+2p_2\,((n-1)w_5+w_1+w_3+2w_4))$$
$$+4p_2^2\,(3(n-4)w_4+(8n-26)w_5+2w_1+6w_3)$$
$$+2p_2p_3\,(2(n-3)w_1+(8n-26)w_3+n\,((n-5)w_4+2(2n-7)w_5)+2w_2+6w_4-6w_5)$$
$$+4p_3^2\,((n-4)w_1+(2n-7)w_3+(n-4)\,((n-4)w_4+(4n-17)w_5))+4p_1^2w_5]$$
$$+(n-3)u_1\,[2p_1\,((n-3)p_3\,((n-4)w_4+2w_3+2w_5)+2p_2\,((n-1)w_3+(n-3)\,(w_4+w_5)+w_1+w_2))$$
$$+(n-3)p_3^2\,(2(n-4)w_4+4(n-3)w_5)+2(n-3)p_2p_3\,(nw_4+8nw_5+2w_1+2w_3-26w_5)$$
$$+4p_2^2\,((n-2)w_1+3(n-2)w_3+(n-3)(n+2)w_5)+4p_1^2w_3]\}\,, \tag{D.42}$$

$$\sum_{(ef)}\gamma^{(4)}_{ab,bc,cd,ef}|_{q_k} = u_1\,, \tag{D.43}$$

and we do not give the expression of $f^{(3),(3),(3)}_{ab,bc,cd}(0)|_{q_k}$.

D.5.4 Results: additional plots

We give additional results for the NPRG-1 (A).

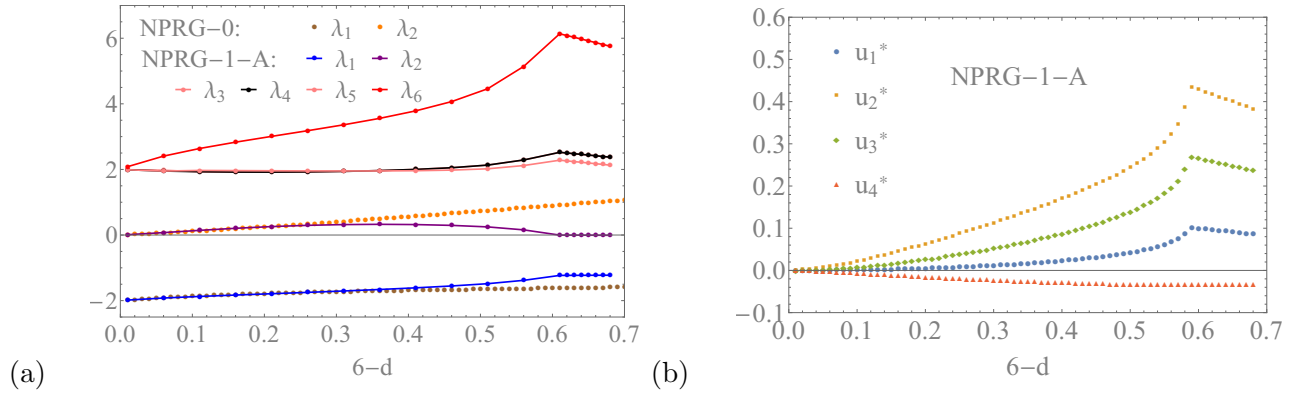

Figure D.1: Fixed point solution for the critical point of the Ising spin glass at the next order NPRG-1 (A) of the truncation of the nonperturbative RG approach versus $6-d$. We also display in brown the results of the NPRG-0. (a) Relevant (λ_1) and irrelevant (λ_i, $i\neq 1$) eigenvalues of the stability matrix at the critical fixed point; and (b) dimensionless quartic constants $u_i^\star$.

D.6 One-loop-improved approximation

D.6.1 Expression of the n-point 1-PI vertices $\gamma^{(n)}$

The function $d^{(3)}_{ab}(0)$ defined in (D.19) appearing in the flow of q_k and the function $e^{(3),(3)}_{ab,ab}(\hat{p}^2)$ defined in (D.20) appearing in η_k, both involve the 3-point 1-PI vertices $\gamma^{(3)}_{ab,cd,ef}(0,\hat{q},-\hat{q})$. The functions needed for the flow of $w_{k,1}$ are directly visible in (6.69), and they require 3 to 5-point vertices $\gamma^{(3)}_{ab,cd,ef}(0,\hat{q},-\hat{q})$, $\gamma^{(4)}_{ab,cd,ef,gh}(0,0,\hat{q},-\hat{q})$ and $\gamma^{(5)}_{ab,cd,ef,gh,ij}(0,0,0,\hat{q},-\hat{q})$. Finally, the three flow equations contains the 2-point vertices $\gamma^{(2)}_{ab,cd}(\hat{q},-\hat{q})$, explicitly used in the propagators.

All the 1-PI vertices $\gamma^{(n)}_{k;a_1b_1,\ldots,a_nb_n}$ for $n=2,3,4,5$ that are nonzero are listed below for the choice of solution (A) of the constants $\{b_{ij},c_i\}$ of the exact potential (the choice (B) is also feasible, other similar relations are obtained). These field derivatives of the effective average action are potentially

functions of *all* the couplings of the expansion in invariants of the potential. Actually, with the choice of solution (A), the derivatives $\gamma^{(2)}_{k;ab,ab}(0)|_{q_k}$, $\gamma^{(2)}_{k;ab,bc}(0)|_{q_k}$, $\gamma^{(2)}_{k;ab,cd}(0)|_{q_k}$, $\gamma^{(3)}_{k;ab,bc,ca}(0)|_{q_k}$ and $\gamma^{(3)}_{k;ab,ab,cd}(0)|_{q_k}$ (with $a,b,c,d \neq$) are exactly given by the following expressions at the minimum, involving orders until $O(Q^4)$ of the expansion. All the others receive contributions from the higher order terms of the development, involving couplings $v_{k,i}$, $t_{k,i}$ ($O(Q^6)$ terms), etc. (In the following list of definitions, from (D.44) to (D.47), all indices are distinct two by two $(a,b,c,d,e,f,g \neq)$.) We obtain:

$$
\begin{aligned}
\gamma^{(2)}_{k;ab,ab}(0)|_{q_k} &= -(n-2)q_k\, w_{k,1} - (n-2)(n-3)q_k^2 u_{k,1} + \frac{1}{3}q_k^2 u_{k,2} \\
\gamma^{(2)}_{k;ab,bc}(0)|_{q_k} &= q_k\, w_{k,1} + (n-3)q_k^2 u_{k,1} + q_k^2 u_{k,3} \\
\gamma^{(2)}_{k;ab,cd}(0)|_{q_k} &= 2q_k^2 u_{k,1} + q_k^2 u_{k,4} \\
\gamma^{(3)}_{k;ab,bc,ca}(0)|_{q_k} &= w_{k,1} \\
\gamma^{(3)}_{k;ab,ab,ab}(0)|_{q_k} &= q_k u_{k,2} - \frac{1}{2}(n-2)q_k^2\,(6(n-4)(n-3)v_{k,1} + 3(n-3)\,((n-4)v_{k,4} + 2v_{k,3}) + 8v_{k,2}) + O(q_k^3 t_{k,i}) \\
\gamma^{(3)}_{k;ab,ab,bc}(0)|_{q_k} &= q_k u_{k,3} + \frac{1}{6}q_k^2\,(6(n-4)(n-3)v_{k,1} + 3(n-4)(n-3)v_{k,4} + 8v_{k,2}) + O(q_k^3 t_{k,i}) \\
\gamma^{(3)}_{k;ab,ab,cd}(0)|_{q_k} &= q_k u_{k,4} \\
\gamma^{(3)}_{k;ab,bc,cd}(0)|_{q_k} &= q_k u_{k,1} - \frac{1}{2}q_k^2\,(2(n-4)v_{k,1} + (n-4)v_{k,4} - 2v_{k,3}) + O(q_k^3 t_{k,i}) \\
\gamma^{(3)}_{k;ab,ac,ad}(0)|_{q_k} &= 3q_k^2 v_{k,3} + O(q_k^3 t_{k,i}) \\
\gamma^{(3)}_{k;ab,ac,de}(0)|_{q_k} &= q_k^2\,(2v_{k,1} + v_{k,4}) + O(q_k^3 t_{k,i}) \\
\gamma^{(3)}_{k;ab,cd,ef}(0)|_{q_k} &= O(q_k^3 t_{k,i})\,,
\end{aligned}
\tag{D.44}
$$

$$
\begin{aligned}
\gamma^{(4)}_{k;ab,bc,cd,da}(0)|_{q_k} &= u_{k,1} - \frac{1}{2}q_k\,(4(n-4)v_{k,1} + (n-4)v_{k,4} + 2v_{k,3}) + O(q_k^2 t_{k,i}) \\
\gamma^{(4)}_{k;ab,ab,ab,ab}(0)|_{q_k} &= u_{k,2} - \frac{1}{2}(n-2)q_k\,(6(n-4)(n-3)v_{k,1} + 3(n-3)\,((n-4)v_{k,4} + 2v_{k,3}) + 10v_{k,2}) + O(q_k^2 t_{k,i}) \\
\gamma^{(4)}_{k;ab,ab,bc,bc}(0)|_{q_k} &= u_{k,3} + \frac{1}{6}q_k\,(6(n-4)(n-3)v_{k,1} + 3(n-3)\,((n-4)v_{k,4} - 2v_{k,3}) + 2v_{k,2}) + O(q_k^2 t_{k,i}) \\
\gamma^{(4)}_{k;ab,ab,cd,cd}(0)|_{q_k} &= u_{k,4} - (n-4)q_k v_{k,4} - 2q_k v_{k,3} + O(q_k^2 t_{k,i})\,,
\end{aligned}
\tag{D.45}
$$

$$
\begin{aligned}
\gamma^{(4)}_{k;ab,ab,ac,bc}(0)|_{q_k} &= q_k v_{k,2} + O(q_k^2 t_{k,i}) & \gamma^{(4)}_{k;ab,ab,cd,ce}(0)|_{q_k} &= q_k v_{k,4} + O(q_k^2 t_{k,i}) \\
\gamma^{(4)}_{k;ab,ac,bc,cd}(0)|_{q_k} &= q_k v_{k,3} + O(q_k^2 t_{k,i}) & \gamma^{(4)}_{k;ab,bc,cd,de}(0)|_{q_k} &= q_k v_{k,1} + O(q_k^2 t_{k,i}) \\
\gamma^{(4)}_{k;ab,ac,bc,de}(0)|_{q_k} &= q_k v_{k,4} + O(q_k^2 t_{k,i}) & \gamma^{(4)}_{k;ab,bc,cd,ef}(0)|_{q_k} &= O(q_k^2 t_{k,i}) \\
\gamma^{(4)}_{k;ab,ab,ab,bc}(0)|_{q_k} &= q_k v_{k,2} + O(q_k^2 t_{k,i}) & \gamma^{(4)}_{k;ab,bc,cd,ce}(0)|_{q_k} &= O(q_k^2 t_{k,i}) \\
\gamma^{(4)}_{k;ab,ab,bc,bd}(0)|_{q_k} &= q_k v_{k,3} + O(q_k^2 t_{k,i}) & \gamma^{(4)}_{k;ab,ac,ad,ae}(0)|_{q_k} &= O(q_k^2 t_{k,i}) \\
\gamma^{(4)}_{k;ab,ab,bc,cd}(0)|_{q_k} &= q_k v_{k,3} + O(q_k^2 t_{k,i}) & \gamma^{(4)}_{k;ab,cd,ce,cf}(0)|_{q_k} &= O(q_k^2 t_{k,i}) \\
\gamma^{(4)}_{k;ab,ab,bc,de}(0)|_{q_k} &= O(q_k^2 t_{k,i}) & \gamma^{(4)}_{k;ab,ac,de,df}(0)|_{q_k} &= O(q_k^2 t_{k,i}) \\
\gamma^{(4)}_{k;ab,ab,ac,bd}(0)|_{q_k} &= O(q_k^2 t_{k,i}) & \gamma^{(4)}_{k;ab,ac,ef,gh}(0)|_{q_k} &= O(q_k^2 t_{k,i})\,,
\end{aligned}
\tag{D.46}
$$

$$
\begin{aligned}
\gamma^{(5)}_{k;ab,bc,cd,de,ea}(0)|_{q_k} &= v_{k,1} + O(q_k t_{k,i}) \\
\gamma^{(5)}_{k;ab,bc,ca,ab,ab}(0)|_{q_k} &= v_{k,2} + O(q_k t_{k,i}) \\
\gamma^{(5)}_{k;ab,bc,ca,ad,ad}(0)|_{q_k} &= v_{k,3} + O(q_k t_{k,i}) \\
\gamma^{(5)}_{k;ab,bc,ca,de,de}(0)|_{q_k} &= v_{k,4} + O(q_k t_{k,i}) \\
\gamma^{(5)}_{k;ab,bc,ca,ab,bc}(0)|_{q_k} &= O(q_k t_{k,i}) \\
\gamma^{(5)}_{k;ab,bc,ca,ab,ad}(0)|_{q_k} &= O(q_k t_{k,i}) \\
\gamma^{(5)}_{k;ab,bc,ca,ad,ae}(0)|_{q_k} &= O(q_k t_{k,i}) \\
\gamma^{(5)}_{k;ab,bc,ca,ad,bd}(0)|_{q_k} &= O(q_k t_{k,i})
\end{aligned}
\qquad
\begin{aligned}
\gamma^{(5)}_{k;ab,bc,ca,ad,de}(0)|_{q_k} &= O(q_k t_{k,i}) \\
\gamma^{(5)}_{k;ab,bc,ca,ab,de}(0)|_{q_k} &= O(q_k t_{k,i}) \\
\gamma^{(5)}_{k;ab,bc,ca,de,df}(0)|_{q_k} &= O(q_k t_{k,i}) \\
\gamma^{(5)}_{k;ab,bc,ca,ab,cd}(0)|_{q_k} &= O(q_k t_{k,i}) \\
\gamma^{(5)}_{k;ab,bc,ca,ad,be}(0)|_{q_k} &= O(q_k t_{k,i}) \\
\gamma^{(5)}_{k;ab,bc,ca,ad,ef}(0)|_{q_k} &= O(q_k t_{k,i}) \\
\gamma^{(5)}_{k;ab,bc,ca,de,fg}(0)|_{q_k} &= O(q_k t_{k,i})\,.
\end{aligned}
\tag{D.47}
$$

For simplicity, we will take a truncation of the exact potential in equation (6.68) at order $O(Q^5)$, hence all the dependence on the $t_{k,i}$'s are set to zero in the above expressions.

D.6.2 One-loop-improved prescriptions

After neglecting all $t_{k,i}$'s and higher order coupling constants in equation (D.47), the four $v_{k,i}$'s are exactly determined by the following expressions (distinct a, b, c, d, e)

$$
\begin{aligned}
v_{k,1} &= \gamma^{(5)}_{k;ab,bc,cd,de,ea}(0)|_{q_k}\,, \\
v_{k,2} &= \gamma^{(5)}_{k;ab,bc,ca,ab,ab}(0)|_{q_k}\,, \\
v_{k,3} &= \gamma^{(5)}_{k;ab,bc,ca,ad,ad}(0)|_{q_k}\,, \\
v_{k,4} &= \gamma^{(5)}_{k;ab,bc,ca,de,de}(0)|_{q_k}\,,
\end{aligned}
\tag{D.48}
$$

and from (D.45), the four $u_{k,i}$'s are given by (distinct a, b, c, d)

$$
\begin{aligned}
u_{k,1} &= \gamma^{(4)}_{k;ab,bc,cd,da}(0)|_{q_k} + \frac{1}{2} q_k \left(4(n-4)v_{k,1} + (n-4)v_{k,4} + 2v_{k,3}\right)\,, \\
u_{k,2} &= \gamma^{(4)}_{k;ab,ab,ab,ab}(0)|_{q_k} + \frac{1}{2}(n-2) q_k \left(6(n-4)(n-3)v_{k,1} + 3(n-3)\left((n-4)v_{k,4} + 2v_{k,3}\right) + 10 v_{k,2}\right)\,, \\
u_{k,3} &= \gamma^{(4)}_{k;ab,ab,bc,bc}(0)|_{q_k} - \frac{1}{6} q_k \left(6(n-4)(n-3)v_{k,1} + 3(n-3)\left((n-4)v_{k,4} - 2v_{k,3}\right) + 2v_{k,2}\right)\,, \\
u_{k,4} &= \gamma^{(4)}_{k;ab,ab,cd,cd}(0)|_{q_k} + (n-4) q_k v_{k,4} + 2 q_k v_{k,3}\,.
\end{aligned}
\tag{D.49}
$$

After, the 1-PI vertices $\gamma^{(5)}$ and $\gamma^{(4)}$ are given by their one-loop-improved prescriptions (distinct a, b, c, d, e), namely,

$$
\begin{aligned}
&\gamma^{(5)}_{k;ab,bc,cd,de,ea}(0)|_{q_k} \\
&= \frac{1}{2}\left\{ \overline{h}^{(3),(3),(3),(3),(3)}_{ab,bc,cd,de,ea}(0) + \overline{h}^{(3),(3),(3),(3),(3)}_{ab,de,bc,ea,cd}(0) + 5\,\overline{h}^{(3),(3),(3),(3),(3)}_{ab,bc,de,ea,cd}(0) + 5\,\overline{h}^{(3),(3),(3),(3),(3)}_{ab,bc,ea,de,cd}(0) \right\}\,, \\
&\gamma^{(5)}_{k;ab,bc,ca,ab,ab}(0)|_{q_k} = 3\,\overline{h}^{(3),(3),(3),(3),(3)}_{ab,bc,ca,ab,ab}(0) + 3\,\overline{h}^{(3),(3),(3),(3),(3)}_{ab,bc,ab,ca,ab}(0)\,, \\
&\gamma^{(5)}_{k;ab,bc,ca,ad,ad}(0)|_{q_k} = \overline{h}^{(3),(3),(3),(3),(3)}_{ad,bc,ad,ca,ab}(0) + \overline{h}^{(3),(3),(3),(3),(3)}_{ad,ad,ca,bc,ab}(0) + 2\,\overline{h}^{(3),(3),(3),(3),(3)}_{ad,ca,bc,ad,ab}(0) + 2\,\overline{h}^{(3),(3),(3),(3),(3)}_{ad,ad,bc,ca,ab}(0), \\
&\gamma^{(5)}_{k;ab,bc,ca,de,de}(0)|_{q_k} = 3\,\overline{h}^{(3),(3),(3),(3),(3)}_{ab,bc,ca,de,de}(0) + 3\,\overline{h}^{(3),(3),(3),(3),(3)}_{ab,de,bc,ca,de}(0)\,,
\end{aligned}
\tag{D.50}
$$

and

$$\begin{aligned}
\gamma^{(4)}_{k;ab,bc,cd,da}(0)|_{q_k} &= -\frac{1}{2}\left\{\overline{g}^{(3),(3),(3),(3)}_{ab,bc,cd,da}(0) + 2\,\overline{g}^{(3),(3),(3),(3)}_{ab,bc,da,cd}(0)\right\}, \\
\gamma^{(4)}_{k;ab,ab,ab,ab}(0)|_{q_k} &= -\frac{3}{2}\overline{g}^{(3),(3),(3),(3)}_{ab,ab,ab,ab}(0), \\
\gamma^{(4)}_{k;ab,ab,bc,bc}(0)|_{q_k} &= -\frac{1}{2}\left\{2\,\overline{g}^{(3),(3),(3),(3)}_{ab,ab,bc,bc}(0) + \overline{g}^{(3),(3),(3),(3)}_{ab,bc,ab,bc}(0)\right\}, \\
\gamma^{(4)}_{k;ab,ab,cd,cd}(0)|_{q_k} &= -\frac{1}{2}\left\{2\,\overline{g}^{(3),(3),(3),(3)}_{ab,ab,cd,cd}(0) + \overline{g}^{(3),(3),(3),(3)}_{ab,cd,ab,cd}(0)\right\}.
\end{aligned} \tag{D.51}$$

where the functions $\overline{h}^{(3),(3),(3),(3),(3)}$ and $\overline{g}^{(3),(3),(3),(3)}$ read (for all $a \neq b$, $c \neq d$, $e \neq f$, $g \neq h$ and $i \neq j$):

$$\begin{aligned}
\overline{h}^{(3),(3),(3),(3),(3)}_{ab,cd,ef,gh,ij}(0) = \sum_{(kl),(mn),(op),(qr),(st),(uv),(wx),(yz),(\alpha\beta),(\gamma\delta)} \int_{\hat{q}} \times \\
\overline{\gamma}^{(3)}_{ab,kl,mn}(0,\hat{q},-\hat{q})\,\overline{p}_{mn,op}(\hat{q},-\hat{q})\,\overline{\gamma}^{(3)}_{cd,op,qr}(0,\hat{q},-\hat{q})\,\overline{p}_{qr,st}(\hat{q},-\hat{q}) \\
\overline{\gamma}^{(3)}_{ef,st,uv}(0,\hat{q},-\hat{q})\,\overline{p}_{uv,wx}(\hat{q},-\hat{q})\,\overline{\gamma}^{(3)}_{gh,wx,yz}(0,\hat{q},-\hat{q})\,\overline{p}_{yz,\alpha\beta}(\hat{q},-\hat{q}) \\
\overline{\gamma}^{(3)}_{ij,\alpha\beta,\gamma\delta}(0,\hat{q},-\hat{q})\,\overline{p}_{\gamma\delta,kl}(\hat{q},-\hat{q}),
\end{aligned} \tag{D.52}$$

and

$$\begin{aligned}
\overline{g}^{(3),(3),(3),(3)}_{ab,cd,ef,gh}(0) = \sum_{(kl),(mn),(op),(qr),(st),(uv),(wx),(yz)} \int_{\hat{q}} \times \\
\overline{\gamma}^{(3)}_{ab,kl,mn}(0,\hat{q},-\hat{q})\,\overline{p}_{mn,op}(\hat{q},-\hat{q})\,\overline{\gamma}^{(3)}_{cd,op,qr}(0,\hat{q},-\hat{q})\,\overline{p}_{qr,st}(\hat{q},-\hat{q}) \\
\overline{\gamma}^{(3)}_{ef,st,uv}(0,\hat{q},-\hat{q})\,\overline{p}_{uv,wx}(\hat{q},-\hat{q})\,\overline{\gamma}^{(3)}_{gh,wx,yz}(0,\hat{q},-\hat{q})\,\overline{p}_{yz,kl}(\hat{q},-\hat{q}).
\end{aligned} \tag{D.53}$$

The functions $\overline{h}^{(3),(3),(3),(3),(3)}$ and $\overline{g}^{(3),(3),(3),(3)}$ involve integrals over products of respectively 4 and 5 propagators $\overline{p}_{k;ab,cd}(\hat{q},-\hat{q})$. To compute these integrals, the propagators are transformed into sums of diagonal propagators, following the expressions given in equation (6.36) (for $n \to 0$). Following equations (6.34) and (6.35), the diagonal masses can be found as

$$\begin{aligned}
\overline{u}^{(2)}_{k;R} &= 0, \\
\overline{u}^{(2)}_{k;A} &= -2q_k\,w_{k,1}, \\
\overline{u}^{(2)}_{k;AL} &= -q_k\,w_{k,1}.
\end{aligned} \tag{D.54}$$

The zero replicon mass simplifies the replicon diagonal propagator to $\overline{p}_R(\hat{q}^2) = r_k(\hat{q}^2)^{-1}$. The different integrals hence appearing are composed by a product of $4 \leq m_R + m_A \leq 10$ propagators $\overline{p}_R(\hat{q}^2)^{m_R}\,\overline{p}_A(\hat{q}^2)^{m_A}$, and they are given by the generic expression

$$\overline{j}(R,m_R;A,m_A) = v_d \int_0^\infty d\hat{q}\,\hat{q}^{d-1}\,\overline{p}_R(\hat{q}^2)^{m_R}\,\overline{p}_A(\hat{q}^2)^{m_A}. \tag{D.55}$$

The integrals can be computed for the Litim regulator, one part of the integral can be expressed exactly when the other involves the hypergeometric function ${}_2F_1$ defined for $m_R + m_A > \frac{d}{2}$ and $\overline{u}^{(2)}_{k;A} > 0$. The integral is then given by

$$\begin{aligned}
&\overline{j}(R,m_R;A,m_A) = \\
&\frac{1}{2}v_d\left\{\frac{2}{d}\frac{1}{(1+\overline{u}^{(2)}_{k;A})^{m_2}} + \frac{{}_2F_1\left(m_A, -\frac{d}{2}+m_R+m_A, 1-\frac{d}{2}+m_R+m_A, -\overline{u}^{(2)}_{k;A}\right)}{\Gamma(m_A)\,\Gamma\left(1-\frac{d}{2}+m_R+m_A\right)\,\Gamma\left(-\overline{u}^{(2)}_{k;A}\right)}\right\}.
\end{aligned} \tag{D.56}$$

The second part of $\bar{j}(R, m_R; A, m_A)$ involves an integration on $\hat{q}$ over a range $[1; \infty[$ which is ultraviolet divergent if the condition $m_R + m_A > \frac{d}{2}$ is not respected; as soon as this is verified, like in our case as $m_R + m_A \geq 4$ and $\frac{d}{2} \leq 3$, the integral is convergent and finite. However, one has to be careful as it leads to large values for the limiting case when $m_R + m_A = \frac{d}{2}$, which could then give a too large importance to secondary couplings supposed to be perturbative: this indeed occurs when one aims to compute third order derivatives $\gamma^{(3)}$ by the one loop improved prescription. Since our choice is limited to $m_R + m_A \geq 4$, no such problems occur and we obtain only small corrections to the independent couplings.

Using the above equations, one obtains expressions for the $v_{k,i}$'s and the $u_{k,i}$'s that are functions of only q_k and $w_{k,1}$.

D.6.3 Additional results for the $O(Q^5)$ truncation of the potential

All the results of this appendix have been obtained for the choice (A) of the potential (6.68). The same study has also been performed for the choice (B), but as the results are almost indistinguishable from those for the choice (A), they have not been represented.

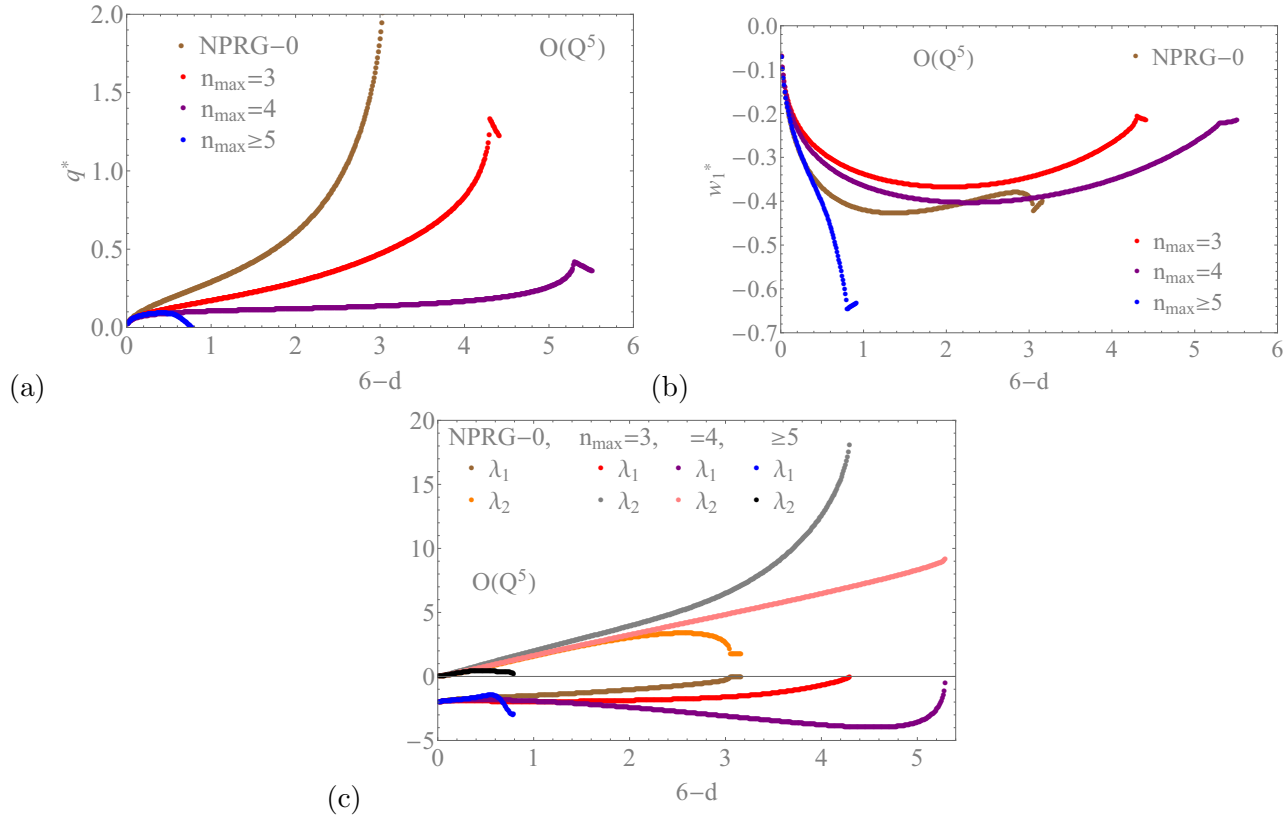

Figure D.2: Fixed point solution for the critical point of the Ising spin glass at the $O(Q^5)$ truncation of the potential in the one-loop improved approximation of the nonperturbative RG versus $6 - d$. We compare three situations where the maximal number of replicas n_{max} appearing in the vertices is varied: $n_{max} = 3$ (red/gray), $n_{max} = 4$ (purple/pink) and $n_{max} = 5$ (blue/black). We also display the results of the NPRG-0 (in brown/orange). (a) Dimensionless minimum $q^\star$; (b) dimensionless cubic coupling constant $w_1^\star$; and (c) relevant (λ_1) and irrelevant eigenvalues (λ_i, $i \neq 1$) of the stability matrix at the critical fixed point.

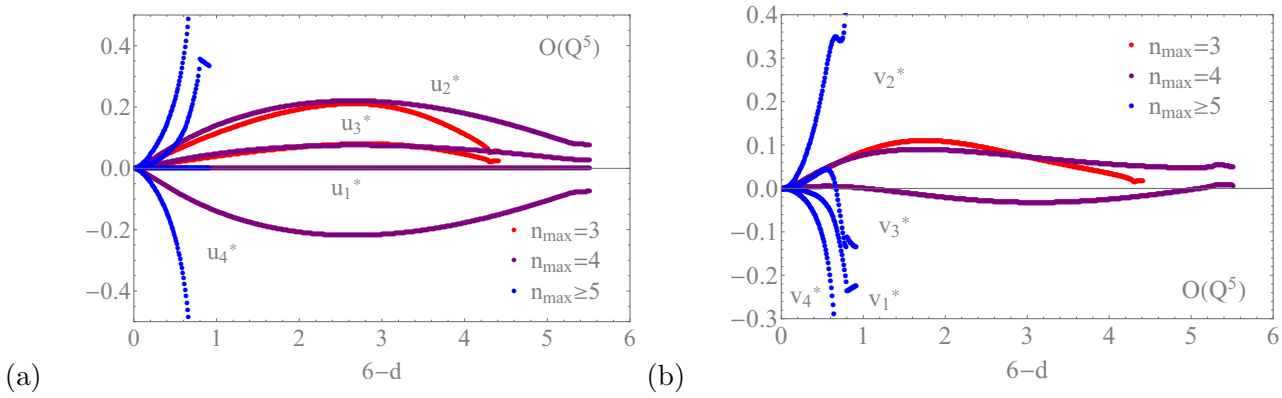

Figure D.3: Fixed point solution for the critical point of the Ising spin glass at the $O(Q^5)$ truncation of the potential in the one-loop improved approximation of the nonperturbative RG versus $6-d$. We compare three situations where the maximal number of replicas n_{max} appearing in the vertices is varied: $n_{max}=3$ (red/gray), $n_{max}=4$ (purple/pink) and $n_{max}=5$ (blue/black). We also display the results of the NPRG-0 (in brown/orange). (a) Dimensionless quartic couplings $u_i^\star$; and (b) dimensionless quintic couplings $v_i^\star$.

D.6.4 Results for the $O(Q^4)$ truncation of the potential

All the results shown here have been obtained for the choice (A) of the potential for the same reason as given above.

With this truncation, setting $n_{max}=3$ gives results which are qualitatively in agreement with the NPRG-0 ones; in particular, the critical exponents behave similarly, also do $q^\star$ and $w_1^\star$; differences appear however in the behavior of λ_2 which does not diverge between $d=2$ and $d=3$ and the anomalous mass which remains quite small. The same truncation with $n_{max}=4$ gives poor results, very far from the NPRG-0 ones: indeed ν is decreasing, there is no lower critical dimension as no divergence nor instability of the fixed point appear. However, we observe that going to the next order of truncation of the potential substantially improves the behavior and restores in large part the good properties and the behavior of the NPRG-0 (see main text).

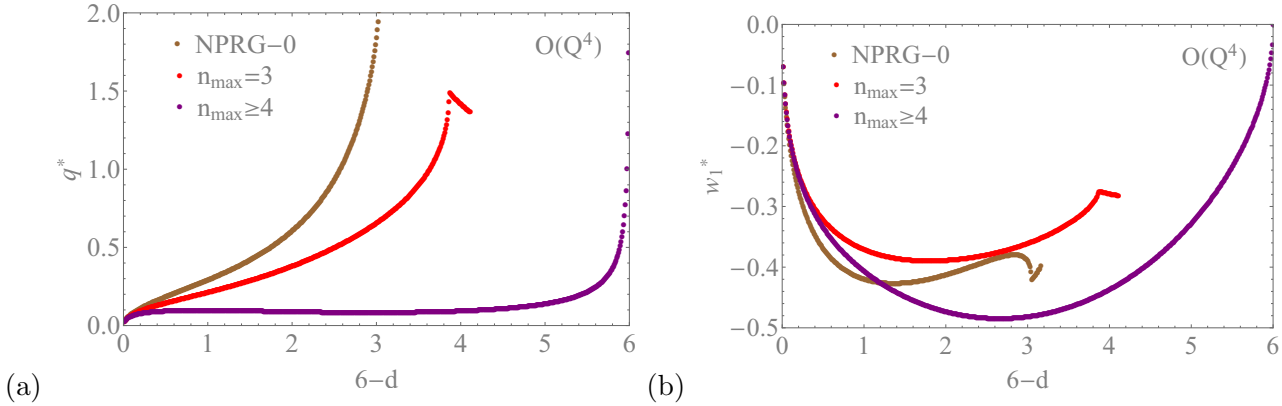

Figure D.4: Fixed point solution for the critical point of the Ising spin glass at the $O(Q^4)$ truncation of the potential in the one-loop improved approximation of the nonperturbative RG versus $6-d$. We compare two situations where the maximal number of replicas n_{max} appearing in the vertices is varied: $n_{max}=3$ (red/gray) and $n_{max}=4$ (purple/pink). We also display the results of the NPRG-0 (in brown/orange). (a) dimensionless minimum $q^\star$; and (b) dimensionless cubic coupling constant $w_1^\star$.

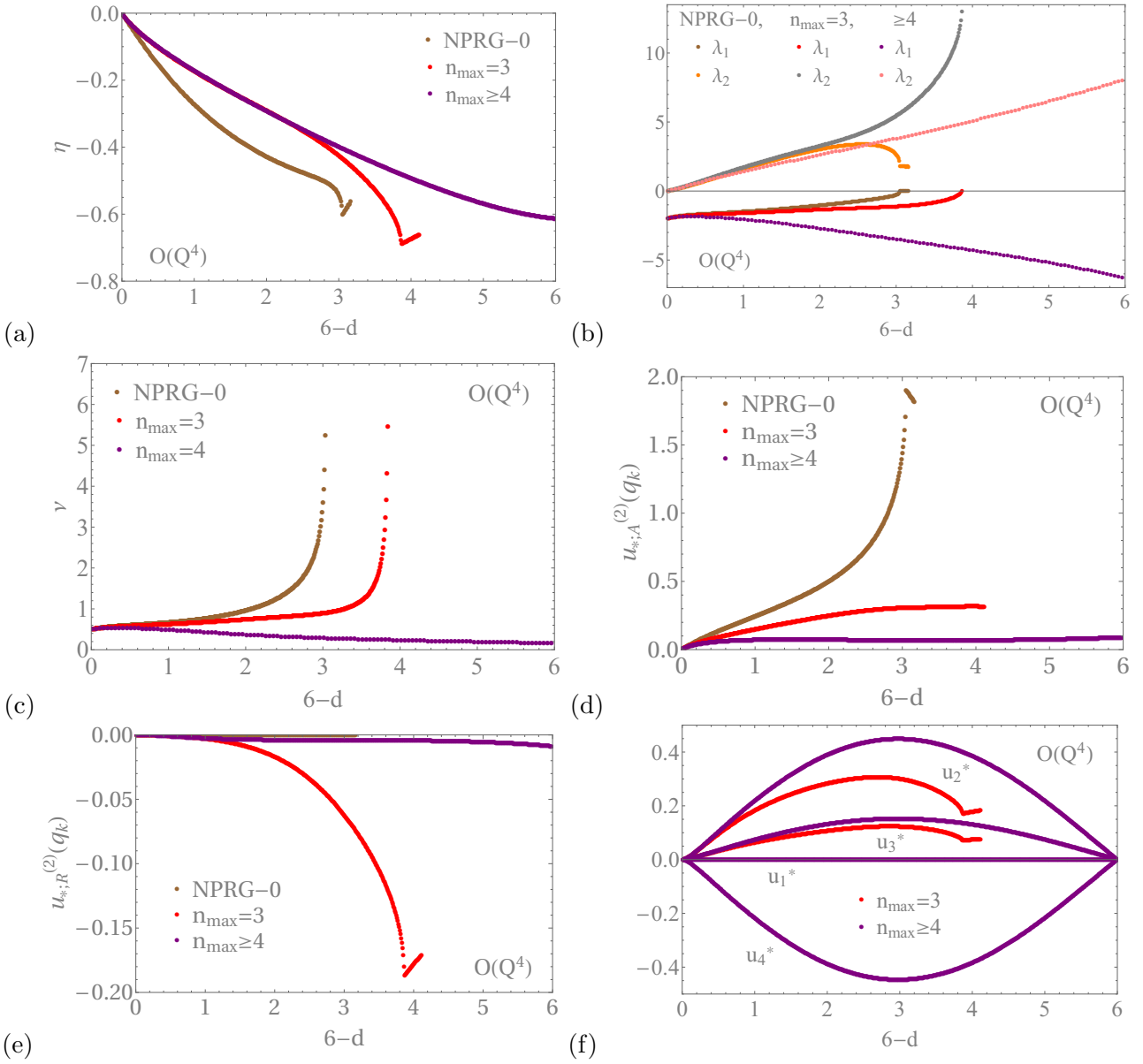

Figure D.5: Fixed point solution for the critical point of the Ising spin glass at the $O(Q^4)$ truncation of the potential in the one-loop improved approximation of the nonperturbative RG versus $6-d$. We compare two situations where the maximal number of replicas n_{max} appearing in the vertices is varied: $n_{max}=3$ (red/gray) and $n_{max}=4$ (purple/pink). We also display the results of the NPRG-0 (in brown/orange). (a) Anomalous dimension η; (b) relevant (λ_1) and irrelevant eigenvalues (λ_i, $i\neq 1$) of the stability matrix at the critical fixed point; (c) correlation length critical exponent ν; (d) dimensionless anomalous/longitudinal mass $u^{(2)}_{\star;A}(q_k)$; (e) dimensionless replicon mass $u^{(2)}_{\star;R}(q_k)$; and (f) dimensionless quartic couplings $u^{\star}_i$.

Bibliography

[1] G. Tarjus, *An overview of the theories of the glass transition*, pp. 39–62. Eds: L. Berthier, G. Biroli and J.-P. Bouchaud and L. Cipelletti and W. van Saarloos (Oxford University Press, New York), 2011. (Cited on pages 1 and 7.)

[2] A. Cavagna, "Supercooled liquids for pedestrians," *Physics Reports*, vol. 476, pp. 51–124, 2009. (Cited on pages 1 and 6.)

[3] L. Berthier and G. Biroli, "Theoretical perspective on the glass transition and amorphous materials," *Rev. Mod. Phys.*, vol. 83, p. 587, 2011. (Cited on pages 1, 6, 7, 8, 9, 10 and 16.)

[4] P. G. Wolynes and V. Lubchenko, *Structural Glasses and Supercooled Liquids: Theory, Experiment, and Applications*. V. Lubchenko and P. G. Wolynes Eds. (Wiley), 2012. (Cited on pages 1 and 6.)

[5] K. Binder and A. P. Young, "Spin glasses: Experimental facts, theoretical concepts, and open questions," *Rev. Mod. Phys.*, vol. 58, pp. 801–976, Oct 1986. (Cited on pages 1 and 25.)

[6] M. Mézard, G. Parisi, and M. Virasoro, *Spin Glass Theory and Beyond*. World Scientific Lecture Notes in Physics: Volume 9, 1987. (Cited on pages 1, 15, 118 and 123.)

[7] T. R. Kirkpatrick, D. Thirumalai, and P. G. Wolynes, "Scaling concepts for the dynamics of viscous liquids near an ideal glassy state," *Phys. Rev. A*, vol. 40, p. 1045, 1989. (Cited on pages 1, 11, 17, 20 and 132.)

[8] G. Tarjus, S. A. Kivelson, Z. Nussinov, and P. Viot, "The frustration-based approach of supercooled liquids and the glass transition: a review and critical assessment," *J. Phys. Condens. Matt.*, vol. 17, p. R1143, 2005. (Cited on pages 1 and 22.)

[9] G. Biroli and J.-P. Bouchaud, *Structural Glasses and Supercooled Liquids, Chap. 2: The Random First-Order Transition Theory of Glasses: A Critical Assessment*. V. Lubchenko and P. G. Wolynes Eds. (Wiley), 2009. (Cited on pages 1 and 11.)

[10] W. Götze, *Liquids, Freezing, and the Glass Transition*. Eds.: J. P. Hansen, D. Levesque and J. Zinn-Justin (North Holland, Amsterdam), 1991. (Cited on pages 1 and 9.)

[11] J. P. Garrahan, P. Sollich, and C. Toninelli, *Kinetically constrained models*. Eds: L. Berthier, G. Biroli, J.-P. Bouchaud, L. Cipelletti and W. van Saarloos (Oxford University Press, New York), 2011. (Cited on pages 1, 22 and 131.)

[12] G. Parisi, "The order parameter for spin glasses: a function on the interval $0 - 1$," *J. Phys. A*, vol. 13, p. 1101, 1980. (Cited on pages 2, 13, 14, 26 and 132.)

[13] A. J. Bray and M. A. Moore, "Nonanalytic magnetic field dependence of the magnetisation in spin glasses," *J. of Phys. C: Sol. St. Phys.*, vol. 17, no. 23, p. L613, 1984. (Cited on pages 2 and 26.)

[14] D. S. Fisher and D. A. Huse, "Ordered phase of short-range ising spin-glasses," *Phys. Rev. Lett.*, vol. 56, p. 1601, 1985. (Cited on pages 2 and 26.)

[15] D. Sherrington and S. Kirkpatrick, "Solvable model of a spin-glass," *Phys. Rev. Lett.*, vol. 35, p. 1792, 1975. (Cited on pages 2, 24 and 110.)

[16] G. Parisi, "Infinite number of order parameters for spin glasses," *Phys. Rev. Lett.*, vol. 43, p. 1754, 1979. (Cited on pages 2, 13, 14, 26 and 132.)

[17] T. Castellani and A. Cavagna, "Spin-glass theory for pedestrians," *J. Stat. Mech.*, p. P05012, 2005. (Cited on pages 2, 13 and 15.)

[18] F. Guerra and F. L. Toninelli, "The thermodynamic limit in mean field spin glass models," *Commun. Math. Phys.*, vol. 230, p. 71, 2002. (Cited on pages 2 and 26.)

[19] F. Guerra, "Broken replica symmetry bounds in the mean field spin glass model," *Commun. Math. Phys.*, vol. 233, pp. 1–12, 2003. (Cited on pages 2 and 26.)

[20] M. Talagrand, "The generalized parisi formula," *C. R. Acad. Sci. Paris, Ser. I*, vol. 337, p. 111, 2003. (Cited on pages 2 and 26.)

[21] J. Kurchan, G. Parisi, and F. Zamponi, "Exact theory of dense amorphous hard spheres in high dimension i. the free energy," *J. Stat. Mech.*, vol. P10012, 2012. (Cited on pages 2 and 15.)

[22] J. Kurchan, G. Parisi, P. Urbani, and F. Zamponi, "Exact theory of dense amorphous hard spheres in high dimension. ii. the high density regime and the gardner transition," *J. Phys. Chem. B*, vol. 117, p. 12979, 2013. (Cited on pages 2 and 15.)

[23] M. Mézard, G. Parisi, N. Sourlas, G. Toulouse, and M. Virasoro, "Replica symmetry breaking and the nature of the spin-glass phase," *J. Phys. France*, vol. 45, pp. 843–854, 1984. (Cited on pages 2 and 26.)

[24] K. G. Wilson and I. G. Kogut, "The renormalization group and the ε expansion," *Phys. Rep. C*, vol. 12, p. 75, 1974. (Cited on pages 2, 32 and 33.)

[25] J. Berges, N. Tetradis, and C. Wetterich, "Non-perturbative renormalization flow in quantum field theory and statistical physics," *Phys. Rep.*, vol. 363, p. 223, 2002. (Cited on pages 2, 3, 34, 35, 40, 112, 142 and 143.)

[26] B. Delamotte, *An Introduction to the Nonperturbative Renormalization Group*, pp. 49–132. Springer Berlin Heidelberg, 2012. (Cited on pages 2, 3, 33, 34 and 41.)

[27] F. Ritort and P. Sollich, "Glassy dynamics of kinetically constrained models," *Adv. Phys.*, vol. 52, p. 219, 2003. (Cited on pages 3, 22, 23, 64 and 131.)

[28] P. G. Debenedetti, *Metastable Liquids: Concepts and Principles*. Physical Chemistry: Science and Engineering, J. M. Prausnitz and L. Brewer Eds, 1997. (Cited on pages 6 and 18.)

[29] K. A. Ross, S. D. Arntfield, and S. Cenkowski, *A Polymer Science Approach to Physico-Chemical Characterization and Processing of Pulse Seeds, Chap. 3*. Polymer Science, Dr. Faris Yilmaz (Ed.), 2013. (Cited on page 6.)

[30] P. G. Debenedetti and F. H. Stillinger, "Supercooled liquids and the glass transition," *Nature*, vol. 410, pp. 259–267, 2001. (Cited on page 6.)

[31] C. A. Angell, *Relaxations in Complex Systems*. K. L. Ngai and G. B. Wright Eds. (NRL, Washington), 1985. (Cited on page 6.)

[32] L.-M. Martinez and C. A. Angell, "A thermodynamic connection to the fragility of glass-forming liquids," *Nature*, vol. 410, pp. 663–667, 2001. (Cited on page 6.)

[33] H. Vogel *Phys. Z*, vol. 22, p. 645, 1921. (Cited on page 7.)

[34] G. S. Fulcher, "Analysis of recent measurements of the viscosity of glasses," *J. Am. Cer. Soc.*, vol. 8, p. 339, 1925. (Cited on page 7.)

[35] G. Tammann and G. Hesse, "Die abhängigkeit der viscosität von der temperatur bie unterkühlten flüssigkeiten," *Z Anorg. Allg. Chem.*, vol. 156, p. 245, 1926. (Cited on page 7.)

[36] A. Montanari and G. Semerjian, "Rigorous inequalities between length and time scales in glassy systems," *J. Stat. Phys.*, vol. 125, p. 23, 2006. (Cited on pages 7 and 20.)

[37] W. Kob, *Supercooled Liquids, the Glass Transition and Computer Simulations*. ADP Sciences, Les Ulis; Springer-Verlag, Berlin, 2003, 2002. (Cited on page 7.)

[38] W. Kauzmann, "The nature of the glassy state and the behavior of liquids at low temperatures," *Chem. Review*, vol. 43, p. 219, 1948. (Cited on pages 7 and 8.)

[39] M. D. Ediger, "Spatially heterogeneous dynamics in supercooled liquids," *Annual Review of Physical Chemistry*, vol. 51, pp. 99–128, 2000. (Cited on pages 8 and 9.)

[40] L. Berthier, G. Biroli, J.-P. Bouchaud, L. Cipelletti, and W. van Saarloos, *Dynamical heterogeneities in glasses, colloids and granular media*. Oxford University Press, 2011. (Cited on pages 8, 9, 77 and 131.)

[41] L. O. Hedges, "Theory of nanostructured materials facility, lawrence berkeley national lab.." http://nanotheory.lbl.gov/people/LesterHedges.html. Accessed: 2017-07-13. (Cited on page 8.)

[42] E. Guillaud, S. Merabia, D. de Ligny, and L. Joly, "Decoupling of viscosity and relaxation processes in supercooled water: a molecular dynamics study with the tip4p/2005f model," *Phys. Chem. Chem. Phys.*, vol. 19, pp. 2124–2130, 2017. (Cited on page 10.)

[43] R. Zwanzig, *Lectures in Theoretical Physics*, vol. 135. W.E. Britton, B.W. Downs and J. Downs (Wiley, New York), 1961. (Cited on pages 10, 79 and 80.)

[44] H. Mori, "Transport, collective motion, and brownian motion," *Prog. Theor. Phys.*, vol. 33, p. 423, 1965. (Cited on pages 10, 79 and 80.)

[45] W. Petry, E. Bartsch, F. Fujara, M. Kiebel, H. Sillescu, and B. Farago, "Dynamic anomaly in the glass transition region of orthoterphenyl," *Z. Phys. B*, vol. 83, p. 175, 1991. (Cited on page 11.)

[46] M. Goldstein, "Viscouss liquids and the glass transition: A potential energy barrier picture," *J. Chem. Phys.*, vol. 51, p. 3728, 1969. (Cited on page 11.)

[47] Y. Singh, J. P. Stoessel, and P. G. Wolynes, "Hard-sphere glass and the density-functional theory of aperiodic crystals," *Phys. Rev. Lett.*, vol. 54, p. 1059, 1985. (Cited on pages 11 and 15.)

[48] T. R. Kirkpatrick and P. G. Wolynes, "Connections between some kinetic and equilibrium theories of the glass transition," *Phys. Rev. A*, vol. 35, p. 3072, 1987. (Cited on page 11.)

[49] T. R. Kirkpatrick and D. Thirumalai, "Dynamics of the structural glass transition and the p-spin-interaction spin-glass model," *Phys. Rev. Lett.*, vol. 58, p. 2091, 1987. (Cited on page 11.)

[50] R. W. Hall and P. G. Wolynes, "The aperiodic crystal picture and free energy barriers in glasses," *J. Chem. Phys.*, vol. 86, p. 2943, 1987. (Cited on page 11.)

[51] V. Lubchenko and P. G. Wolynes, "Theory of structural glasses and supercooled liquids," *Ann. Rev. Phys. Chem.*, vol. 58, p. 235, 2007. (Cited on page 11.)

[52] S. Crisanti and H.-J. Sommers, "The spherical p-spin interaction spin glass model: the statics," *Z. Phys. B*, vol. 87, p. 341, 1992. (Cited on pages 11 and 13.)

[53] D. J. Thouless, P. W. Anderson, and R. G. Palmer, "Solution of "solvable model of a spin glass"," *Philos. Mag.*, vol. 35, p. 593, 1977. (Cited on page 12.)

[54] L. F. Cugliandolo and J. Kurchan, "Analytical solution of the off-equilibrium dynamics of a long-range spin-glass model," *Phys. Rev. Lett.*, vol. 71, p. 173, 1993. (Cited on page 13.)

[55] G. Parisi, "Magnetic properties of spin glasses in a new mean field theory," *J. Phys. A*, vol. 13, p. 1887, 1980. (Cited on pages 13 and 26.)

[56] G. Parisi, "A sequence of approximated solutions to the s-k model for spin glasses," *J. Phys. A*, vol. 13, p. L115, 1980. (Cited on pages 13 and 26.)

[57] G. Parisi, "The magnetic properties of the sherrington-kirkpatrick model for spin glasses," *Philos. Mag. B*, vol. 41, p. 677, 1980. (Cited on pages 13 and 26.)

[58] G. Parisi, "Mean field theory for spin glasses," *Phys. Rep.*, vol. 67, p. 97, 1980. (Cited on pages 13, 26 and 132.)

[59] S. Edwards and P. Anderson, "Theory of spin glasses," *J. Phys. F*, vol. 5, p. 965, 1975. (Cited on pages 14, 24, 110 and 132.)

[60] C. Dasgupta and O. T. Valls, "Free-energy landscape of simple liquids near the glass transition," *J. Phys. C*, vol. 12, no. 29, p. 6553, 2000. (Cited on page 15.)

[61] S. Franz, C. Donati, G. Parisi, and S. C. Glotzer, "On dynamical correlations in supercooled liquids," *Philos. Mag. B*, vol. 79, p. 1827, 1999. (Cited on page 15.)

[62] G. Parisi and F. Zamponi, "Mean-field theory of hard sphere glasses and jamming," *Rev. Mod. Phys.*, vol. 82, p. 789, 2010. (Cited on page 15.)

[63] P. Charbonneau, J. Kurchan, G. Parisi, P. Urbani, and F. Zamponi, "Exact theory of dense amorphous hard spheres in high dimension. iii. the full replica symmetry breaking solution," *J. Stat. Mech.*, vol. P10009, 2014. (Cited on page 15.)

[64] T. Maimbourg, J. Kurchan, and F. Zamponi, "Solution of the dynamics of liquids in the large-dimensional limit," *Phys. Rev. Lett.*, vol. 116, p. 015902, 2016. (Cited on page 15.)

[65] R. Monasson, "Structural glass transition and the entropy of the metastable states," *Phys. Rev. Lett.*, vol. 75, p. 2847, 1995. (Cited on page 15.)

[66] S. Franz and G. Parisi, "Effective potential in glassy systems: theory and simulations," *Physica (Amsterdam)*, vol. 261, p. 317, 1998. (Cited on page 15.)

[67] S. Franz and G. Parisi, "Recipes for metastable states in spin glasses," *J. Phys. (Paris) I*, vol. 5, p. 1401, 1995. (Cited on pages 15 and 63.)

[68] S. Franz and G. Parisi, "Phase diagram of coupled glassy systems: A mean-field study," *Phys. Rev. Lett.*, vol. 79, p. 2486, 1997. (Cited on pages 16 and 63.)

[69] M. Mézard, "How to compute the thermodynamics of a glass using a cloned liquid," *Physica A*, vol. 265, p. 352, 1999. (Cited on page 16.)

[70] J. Langer, "Statistical theory of the decay of metastable states," *Ann. Phys.*, vol. 54, p. 258, 1969. (Cited on page 18.)

[71] J.-P. Bouchaud and G. Biroli, "On the adam-gibbs-kirkpatrick-thirumalai-wolynes scenario for the viscosity increase in glasses," *J. Chem. Phys.*, vol. 121, p. 7347, 2004. (Cited on pages 19 and 20.)

[72] S. Franz and A. Montanari, "Analytic determination of dynamical and mosaic length scales in a kac glass model," *J. Phys. A: Math. Gen.*, vol. 40, p. F251, 2007. (Cited on pages 19 and 20.)

[73] A. Cavagna, T. S. Grigera, and P. Verrochio, "Mosaic multistate scenario versus one-state description of supercooled liquids," *Phys. Rev. Lett.*, vol. 98, p. 187801, 2007. (Cited on page 19.)

[74] G. Biroli, J.-P. Bouchaud, A. Cavagna, T. S. Grigera, and P. Verrochio, "Thermodynamic signature of growing amorphous order in glass-forming liquids," *Nature Phys.*, vol. 4, p. 771, 2008. (Cited on page 19.)

[75] C. Cammarota, A. Cavagna, G. Gradenigo, T. S. Grigera, and P. Verrocchio, "Evidence for a spinodal limit of amorphous excitations in glassy systems," *J. Stat. Mech.*, p. L12002, 2009. (Cited on page 19.)

[76] T. M. Group, "Glassy systems, stanford." https://web.stanford.edu/group/markland/research.html. Accessed: 2017-04-27. (Cited on page 19.)

[77] S. Franz and G. Semerjian, *Analytical approaches to time and length scales in models of glasses*. Eds: L. Berthier, G. Biroli, J.-P. Bouchaud, L. Cipelletti and W. van Saarloos (Oxford University Press, New York), 2011. (Cited on page 20.)

[78] S. Franz, "First steps of a nucleation theory in disordered systems," *J. Stat. Mech.*, vol. P04001, 2005. (Cited on page 20.)

[79] M. Dzero, J. Schmalian, and P. G. Wolynes, "Replica theory for fluctuations of the activation barriers in glassy systems," *Phys. Rev. B*, vol. 80, p. 024204, 2009. (Cited on page 20.)

[80] M. Dzero, J. Schmalian, and P. G. Wolynes, "Activated events in glasses: The structure of entropic droplets," *Phys. Rev. B*, vol. 72, p. 100201, 2005. (Cited on page 20.)

[81] S. Franz, "Metastable states, relaxation times and free-energy barriers in finite-dimensional glassy systems," *Euro. Phys. Lett.*, vol. 73, p. 492, 2006. (Cited on page 20.)

[82] M. Castellana, A. Decelle, S. Franz, M. Mézard, and G. Parisi, "Hierarchical random energy model of a spin glass," *Phys. Rev. Lett.*, vol. 104, p. 127206, 2010. (Cited on page 20.)

[83] M. C. Angelini and G. Biroli, "Real space renormalization group theory of disordered models of glasses," *PNAS*, vol. 114, p. 3328, 2017. (Cited on page 20.)

[84] F. Caltagirone, U. Ferrari, L. Leuzzi, G. Parisi, F. Ricci-Tersenghi, and T. Rizzo, "Evidence for a spinodal limit of amorphous excitations in glassy systems," *Phys. Rev. Lett.*, vol. 108, p. 085702, 2012. (Cited on page 21.)

[85] G. Parisi and T. Rizzo, "Critical dynamics in glassy systems," *Phys. Rev. E*, vol. 87, p. 012101, 2013. (Cited on page 21.)

[86] T. Rizzo, "Long-wavelength fluctuations lead to a model of the glass crossover," *Eur. Phys. Lett.*, vol. 106, p. 56003, 2014. (Cited on pages 21 and 132.)

[87] T. Rizzo and T. Voigtmann, "Qualitative features at the glass crossover," *Eur. Phys. Lett.*, vol. 111, p. 56008, 2015. (Cited on page 21.)

[88] T. Rizzo, "The glass crossover from mean-field spin-glasses to supercooled liquids," *Philos. Mag.*, vol. 96, p. 636, 2015. (Cited on page 21.)

[89] T. Rizzo, "Dynamical landau theory of the glass crossover," *Phys. Rev. B*, vol. 94, p. 014202, 2016. (Cited on pages 21 and 132.)

[90] Y. Imry and S. Ma, "Random-field instability of the ordered state of continuous symmetry," *Phys. Rev. Lett.*, vol. 35, p. 1399, 1975. (Cited on pages 21, 67 and 132.)

[91] T. Schneider and E. Pytte, "Random-field instability of the ferromagnetic state," *Phys. Rev. B*, vol. 15, p. 1519, 1977. (Cited on page 21.)

[92] J. Villain, "Nonequilibrium "critical" exponents in the random-field ising model," *Phys. Rev. Lett.*, vol. 52, p. 1543, 1984. (Cited on page 21.)

[93] A. J. Bray and M. A. Moore, "Scaling theory of the random-field ising model," *J. Phys. C: Solid. State Phys.*, vol. 18, p. L927, 1985. (Cited on page 21.)

[94] T. Nattermann, *Theory of the Random Field Ising Model*. World scientific, Singapore, 1998. (Cited on pages 21, 67 and 132.)

[95] S. Franz, G. Parisi, F. Ricci-Tersenghi, and T. Rizzo, "Field theory of fluctuations in glasses," *Eur. Phys. J. E*, vol. 34, p. 102, 2011. (Cited on pages 21 and 132.)

[96] G. Biroli, C. Cammarota, G. Tarjus, and M. Tarzia, "Ising-like effective theory of the glass transition," *To be published*, 2017. (Cited on page 21.)

[97] S. Franz, M. Cardenas, and G. Parisi, "Glass transition and effective potential in the hypernetted chain approximation," *J. Phys. A*, vol. 31, p. L163, 1998. (Cited on pages 21 and 61.)

[98] L. Berthier, "Overlap fluctuations in glass-forming liquids," *Phys. Rev. E*, vol. 88, p. 022313, 2013. (Cited on pages 21 and 61.)

[99] G. Parisi and B. Seoane, "Liquid-glass transition in equilibrium," *Phys. Rev. E*, vol. 89, p. 022309, 2014. (Cited on pages 21 and 61.)

[100] L. Berthier and R. L. Jack, "Evidence for a disordered critical point in a glass-forming liquid," *Phys. Rev. Lett.*, vol. 114, p. 205701, 2015. (Cited on pages 21 and 61.)

[101] S. Franz and G. Parisi, "Universality classes of critical points in constrained glasses," *J. Stat. Mech.*, vol. P11012, 2013. (Cited on pages 21, 66 and 67.)

[102] G. Biroli, C. Cammarota, G. Tarjus, and M. Tarzia, "Random-field-like criticality in glass-forming liquids," *Phys. Rev. Lett.*, vol. 112, p. 175701, 2014. (Cited on pages 21, 46, 66, 67 and 132.)

[103] G. Biroli and C. Cammarota, "Ideal glass transitions by random pinning," *Proc. Natl. Acad. Sci.*, vol. 109, p. 8850, 2012. (Cited on page 21.)

[104] W. Kob and L. Berthier, "Probing a liquid to glass transition in equilibrium," *Phys. Rev. Lett.*, vol. 110, p. 245702, 2013. (Cited on page 21.)

[105] S. Franz, G. Parisi, and F. Ricci-Tersenghi, "Glassy critical points and the random field ising model," *J. Stat. Mech.*, vol. L02001, 2013. (Cited on pages 21 and 132.)

[106] C. Cammarota and G. Biroli, "Random pinning glass transition: Hallmarks, mean-field theory and renormalization group analysis," *J. Chem. Phys.*, vol. 138, p. 12A547, 2013. (Cited on page 21.)

[107] J. D. Stevenson, A. M. Walczak, R. W. Hall, and P. G. Wolynes, "Constructing explicit magnetic analogies for the dynamics of glass forming liquids," *J. Chem. Phys.*, vol. 129, p. 194505, 2008. (Cited on page 21.)

[108] R. M. Turner, R. L. Jack, and J. P. Garrahan, "Overlap and activity glass transitions in plaquette spin models with hierarchical dynamics," *Phys. Rev. E*, vol. 92, p. 022115, 2015. (Cited on pages 21, 61, 63, 65, 66, 67, 72 and 74.)

[109] R. L. Jack and J. P. Garrahan, "Phase transition for quenched coupled replicas in a plaquette spin model of glasses," *Phys. Rev. Lett.*, vol. 116, p. 055702, 2016. (Cited on pages 21, 61, 63, 66, 70, 72, 73 and 74.)

[110] M. Moore, "Interface free energies in p-spin glass models," *Phys. Rev. Lett.*, vol. 96, p. 137202, 2006. (Cited on pages 21 and 132.)

[111] J. Yeo and M. A. Moore, "Renormalization group analysis of the $m - p$-spin glass model with $p = 3$ and $m = 3$," *Phys. Rev. B*, vol. 85, p. 100405(R), 2012. (Cited on page 21.)

[112] C. P. Royall and S. R. Williams, "The role of local structure in dynamical arrest," *Phys. Rep.*, vol. 560, p. 1, 2015. (Cited on page 22.)

[113] J. P. Garrahan and D. Chandler, "Geometrical explanation and scaling of dynamical heterogeneities in glass forming systems," *Phys. Rev. Lett.*, vol. 89, p. 035704, 2002. (Cited on page 22.)

[114] J. P. Garrahan, "Glassiness through the emergence of effective dynamical constraints in interacting systems," *J. Phys. Condens. Matter*, vol. 14, p. 1571, 2002. (Cited on pages 22 and 23.)

[115] G. H. Fredrickson and H. C. Andersen, "Kinetic ising model of the glass transition," *Phys. Rev. Lett.*, vol. 53, p. 1244, 1984. (Cited on page 22.)

[116] J. Jäckle and S. Eisinger, "A hierarchically constrained kinetic ising model," *Z. Phys. B*, vol. 84, p. 115, 1991. (Cited on page 22.)

[117] Y. S. Elmatad, R. L. Jack, D. Chandler, and J. P. Garrahan, "Finite-temperature critical point of a glass transition," *PNAS*, vol. 107, pp. 12793–12798, 2010. (Cited on page 22.)

[118] M. E. J. Newman and C. Moore, "Glassy dynamics and aging in an exactly solvable spin model," *Phys. Rev. E*, vol. 60, p. 5068, 1999. (Cited on pages 22 and 64.)

[119] J. P. Garrahan and M. E. J. Newman, "Glassiness and constrained dynamics of a short-range nondisordered spin model," *Phys. Rev. E*, vol. 62, p. 7670, 2000. (Cited on pages 22, 23 and 64.)

[120] A. Lipowski, "Glassy behaviour and semi-local invariance in ising model with four-spin interaction," *J. Phys. A: Math. Gen.*, vol. 30, p. 7365, 1997. (Cited on page 23.)

[121] A. Lipowski and D. Johnston, "Metastability in a four-spin ising model," *J. Phys. A: Math. Gen.*, vol. 33, p. 4451, 2000. (Cited on page 23.)

[122] R. L. Jack, L. Berthier, and J. P. Garrahan, "Static and dynamic length scales in a simple glassy plaquette model," *Phys. Rev. E*, vol. 72, p. 016103, 2005. (Cited on page 23.)

[123] R. L. Jack and J. P. Garrahan, "Caging and mosaic length scales in plaquette spin models of glasses," *J. Chem. Phys.*, vol. 123, p. 164508, 2005. (Cited on pages 23 and 74.)

[124] G. Toulouse, "Theory of the frustration effect in spin glasses: I," *Commun. Phys.*, vol. 2, p. 115, 1977. (Cited on page 23.)

[125] H. Kawamura and T. Taniguchi, *Spin Glasses*, vol. 24. 2015. (Cited on page 24.)

[126] K. Gunnarsson, P. Svedlindh, P. Nordblad, L. Lundgren, H. Aruga, and A. Ito, "Static scaling in a short-range ising spin glass," *Phys. Rev. B*, vol. 43, p. 8199, 1991. (Cited on page 23.)

[127] A. P. Young, *Spin Glasses and Random Fields*. World Scientific Publishing Co. Pte. Ltd., 1997. (Cited on page 23.)

[128] A. T. Ogielski and I. Morgenstern, "Critical behavior of three-dimensional ising spin-glass model," *Phys. Rev. Lett.*, vol. 54, p. 928, 1985. (Cited on page 24.)

[129] R. N. Bhatt and A. P. Young, "Search for a transition in the three-dimensional j ising spin-glass," *Phys. Rev. Lett.*, vol. 54, p. 924, 1985. (Cited on page 24.)

[130] A. J. Bray and M. A. Moore, "Critical behavior of the three-dimensional ising spin glass," *Phys. Rev. B*, vol. 31, p. 631, 1985. (Cited on pages 24 and 27.)

[131] J. Collaboration, "Nature of the spin-glass phase at experimental length scales," *J. Stat. Mech.*, vol. P06026, 2010. (Cited on page 24.)

[132] J. Collaboration, "Sample-to-sample fluctuations of the overlap distributions in the three-dimensional edwards-anderson spin glass," *Phys. Rev. B*, vol. 84, p. 174209, 2011. (Cited on page 24.)

[133] W. L. McMillan, "Domain-wall renormalization-group study of the three-dimensional random ising model," *Phys. Rev. B*, vol. 30, p. 476, 1984. (Cited on page 24.)

[134] A. J. Bray and M. A. Moore, "Lower critical dimension of ising spin glasses: a numerical study," *J. of Phys. C: Sol. St. Phys.*, vol. 17, no. 18, p. L463, 1984. (Cited on pages 24 and 27.)

[135] S. Franz, G. Parisi, and M. A. Virasoro, "Interfaces and lower critical dimension in a spin glass model," *J. Physique I*, vol. 4, p. 1657, 1994. (Cited on page 24.)

[136] H. Rieger, L. Santen, U. Blasum, M. Diehl, M. Jünger, and G. Rinaldi, "The critical exponents of the two-dimensional ising spin glass revisited: exact ground-state calculations and monte carlo simulations," *J. of Phys. A: Math. and Gen.*, vol. 29, no. 14, p. 3939, 1996. (Cited on page 24.)

[137] C. Amoruso, E. Marinari, O. C. Martin, , and A. Pagnani, "Scalings of domain wall energies in two dimensional ising spin glasses," *Phys. Rev. Lett.*, vol. 91, p. 087201, 2003. (Cited on page 24.)

[138] F. Zamponi, "Mean field theory of spin glasses," *arXiv:1008.4844v5*, 2010. (Cited on page 25.)

[139] A. B. Harris, T. C. Lubensky, and J.-H. Chen, "Critical properties of spin-glasses," *Phys. Rev. Lett.*, vol. 36, p. 415, 1976. (Cited on pages 25, 26, 109, 110 and 123.)

[140] J. de Almeida and D. Thouless, "Stability of the sherrington-kirkpatrick solution of a spin glass model," *J. Phys. A*, vol. 11, p. 983, 1978. (Cited on page 25.)

[141] C. D. Dominis, I. Kondor, and T. Temesvári, *Beyond the Sherrington-Kirkpatrick model*. World Scientific Publishing Co. Pte. Ltd., Ed. A. P. Young, 1997. (Cited on pages 26 and 129.)

[142] M. Moore and A. J. Bray, "The nature of the spin-glass phase and finite size effects," *J. of Phys. C: Sol. St. Phys.*, vol. 18, no. 23, p. L699, 1985. (Cited on page 26.)

[143] A. J. Bray and M. A. Moore, *Heidelberg Colloquium on Glassy Dynamics: Proceedings of a Colloquium on Spin Glasses, Optimization and Neural Networks Held at the University of Heidelberg June 9–13, 1986*. Springer Berlin Heidelberg, 1987. (Cited on page 26.)

[144] D. S. Fisher and D. A. Huse, "Nonequilibrium dynamics of spin glasses," *Phys. Rev. B*, vol. 38, p. 373, 1988. (Cited on page 26.)

[145] D. S. Fisher and D. A. Huse, "Equilibrium behavior of the spin-glass ordered phase," *Phys. Rev. B*, vol. 38, p. 386, 1988. (Cited on page 26.)

[146] W. L. McMillan, "Scaling theory of ising spin glasses," *J. Phys. C*, vol. 17, p. 3179, 1984. (Cited on page 27.)

[147] R. Rajaraman, *Solitons and Instantons: An Introduction to Solitons and Instantons in Quantum Field Theory*. North-Holland Pub. Comp., Amsterdam, New-York, Oxford, 1982. (Cited on page 29.)

[148] S. Coleman, *Aspects of symmetry*. Cambridge Univ. Press, Cambridge, 1985. (Cited on pages 29, 30 and 31.)

[149] J. Zinn-Justin, *Quantum field theory and critical phenomena*. Clarendon, Oxford, 1989. (Cited on pages 29, 31, 51 and 145.)

[150] L. Kadanoff, "Scaling laws for ising models near t_c," *Physics*, vol. 2, p. 263, 1966. (Cited on page 32.)

[151] A. Migdal *Z. Eksper. Teoret. Fiz.*, vol. 69, p. 810, 1975. (Cited on page 32.)

[152] A. Migdal, "Phase transitions in gauge and spin-lattice system," *Z. Eksper. Teoret. Fiz.*, vol. 69, p. 1457, 1975. (Cited on page 32.)

[153] L. Kadanoff, "Notes on migdal's recursion formulas," *Annals of Physics*, vol. 100, pp. 359–394, 1976. (Cited on page 32.)

[154] F. J. Wegner and A. Houghton, "Renormalization group equation for critical phenomena," *Phys. Rev. A*, vol. 8, p. 401, 1973. (Cited on page 33.)

[155] J. Polchinski, "Renormalization and effective lagrangians," *Nucl. Phys. B*, vol. 231, p. 269, 1984. (Cited on page 33.)

[156] A. Hasenfratz and P. Hasenfratz, "Renormalization group study of scalar field theories," *Nucl. Phys. B*, vol. 270, p. 687, 1986. (Cited on pages 33 and 41.)

[157] C. Wetterich, "Average action and the renormalization group equations," *Phys. Lett. B*, vol. 352, p. 529, 1991. (Cited on page 34.)

[158] C. Wetterich, "The average action for scalar fields near phase transitions," *Z. Phys. C*, vol. 57, p. 451, 1993. (Cited on page 34.)

[159] C. Wetterich, "Improvement of the average action," *Z. Phys. C*, vol. 60, p. 461, 1993. (Cited on page 34.)

[160] C. Wetterich, "Exact evolution equation for the effective potential," *Phys. Lett. B*, vol. 301, p. 90, 1993. (Cited on pages 34 and 35.)

[161] N. Tetradis and C. Wetterich, "The high temperature phase transition for φ^4 theories," *Nucl. Phys. B*, vol. 398, p. 659, 1993. (Cited on pages 34 and 35.)

[162] D. Litim, "Optimized renormalization group flows," *Phys. Rev. D*, vol. 64, p. 105007, 2001. (Cited on pages 35 and 48.)

[163] C. Wetterich, "Exact evolution equation for the effective potential," *Phys. Lett. B*, vol. B301, p. 90, 1993. (Cited on page 35.)

[164] T. R. Morris, "Derivative expansion of the exact renormalization group," *Phys. Lett. B*, vol. 329, p. 241, 1994. (Cited on page 41.)

[165] G. Grinstein, "Ferromagnetic phase transitions in random fields: The breakdown of scaling laws," *Phys. Rev. Lett.*, vol. 37, p. 944, 1976. (Cited on page 43.)

[166] C. Rulquin, P. Urbani, G. Biroli, G. Tarjus, and M. Tarzia, "Nonperturbative fluctuations and metastability in a simple model: from observables to microscopic theory and back," *J. Stat. Mech.: Th. and Exp.*, vol. 2, p. 023209, 2016. (Cited on page 45.)

[167] L. Berthier and D. Coslovich, "A novel approach to numerical measurements of the configurational entropy in supercooled liquids," *PNAS (USA)*, vol. 111, p. 11668, 2014. (Cited on page 46.)

[168] T. Antal, M. Droz, and Z. Rácz, "Probability distribution of magnetization in the one-dimensional ising model: effects of boundary conditions," *J. Phys. A: Math. Gen.*, vol. 37, pp. 1465–1478, 2004. (Cited on pages 52, 53 and 135.)

[169] A. S. Kapoyannis and N. Tetradis, "Quantum-mechanical tunnelling and the renormalization group," *Phys. Lett. A*, vol. 276, p. 225, 2000. (Cited on pages 59 and 140.)

[170] K. I. Aoki and *et al.*, "Non-perturbative renormalization group analysis in quantum mechanics," *Prog. Theor. Phys.*, vol. 108, p. 571, 2002. (Cited on pages 59 and 140.)

[171] D. Zappala, "Improving the renormalization group approach to the quantum-mechanical double well potential," *Phys. Lett. A*, vol. 290, p. 35, 2001. (Cited on page 59.)

[172] M. Weyrauch, "Functional renormalization group and quantum tunnelling," *J. Phys. A*, vol. 39, p. 649, 2006. (Cited on pages 59 and 140.)

[173] G. Biroli, C. Rulquin, G. Tarjus, and M. Tarzia, "Role of fluctuations in the phase transitions of coupled plaquette spin models of glasses," *SciPost Phys.*, vol. 1, p. 007, 2016. (Cited on page 61.)

[174] J. P. Garrahan, "Transition in coupled replicas may not imply a finite-temperature ideal glass transition in glass-forming systems," *Phys. Rev. E*, vol. 89, p. 030301, 2014. (Cited on pages 61, 63, 64, 65, 66 and 74.)

[175] J. R. Heringa, H. W. J. Blöte, and A. Hoogland, "Phase transitions in self-dual ising models with multispin interactions and a field," *Phys. Rev. Lett.*, vol. 63, p. 1546, 1989. (Cited on page 65.)

[176] S.-I. Sasa, "Thermodynamic transition associated with irregularly ordered ground states in a lattice gas model," *J. Phys. A: Math. Theor.*, vol. 43, p. 465002, 2010. (Cited on page 65.)

[177] Y. Deng, W. Guo, J. R. Heringa, H. W. J. Blöte, and B. Nienhuis, "Phase transitions in self-dual generalizations of the baxter-wu model," *Nucl. Phys. B*, vol. 827, p. 406, 2010. (Cited on page 65.)

[178] M. Aizenman and J. Wehr, "Rounding of first-order phase transitions in systems with quenched disorder," *Phys. Rev. Lett.*, vol. 62, p. 2503, 1989. (Cited on page 67.)

[179] S. Franz, M. Mézard, F. Ricci-Tersenghi, M. Weigt, and R. Zecchina, "A ferromagnet with a glass transition," *Europhys. Lett.*, vol. 55, p. 465, 2001. (Cited on pages 67, 68, 69 and 70.)

[180] M. Mézard and G. Parisi, "The bethe lattice spin glass revisited," *Europhys. J. B*, vol. 20, p. 217, 2001. (Cited on page 68.)

[181] M. Mézard and G. Parisi, "The cavity method at zero temperature," *J. Stat. Phys.*, vol. 111, p. 1, 2003. (Cited on pages 68 and 69.)

[182] L. Zdeborová and F. Krzakala, "Phase transitions in the coloring of random graphs," *Phys. Rev. E*, vol. 76, p. 031131, 2007. (Cited on pages 68 and 69.)

[183] M. Mézard, F. Ricci-Tersenghi, and R. Zecchina, "Two solutions to diluted p-spin models and xorsat problems," *J. Stat. Phys.*, vol. 111, p. 505, 2003. (Cited on page 70.)

[184] S. Cocco, O. Dubois, J. Mandler, and R. Monasson, "Rigorous decimation-based construction of ground pure states for spin-glass models on random lattices," *Phys. Rev. Lett.*, vol. 90, p. 047205, 2003. (Cited on page 70.)

[185] L. Zdeborová and F. Krzakala, "Generalization of the cavity method for adiabatic evolution of gibbs states," *Phys. Rev. B*, vol. 81, p. 224205, 2010. (Cited on page 70.)

[186] Y. Matsuda, H. Nishimori, L. Zdeborová, and F. Krzakala, "Random-field p-spin-glass model on regular random graphs," *J. Phys. A: Math. Theor.*, vol. 44, p. 185002, 2011. (Cited on page 70.)

[187] C. Cammarota, G. Tarzia, G. Biroli, and G. Tarjus, "Fragility of the mean-field scenario of structural glasses for disordered spin models in finite dimensions," *Phys. Rev. B*, vol. 87, p. 064202, 2013. (Cited on page 72.)

[188] L. Foini, F. Krzakala, and F. Zamponi, "On the relation between kinetically constrained models of glass dynamics and the random first-order transition theory," *JSTAT*, vol. P06013, 2012. (Cited on page 73.)

[189] L. Berthier, G. Biroli, J.-P. Bouchaud, W. Kob, K. Miyazaki, and D. Reichman, "Spontaneous and induced dynamic fluctuations in glass formers. i. general results and dependence on ensemble and dynamics," *J. Chem. Phys.*, vol. 126, p. 184503, 2007. (Cited on page 78.)

[190] L. Berthier, G. Biroli, J.-P. Bouchaud, W. Kob, K. Miyazaki, and D. Reichman, "Spontaneous and induced dynamic correlations in glass formers. ii. model calculations and comparison to numerical simulations," *J. Chem. Phys.*, vol. 126, p. 184504, 2007. (Cited on page 78.)

[191] G. W. Ford, M. Kac, and P. Mazur, "Statistical mechanics fo assemblies of coupled oscillators," *J. of Math. Phys.*, vol. 6, p. 504, 1965. (Cited on pages 79 and 80.)

[192] K. Lindenberg and E. Cortés, "Thermal relaxation of systems with quadratic heat bath coupling," *Physica A*, vol. 126, pp. 489–503, 1984. (Cited on pages 79 and 87.)

[193] R. Zwanzig, "Nonlinear generalized langevin equations," *J. Stat. Phys.*, vol. 9, pp. 215–220, 1973. (Cited on pages 79 and 80.)

[194] A. O. Caldeira and A. J. Leggett, "Influence of dissipation on quantum tunneling in macroscopic systems," *Phys. Rev. Lett.*, vol. 46, p. 211, 1981. (Cited on pages 79 and 80.)

[195] A. O. Caldeira and A. J. Leggett, "Quantum tunneling in a dissipative system," *Ann. of Phys.*, vol. 149, p. 374, 1983. (Cited on pages 79 and 80.)

[196] P. C. Martin, E. D. Siggia, and H. A. Rose, "Statistical dynamics of classical systems," *Phys. Rev. A*, vol. 8, p. 423, 1973. (Cited on pages 79 and 88.)

[197] K.-K. Janssen, "On a lagrangean for classical field dynamics and renormalization group calculations of dynamical critical properties," *Z. Phys. B*, vol. 23, pp. 377–380, 1976. (Cited on pages 79 and 88.)

[198] D. Dominicis and C., "Techniques de renormalisation de la théorie des champs et dynamique des phénomènes critiques," *J. Phys. Colloq.*, vol. 37, pp. C1–247, 1976. (Cited on pages 79 and 88.)

[199] C. Kittel, *Introduction to Solid State Physics - 8th ed.* John Wiley and Sons, Inc, 2005. (Cited on page 81.)

[200] O. S. Duarte and A. O. Caldeira, "Effective coupling between two brownian particles," *Phys. Rev. Lett.*, vol. 97, p. 250601, 2006. (Cited on page 83.)

[201] E. Cortés, B. J. West, and K. Lindenberg, "On the generalized langevin equation: Classical and quantum mechanical," *J. Chem. Phys.*, vol. 82, p. 2708, 1985. (Cited on page 87.)

[202] E. Brezin, G. Parisi, and J. Zinn-Justin, "Perturbation theory at large orders for a potential with degenerate minima," *Phys. Rev. D*, vol. 16, p. 408, 1977. (Cited on page 94.)

[203] E. Pollak, S. C. Tucker, and B. J. Berne, "Variational transition-state theory for reaction rates in dissipative systems," *Phys. Rev. Lett.*, vol. 65, p. 1399, 1990. (Cited on page 107.)

[204] J.-H. Chen and T. C. Lubensky, "Mean field and ε-expansion study of spin glasses," *Phys. Rev. B*, vol. 16, p. 2106, 1977. (Cited on page 109.)

[205] A. J. Bray and M. A. Moore, "Replica symmetry and massless modes in the ising spin glass," *J. Phys. C*, vol. 12, p. 79, 1979. (Cited on page 109.)

[206] J. Hubbard, "Calculation of partition functions," *Phys. Rev. Lett.*, vol. 3, p. 77, 1959. (Cited on page 110.)

[207] T. Temesvári, C. D. Dominicis, and I. R. Pimentel, "Generic replica symmetric field-theory for short range ising spin glasses," *Eur. Phys. J. B*, vol. 25, pp. 361–372, 2002. (Cited on pages 110 and 113.)

[208] D. J. Elderfield and A. J. McKane, "Relevance of φ^4 operators in the edwards-anderson model," *Phys. Rev. B*, vol. 18, p. 3730, 1978. (Cited on page 110.)

[209] J. E. Green, "ε-expansion for the critical exponents of a vector spin glass," *J. Phys. A: Math. Gen.*, vol. 18, p. L43, 1985. (Cited on pages 110 and 123.)

[210] J. Yeo, M. A. Moore, and T. Aspelmeier, "Nature of perturbation theory in spin glasses," *J. Phys. A: Math. and Gen.*, vol. 38, p. 4027, 2005. (Cited on page 110.)

[211] J. Collaboration, "Critical parameters of the three-dimensional ising spin glass," *J. Stat. Mech.*, vol. P05014, 2014. (Cited on pages 111 and 123.)

[212] P. H. Lundow and I. A. Campbell, "The ising spin glass in dimension four," *Physica A*, vol. 434, p. 181, 2015. (Cited on pages 111 and 123.)

[213] P. H. Lundow and I. A. Campbell, "Ising spin glasses in dimension five," *Phys. Rev. E*, vol. 95, p. 012112, 2017. (Cited on pages 111 and 123.)

[214] G. Tarjus and M. Tissier, "Nonperturbative functional renormalization group for random field models and related disordered systems. i. effective average action formalism," *Phys Rev. B*, vol. 78, p. 024203, 2008. (Cited on page 112.)

[215] I. R. Pimentel, T. Temesvári, and C. D. Dominicis, "Spin-glass transition in a magnetic field: A renormalization group study," *Phys. Rev. B*, vol. 65, p. 224420, 2002. (Cited on pages 113 and 123.)

[216] V. Jovovic, "Number of multigraphs on infinite set of nodes with n edges." http://oeis.org/A050535. Accessed: 2017-10-25. (Cited on page 114.)

[217] F. Harary, "The number of linear, directed, rooted, and connected graphs," *Trans. Am. Math. Soc.*, vol. 78, pp. 445–463, 1955. (Cited on page 114.)

[218] F. Harary and E. M. Palmer, *Graphical Enumeration, Chap. 4*. Academic Press, NY, 1973. (Cited on page 114.)

[219] H. Li and D. C. Torney, "Enumerations of multigraphs," 2002. (Cited on page 114.)

[220] H. Li and D. C. Torney, "Number of different euler multigraphs with n edges, loops forbidden." http://oeis.org/A068592. Accessed: 2017-10-25. (Cited on page 114.)

[221] H. Ballhausen, J. Berges, and C. Wetterich, "Critical phenomena in continuous dimension," *J. Phys. Lett. B*, vol. 582, pp. 144–150, 2004. (Cited on page 123.)

[222] T. Papenbrock and C. Wetterich, "Two-loop results for improved one loop computations," *Z. Phys. C*, vol. 65, pp. 519–535, 1995. (Cited on page 126.)

[223] R. J. Baxter, *Exactly solved models in statistical mechanics*. Courier Corporation, 2007. (Cited on pages 135 and 138.)

[224] J.-P. Blaizot, R. Mendez-Galain, and N. Wschebor, "A new method to solve the non-perturbative renormalization group equations," *Phys. Lett. B*, vol. 632, p. 571, 2006. (Cited on page 142.)

[225] A. Parola and L. Reatto, "Liquid state theories and critical phenomena," *Adv. in Phys.*, vol. 44, p. 211, 1995. (Cited on pages 142 and 143.)

[226] N. Tetradis and C. Wetterich, "Scale dependence of the average potential around the maximum in φ^4 theories," *Nucl. Phys. B*, vol. 383, p. 197, 1992. (Cited on pages 142 and 143.)

[227] D. Baeriswyl, A. Bishop, and J. Camelo, *Applications of statistical and field theory methods to condensed matter*. Springer Science and Business Media, 2012. (Cited on page 143.)

[228] A. Ringwald and C. Wetterich, "Average action for the $n-$component ϕ^4 theory," *Nucl. Phys. B*, vol. 334, p. 506, 1990. (Cited on page 143.)

Le rôle des fluctuations dans les systèmes vitreux de dimension finie

Résumé : Les systèmes vitreux sujets à une diminution de la température présentent une dynamique très lente, et à une valeur suffisamment faible de celle-ci se trouvent dans un état désordonné dit "gelé". Cette thèse traite du cas des verres structuraux, comme les liquides surfondus, et du cas des verres de spins. Dans les deux cas, les scénarios physiques issus des théories de champ moyen sont connus et pourraient être sensibles à l'introduction des fluctuations présentes dans les systèmes de dimension finie. L'étude de leur effet dans les systèmes vitreux étant difficile, nous avons étudié des modèles simples reliés au problème de la transition vitreuse dans lesquels l'effet des fluctuations peut être analysé en détail.

Concernant les verres structuraux, nous étudions tout d'abord le retour à la convexité de l'énergie libre d'un système unidimensionnel où les fluctuations sont contraintes par la taille finie du système. Ensuite, nous étudions le rôle des fluctuations de "courte" et de "longue" portée dans un système vitreux appelé "modèle de plaquette" en comparant les propriétés thermodynamiques du système connues sur réseaux Euclidiens à celles que nous avons obtenues sur un réseau "en arbre". Enfin, nous étudions l'existence de fluctuations spatio-temporelles au sein d'un modèle de systèmes à dynamique activée couplés *via* un bain thermal à faible température.

Concernant les verres de spins, nous construisons une approche du groupe de renormalisation non-perturbatif afin de décrire l'effet des fluctuations critiques sur les propriétés critiques du verre de spin d'Ising en champ nul en dimensions inférieures à six.

The role of fluctuations in finite-dimensional glassy systems

Abstract: When the temperature diminishes, glassy systems present a very sluggish dynamics and at low enough temperature can finish in some arrested disordered state. This thesis deals about the case of structural glasses, to which category supercooled liquids belong to, and spin glasses. In these two cases the physical scenarios issued from the mean-field theories are known and could be fragile to the introduction of fluctuations that are present in finite-dimensional systems. Since the study of the effect of fluctuations in glassy systems is a daunting task, the aim of this thesis is to study simple related problems in which the effect of fluctuations can be thoroughly investigated.

For the structural-glass case, we study first the return to convexity of the free energy of a unidimensional finite-size system where fluctuations are restricted by the finite size of the system. Then, we study the role of "short"- and "long"-range fluctuations in a glass-former model called "plaquette model" in comparing the thermodynamic properties of the system which are known on Euclidean lattices with the ones we obtained on a "tree" lattice. Finally, we study the existence of space-time fluctuations in a model made of activated-dynamics systems coupled *via* a thermal bath at low temperature.

For the spin-glass case, we construct a scheme for the nonperturbative renormalization group to describe the effect of critical fluctuations on the critical properties of the Ising spin glass in zero field in dimensions lower than six.